Publicacao mais relevante 2/2

Data Acquisition and Trigger System of the Gamma Ray Energy Tracking In-Beam Nuclear Array (GRETINA)

John Anderson, Renato Brito, Dionisio Doering, Todd Hayden, Bryan Holmes, John Joseph, Harold Yaver, and Sergio Zimmermann, *Senior Member, IEEE*

***Abstract*—The Gamma Ray Energy Tracking In-Beam Nuclear Array (GRETINA), capable of determining the energy and position (within 2 mm) of each gamma-ray interaction point and tracking multiple gamma-ray interactions, has been designed. GRETINA will be composed of seven detector modules, each with four highly pure germanium crystals. Each crystal has 36 segments and one central contact instrumented by charge sensitive amplifiers. Two custom designed modules, the Digitizer/Digital Signal Processing (DSP) and the Trigger Timing and Control, compose the electronics of this system. The Digitizer/DSP converts the analog information with 14-bit analog to digital converters (operating at 100 MS/s, and digitally processes the data to determine the energy and timing information of the gamma interactions with the crystal. Each Digitizer/DSP is controlled by and sends trigger information to the Trigger Timing & Control system through a bidirectional Gbit link. Presently four different trigger algorithms are planned for the trigger system and can be selected for trigger decision. In this paper the details of the electronics and algorithms of the GRETINA data acquisition and trigger system are presented and the performance is reviewed.**

***Index Terms*—Data acquisition systems, digital signal processing, gamma-ray spectrometer, trigger systems.**

I. Introduction

We have designed a data acquisition and trigger system for the Gamma Ray Energy Tracking In-Beam Nuclear Array (GRETINA). GRETINA is based on germanium detectors and it will be capable of determining the energy and position (within 2 mm) of the points of interaction of the gamma-rays with the germanium crystal and of tracking multiple gamma-ray interactions [1], [2]. GRETINA is composed of seven detector modules, each with four high purity germanium crystals (see Fig. 1), comprising a quarter or 1-π of a sphere. The detector module components include charge sensitive amplifiers [3] assembled inside the detector enclosure to instrument each of the 36 segments and the central contact. The gamma ray interaction with the germanium crystal induces charge on the segments and central contact. The amplifiers integrate this charge and drive an analog voltage to the GRETINA front-end electronics.

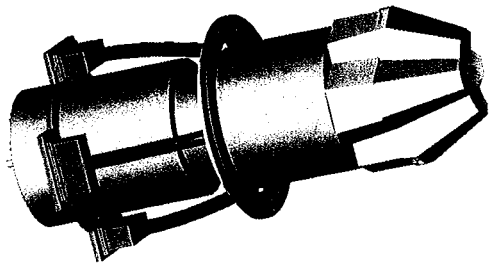

Fig. 1. GRETINA detector module.

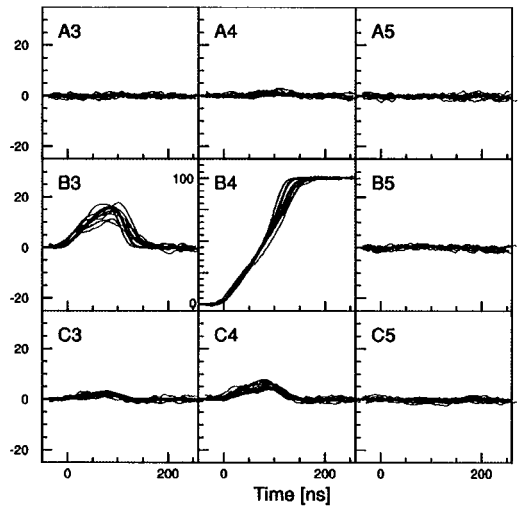

Fig. 2. Waveforms for interactions below segment B4.

For illustration, Fig. 2 shows examples of typical waveforms on the output of the amplifiers. The gamma-rays from a collimated ^{137}Cs source are interacting with the detector at a specific location below the B4 segment. The segments shown are the one that collects the charge (B4) and its eight nearest neighbor segments. The neighbor segments detect induced charge. A total of 16 measured shapes are plotted in gray and calculated signals at this given position are plotted in black; the agreement between calculation and measurement is very good. Observe that the measured signals include noise.

The detector modules are supported by a mechanical structure composed of two quasi-hemispheres shells that surround

Manuscript received January 22, 2008; revised August 14, 2008. Current version published February 11, 2009. This work was supported by the Director, Office of Science, Office of Nuclear Physics, of the U.S. Department of Energy under Contract DE-AC02-05CH11231.

J. Anderson and T. Hayden are with Argonne National Laboratory, Argonne, IL 60439 USA.

R. Brito was with the Lawrence Berkeley National Laboratory, Berkeley, CA 94720 USA. He is now with the Department of Electrical Engineering, Federal University of Rio Grande do Sul, Porto Alegre, RS 90035, Brazil.

D. Doering, B. Holmes, J. Joseph, H. Yaver, and S. Zimmermann are with the Lawrence Berkeley National Laboratory, Berkeley, CA 94720 USA (e-mail: szimmermann@lbl.gov).

Digital Object Identifier 10.1109/TNS.2008.2009444

0018-9499/$25.00 © 2009 IEEE

Authorized licensed use limited to: Lawrence Berkeley National Laboratory. Downloaded on November 21, 2009 at 12:25 from IEEE Xplore. Restrictions apply.

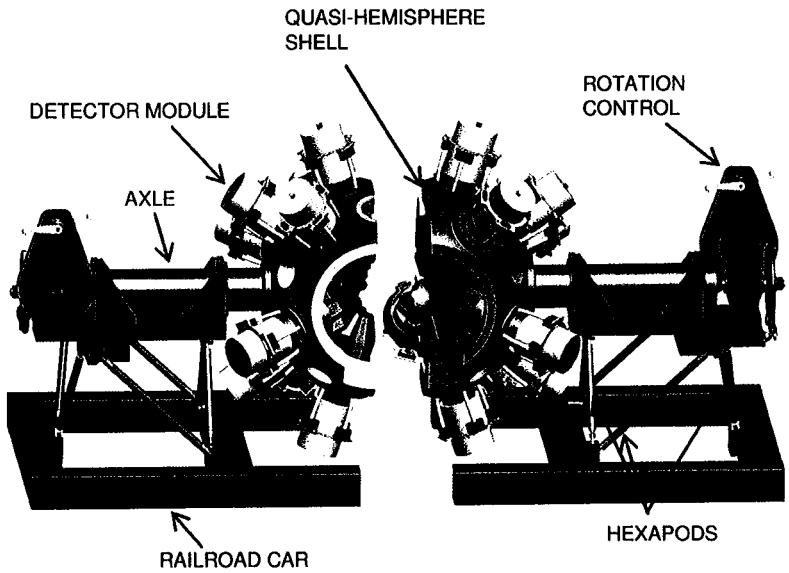

Fig. 3. GRETINA mechanical support structure.

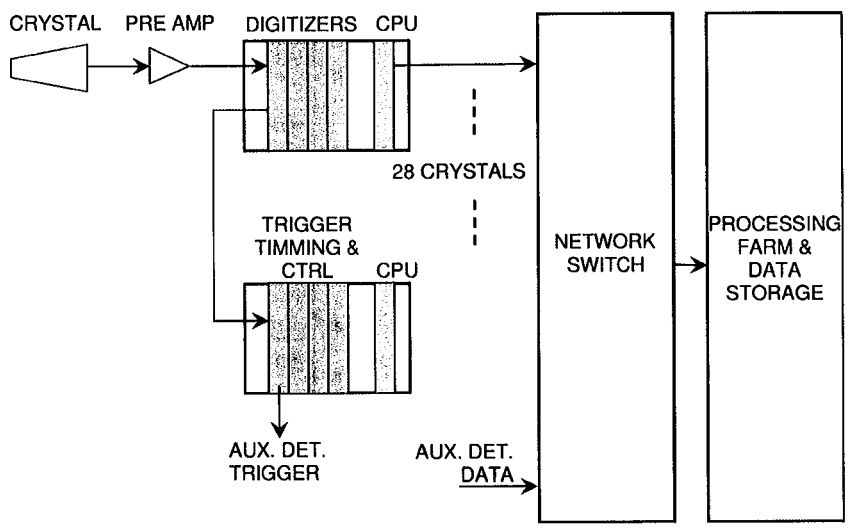

Fig. 4. GRETINA electronics and computing systems.

the target chamber. This shell structure is capable of supporting 21 detector modules. The structure allows rotation for detector mounting (through a gear box in the end of the axles) and translation to access the target chamber (through railroad cars). Hexapods connect the structure to the railroad cars. Fig. 3 shows a sketch of the support structure, with all possible positions instrumented with a detector module. There are plans to construct the full 4-π detector module array, GRETA [4], and the electronics system foresees this possible scenario.

In this paper the details of the electronics and algorithms of the GRETINA data acquisition and trigger system will be presented and the performance will be reviewed. In addition, grounding and filtering techniques used to achieve the 14-bit analog to digital conversion (ADC) performance will be discussed, as well as transmission line techniques for the very low bit error rate of the gigabit links.

II. System Architecture

Fig. 4 shows a block diagram of the GRETINA Electronics and Computing Systems. The oblong shape on the left represents the detector modules and its crystals. Charge sensitive amplifiers instrument the segments and central contact. Fifteen meters of shielded twisted pair cable connect the pre-amplifier outputs to the digitizer modules. Two custom designed modules, the Digitizer/Digital Signal Processing (Digitizer/DSP) and the Trigger Timing & Control (TTC), compose the electronics of this system. Four Digitizer/DSP modules instrument one crystal: each master Digitizer/DSP interfaces with the TTC system and controls three slave Digitizer/DSP modules. A digital bus in the front panel allows the digitizers serving a crystal to synchronize among themselves for clock and trigger information. A very simple communication protocol based on a single master controlling the operations is used.

Authorized licensed use limited to: Lawrence Berkeley National Laboratory. Downloaded on November 21, 2009 at 12:25 from IEEE Xplore. Restrictions apply.

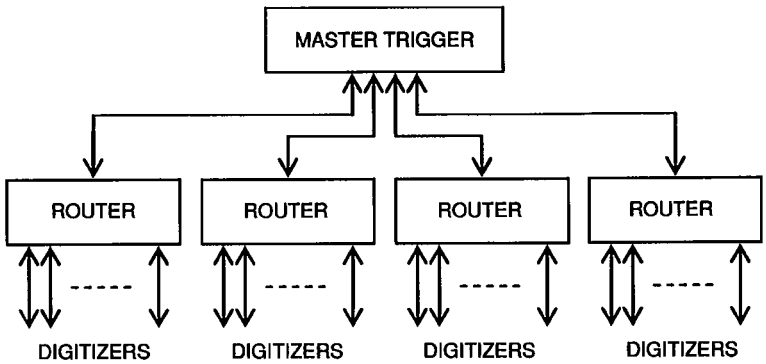

Fig. 5. TTC router and master connection.

The master digitizer monitors the crystal central contact. If a gamma ray deposits charge in the crystal above the programmable threshold of the leading edge (LE) discriminator, the master Digitizer/DSP recognizes the event and reads the segment hit pattern using the front panel bus. In parallel the Master digitizer estimates the energy of the central contact signal using a fast algorithm. It then assembles the trigger information (time stamp (TS) of the LE discriminator, central contact energy and segment hit pattern) and sends it to the TTC over one pair of a bidirectional 1 Gb/s serial link. A buffer records the timestamps of all recent discriminator decisions.

The serial link connecting the TTC and Digitizer/DSP modules is implemented using the National Semiconductor DS92LV18 Serializer/Deserializer (SerDes). It transmits 20 bits per word at a 50 MHz rate, where 18 bits are available for trigger and control information. The link meets the stability requirement of the system and has a predictable latency. The predictable latency allows the same twisted pair to transmit control information and provide the 50 MHz master clock to each Digitizer/DSP. The trigger information exchange between the master trigger and Digitizer/DSP employs a synchronous protocol and the master trigger module determines the synchronism. A synchronous implementation is easier to implement and maintain. The protocol consists of an endlessly repeating series of 20 command frames transmitted every 2 μs that allows the TTC system to regularly synchronize and control activities at the Digitizer/DSPs. Also, all trigger information from the Digitizer/DSP is transmitted to the TTC within this 2 μs window. The reason for a 2 μs period is to accommodate instantaneous fluctuations on the maximum average of one gamma interaction per crystal every 20 μs.

The whole TTC system is assembled around the same hardware module. The firmware is configured for two different functions: the Router module and the Master TTC. The Router routes all information between the Master TTC and the Digitizer/DSP modules and assists in fast multiplicity trigger decisions. The Master TTC collects all messages from the Routers plus additional information from auxiliary trigger modules and uses it to make a global trigger decision (refer to Fig. 5). Once a global trigger decision is made, the TTC system sends a trigger decision command to the Routers for distribution to all master Digitizer/DSP modules and auxiliary detectors. Each master Digitizer/DSP identifies a match between the timestamp embedded within the trigger decision message and the saved LE discriminator timestamps, and requests all slave Digitizer/DSP to transfer the data from the circular buffer into its own readout FIFO. Later, the VME readout CPUs in the digitizer crates read the event data from each Digitizer/DSP FIFO, assemble the crystal event, and send the data to the network switch. The switch routes the events to the computing farm where they are processed. The processing uses the segment information to estimate the position (r, θ, z) and energy of the interaction points. Additional processing establishes the tracks by connecting the individual interaction points.

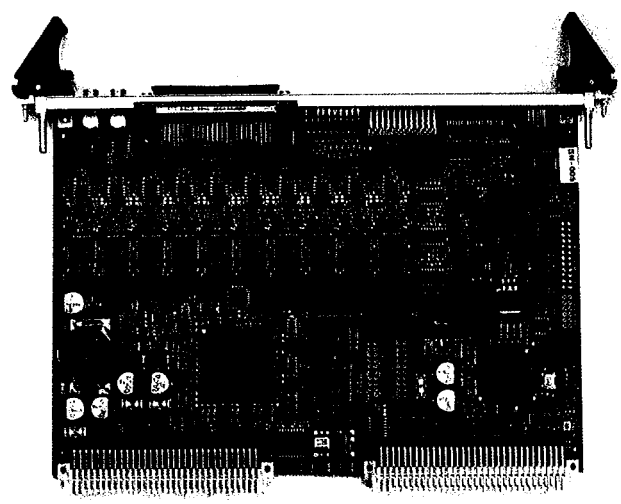

Fig. 6. Digitizer/DSP module.

We have extensively tested the performance of the DS92LV18 SerDes for bit error rate (BER). We have run 12 SerDes links in parallel for more than 10 consecutive days with no errors, which corresponds to a BER better than 10^{-16} or less than one error per day for GRETINA (four per day for GRETA). This component is a very simple SerDes that adds minimum protocol (an important characteristic for the constant latency). In order to guarantee the DC balancing of the communication we encoded the data stream in the FPGA. This encoding operates in the following way. First, before sending a word, the FPGA sums the number of zero and one bits in the word. Then it determines the DC balance of the line due to previous transmissions (i.e., if it has sent more zero bits or more one bits). Finally, to keep

Authorized licensed use limited to: Lawrence Berkeley National Laboratory. Downloaded on November 21, 2009 at 12:25 from IEEE Xplore. Restrictions apply.

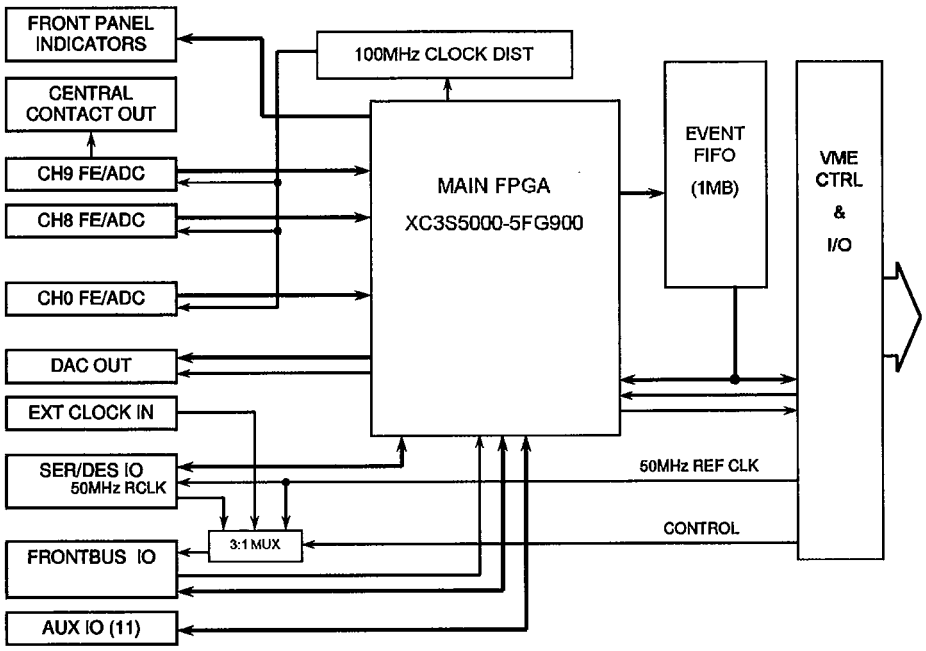

Fig. 7. Digitizer/DSP block diagram.

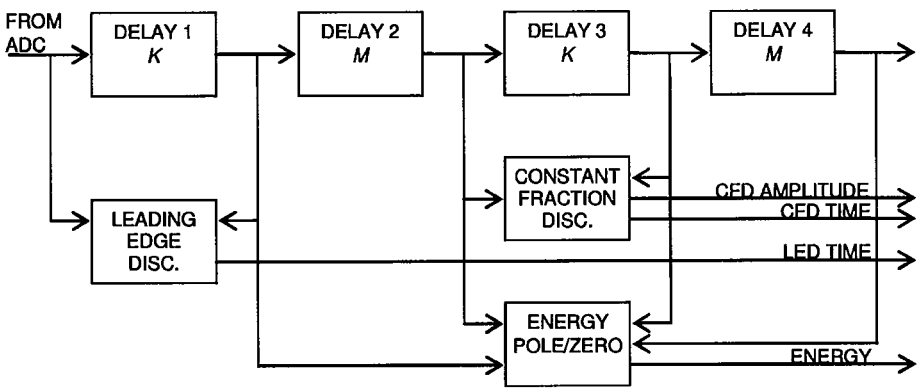

Fig. 8. Digital signal processing.

the line balanced, it then transmits the word itself or its complement. A dedicated bit in the word is set or reset to indicate to the receiver how to decode it. Also, we observed that replacing the cable from unshielded CAT5 to a good quality shielded CAT5 decreased the BER to the level reported above. LVDS drivers (DS90LV004) with programmable pre-emphasis are used in all modules to compensate for cable losses.

Each Digitizer/DSP and TTC module is implemented using two field programmable gate arrays (FPGA): one is a smaller FPGA, which controls the VME interface and has a steady configuration, and the other is a larger FPGA which executes the module specific algorithms and is easily re-configured through VME.

III. Digitizer/DSP

The Digitizer/DSP module samples the crystal segment and central contact analog information using 14-bit ADC operating at 100 MS/s. The ADC used is the AD6645 from Analog Devices. Fig. 6 shows a picture of the module and Fig. 7 shows its block diagram. The Digitizer/DSP has a total of 10 analog inputs. The ADCs are connected to an FPGA, which digitally processes the conversion and executes the following operations: leading and constant fraction discrimination, trapezoidal filtering, energy determination, and pole/zero cancellation.

Fig. 8 shows a block diagram of the digital processing algorithms and how they interconnect and Table I describes the algorithms. The processing is optimized to be implemented using the internal FPGA resources and occurs at a clock rate of 100 MHz, which is generated inside the FPGA by multiplying the 50 MHz master clock distributed from the TTC. This results in approximately 20 giga-operations/s. While the processing occurs, the raw data is stored in 40 μsec circular buffers (designed around the FPGA block RAMs). For further details about these algorithms refer to [5].

The present noise performance of the ADC inputs at full digital processing rate is approximately 1.5 RMS counts for all inputs (refer to Fig. 9). Achieving this performance in a board with digital power supplies and heavy digital activity required special

Authorized licensed use limited to: Lawrence Berkeley National Laboratory. Downloaded on November 21, 2009 at 12:25 from IEEE Xplore. Restrictions apply.

TABLE I
DIGITAL SIGNAL PROCESSING

Leading Edge Discrimination
$y(n)=x(n) - x(n-k)$ (differentiation)
$y(n)=(x(n) + x(n-2)) + x(n-1)<<1$ (×4, Gaussian filtering)
Threshold comparison → LE discriminator time
Constant Fraction Discrimination
$y(n)=x(n) - x(n-k)$ (differentiation)
$y(n)=(x(n) + x(n-2)) + x(n-1)<<1$ (×2, Gaussian filtering)
$y(n)=x(n-k)<<ab - x(n)$ (constant fraction)
Zero crossing comparison → CFD time
Trapezoidal filter and energy determination [6]
$y(n)=y(n-1) + ((x(n) + x(n-2m-k)) - (x(n-m) + x(n-m-k))$
Maximum tracking → energy
Pole-Zero cancellation
$I(n)=I(n-1) + x(n)$
$y(n)=x(n) + I(n)/t$ (where t is the pre-amp time constant)

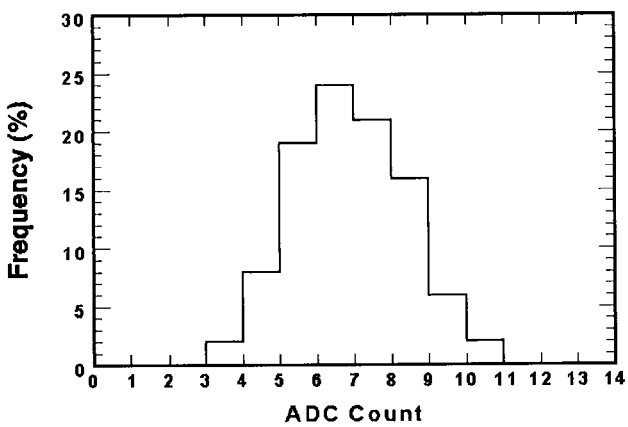

Fig. 9. Noise distribution: $\sigma = 1.5$ counts.

attention. We have filtered the +5 V with a π-filter (observe the inductor on the left portion of Fig. 6). Also, the analog inputs are all implemented using balanced differential techniques.

During prototyping we found two sources of noise due to board layout: one associated with a stray capacitance and the other with the analog and digital ground separation. For the first source we measured about 15 RMS counts and we observed that the ADC noise spectrum was not constant: it was mostly flat until $\sim$ 15 MHz; then it increased by 6 dB/oct until $\sim$ 30 MHz where it became mostly flat again. The increase at 15 MHz was traced to a stray capacitance between the input of the differential amplifier and the ground plane. This capacitance limited the amplifier feedback and, therefore, increasing the gain for higher frequencies (i.e., larger than $\sim$ 15 MHz). At $\sim$ 30 MHz the amplifier reached the maximum frequency response and the gain stabilized again. To reduce this stray capacitance we modified the layout and removed the ground plane right below the differential amplifier inputs. For the second source of noise we observed that the RMS noise performance was not similar for all ADC channels: the ADCs on the left portion of the board (i.e., close to the π-filter, refer to Fig. 6) had approximately 1.5 RMS counts while the ones on the right had approximately 3 RMS counts. We then changed the layout and cut the ground plane around the analog section to create an analog ground mostly free of digital switching. We connected the analog ground together with the digital ground under the ADCs (as suggested on the datasheet) and also close to the π-filter. With these two layout changes we now obtain approximately the same noise performance to all channels.

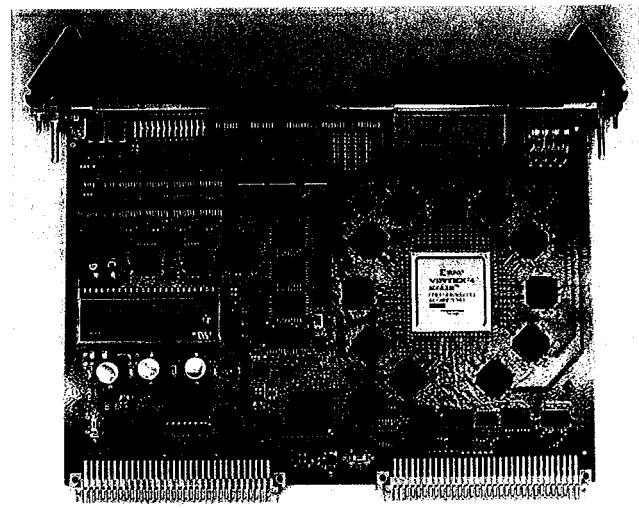

Fig. 10. Trigger, timing and control module.

The Digitizer/DSP module also has programmable digital inputs and outputs for interfacing with other units and front panel LE discriminators for status. All the processing described above is done in a XC3S5000 FPGA from Xilinx. Presently about 50% of the FPGA is utilized, allowing for further increase in algorithm complexity.

IV. TRIGGER, TIMING AND CONTROL

Fig. 10 and 11 show the picture and block diagram of the TTC module, respectively. The TTC is presently configured for multiplicity algorithm, and we intend to add three more in the next few months. When completed, the trigger algorithms will be:

a) *Multiplicity*: Uses the LE discriminator detection of the crystals central contacts. The TTC generates a trigger when it detected that the sum of LE discriminators crosses some threshold within a time window.
b) *Energy*: uses the energy of a central contact or the sum of energies of central contacts. When this energy falls within some programmable window the TCC generates a trigger.
c) *Pattern distribution*: It also uses central contact energy as described above. The TTC triggers when it detects coincidence of gamma-rays energy above threshold in any two pre-programmed crystals.
d) *Auxiliary detector trigger*: The TTC receives an external trigger within the 40 μsec pipeline depth of the Digitizer/DSP.

We call these algorithms prompt triggers, because a trigger is generated as soon as the proper condition is detected. A delayed coincidence trigger can further refine the meaning of these prompt triggers. When this option is enabled, the TTC generates a trigger command when it detects two prompt trigger conditions (e.g., two multiplicity triggers) in two time windows within the allowed overall trigger window. Finally, observe that all the trigger parameters are configurable through VME.

Authorized licensed use limited to: Lawrence Berkeley National Laboratory. Downloaded on November 21, 2009 at 12:25 from IEEE Xplore. Restrictions apply.

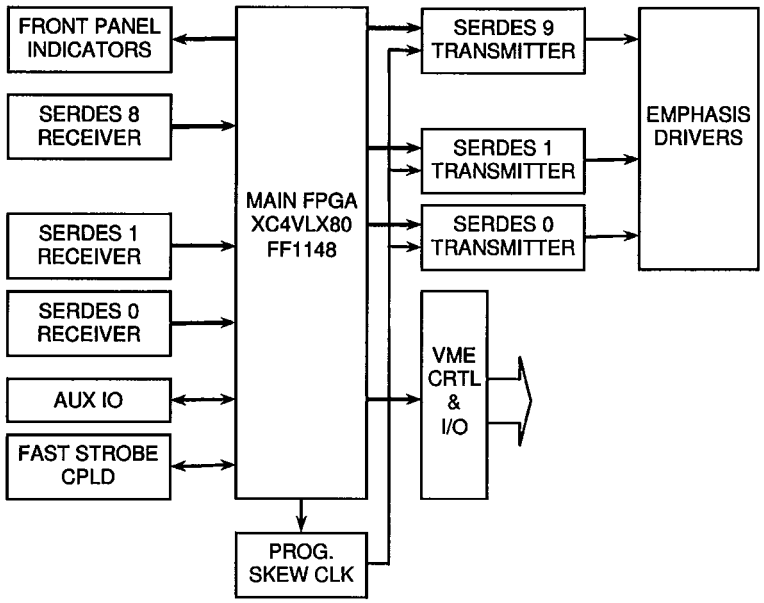

Fig. 11. Trigger, timing and control block diagram.

The main FPGA in the TTC module is the Virtex 4 series XC4VLX80 FPGA. This part executes the trigger algorithms and interfaces with eight SerDes. As already described, the SerDes components transfer information between the Digitizers/DSP. The base multiplicity algorithm presently uses only 15% of the resources inside this FPGA, which allows for further development of the trigger algorithms.

The high-speed switching of the SerDes has edge transition times in the order of 100 ps range. These high-speed signals require special attention during layout, and are more critical on the TTC (when compared with the Digitizer/DSP module), since it has eight SerDes and not all can be mounted close to the connector. Carefully matched, impedance controlled differential traces are used. Additionally, the number of vias was minimized: the component side transmits trigger information, and it does not have any vias, while the solder side is used to receive trigger information, and it has just one via per trace of the differential signal. To further improve signal fidelity, a mixed stackup is used where the dielectric under the component and solder layers of the board is Rogers 4350, which has lower losses than FR4.

The electronics requirements [7] state that the Digitizers/DSPs shall sample all crystals within a 2 ns clock phase window. To synchronize all these modules, all CAT5 cables between the TTC and the Digitizer/DSP are approximately of the same length. However, small cable and component delay differences may generate delays that exceed this limit. To compensate for small delay variations and allow field tuning without recompiling the FPGA firmware, the TTC uses programmable skew clock buffers (Cypress Semiconductor CY7B992) to adjust the delay of the transmit clock (TCLK) of each SerDes. This, in turn, changes the delay of the sampling clock of the Digitizer/DSP at the other end of the cable. To adjust the clock phases we intend to use an oscilloscope monitoring multiple clock outputs on the front bus of master digitizers followed by manual reconfiguration of the VME registers controlling the programmable skew clock buffers. Also, the system phase adjustment can be validated before, during and after an experiment by measuring coincidences between any pair of detectors using a radioactive ^{60}Co source that provides two gamma-rays in prompt coincidence.

GRETINA may provide trigger to auxiliary detectors. Some of these detectors use old technology and they do not have digital pipelines; the trigger decision has to be done when the signals are actually traveling on cables, and the sampling has to start when they arrived at the auxiliary electronics. Only the multiplicity algorithm will be used when interfacing with this type of auxiliary detectors. We have implemented a parallel path that by-passes the SerDes to meet the more stringent timing requirements. The SerDes add a delay of approximately 70 ns to serialize and de-serialize the data. This new path uses a dedicated available pair of the CAT5 cable to transmit from the Digitizer/DSP to the TTC system the status of the central contact LE discriminator detection. To determine multiplicity, the TTC makes the sum of the LE discriminators using front panel connectors and CPLDs. The partial sums travel from the Routers to the Master Trigger module, which executes the final sum and determines the multiplicity. We estimate that this processing will take less than 250 ns. Also, it is interesting to highlight that this requirement also imposed one of the criteria to select the ADC: the latency of the AD6645 is just three clock cycles, which allows for faster LE discriminator determination.

The TTC module also has programmable digital inputs and outputs for interfacing with other units (e.g., auxiliary detectors & NIM electronics) plus front panel LED for status.

V. Cable and Connector Selection

We have dedicated substantial effort in selecting the proper cabling for this electronics. One example already discussed is

Authorized licensed use limited to: Lawrence Berkeley National Laboratory. Downloaded on November 21, 2009 at 12:25 from IEEE Xplore. Restrictions apply.

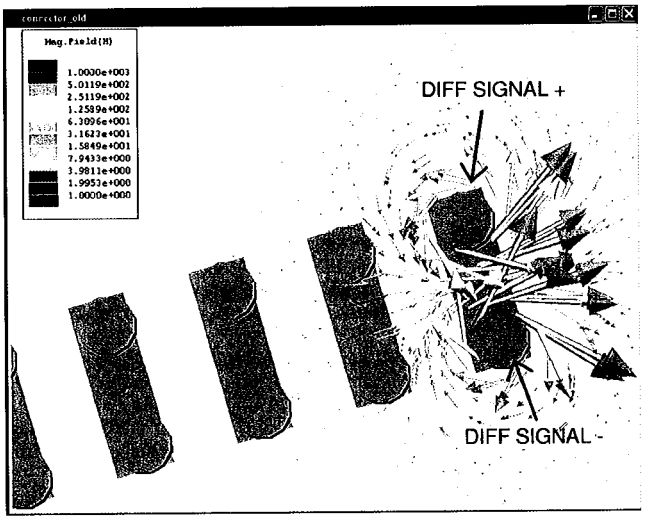

Fig. 12. Magnetic coupling in 0.1" spacing connectors.

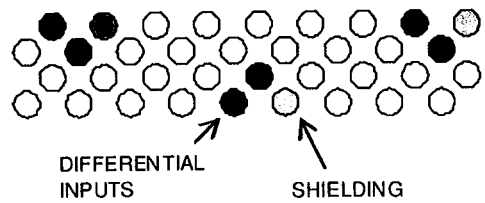

Fig. 13. IIT-Cannon connector pin assignment.

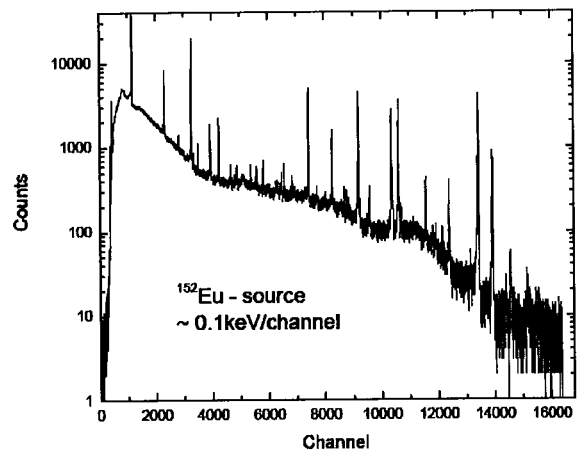

Fig. 14. Energy spectrum for a ^{152}Eu source.

the CAT5 cable for the SerDes. We will now describe the selection of another very important cable, the one that connects the detector pre-amplifiers to the Digitizers/DSPs, which carries the crystal interaction information. Reducing crosstalk between the signals in this interconnection is very important for estimating the position (r, θ, z) of the interactions points: excessive crosstalk decreases the position resolution of the gamma ray interaction. The requirement of total crosstalk in the detector module is less than 0.2% and, therefore, the rest of the electronics crosstalk has to be substantially less than this (required of $< 0.04\%$). To avoid ground loops we decided that the input of the Digitizers/DSPs would be differential and that we would employ twisted pairs. We tested several cables. We obtained the best performance with twisted individually shielded pairs. The crosstalk between adjacent pairs was $< 0.04\%$ for a 15 m cable span. For comparison, a similar cable, but non-twisted (used for LVDS transmission), had a crosstalk of $\sim 2.5\%$. This crosstalk is explained by the magnetic field created in one pair passing through the shielding and magnetically coupling to an adjacent pair. The shielding between pairs is a thin aluminum layer, and it does not attenuate the magnetic field significantly for these speeds. These tests considered a constant rise time (10%–90%) of 30 nsec, well within the expected rise times in GRETINA.

For the connector between the cable and the digitizer we have also tested several connector types, and we also observed crosstalk between signals. We traced the crosstalk, again, to the magnetic field of one signal coupling into the next signal. This can be visualized in Fig. 12. This figure shows the results of Maxwell simulations [from Ansoft] where the arrows represent the direction and the magnitude of the magnetic field. These simulations were done considering that the positive input of the differential signals are connected on the top row and the negative on the bottom row, forming these differential connections. The offending signal uses the differential connection on the right. One can observe that the magnetic field propagates well into the adjacent differential connections, causing crosstalk. The connector simulated has 0.1" pin spacing. Ways to mitigate this effect are threefold: (a) increasing the distance between differential connections, (b) selecting the direction of the pairs (ideally in an angle of 90°), and (c) short circuiting unused connector pairs (to create an opposing magnetic field that decreasing the offending field). For example, the simulations and subsequent tests have demonstrated that skipping two differential connections (on the right of the offending differential connection) and using the third for the next signal decreased the crosstalk by $\sim 10\times$, and that short circuiting these two unused set of pins reduces the crosstalk on the third pair by a further $\sim 2.5\times$. These tests were run with a 100 MHz sinusoidal signal. To meet the crosstalk mitigation strategies outlined above we used a 100 pin Double Density, Subminiature D type connector manufactured by ITT-Cannon. Fig. 13 shows a sketch of how we connected the differential pairs (represented by back circles) and its individual shielding (represented by gray circles). The figure shows the sketch of just a portion of the connector. The unused pins were short circuited in pairs. With this arrangement the measured crosstalk was below what we can measure using 14-bits ADC of the Digitizer/DSP (i.e., crosstalk $< 0.025\%$). The signal used had a constant rise time (10–90%) of 30 nsec.

VI. Test Results and Conclusions

We have tested the performance of the DAQ and trigger system connected to a detector module and we will now describe a few results we have obtained. For these tests we used the production cables and floating low- and high-voltage (bias) supplies. Fig. 14 shows a ^{152}Eu source energy spectrum obtained with the central contact of one of the crystals.

Authorized licensed use limited to: Lawrence Berkeley National Laboratory. Downloaded on November 21, 2009 at 12:25 from IEEE Xplore. Restrictions apply.

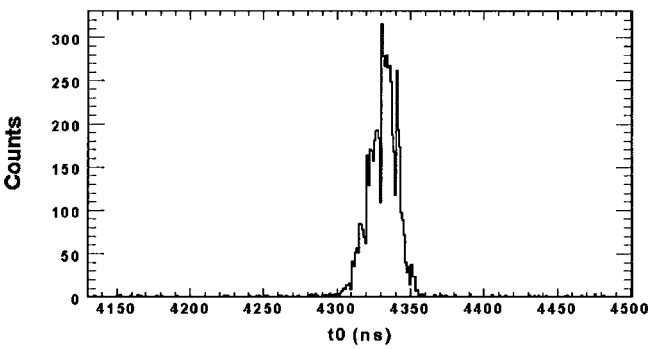

Fig. 15. Constant Fraction discriminator performance.

Fig. 2 shows waveforms that are similar to the waveforms the DSP/Digitizer module records. Fig. 15 shows a time spectrum used to measure the performance of the constant fraction discriminator in the digital processing. The T_O, derived from the FPGA algorithm is referenced to a very fast external trigger provided by a CsF scintillator with essentially no contribution to the width. The standard deviation of the Gaussian fit is 9 ns.

All tests with the prototype system indicate that the DAQ and Trigger systems for GRETINA will meet the requirements. We are presently preparing the production of the system to enter in operation in 2011.

ACKNOWLEDGMENT

The authors would like to thank the GRETINA Advisory Committee and M. Cromaz, S. Gros, I-Y. Lee, A. Macchiavelli and D. Radford for their valuable suggestions.

REFERENCES

[1] I. Y. Lee, "Gamma-ray tracking detectors," *Nucl. Instrum. Methods Phys. Res. A*, vol. A422, pp. 195–200, Feb. 1999.

[2] M. A. Deleplanque *et al.*, "GRETA: utilizing new concepts in γ-ray detection," *Nucl. Instrum. Methods Phys. Res. A*, vol. A430, pp. 292–310, Jul. 1999.

[3] F. S. Goulding and D. A. Landis, "Semiconductor detector spectrometer electronics," in *Nuclear Spectroscopy and Reactions Part A*, J. Cerny, Ed. New York: Academic, 1974, pp. 413–481.

[4] The Future of Gamma-Ray Spectroscopy: GRETA, the Gamma-Ray Energy Tracking, 2006 [Online]. Available: http://fsunuc.physics.fsu.edu/~gretina/GRETA_WP_Jan07_4.pdf

[5] M. Cromaz *et al.*, "A digital signal processing module for gamma-ray tracking detectors," *Nucl. Instrum. Methods Phys. Res. A*, vol. A597, pp. 233–237, Dec. 2008.

[6] V. T. Jordanov and G. F. Knoll, "Digital synthesis of pulse shapes in real time for high resolution radiation spectroscopy," *Nucl. Instrum. Methods Phys. Res. A*, vol. A345, pp. 337–345, Jun. 1994.

[7] F. Bieser, I.-Y. Lee, A. Macchiavelli, J. Weizeorick, and S. Zimmermann, GRETINA Electronics Requirement Document LBNL, Berkeley, 2005, Doc. GRT-3-041115.

Authorized licensed use limited to: Lawrence Berkeley National Laboratory. Downloaded on November 21, 2009 at 12:25 from IEEE Xplore. Restrictions apply.

ELSEVIER

Nuclear Instruments and Methods in Physics Research A 422 (1999) 195–200

NUCLEAR INSTRUMENTS & METHODS IN PHYSICS RESEARCH Section A

Gamma-ray tracking detectors

I.Y. Lee

Lawrence Berkeley National Laboratory, Berkeley, CA 94720, USA

Abstract

A gamma-ray tracking detector is a new concept for a detector array composed of about 100 highly segmented Ge detector elements. The detector would give the energy and the position of all the interaction points and by using the angle–energy relation of the Compton scattering, the scattering sequence of the gamma rays can be reconstructed. Such a detector will have a high efficiency and a good peak-to-background ratio. Research and development are being carried in the production of highly segmented Ge detectors, understanding the signal, and development of tracking algorithms. Recent progress indicated that this type of detector system appears to be feasible and would have a large impact on a wide variety of physics. © 1999 Elsevier Science B.V. All rights reserved.

1. Introduction

Gamma-ray detector systems are important in a broad range of science and new capabilities are continuously being developed. The most recent step in the evolution of detectors for nuclear spectroscopy is the construction of large arrays such as GAMMASPHERE and Euroball. These arrays, consisting of approximately 100 modules of Compton suppressed Ge detectors, have a total peak efficiency of about 0.1 (for a 1.3 MeV gamma ray) and a peak-to-total ratio (P/T) of about 0.6. To improve this performance, the efficiency and/or the P/T have to be increased. However, the highest efficiency that can be reasonably achieved for a Compton suppressed Ge detector array is limited to about 0.15. This is partly due to the scattered gamma rays escaping from the Ge detector (a 1.3 MeV gamma ray deposits full energy in a 7 cm-by-7 cm detector only 20% of the time) and partly due to the solid angle lost to the Compton shield (about 50% for GAMMASPHERE).

A shell consisting of closely packed Ge detectors has been suggested as the solution to the efficiency limitation. In this case, the entire solid angle is covered by Ge detectors, and by adding the signal from neighboring detectors, the escaped energy is recovered and much higher efficiency can be achieved. For example, a 9 cm thick shell of Ge will have an efficiency of about 0.6 for a 1.3 MeV gamma ray. However, for events with many coincident gamma rays, such as long cascades in the decay of nuclear high-spin states, the summing of two gamma rays hitting neighboring detectors reduces the efficiency and increases the background. In order to reduce this summing, a large number of detectors, of the order of 1000, is required. The cost of such a detector array will be prohibitive.

We have developed a new concept, the Gamma-Ray Energy Tracking Array (GRETA), which uses

0168-9002/99/$ – see front matter © 1999 Elsevier Science B.V. All rights reserved.
PII: S0168-9002(98)01093-6

highly segmented Ge detector elements to determine the location and energy of every interaction of each gamma ray. The interaction points belonging to a particular gamma ray would then be identified from the position and energy using a procedure called "tracking". The full gamma-ray energy is obtained by summing only the interactions belonging to that gamma-ray and the problem of summing two gamma rays is avoided. Tracking makes use of all the information deposited in the detector and the energy–angle relation given by the Compton scattering formula. Such an array could be constructed from 100 to 200 highly segmented Ge detectors and with a cost comparable to that of GAMMASPHERE.

2. Tracking principle

For a gamma ray with an energy up to about 2 MeV, the dominant interaction modes are photo absorption and Compton scattering. In Compton scattering, the energy of the scattered photon E'_γ (in MeV) is related to the energy of the incident photon E_γ and the scattering angle θ by the formula

$$E'_\gamma = \frac{E_\gamma}{1 + E_\gamma(1 - \cos\theta)/0.511}.$$

The energy transferred to the electron which is measured by the detector is

$$E_e = E_\gamma - E'_\gamma.$$

If the energy and the direction of the incident photon is known, then there is a definite relation between the scattering angle and the detected energy. As the photon makes successive Compton scatterings in a detector, this relation is valid for each scattering until a photo absorption terminates the scattering process. Thus, from the measured position and the energy deposited at each of the Compton interaction point, we can determine uniquely the sequence of the scattering and thus "track" the path of the photon in the detector.

Tracking has already been used to determine the energy and direction of incident photons. For example, in astronomy Compton telescopes are surveying the sky for gamma ray emitting sources. In laboratory applications such as gamma-ray spectroscopy, since the source position is known, the use of tracking will give both the energy and direction of the gamma-ray on a event-by-event basis. To start the tracking, we need to make a first guess of the incident energy. This is done by summing the energy from individual interactions which are assumed to originate from a single gamma ray and that it has deposit its full energy in the detector. For an event with N interaction points, there are $N!$ possible scattering sequences. They are evaluated, using the angle-energy relation of Compton scattering, to determine the correct sequence. If this sequence is from a full energy gamma-ray, then the relation will be satisfied exactly. In practice, we use a parameter to characterize the deviation from the ideal relation such as the square deviation (χ^2) of the measured scattering angle from the predicted scattering angle based on the deposited energy. The correct sequence will have a χ^2 value of 0. On the other hand, if the gamma ray did not deposit all of its energy in the detector, the sum energy of the interaction points will be less than the true energy and the Compton condition will not be satisfied. In such cases, the χ^2 value will in general have a non-zero value and, based on this value, these partial-energy (Compton) events can be rejected. This method of Compton rejection had the advantages of a Compton shielded detector (good peak-to-total) and sum spectrometer (high efficiency), but not the disadvantages such as low efficiency and false veto of the Compton shielded detector and false summing of the sum spectrometer.

In a detector with finite energy and position resolution, the correctly identified full energy sequence will have a non-zero χ^2 and it cannot be separated cleanly, from the Compton events. Fig. 1 shows the χ^2 distributions for position resolution of 1 and 3 mm, respectively. These results are from calculated simulations for 1.2 MeV gama rays emitted from the center of a spherical shell with an inner radius of 12 cm and an outer radius of 21 cm. Comparing with the position resolution of the order of a few mm, the energy resolution of a Ge detector of the order of a few keV makes negligible contributions to the uncertainties of the tracking. With the finite value of χ^2, there is no exact criterion for separating the full-energy events from Compton

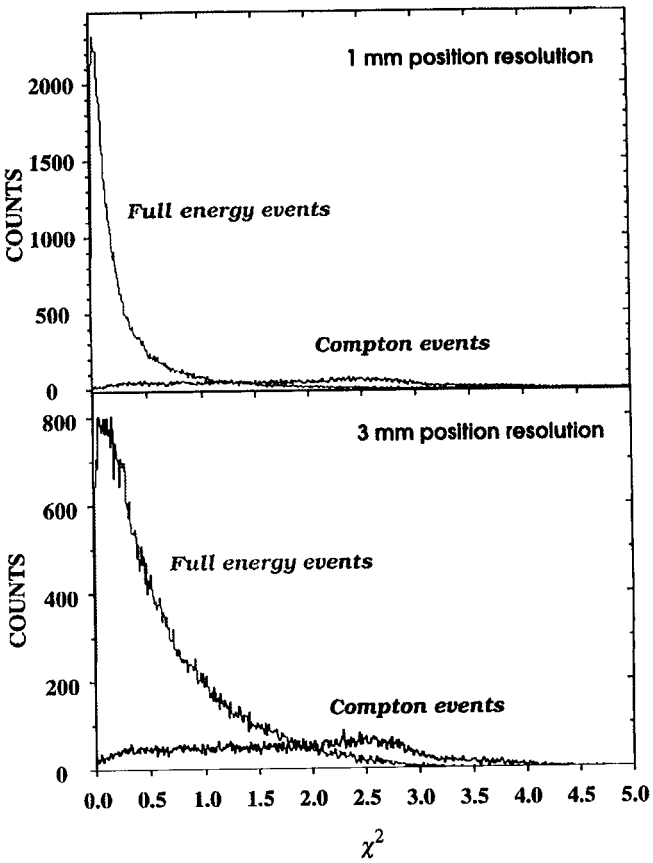

Fig. 1. The χ^2 distributors for full energy events and Compton events from tracking 10 000 simulated gamma rays with an energy of 1.2 MeV. These gamma rays are emitted from the center of a spherical shell with an inner radius of 12 cm and an outer radius of 21 cm. Results are shown for position resolutions of 1 and 3 mm, respectively.

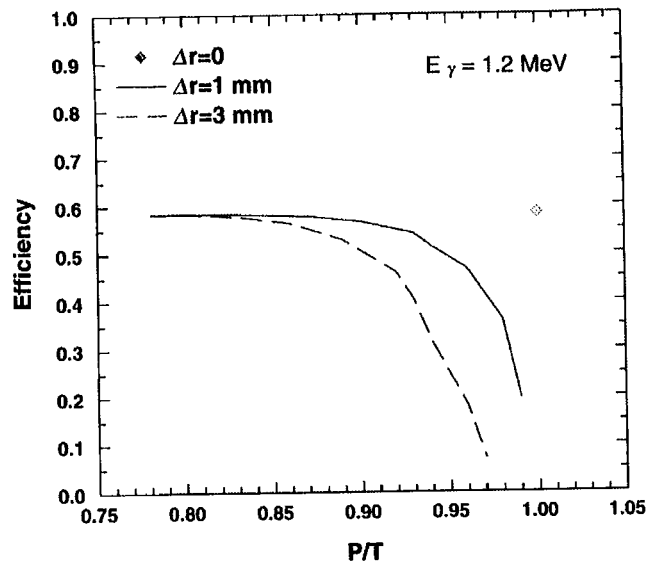

Fig. 2. Trade off between efficiency and peak-to-total ratio for a 1.2 MeV gamma ray from the simulations shown in Fig. 1. The diamond indicates result for a detector with infinite position resolution, the solid and dashed lines represent the results for position resolution of 1 and 3 mm, respectively.

events. A narrower cut will produce a better P/T and lower efficiency. Fig. 2 shows such trade off between efficiency and P/T for a 1.2 MeV gamma ray from the simulations shown in Fig. 1. Other important factors which can affect the tracking efficiency include absorption and scattering of gamma rays in detector packaging material and the ability of separating coincidence gamma rays in an event.

3. Status of development

The technology needed to realize the gamma ray energy tracking array (GRETA) can be divided in to three areas. They are: (1) manufacture of segmented detectors which can provide signals for resolving and locating individual interaction points; (2) electronics and signal processing methods for determining energy, time and position based on pulse shape digitization and digital processing of signals; and (3) tracking algorithms, using the energy and position information, to identify interaction points belonging to a particular gamma ray.

The basic element of GRETA is a Ge detector which can give three dimensional position information of the gamma-ray interaction points. This can be achieved by segmenting one of the electrodes in two dimensions to provide two of the coordinates while the third coordinate can be derived from the drift time of the charges. There are many possible segmentation and packing schemes. One possibility is spherical packing, as is used in Gammasphere, using tapered hexagonal and pentagonal shaped detectors with a segmented outside surface. a prototype detector of this type has been designed, produced and extensively tested. As shown in Fig. 3, this detector has a tapered hexagonal shape with six longitudinal segmentations and one transverse segmentation which divide the outer surface

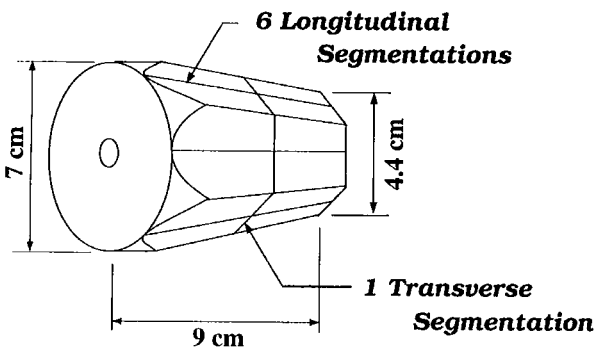

Fig. 3. The prototype of GRETA detector has a tapered hexagonal shape with six longitudinal segmentations and one transverse segmentation.

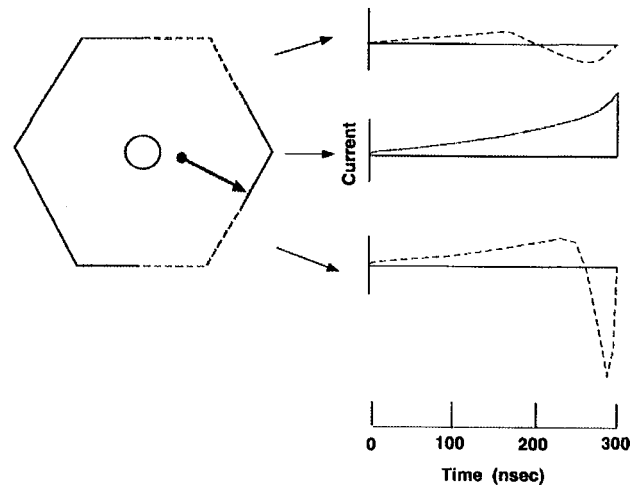

Fig. 4. Current signal on three electrodes from a charge drifting toward the outside electrodes.

into 12 segments. Signals from each of the segments, as well as from the center electrode, are read out. This detector has an energy resolution of 1.8 keV for all the segments which is better than unsegmented detectors due to the low capacitance of each of the segments. Currently, we are in the process of having this detector further segmented into a 6-by-6 configuration. According to our simulation studies, this segmentation will be sufficient for achieving a position resolution of 1–2 mm under ideal conditions. This second prototype will be available in the fall of 1998. The goal of this prototype is to push the segmentation technology and to determine the performance of the detector electronics. New miniaturized preamplifiers will be tested for their wider bandwidth and their noise and cross talk properties. With this prototype, the performance of a single element of GRETA can be fully characterized.

To determine the position in three dimensions accurately, a detailed understanding of the signal shape is necessary. A signal is produced when electrons and holes, formed by the slowing down of the photo- or Compton-electrons, produce induced charges of opposite sign on the electrodes. As the charge drifts toward the electrodes, the amount of the image charge changes and it causes current to flow in or out of the electrodes. Fig. 4 shows a schematic diagram of the current signal expected from a segmented detector. When the charge is at a large distance from the electrodes, the induced charge is distributed over several electrodes and their current signals are similar. As the charge moves closer to the destination electrode, the induced charge on this electrode increases and charge on the other electrode decreases. The current continues to increase on the destination electrode until the charge finally reaches the electrode and neutralizes the image charge and the current stops. The duration of the current signal (drift time) can be used to determine the drift distance. The integral of the current gives the charge which provides the energy measurement. The signal from the neighboring electrode has a bipolar shape with a zero net charge. This fact can be used to identify the electrode where the charge is collected which gives a position resolution of the size of the electrode. Actually, a better position resolution can be obtained ny analyzing the shape of the induced signal from the neighboring electrodes. As shown in Fig. 4, the maximum amplitude and time of zero crossing of these signal are sensitive to the transverse position and they can be used as parameters for the shape analysis.

We are developing algorithms to analyze the digitized signal to obtain the position of the interaction points. The goal of this on-going study is to determine the segmentation needed to achieve a given position resolution. As a first step we have compared the measured signal form the first

prototype with calculated signals and confirmed the accuracy of our calculations. Analysis of the measured signals using a simple algorithm indicated that a radial position resolution of about 3–4 mm can be obtained from the charge drift time. The transverse position can be obtained with a position resolution about 3 mm if the interaction point is within 1 cm from the neighboring segment so that the induced signal is strong enough to be used. Further refinement of the algorithms would improve these numbers. Algorithms are also being developed to include the capability of separating multiple interaction points in one segment which will further enhance the resolving power of the detector.

Algorithms are being developed for identifying interaction points belonging to a given gamma ray. The current algorithm consists of three steps. Cluster identification is the first step of the algorithm. The interaction points within a given angular separation as viewed from the target are grouped in to a cluster. In the second step, each cluster was evaluated by tracking to determine whether it contains all the interaction points belonging to a single gamma ray. The tracking algorithm uses the angle-energy relation of the Compton scattering to determine the most likely scattering sequence from the position and energy of the interaction points. If the interaction points have infinite position and energy resolution, the tracking would be exact and the proper identified full-energy cluster will show no deviation from the scattering formula. Wrongly identified clusters or partial-energy clusters will deviate from the formula. Therefore, the separation of the good clusters from the bad clusters is easy to achieve. However, with finite resolutions the good cluster will also have a non-zero deviation and they cannot be separated cleanly from the bad clusters. This causes lower efficiency and a worse P/T ratio. In the third step, we try to recover some of the wrongly identified gamma rays. For example, one type of incorrectly identified cluster is a gamma ray being separated into two clusters. These clusters can be identified by tracking two clusters together. If the result gives a small deviation the gamma ray is recovered by adding the two clusters. Similarly, the case of two gamma rays wrongly identified as one can also be separated by tracking. The cluster which did not satisfy any of the above criteria are rejected. This simulation was carried out for a number of different conditions such as the multiplicity and energies of the gamma rays as well as for changing position resolution of the detector. Fig. 5 shows the efficiency and P/T achieved so far for simulated events with 25 gamma rays, each with an energy of 1.33 MeV, and a detector position resolution of 1 mm. Several improvements of this algorithm are being developed. Information such as the energy dependence of the angular distribution of

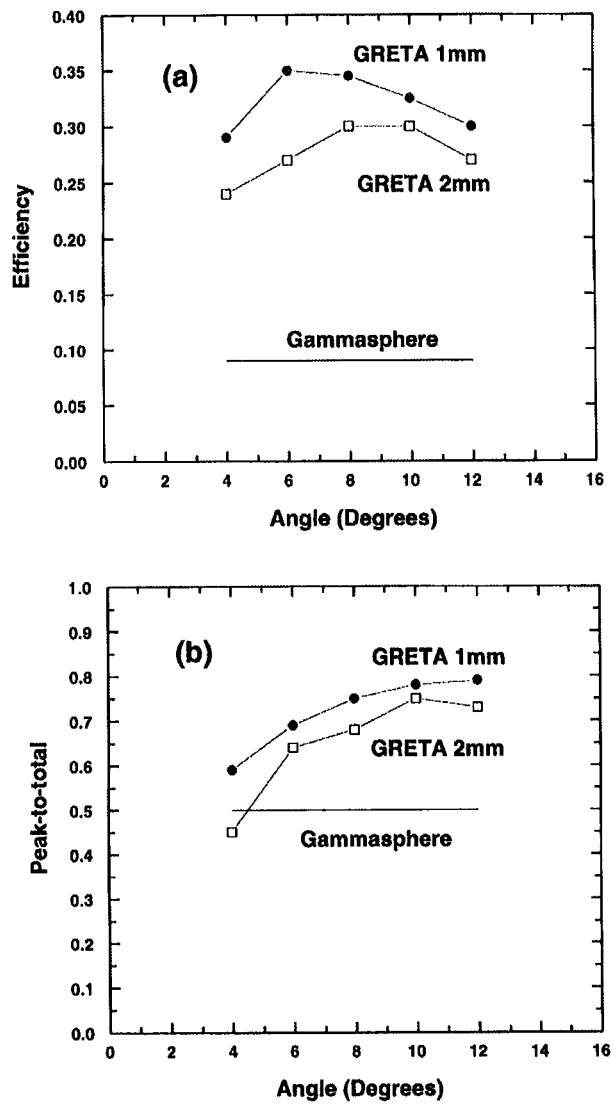

Fig. 5. Efficiency (a) and peak-to-total ratio (b) achieved so far for simulated events of 25 coincident gamma rays with energy of 1.33 MeV and a detector position resolution of 1 and 2 mm, respectively. The curves are plotted as a function of the angle parameter used in the cluster identification.

the Compton scattering cross section and the distribution of the distance between two interaction points will be used in the tracking. Other methods such as neural networks are also being considered. As the next step, we will be using multiple detectors, to measure the scattering between them. These data will be used to tract the gamma ray across detector boundaries and compared the results with the simulations. The importance of the effects of the gap and absorbing material will be quantified in a realistic design of detector packaging. These information will be used to extend the tracking algorithm to handle the realistic detector design.

4. Expected performance

Based on a conservative estimate of an efficiency of 30%, GRETA will improve the sensitivity by a factor of 100 for high-spin nuclear-structure studies. Such sensitivity will be important in the study of very rare cascades, such as hyperdeformation bands populated in fusion reactions. Due to the energy add back feature, GRETA would also have a much higher efficiency for detecting high-energy gamma rays (e.g. 20% for a 10 MeV gamma ray). This feature will enable the high-resolution studies of high-energy gamma rays such as those from the gamma decay of giant resonances. The large segmentation, as well as the use of digital electronics and signal processing, will result in a factor of 30 improvement in the counting rate. This will further enhance the ability of detecting weak cascades.

The localization of the first interaction point in a detector defines the angle of emission of that gamma ray. Tracking will locate the position with an accuracy about 2 mm (FWHM) and at a typical source–detector distance of 15 cm the corresponding angular accuracy is about 0.8° which is 10 times better than existing detectors. This is especially important when the gamma rays are emitted by a moving source because its energy has an angular dependent Doppler shift. A detector with a better angular resolution will give a narrower energy spread. For example, nuclei produced by projectile fragmentation reactions usually have a recoil velocity of $v/c = 30\%$. For a 1 MeV gamma ray emitted at 90° to the recoil direction, the Doppler broadening would be 39 keV with a Gammasphere detector, but only 3.7 keV with GRETA. In addition, the location of the first and the second interaction points give the scattering angle which provides information about the linear polarization of a gamma ray. This information is essential in determining the parity of nuclear levels. Tracking can also distinguish gamma rays emitted by the source from those originating outside the detector array, providing a new method of reducing the background in experiments measuring low intensity gamma rays.

5. Conclusion

A gamma ray energy tracking array which is based on highly segmented Ge detector elements would provide far better efficiency, peak-to-background, counting rate and localization than any existing gamma ray array. These new capabilities will have a major impact in many areas of physics. Recent progress in detector segmentation, signal processing and gamma ray tracking indicate that this new concept is feasible and a cost effective array can be constructed.

Acknowledgements

This work was carried out by the nuclear structure group at the 88-Inch Cyclotron of Lawrence Berkeley Laboratory. The gamma-ray tracking work was carried out mainly by Greg Schmid. Kai Vetter did the measurements and calculations of the segmented detector signals. Other members of this effort include Marie-Agnes Deleplanque, Paul Fallon, Augusto Macchiavelli and Frank Stephens. This work is supported by the U.S. DOE (contract number DE-AC03-76SF000098).

ELSEVIER

Nuclear Instruments and Methods in Physics Research A 430 (1999) 292–310

NUCLEAR INSTRUMENTS & METHODS IN PHYSICS RESEARCH Section A

www.elsevier.nl/locate/nima

GRETA: utilizing new concepts in γ-ray detection☆

M.A. Deleplanque*, I.Y. Lee, K. Vetter, G.J. Schmid[1], F.S. Stephens, R.M. Clark, R.M. Diamond, P. Fallon, A.O. Macchiavelli

Nuclear Science Division, Lawrence Berkeley National Laboratory, Berkeley, CA 94720, USA

Received 4 November 1998; accepted 11 January 1999

Abstract

We present a new concept for γ-ray detector arrays. An example, called GRETA (Gamma-Ray Energy Tracking Array), consists of highly segmented HPGe detectors covering 4π solid angle. The new feature is the ability to track the scattering sequence of incident γ-rays and in every event, this potentially allows one to measure with high resolution the energy deposited, the location (incident angle) and the time of each γ-ray that hits the array. GRETA will be of order of 1000 times more powerful than the best present arrays, such as Gammasphere or Euroball, and will provide access to new physics. © 1999 Published by Elsevier Science B.V. All rights reserved.

1. Introduction

Much of what we known about nuclear energy levels has come from studying the electromagnetic radiation emitted when the system makes a transition from one state to another. For a nucleus, the order of magnitude of the transition energy is 1 MeV. For about 30 years, high-purity germanium (Ge) crystals have been the detectors of choice for such studies. Improvement in detector properties (size, energy resolution) and in detector number (large arrays) has recently culminated in the construction of Gammasphere [1], Eurogam [2,3] and Euroball [2–4]. These arrays all use the concept of Compton suppression to improve the peak-to-background ratio in the γ-ray spectra. In this paper, we present a new concept for a γ-ray detector array, illustrated in the detector system called GRETA (Gamma-Ray Energy Tracking Array), that will have a resolving power[2] 100–1000 times greater than Gammasphere. GRETA consists of a "solid" shell of about 100 highly segmented Ge detectors. The solid angle subtended by the Ge detectors will be 4π (instead of approximately 2π as in a Compton-suppressed array), and the Compton-scattered γ-rays will be recovered (instead of rejected) by tracking the γ-ray interactions from one detector to the next.

These γ-ray detector arrays are primarily used to study nuclear structure and reactions. However, they can also play an important role in other fields

☆This paper should have been published together with the paper "A γ-ray tracking alogorithm for the GRETA spectrometer" (Nucl. Instr. and Meth. A 430 (1999) 69).

* Corresponding author. Tel.: + 1-510-486-5384; fax: + 1-510-486-7983.

E-mail address: mads@lbl.gov (M.A. Deleplanque)

[1] Present address: Lawrence Livermore National Laboratory, Livermore, CA 94550, USA.

[2] As will be discussed later (Section 2.2.4), the resolving power of such arrays depends to some extent on the experiment considered.

0168-9002/99/$ - see front matter © 1999 Published by Elsevier Science B.V. All rights reserved.
PII: S0168-9002(99)00187-4

in which the nucleus is used as a laboratory; for example, in studying fundamental interactions or astrophysics; or in searches for exotic forms of matter such as strange matter. The unique characteristics of GRETA will enable us to address new kinds of physics.

The next section will review the development of γ-ray detectors, leading to the need for a new concept. Section 3 will present the GRETA concept. Section 4 will outline the methods used to design such a detector array and the present status of the research and development. Section 5 will briefly review the new physics that can be done with such an array.

2. Development of γ-ray detectors

We will first present the characteristics of a good γ-ray detector array and then review the development of the Ge detectors. Some of the new physics discoveries made using such arrays will be mentioned at the end of each section.

2.1. Characteristics of a γ-ray detector array

An ultimate goal of a γ-ray detector array is to resolve all possible γ-ray decay sequences. Usually, detectors, such as microscopes or telescopes, are characterized by their resolving power. In nuclear structure physics, there are many weakly populated sequences embedded in large and complex backgrounds and the ability of the instrument to resolve such sequences depends on the detailed nature of both the sequence and the background, so that there is no unique definition of the "resolving power" of the detector. However, the concept of resolving power has proved useful and will be discussed in more detail in Section 2.2.4 when evaluating the performance of detector arrays. Even without an explicit definition, it is clear that the important properties of a γ-ray detector are: (1) high efficiency in detecting incident γ-rays; (2) high energy resolution; (3) high ratio of full-energy events to total (full energy and partial energy) events (called the peak-to-total ratio or P/T ratio); (4) high granularity to localize individual γ-rays; and (5) stable operation and long life. The basic element of such a detector system is (and has been for more than 30 years) a semiconductor detector made of germanium, and the main reason for this has been their high γ-ray energy resolution. Progress has been made in both the size of these detectors and their arrangement into efficient arrays.

2.2. Development of Ge detector systems

2.2.1. The first Ge detectors

In 1962, the first Li-drifted Ge detectors were made [5]. The new feature was their excellent γ-ray energy resolution (6 keV at 1 MeV) – about a factor of 10 better than that of their predecessor, the NaI scintillator. The first detectors had a small volume ($\sim$ 1 ml) and a very small full-energy efficiency, $\sim$ 1% of that of the standard NaI scintillator (7.5 cm diameter $\times$ 7.5 cm long at 25 cm from the source). But soon thereafter, Ge detectors with efficiencies around 10% were used. By 1970, γ–γ coincidence measurements using two Ge detectors were routinely used to construct complicated nuclear level schemes. A major discovery in nuclear structure using these detectors was the so-called "backbending" in ground-state rotational bands of moderately deformed nuclei in 1971 [6]. Because of the high energy resolution of these Ge detectors, weak γ-ray transitions could be seen for the first time up to and above spin 14. Around that spin, irregularities (backbendings) in the rotational bands revealed Coriolis effects [7] aligning single-particle angular momentum along the rotation axis. This "alignment" concept led to the study of single-particle motion in a rotating potential and the development of the cranking models. Such models have formed the basis for understanding the properties of nuclei at high spins and have been used ever since in both theoretical and experimental developments in nuclear structure.

2.2.2. High-purity Ge detectors

A milestone in the development of Ge detectors came in 1971 [8] with the development of high-purity Ge detectors. This meant that there was no longer a need for Li drift and bigger detectors could be made, providing much greater efficiency, particularly important in coincidence experiments.

2.2.3. Compton suppression and detector arrays

In 1980, a big step was made with the development of arrays of Compton-suppressed Ge detectors. One way to decrease the background of partial-energy γ-ray events is to veto these events whenever possible. The large majority of these occurs when a γ-ray Compton scatters in the Ge detector and the scattered γ-ray escapes the detector, leaving only a partial energy signal that is of no interest. It is then advantageous to suppress this event. This is done by surrounding each Ge detector with another efficient γ-ray detector which catches the escaped Compton-scattered γ-ray and vetoes the recording of the signal from the Ge detector. This is the Compton-suppression technique. Typically, it increases the peak-to-total ratio of a 1.3 MeV γ-ray from 20%, for a bare Ge detector (of size 7 cm diameter by 8 cm long), to 50%, for a Compton suppressed detector. This well-known technique was "revived" around 1980 in the construction in Copenhagen of the first "array" of five elements, each composed of a Ge detector which is Compton-suppressed by a large NaI scintillator [9,10]. At that time, a more efficient scintillator, bismuth germanate (BGO), was being developed. Due to its high density and Z, this material is about three times more efficient per unit length than NaI in interacting with gamma rays. The Berkeley Nuclear Structure group pioneered the BGO Compton suppressors and assembled the first large array of 21 Compton-suppressed Ge detectors called HERA [11,12]. Such arrays were developed in parallel in Europe, particularly in Daresbury, UK where various configurations of arrays called TESSA were set up. It was with one of these arrays that "superdeformed nuclei at high spins" were discovered in 1986 [13]. Superdeformed nuclei are loosely referred to as nuclei which are more deformed than "usual", i.e. typically they have the shape of an axially symmetric ellipsoid with a ratio of the long to short axis around 2. They are interesting because the forces that the nucleons feel in such nuclei differ in systematic ways from those felt in "normal" nuclei. For example, the Coriolis and centrifugal forces due to rotation are weaker relative to the coupling to deformation than in normal nuclei and this gives us a chance to study nuclei under new conditions. An important resulting property of superdeformed nuclei is that they are the best (nuclear) rotors known, giving deexcitation spectra of equally spaced gamma rays which are relatively easy to search for in two- or three-dimensional γ-ray spectra. Except for the heaviest (the fission isomers), the superdeformed nuclei are populated in nuclear reactions only at very high spins (40–60 $\hbar$), and the reaction mechanism is such that their population is very small, typically only about 1% of the total reaction cross section. The key to finding and studying these nuclei was to make use of the regular spectra and of the increased efficiency of multidetector arrays, which provide higher-order coincidence spectra and thus higher resolving power.

2.2.4. Resolving power and 4 π arrays

To quantify the performance of 4π arrays and plan new ones, the concept of resolving power – the ability to isolate a given sequence of gamma rays from a complex spectrum – was introduced [1]. Our precise definition of the resolving power [14] is dependent on assumptions related to the type of spectra. (Other formulations have been given by Radford [15]).

We consider the γ-ray spectra typically produced in nuclear fusion reactions, which consist of a number of γ-rays per cascade extending over a certain energy range. This determines an average energy spacing per transition (SE). We further assume that the background is essentially unrelated to the peaks (which means that the cascade of interest has a small intensity and is not in coincidence with the bulk of the background). To be "resolved", a peak must stand out above the background and also be statistically significant. We take as criteria for a peak to be "resolved" from the background that the peak-to-background ratio is one and that there must be N counts in the peak.

The peaks are measured with an energy resolution δE, so that every time we set a gate on such a peak (i.e., a coincidence gate of width δE), we improve the peak-to-background ratio for that sequence by a factor around SE/δE. We also take into account that a γ-ray peak represents only a fraction P/T of the γ-ray total intensity (see Section 2.1), and further that a typical gate includes only a fraction

of the full-energy peak (a realistic number for a FWHM gate on a Gaussian peak is 76%). The improvement in peak-to-background is then given by $R = 0.76(\mathrm{SE}/\delta E)P/T$. In this derivation of the resolving power, we assume that for any fold considered, the peaks to resolve are much smaller than the background. Thus, the peak-to-background ratio in the one-fold spectrum for a branch of intensity α is αR, and for an f-fold coincidence spectrum (i.e. one where f γ-rays are detected) this ratio is αR^f. Thus, for a peak-to-background ratio of one, $\alpha R^f = 1$.

The number of counts n in the peaks of an f-fold coincidence spectrum for a branch of intensity α is $n = \alpha N_0 \varepsilon^f$, where N_0 is the total number of events, and ε is the total full-energy peak efficiency of the array for a typical energy.

We now apply the criteria given above to define the resolving power. The conditions for a cascade of minimum intensity (α_0) to be "resolved" (N counts in a peak with peak-to-background ratio one) define an "optimum-fold" (F) that will just satisfy the criteria given above. Thus we have $N = \alpha_0 N_0 \varepsilon^F$ and $\alpha_0 R^F = 1$. The intensity of that cascade $\alpha_0 = 1/R^F$ defines the resolving power RP as $1/\alpha_0 = R^F$. At this optimum fold, F, α_0 represents the smallest sequence intensity that can be "resolved" in that spectrum. By eliminating F using the equations for α_0 and N, one obtains the expression for the resolving power as a function of ε and R:

$$\mathrm{RP} = \exp[\ln(N_0/N)/(1 - \ln \varepsilon/\ln R)]. \quad (1)$$

This formula shows that the important parameters which determine the performance of this type of γ-ray array are the energy resolution, δE, of the detectors, their characteristic peak-to-total ratio, P/T, and the full-energy peak efficiency, ε. What the first generation arrays such as HERA have done over previous systems of three or four Ge detectors is to improve (1) the P/T through Compton suppression and (2) the full-energy peak efficiency through the number of detectors used. If we take $N = 100$ and a typical value of $N_0 = 2.88 \times 10^{10}$, corresponding to a reaction rate of 10^5/s for a duration of 80 h, then $\ln(N_0/N) = 19.5$. We can evaluate the resolving power of the HERA array mentioned in the previous paragraph. In the evaluation one takes into account realistic experimental conditions and defines δE_{eff} as an "effective" energy resolution, which includes not only the intrinsic resolution of Ge detectors (approximately 2 keV for a 1 MeV gamma ray), but also other effects that might affect the peak width, such as the Doppler broadening due to the recoil velocity of the product nuclei that emit the γ-rays and the finite size of the Ge detector. For HERA, $\varepsilon = 0.012$, $\delta E_{\mathrm{eff}} = 6.1$ keV, P/T = 0.40. We take SE = 60 keV for all our evaluations. The resolving power of HERA is then 50 for γ-rays of approximately 1 MeV.

In 1987, another big step was accomplished when the Berkeley Nuclear Structure group proposed an array design that was optimized to maximize the solid angle covered by the Ge detectors, and that took advantage of the fact that bigger Ge detectors could then be manufactured (efficiency of 75% of that of the standard NaI detector (cf. Section 2.2.1) as compared to 25% for the HERA Ge detectors), which improved the P/T as well as the efficiency. Each Ge detector was still surrounded by a BGO Compton suppressor, and altogether, almost the entire 4π solid angle was covered by 110 Ge detectors and their BGO Compton suppressors. The array is called Gammasphere and it was built at the Lawrence Berkeley National Laboratory with the participation of other US National Laboratories and Universities. Dedicated in December 1995, Gammasphere is a National Facility and was operated at LBNL until September 1997. It was then moved for some period of time to the Argonne National Laboratory. Detector arrays of similar resolving power were constructed in parallel in Europe (Eurogam, succeeded now by the Euroball array).

The Gammasphere detailed design will not be discussed here, but there is one property that should be mentioned because it affects the resolving power: approximately 70 of a total of 110 Ge detectors are segmented into two D-shaped halves through the electrical segmentation of the outer electrode. This feature, which will be discussed in a following paragraph, increases the effective energy resolution of the Ge detectors (δE_{eff} decreases) by reducing the Doppler broadening due to the finite size of the angle subtended by each detector. For Gammasphere, $\delta E_{\mathrm{eff}} = 3.95$ keV, P/T = 0.46,

which gives $R = 5.3$ and $\varepsilon = 0.09$, so that the resolving power is now approximately 3000, about 60 times that of HERA. An example of the increased power of these new arrays is the discovery of the "linking transitions" between superdeformed states and normally deformed states in some nuclei around mass 190 [16]. These transitions are indeed very weak, around 1% of the intensity of the superdeformed bands (which themselves have an intensity around 1% of the total cross section) and their observation corresponds to the gain made possible by the increase in resolving power. Observing these "superdeformed decay" transitions helps understand how the nucleus makes such a dramatic transition between two states where its shape is very different. These links have been observed in very few cases (5–10 out of about 300 bands known) and the full decay mechanism is still not clear. Many failed searches in other nuclei indicate that higher resolving power is needed to elucidate completely the decay mechanism of superdeformed bands.

2.2.5. *Clustering of Ge detectors – towards 4π Ge shell*

In parallel with Gammasphere design and construction, new types of Ge detectors were developed as a means of maximizing the efficiency and P/T of big arrays. The two most important ones are the clover detector [17,18] and the cluster detectors [19,20] which are both components of the Euroball array mentioned earlier. In present arrays, each of these is surrounded by a Compton suppressor. The clover detector is a composite of four coaxial Ge detector elements whose side surfaces have been cut so that they fit together much like the leaves of a clover (see Fig. 1). The main advantage of such detectors is their large efficiency (140%) while the localization remains similar to that of a single detector since one can usually determine which of the four elements is first hit by an incoming gamma ray. Thus the Doppler broadening is reduced to that of one of the elements. Such composite detectors utilize a new concept that considerably increases the efficiency of an array: the concept of "adding back". By adding the energy of signals that scatter between crystals, the efficiency of a clover detector is increased by a factor 1.5 over the sum of the contributions from the individual crystals. The cluster detector is an assembly of seven Ge detectors closely packed in a single cryostat (see Fig. 2). The novelty of this cluster is that each element of this assembly of seven is an encapsulated

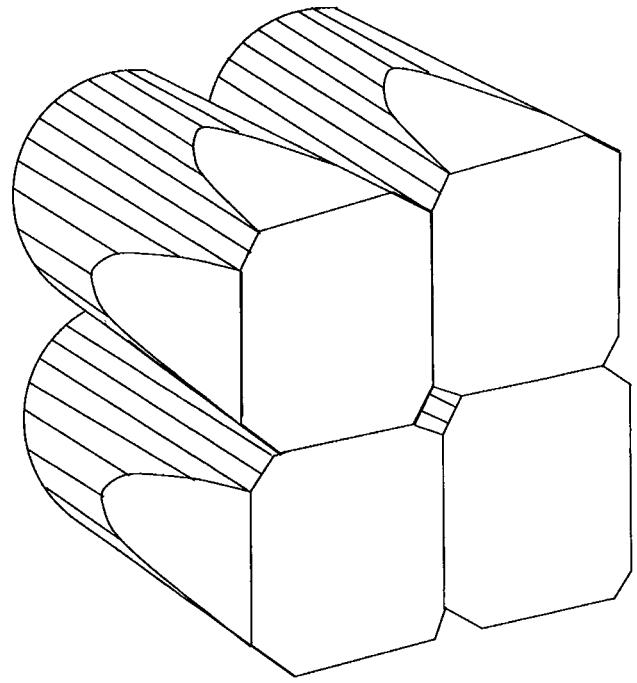

Fig. 1. Schematic drawing of a clover detector (from Ref. [17]).

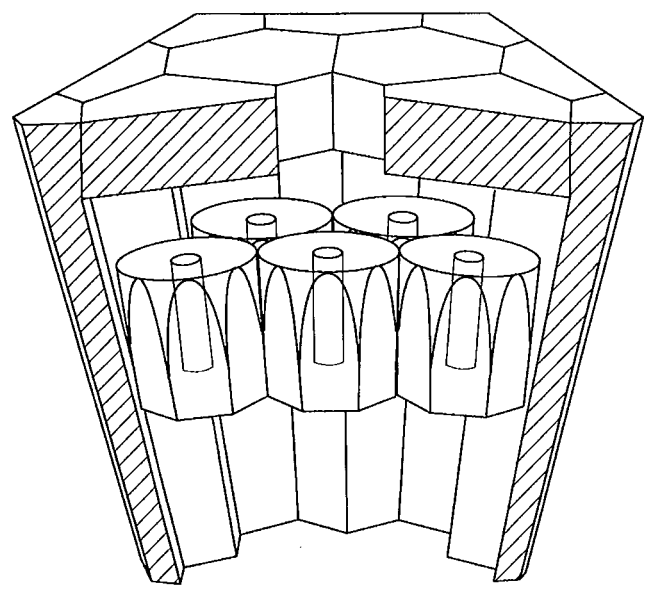

Fig. 2. Schematic diagram (side view cross section) of a cluster of 7 HPGe detectors (5 visible) surrounded by their BGO Compton suppressor (from Ref. [19]).

Ge detector [19,20]. An encapsulated detector is hermetically encased (in vacuum) in an aluminum can which is very close (1 mm) to the Ge crystal and provides electrical shielding. The seven detectors are packed very close together (crystal-to-crystal distance of 2.7 mm) in a cryostat with a ~ 5 mm spacing to the outer can which provides heat shielding. In this way the space between each detector in the group is minimized while retaining flexibility to retrieve individual detectors for repair. Clover and cluster detectors can increase the resolving power of an array, compared with arrays containing only conventional detectors, due to higher efficiency and P/T. However, they suffer to some extent the same limitations as Gammasphere-type detectors: (1) part of the useful solid angle is lost for Compton suppression and (2) the gain in efficiency and P/T is partly offset by summing effects where two γ-rays interacting in the same detector are counted as one, due to the large solid angle of such detectors. The summing effects can be remedied by using many such composite detectors far enough away from the γ-ray source, but the cost of such arrays would be prohibitive. This is where the new concept of GRETA comes in and qualitatively changes what can be achieved in γ-ray detection.

3. GRETA concept

3.1. GRETA principle

GRETA consists of a "solid" shell of (about 100) highly segmented large (e.g., 8 cm diameter by 9 cm long) HPGe detectors. The outer contact (surface of the coaxial detector) is segmented into many "rectangular-like" areas. The full energy and angle with respect to the beam direction of each incident γ-ray are determined by measuring, with high resolution, the energy and position of each of its interactions in the Ge crystals (see Fig. 3). The incident γ-ray is reconstructed by identifying these interactions using a tracking algorithm based on the Compton-scattering formula which describes the interactions. The γ-ray energy is obtained by adding the energy deposited at each interaction, and the emission angle of the incident γ-ray is deduced from the

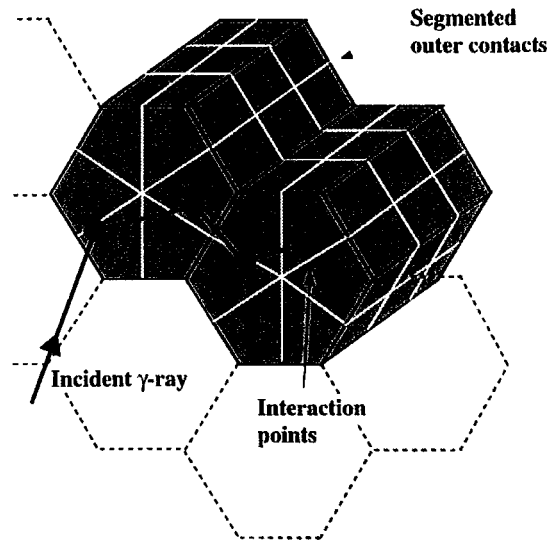

Fig. 3. Schematic view of interactions (dots) of an incident γ-ray in highly segmented HPGe detectors. The positions and energies of the interactions are used to reconstruct the energy and angle of the incident γ-ray.

position of the first interaction. Using fast transient digitizers, an additional gain in efficiency comes from the reduced dead time. In addition, it is expected that, using parallel processing, this analysis can be done in real time. The improvement over previous arrays comes from three areas: (1) the efficiency is increased because nearly 100% of the solid angle is occupied by the Ge detectors which provide a useful high-resolution energy signal (instead of 46% in Gammasphere, for example) and, in addition, most gamma rays Compton-scattered to another crystal can be recovered; (2) because of the high segmentation, each γ-ray interaction can now, in principle, be resolved and attributed (by tracking) to a particular incident gamma ray, thus eliminating the summing problem and improving the peak-to-total ratio; and (3) since the interaction-position resolution is high (of order 2 mm), the position of the first interaction of a γ-ray will give its direction from a target or source with that precision and the Doppler broadening effects due to finite detector size will be greatly reduced.

3.2. Determination of the γ-ray-interaction position

3.2.1. The radial position

It is known [21] that an average radial position of interactions from one γ-ray in a coaxial detector

can be determined by the drift time of the charge toward the electrodes. However, this property has not been used in typical nuclear physics experiments although a hardware circuit to determine the drift time of the main signal has been implemented in Gammasphere [22]. In GRETA, the radial position of an interaction is related to the drift time in the segment that receives the net charge from the interaction as well as to the shape of the transient signals (see Section 3.2.3). It will be deduced from the full decomposition of all the signals in the detector.

3.2.2. Azimuthal and depth position

In the Gammasphere two-fold segmented detector (Section 2.2.4, Fig. 4), the incident γ-ray may be completely absorbed in one half of the crystal, and it is then observed as a net charge signal in the corresponding electrode. If the γ-ray scatters into the other half of the crystal, there is a net charge in each electrode and in that case, its localization is based on the proportion of the energy deposited in each half. This gives a position resolution that is less than the size of the segment and is about a third of the solid angle subtended by the detector. Based on simulations and measurements, an often used procedure of position determination is that if more than 90% of the total γ-ray energy is deposited in one segment, the incident γ-ray is assumed to hit the center (of the front surface) of that segment, and if the energy deposited in one segment is between 10% and 90% of the total γ-ray energy, the incident γ-ray is assumed to hit the center (of the front face)

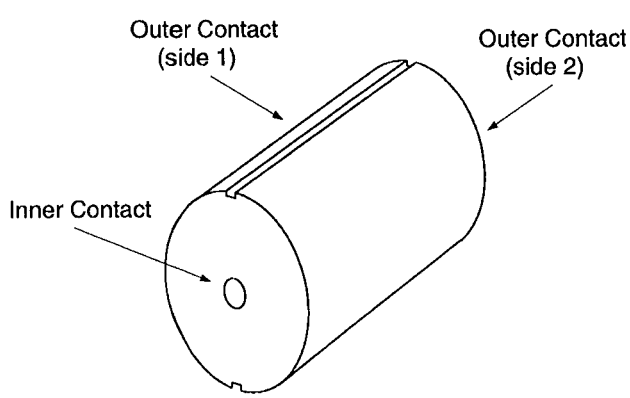

Fig. 4. Schematic view (from the back) of a Gammasphere segmented HPGe detector.

of the detector. Of course, when there is a net charge in both halves, one cannot distinguish between a scattering of one γ-ray from one side to the other and a double hit, but the latter are small (typically $< 10\%$ in Gammasphere). In GRETA, one would like to segment the outer electrode of the Ge detector such that only one γ-ray interaction occurs in each segment. A crude evaluation using the interaction length of γ-rays (of a typical energy of 1 MeV) indicates this requires "rectangular-like" segments 2–3 cm on a side etched onto the outer surface of the detector (i.e., in the length (z) direction, and in the azimuthal ($r\phi$) direction). By just collecting the net charge signals on each segment that fires, the azimuthal- and z-position resolution would correspond to roughly the size of the segment. However, one can do better than this by making use of the transient signals induced in neighboring electrodes.

3.2.3. The transient signal

In the two-fold segmented detectors of Gammasphere, one could analyze the energy distribution of the net charges in adjacent segments to obtain a position resolution better than the size of the segments, but one can do much better by analyzing the transient "induced charges" in neighboring segments. It was realized [23] that the charge drifting towards one electrode induces a signal in the neighboring electrodes and that the characteristics of this transient signal depend on the position of the interaction relative to the boundaries of the electrodes. Fig. 5 shows schematically the current signals produced when the charge from an interaction drifts toward its destination electrode as indicated in the Ge cross-section diagram on the left. The solid line shows the current signal in the segment where the interaction takes place. The signal increases continuously until the charge is neutralized when it reaches the electrode. The dashed lines are the transient currents as a function of time in the two neighboring segments. Their general behavior can be understood simply by considering the field lines that intersect each electrode and generate the image charges. Thus, in the segment where the interaction took place, the image charge always increases until the charge reaches the electrode, while in the neighboring segments, the transient image charge will

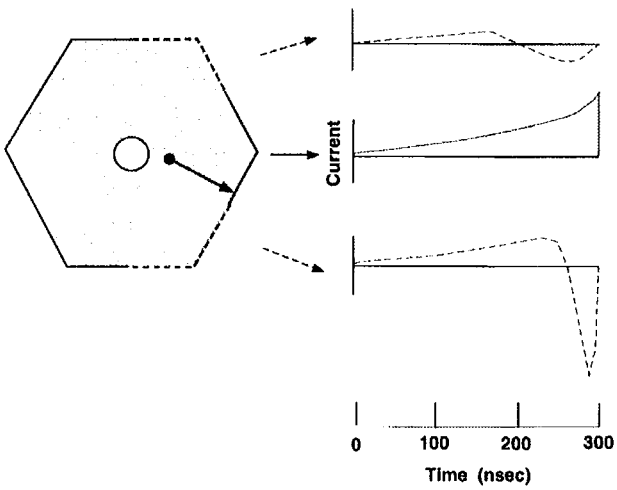

Fig. 5. Current signals on three electrodes (right) from a charge drifting toward the outside electrodes. The position of the interaction is shown as a dot on the detector cross section (left). The current from the destination electrode is the solid line and its integral is the net charge which gives the energy. The current from each neighboring electrode (dashed lines) integrates to zero.

decrease (and therefore the current will change sign) when the charge gets close enough to the destination electrode, and they will decrease more or less rapidly depending on the initial position of the charge. The net charge will be zero in these neighboring segments. Both the amplitude and the time of the maximum of the transient current signals can be used as parameters that define the position of the interaction with greater precision than the size of the segments. Using a prototype 12-segment Ge detector, tests are presently being performed to determine the attainable position resolution (see Section 4.2). A position resolution of a few mm in three dimensions is expected.

3.3. Reconstruction of the incident γ-rays and of their energy

Once the position and energy of each γ-ray interaction in the Ge detectors have been determined (with a known resolution) the next step is to deduce which interactions belong to a given γ-ray, sum up their energies to obtain the incident γ-ray energy and find the first interaction to obtain the γ-ray direction. So far, an algorithm involving a three-step process has been implemented [24,25], which constitutes a preliminary evaluation of this aspect of GRETA. The first step is to group the interactions into "initial clusters", which are assumed to result from the interactions of one incident γ-ray in the Ge detector array (at present considered to be a solid Ge shell). In a second step, the interactions within each cluster are evaluated (tracked) using the Compton formula to determine whether it is a "good" cluster. If not, one tries to maximize the number of good clusters in a third step by rearranging (adding or splitting) the original clusters and then testing the rearranged clusters once more with the Compton formula. This algorithm has been tested using simulated data from GEANT [26] which provides a set of interaction points generated by a number of input γ-rays. The following subsections give a more detailed description of this reconstruction process.

3.3.1. Cluster creation

We define clusters by the angle υ from the center of the array subtended by a pair of interactions. In this step we ignore the depth (z) of the interaction points. If the angle defined by any two interaction points is smaller than υ, these interactions are defined as initially belonging to the same cluster. The cluster is expanded if any additional points are found to be within the angle υ from any cluster point. The set of clusters defined in this way is then tested using the Compton formula.

3.3.2. Tracking

Tracking has been extensively used before in particle detection. It generally uses a trajectory or time sequence of the particle position. This is not possible with γ-rays where all the signals from a series of γ-rays from one event appear simultaneous. In our case, tracking uses the energy deposited and the 3-dimensional position of each interaction point. The energy deposited (E_d) is the energy difference between the incident γ-ray and the scattered γ-ray. It is related to the scattering angle θ by:

$$E_d = E_\gamma - E'_\gamma$$

$$= E - \frac{0.511}{(0.511/E\gamma) + 1 - \cos\theta}, \qquad (2)$$

where E_γ is the sum of the energies of the interaction points in the cluster. From the measured value of E_d, the scattering angle can be determined. However, the scattering angle can also be obtained from the position of the consecutive interaction points. The consistency of these two values is a test of the scattering sequence assumed. This is a very complicated problem since in a typical event, there are of order 20 γ-rays, each having on the average 4 interactions in the Ge shell. Such tracking techniques have not been used before, except perhaps in astronomy in so-called Compton γ-ray observatories to determine the direction of a γ-ray source in the sky. However, tracking is much simpler in this case because the source emits a single γ-ray at a time and only the first Compton interaction is used.

To evaluate a sequence in GRETA we use a figure of merit, which is basically the total χ^2 resulting from the difference of the two scattering angle values for all interaction points in the cluster. For a cluster of n interaction points, there are $n!$ possible scattering sequences. These sequences are tested to find the one with the minimum χ^2. If it is below a predetermined threshold for χ^2, the cluster is defined to represent a "good" γ-ray. If it is above, the clusters are split or added in some prescribed way and then tested again in the same way using the Compton formula. This process produces a set of reconstructed γ-rays which is compared to the known set of input γ-rays to give the peak-to-total ratio and an efficiency curve as a function of υ. Such a study of the dependence of the performance on the angle parameter υ (see Section 4.3) will determine which value(s) of υ to use in the analysis of experimental data.

The above cluster recognition algorithm is one possible approach and shows the "principle" of reconstruction of the incident γ-rays. Other algorithms need to be explored, as well as different techniques such as neural networks.

3.4. Preliminary description of GRETA

The goal of this section is to give the reader a realistic idea of what such an array would look like. Since the design studies are not finished, we will only describe a possible detector configuration, as well as general components of the electronics and acquisition systems.

3.4.1. Detectors

A geometry that keeps the spherical symmetry and in which the Ge material covers the 4π solid angle is similar to that of Gammasphere [1]. It consists of 120 elements, 110 (almost) regular hexagons and 12 pentagons, two of which are used for the entrance and exit beam pipes in nuclear physics experiments at accelerators. Taking into account the present production limitations on the diameter of the Ge detectors (approximately 8 cm), tapered hexagonal detectors with the back part cylindrical, as shown in Fig. 6, optimize the amount of Ge material used without losing too much efficiency: only the last 1.4 cm at the back of the detector will not cover the full space. Using the Gammasphere geometry, this gives an inner radius (to the front face of the crystal) of approximately 12 cm, enough space to accommodate auxiliary detectors. A segmentation into 36 elements corresponds roughly to one interaction length and thus there are approximately 4000 segments in GRETA. Other packing geometries are being considered, for example, using cubic or regular hexagonal shape detectors that will make better use of the Ge material but will no longer have spherical symmetry.

3.4.2. Electronics

The present view is that cold FETs in the same vacuum as the crystal will give the best energy resolution. There is some uncertainty as to whether

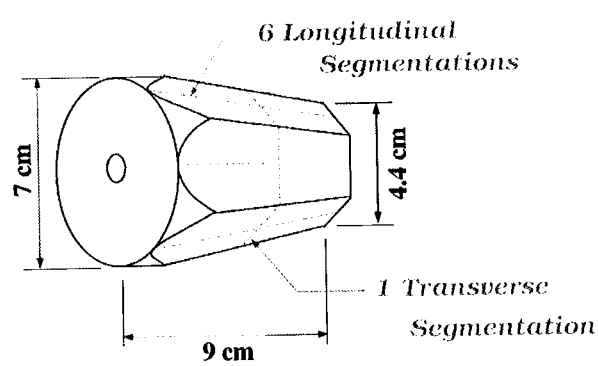

Fig. 6. Schematic perspective view (from the back) of the 12-segmented HPGe first GRETA prototype. The segmentation of the outer electrode is indicated as dashed lines.

36 (or more depending on the packaging chosen) FETs in one cryostat will be reliable enough to be usable. However, the present experience with our 12-segment prototype is encouraging; in a six-month period of continuous operation, and several temperature cyclings, there was no problem associated with the cooled FETs in the detector vacuum container. The preamplifier signal, after digitization, will be filtered in various ways according to the information wanted; primarily low bandwidth for energy information and high bandwidth for shape analysis. Therefore, the preamplifier is designed to have a large enough bandwidth [27] with a minimum rise time of approximately 10 ns. This should be enough to determine the interaction position of the net and transient signals as shown in Fig. 7. In this figure, calculated charge signals are shown for the segment in which an interaction takes place (segment 1) and in the ϕ neighbors (segments 2–4, see inset on top left panel of Fig. 7), as a function of the interaction position for a cylindrical six-fold segmented Ge detector of radius 35 mm. In this two-dimensional simulation, the interaction position is characterized by the Y coordinate (distance perpendicular to one boundary in segment 1 and the radius R. Y and R are each varied at intervals of 3 mm. The detailed shape of the induced signals (whether positive or negative, and the duration of the signal) will be discussed later (Section 4.1). Note that the amplitude of the induced signal depends primarily on how far from the interaction the segment boundary is, and that the risetime of the induced signal depends on the radial position. More details will be given in Ref. [28]. The 10 ns rise time capability of the preamplifier is enough to distinguish the various calculated signals.

3.4.3. Pulse shape analysis and data acquisition

The general data flow is schematically shown in Fig. 8. The goal of on-line data analysis is to deduce

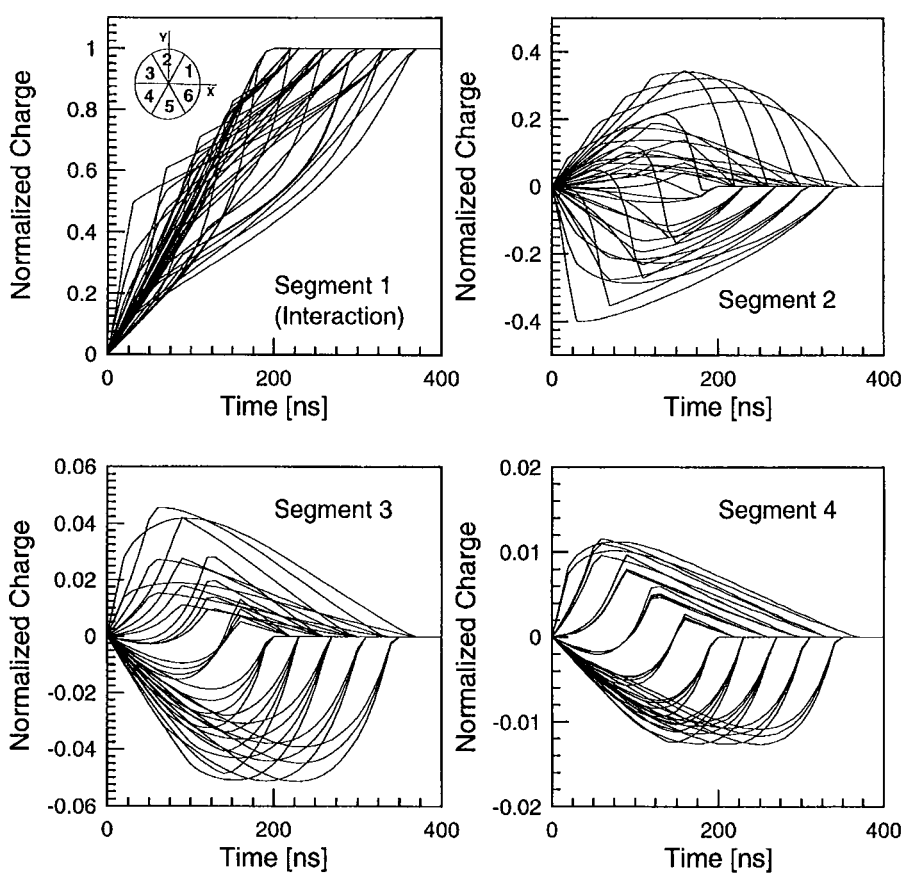

Fig. 7. Charge signals calculated in segments 1–4 (see inset in top left panel), for a grid of interaction points in segment 1 defined by 1 mm $\leq Y \leq$ 28 mm, 6 mm $\leq R \leq$ 33 mm and $\Delta R = \Delta Y =$ 3 mm (see text).

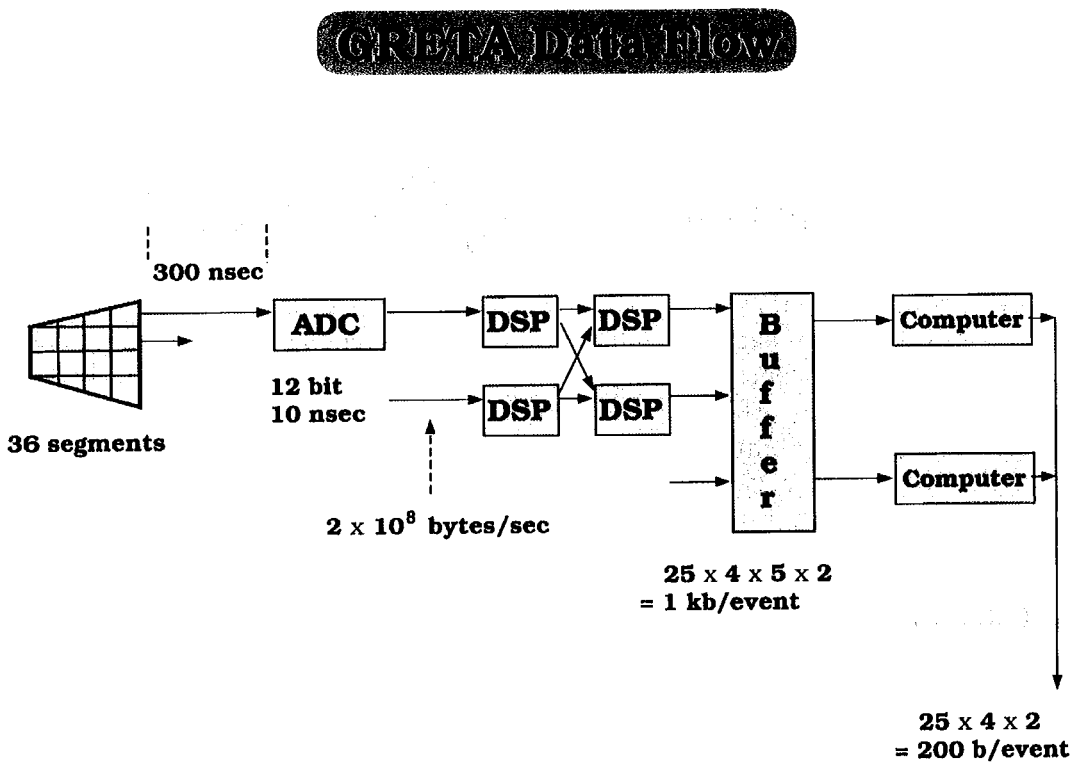

Fig. 8. Schematics of GRETA data flow.

and subsequently store only the direction (first interaction point), energy and time of emission of each γ-ray. The second interaction position will also be stored when polarization analysis is desired. We estimate that, using current algorithms, the computation time for full tracking takes approximately 1 ms, therefore if we use 1000 parallel computers, we will be able to analyze 10^6 events per second. At a cost of $1000 per computer, this is an achievable goal. In addition, we estimate that optimizating both hardware and software may reduce the tracking analysis time by a factor 10. The pulse shape analysis electronics represents a compromise between the needs of sufficient energy resolution and high count rate. A 12-bit, 10-ns ADC will provide a continuous train of 10^8 words or 2×10^8 bytes per second. Thus each segment has its own ADC which digitizes the preamplifier signal in 300 ns, and also provides digitized background information. However, this 12 bit, 10 ns ADC is currently expensive and it is presently advantageous to replace it with a cheaper combination of two ADCs, a slower one (25 ns) with high resolution (12 bits) for energy measurement, and a fast one (10 ns) with lower resolution (8 bits) for signal shape measurement. Two levels of digital signal processors (DSP) could be used to determine the position, energy and time of each γ-ray interaction. In the first level, each ADC is connected to its own DSP which calculates the energy, time and other important characteristics (e.g., shape) of the digitized signal, using a variety of filters and algorithms. The goal is to accomplish this in approximately 1 μs. In addition, the signal from the central detector contact can be used with a slower shaping time to improve the energy resolution when only one γ-ray is absorbed in that detector. At this point, it is conceivable to make a first-level decision to keep an event depending on the number of interactions detected (i.e. γ-ray multiplicity), given an expected average number of four interactions per γ-ray. In the second level, we want to correlate the various first-level DSP signals in order to relate the transient signals to the appropriate interaction points and obtain the interaction position with a desired precision of order 2 mm. This is done in another set

of (4000) DSPs in which we input the signals from each segment and a number of its neighbors, since we expect the transient signals to be strongest in the immediate neighbors. The number of neighbors needed and the details of the algorithm required to deduce the interaction position with the best resolution will be determined shortly using the 36 segments prototype. Again the goal is to process this second level in approximately 1 μs. At this point, typically 5 words (2 bytes each) per interaction (the 3 position coordinates, energy and time of each γ-ray interaction) are sent, with appropriate buffering, to the set of parallel computers. Assuming, as an example, that there are 25 γ-rays emitted in the event, each making an average of 4 interactions in the Ge material, the data flow consists of approximately $25 \times 4 \times 5 \times 2 = 1$ kbyte/event. Each event is processed through a "cluster recognition" algorithm to provide the direction, energy and time of each gamma ray in a time which is currently ~ 1 ms. With a reasonable selection of events (e.g. high multiplicity) and enough computers (~ 1000), events can be processed asynchronously and be stored on tape in this form as fast as they are produced in the experiment.

This represents only the principle of a data acquisition system, the DSP algorithms need to be developed, and the computer configuration is still to be designed. A module for digital signal processing suitable for GRETA detectors is presently being designed by X-ray Instrumentation Associates [29].

3.5. Evaluation

3.5.1. Resolving power

Since the research and development, as well as the design of GRETA, are not complete, a final number for the resolving power cannot be obtained at present. However, we expect a value between a minimum which corresponds to what we estimate can be achieved at present and a maximum which represents a "perfect" performance. Both limits of the resolving power are estimated by assuming the geometry described in Section 3.4.1 and take into account the losses due to gaps and absorption in the Al cans. Also in both cases, it is assumed that the position resolution will be good enough to eliminate the Doppler broadening so that only the intrinsic Ge energy resolution remains, i.e., 2 keV at 1.332 MeV. This assumption is valid in the typical fusion reactions that were considered when evaluating previous arrays and it is used here for comparison purposes. In addition, because of the shorter processing time and the increased number of segments, the event rate can be increased by a factor of approximately 24: i.e., we estimate that with current DSP technology, each sector will be able to sustain 4 times the rate of that of a Gammasphere detector, which, with the 6-fold segmentation of the front face of each detector, results in an overall average factor of 24 improvement in the counting rate (the multiple transverse layers of the detector roughly compensate the 3 or 4 interaction points of each γ-ray in the detector). Here also, the factor 24 represents a maximum of what the array can accomplish since other limits (in beam intensities or in heat that a target can withstand) may decrease this value. Thus, N_0 in formula (1) is increased by a factor 24 (i.e., 2.4×10^6 events/s). For the minimum value of the resolving power, the algorithm used to estimate the efficiency ε and the peak-to-total P/T (see Ref. [24,25] and Section 4.3) assumes an isotropic launch of 25 γ-rays of 1.332 MeV and an interaction position resolution of 2 mm. The photopeak efficiency is found to be 22% and the P/T is 0.62, which gives a resolving power of 1.8×10^6, a gain factor of 600 compared with Gammasphere. For the maximum value of the resolving power, it is assumed that the photopeak efficiency is only limited by the transparency of the Ge material, the gaps between crystals, and by the absorption in the Al cans. This gives a ε value of 54%. Assuming minimal uncertainties in the interaction position resolution, the P/T is estimated at 0.9, and the resolving power is then 1.4×10^8. Even the minimum, 1.8×10^6, is an enormous gain over the present arrays, and Fig. 9 shows that it is a 10 times bigger step than the previous one (e.g. between HERA and Gammasphere). In this figure, the resolving power is plotted against the photopeak efficiency for various values of R, the gain per fold of peak-to-background ratio.

The gain in *energy resolution* over Gammasphere is a factor 2 (for a typical fusion reaction considered

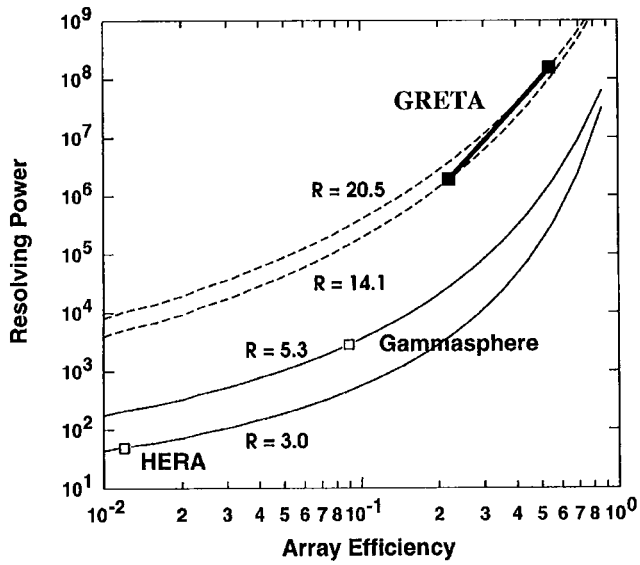

Fig. 9. Resolving power as defined in Eq. (1) as a function of photopeak efficiency for various values of R, the gain in peak-to-background per fold (see Sections 2.2.4 and 3.5.1). The solid lines correspond to $\ln N_0/N$ of Eq. (1) of 19.5, valid for previous arrays. The dashed lines correspond to the value $\ln N_0/N$ of 22.6, valid for GRETA (see text).

in this evaluation) – for γ-rays of approximately 1 MeV – similar to the gain between previous generations – although the reason is different. The gain in energy resolution between HERA and Gammasphere is due to the larger distance between the target and the detectors in the latter as well as the segmentation of 70 of the Gammasphere Ge detectors resulting in a smaller angle subtended by the Ge detectors and therefore a smaller Doppler broadening. In GRETA, the angle subtended by each detector becomes irrelevant since the angle of the incident gamma ray is determined from tracking to within approximately 2 mm. The Doppler broadening is practically eliminated and only the intrinsic Ge resolution remains. The *efficiency* is immediately improved by a factor close to two over Gammasphere due to the gain in solid angle, and by an additional factor due to the add-back and tracking across detectors. The gain in *peak-to-total ratio* in GRETA over Gammasphere is due to the tracking which recognizes and keeps only the full-energy γ-rays. And finally, the *count rate* capabilities of GRETA are higher than those of Gammasphere by more than an order of magnitude.

3.5.2. *Efficiency vs. resolution*

Fig. 9 shows that at high efficiencies, the resolving power increases faster with efficiency than at low values. We can quantify the relative importance of gain per fold, R (proportional to energy resolution), and efficiency, ε, using formula (1), by calculating the percentage change in resolving power, RP, per percentage change of R and ε. We find that the ratio of changes in ln RP relative to ε and R, called $\Delta\varepsilon/\Delta R$, is

$$\frac{\Delta\varepsilon}{\Delta R} = \frac{\delta(\ln RP)/\delta(\ln \varepsilon)}{\delta(\ln RP)/\delta(\ln R)} = \frac{\ln R}{\ln(1/\varepsilon)}. \tag{3}$$

Thus, if ε is close to 1, $\Delta\varepsilon/\Delta R$ tends toward infinity, which means that for GRETA the efficiency is more important than R (i.e. the energy resolution or P/T ratio). In contrast, for the HERA array where the efficiency is small ($\varepsilon \sim 0.012$), $\Delta\varepsilon/\Delta R$ is approximately 0.3, which means the resolving power is more sensitive to R than to the efficiency. For Gammasphere this ratio is close to one and the efficiency and energy resolution have equal importance. This should be taken into consideration when designing GRETA.

4. GRETA development

The concept used in GRETA is new in two main aspects: using the signal shape to determine the interaction position accurately (~ 2 mm), and using a tracking algorithm to select full-energy γ-rays and determine the first interaction point. In addition, there are technical challenges: e.g., building highly segmented HPGe (n-type) detectors, designing fast electronics to analyze the pulse shape online, and developing a powerful analysis system to "track" on line. These problems have never been studied before in this context and therefore simulations are required to prove that such a detector array can be constructed and will function as expected. The general method is to calculate the signals in existing detectors and ensure that they reproduce the measured ones. The calculated signals are then used to determine the pulse parameters that are most sensitive to the interaction position in the crystal. Simulations, as well as

measurements, will use these parameters to deduce the position resolution that can be achieved and to design the optimum detector. A tracking algorithm is developed to reconstruct the γ-rays once the positions of all the interactions in an event are determined. Details of this research and development will be given in two other papers [24,25,28]. We shall give here only the milestones achieved.

4.1. Prototypes

Prototypes are used both for signal measurements and to develop the technology of segmented Ge detectors. The first tests were made using an existing Gammasphere segmented detector. Both the net charge signal and the transient charge signal were calculated and measured. The important conclusion drawn from these tests was that the transient signal does exist and its amplitude is comparable (as much as $\sim 40\%$ of the net charge signal amplitude) to the net signal in the sector hit and agrees well with that calculated. This is the basic information needed to be able to achieve a good position resolution for tracking gamma rays. However, the transient charge signal in the Gammasphere 2-segmented detector, extracted from the outer electrodes, is noisy because of the large capacitance between these electrodes and the Al can. Similar measurements have been made with the 12-segment prototype. In this detector, the noise is much smaller mostly because of the smaller capacitance due to the smaller area of each segment. The energy resolution of each segment is approximately 1.8 keV at 1.332 MeV, exceeding the specifications. Fig. 10 (left panels) shows the measured net charge signals for the interactions A) (top) and B) (bottom) which take place in segment 1 as indicated on the Ge detector schematic at the top of the figure. The incident γ-rays of 662 keV (from a ^{137}Cs source) are collimated from the front in locations A) and B) and the multiple interactions can take place at any depth in the detector (in location B the γ-rays hit the tapered surface of the detector). The central and right panels compare the measured and calculated transient charge signals in segment 6 of the 12-segment prototype for the same locations A) (top) and B) (bottom). The shape of the signals can be understood from the time evolution of the image charges as the electrons and holes move towards the inside and outside electrode respectively. For example, in Fig. 10(A), the electrons, which induce a positive charge on the outer electrode, are close to the center (positive voltage) electrode. Therefore they will contribute very little to the transient signal. The main contribution will come from the holes which induce a negative charge. This is why the transient charge signal is negative in Fig. 10(A). Conversely, in position B) (bottom panels), the electrons are the main contributors to the signal and the transient charge signal will be positive. In the calculation, the measured response from the preamplifier is included. The calculations still need to be refined [28] but the present agreement between the measurements and calculations is encouraging. When the incident γ-ray is close to the boundary between two segments, the amplitude of the transient signal is approximately 40% of that of the net charge signal. The amplitude of the transient signal changes (on average) 2% per mm change in the γ-ray interaction position, for the first cm from the boundary, very close to what is expected from calculations. Measuring such a change in transient signal amplitude appears feasible with existing detectors. The next step is to order a 36-segment prototype, which will test both its feasibility and the expectation that 36 segments are optimum for position resolution.

4.2. Signal processing simulations

As mentioned before, to be able to track γ-rays, one must deduce (within 1–2 mm) the position of each interaction of each γ-ray in the crystal from the measured signals in all the segments. This is not a simple problem since each interaction typically induces signals in several neighboring segments and there will typically be several interactions per γ-ray in the same segment and/or in nearby segments. Therefore, the signals from several interactions may add and will require proper separation into the original interactions. There is also the possibility of nearby γ-ray hits in high-multiplicity events. This question is presently under investigation for a two-dimensional cross section (see Fig. 7) of a crystal. The general method is to generate from simulations a "basis" of signal shapes in each

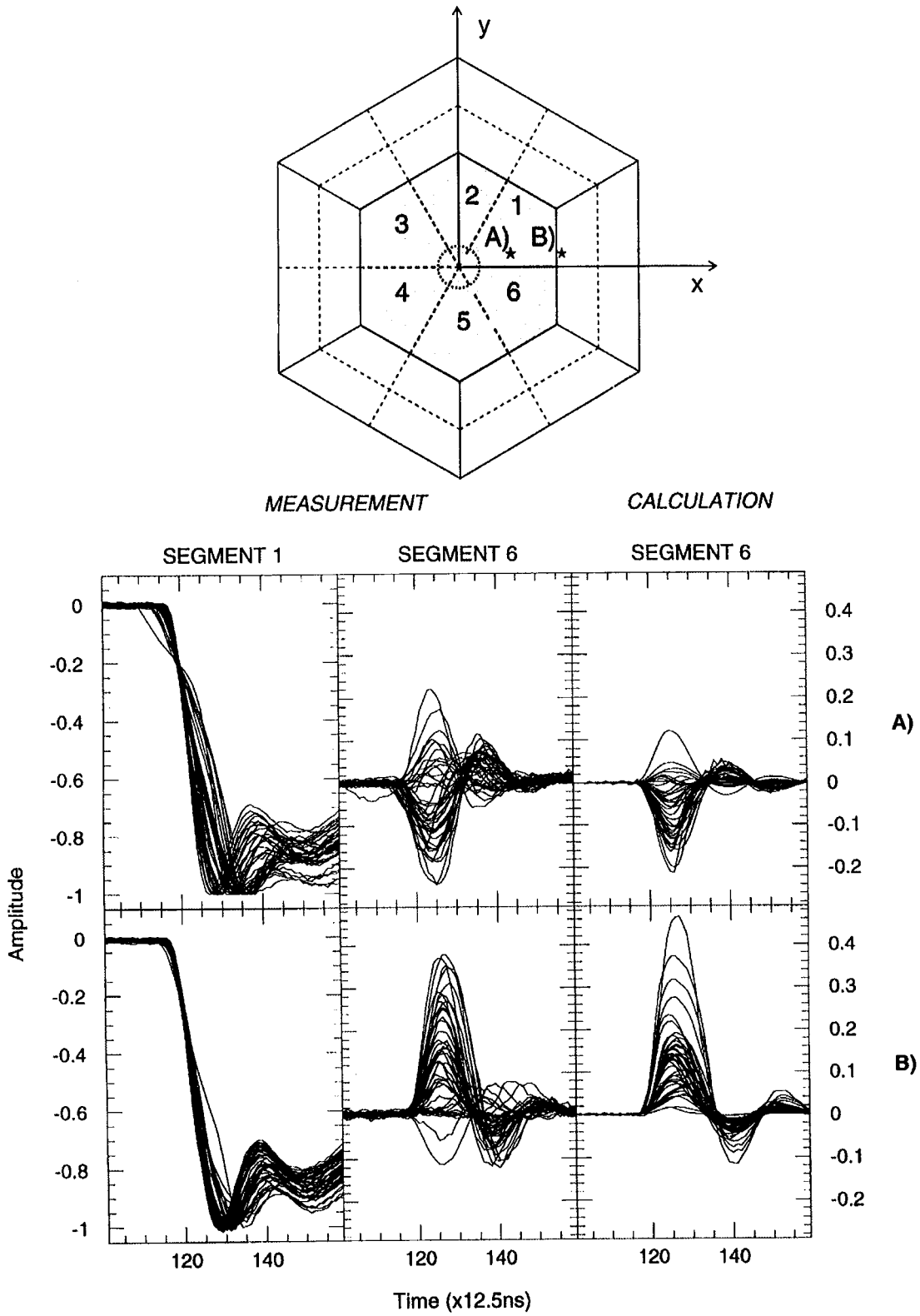

Fig. 10. Signals for incident γ-rays of 662 keV collimated to positions marked A) ($X = 1$ cm, $Y = 0.2$ cm, top) and B) ($X = 2$ cm, $Y = 0.2$ cm, bottom) in the top view of the 12-segmented GRETA prototype shown at the top of the figure. The shaded area represents the front face and the dashed lines are the segmentation lines. Left panels: measured net charge signals (in segment 1). Center (right) panels: measured (calculated) transient charge signals in segment 6.

segment due to interactions occurring in a regular grid spanning the cross-sectional area. One then uses this basis to decompose the observed (or calculated) signals from an event to deduce the position of one (or several) interactions. Fig. 7 shows [28] an example of a set of basis functions calculated in several segments for a regular set of interactions separated by $\Delta R = \Delta Y = 3$ mm. One sees that certain characteristics of the signals (e.g., maximum amplitude, and time of maximum amplitude) clearly depend on the interaction position. Methods of decomposition, as well as other approaches such as neural networks need to be investigated.

4.3. Tracking

A tracking algorithm has been developed [24,25], which reconstructs γ-ray energies and positions from a set of known interactions simulated with the GEANT Monte Carlo program. These interactions are defined by their energy and their position, assumed to be known with a certain accuracy. As already mentioned (see Section 3.3) one uses geometric proximity (angle parameter, see Section 3.3.1) to "define" clusters which are candidate gamma rays and then uses the Compton formula to identify those clusters which indeed represent a γ-ray. The results of the algorithm are compared with the known input and its success is measured by the efficiency and peak-to-total ratio. We consider, as an example, the case of the detector configuration described in Section 3.4.1, with realistic gaps and absorption in the cans. Dependence of the performance on γ-ray energy, multiplicity, and position resolution have been studied, but we shall only discuss one example. Fig. 11 shows efficiency and peak-to-total ratio as functions of the angle parameters for a high-multiplicity case of 25 γ-rays of energy 1.332 MeV. This represents a difficult case, with γ-ray energies that produce on the average four interactions each, for a total of approximately 100 interactions per event. A position resolution of 2 mm is assumed. Under these conditions, an efficiency of 22% and a P/T of 62% can be readily achieved at the optimum angle parameter of 10°. This represents a minimum performance in view of the fact that a search for more sophisticated methods to optimize the number of clusters recovered has not been made. Much remains to be done here since, as mentioned, a "perfect" algorithm would produce an efficiency of 54% and a P/T of 90%.

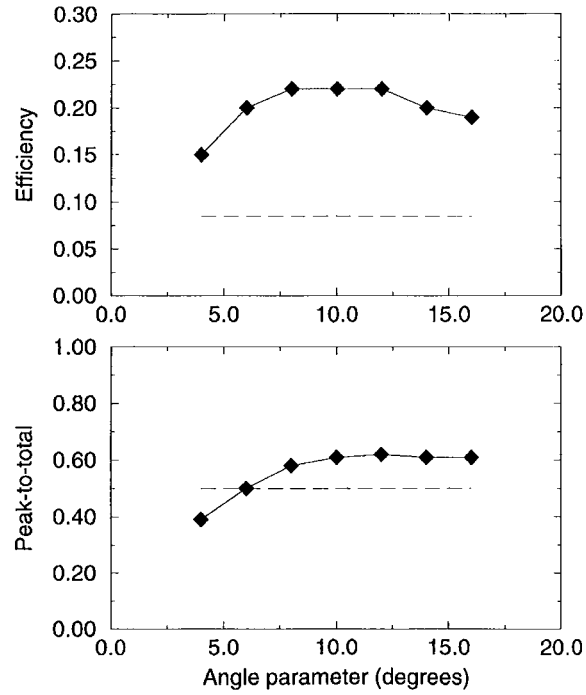

Fig. 11. Efficiency and P/T ratios deduced from the present tracking algorithm of Refs. [24,25] for a realistic GRETA geometry (realistic gaps and absorption in the Al cans) and an assumed position resolution of 2 mm for events consisting of 25 γ-rays of 1.332 MeV. The dashed line represents the performance of Gammasphere.

4.4. Electronics and acquisition

Two prototype preamplifiers have been built, one at LBNL [27] and one at Cologne [30], and are being tested with the 12-segment prototype. Both are expected to be fast enough to be compatible with GRETA requirements. At present, the LBNL preamplifier has a ~ 20 ns rise time and an electronic noise of 900 eV with a cold FET. Fast ADCs with high resolution are expected to be commercially available at a reasonable price when GRETA construction could begin around 2001. We are presently testing a 250 MHz, 8-bit ADC. A prototype digital signal processing module (including filter, ADC and DSP) is being developed in

connection with GRETA by the X-ray Instrumentation Associates company [29] and will be ready for tests soon. Finally, as computer technology keeps improving, we expect that it will be feasible to acquire a set of parallel computers well suited to perform the γ-ray reconstruction analysis. We believe an electronics and acquisition system which can analyze the signals "in flight" is achievable.

4.5. Future developments

We are presently developing algorithms to deduce the γ-ray interaction positions from a composite signal due to multiple hits in one segment. This is the last step needed to prove that the GRETA concept is valid and can be used in an actual detector array. Much remains to be done before finalizing a design for GRETA. Prototypes will be used to compare measurements with calculations, optimize algorithms, and determine characteristics of detectors and electronics. A 36-segment detector has been ordered, and later, a 7- or 9-detector prototype should help finalize the design of the array.

5. GRETA capabilities for new physics

Although the GRETA detector is, in some sense, the next step in the recent development of γ-ray detector systems, it is a very large step. The improvement in performance in some areas is so large that it seems entirely new capabilities are provided. For purposes of discussing the new physics GRETA will enable, we will (somewhat arbitrarily) focus on four areas where such "new" capabilities will be realized.

One area that is entirely new is the *characterization* of an incident γ-ray through tracking; that is, measuring each interaction point and requiring consistency between the total energy and the energy and scattering angle at each point. A major advantage is that close-lying γ-rays can be separated, including ones that hit the same crystal. This also allows one to distinguish full-energy events in the crystal (those that track with low χ^2) from partial-energy events (those that do not track with low χ^2), thereby improving considerably the response function (peak-to-total ratio). This reduction of background is important for almost all experiments involving γ-rays. Measuring the scattering angle between the first and second interaction point gives information on the linear polarization of a γ-ray which defines its electric or magnetic character; essential information in many nuclear structure studies, e.g. the determination of the parity of nuclear levels. From simulations the polarization sensitivity, $Q(E_\gamma)$, is estimated to be 0.35, which is higher than any polarimeter ever built (even those with extremely small efficiencies). A figure of merit for polarimeters is generally taken [31] to be: $\varepsilon[Q(E_\gamma)]^2$, where ε is the efficiency of the detector, and on this basis GRETA is at least 100 times better than any previous system, including Gammasphere and Euroball. In addition, tracking can distinguish γ-rays emitted by the source from those originating outside the detector, important for reducing the background in some types of experiment with low counting rates. The tracking information will become more important when one must be more certain about the nature of an event.

The *localization* of the first interaction point in a detector defines the angle of emission of that γ-ray from a source (target) of known location relative to the detector. Through tracking, GRETA will be able to locate that first interaction point to within 2 mm (FWHM), or at a distance from the source (to the average depth of the first interaction around 1 MeV) of 15 cm, to within a FWHM angle of 0.8°. For a standard Gammasphere-size detector ($\sim$ 7 cm dia.) at a typical distance of 25 cm from the source, this FWHM angle is about 8°, an order of magnitude worse. This angular resolution is especially important when detecting γ-rays emitted by a fast-moving source because such γ-rays have a Doppler energy shift that depends on the angle of emission, and this creates an energy spread in a detector that depends on the uncertainty in the angle of emission defined by the localization. As an example consider the study of neutron-rich light nuclei, where the production of near-drip-line nuclei is by fragmentation reactions resulting in product velocities v/c of 30%, or higher. For a 1 MeV γ-ray emitted at 90° to the beam direction, the contribution to the FWHM of the energy spread due to the Doppler broadening would be

39 keV with a standard Gammasphere detector, while it would be 3.7 keV with GRETA. This improvement can have a large effect on the physics, both in detecting weak γ-rays and in separating nearby peaks. An example of this type of experiment was the Coulomb excitation of a secondary beam of ^{44}S produced in the primary fragmentation reaction ^{48}Ca + ^{9}Be [32]. The ^{44}S beam was subsequently Coulomb excited in a thin gold foil at the center of an array of position-sensitive NaI detectors. Due to its better intrinsic resolution, localization and efficiency, GRETA would have ~ 100 times more sensitivity for detecting the resulting 1.3-MeV γ rays than the NaI array. Localization is important for other experiments involving large recoil velocities, e.g. those using inverse-reaction kinematics and many Coulomb-excitation studies.

GRETA has a much higher *efficiency* for detecting full-energy γ-rays than previous detector systems, especially for high-energy γ-rays; e.g. at 10 MeV the efficiency is more than an order of magnitude larger than in previous arrays. This high efficiency is due to: (1) the 4π germanium coverage, whereas detectors like Gammasphere and Euroball have closer to 2π germanium coverage; and (2) the "add-back" feature of GRETA, where γ-rays can be tracked out of one germanium crystal and into an adjacent one, and by adding the appropriate interaction points, the full energy can be recovered. The gain of GRETA efficiency over Gammasphere efficiency is roughly a factor of 3, 6 and 20, respectively, for the energies of 0.1, 1, and 10 MeV. While the gain is large everywhere, it increases with increasing γ-ray energy due to GRETA's improved ability to collect larger showers. This efficiency will be especially important in ISOL experiments where the beam intensities are likely to be low, and in giant resonance experiments where the combination of high efficiency and high-energy resolution is unprecedented. An interesting example outside the nuclear-structure area is the accurate measurement of the decay probability of positronium into four γ-rays. This experiment requires detection of five γ-rays, the four just mentioned plus one for identification (through the 1.275 MeV γ-ray associated with the decay of ^{22}Na), and GRETA will have about 500 times the probability of detecting such a decay compared with detectors such as Gammasphere or Euroball. The present limit for the decay of triplet positronium into four gamma rays is, $4\gamma/3\gamma < 10^{-5}$, and the estimated five γ-ray detection rate with GRETA is about 10 per second, indicating that the limit could probably be reduced by a factor of 100 or more. This is an enormous improvement in such an experiment.

One of the principal driving forces for the development of detector systems such as Gammasphere and GRETA has been the high-spin studies following fusion reactions. These are cases where there are high multiplicity (20–30) γ-ray cascades and the interesting physics is often in very rare cascades (e.g. superdeformed bands). As discussed earlier, a measure of the *sensitivity* in these kinds of studies is the "resolving power", which combines energy resolution, efficiency, response function, granularity and rate in an appropriate way. An important property of GRETA, due to newly designed electronics, is that it will be able to sustain counting rates more than 20 times higher than Gammasphere (about 4×10^4 per second per sector or more than 2×10^5 per second for each detector) and this large gain in rate is important for many types of experiments. Consider a typical fusion reaction experiment where the average angular momentum left in the product nucleus is around $40\hbar$, resulting in the emission of ~ 20 γ-rays per event with average energy 1 MeV. Gammasphere would catch an average of 2 full-energy γ-rays per event, whereas, GRETA will catch between 5 and 10, and these 5 or 10 could be accumulated at more than 20 times the rate. It is clear that this will bring a qualitative improvement in the experiments. For example, the linking transitions between superdeformed and normally deformed states are very difficult to detect now – only a few cases known with several linking transitions in those cases – but GRETA's much greater sensitivity may be able to resolve completely this decay (perhaps hundreds of pathways), providing unprecedented information on the energy levels between the superdeformed band and the ground state. There are many other examples where the large gain in sensitivity with GRETA will be crucial.

GRETA has a variety of new capabilities which will be used in various combinations to accomplish

the goals of many types of physics. The objective of this section has been to give some hint of this variety.

6. Conclusion

GRETA, the next generation γ-ray detector array, successor of Gammasphere and Euroball, goes beyond the limit reached by these arrays which were based on Compton suppression. GRETA uses the new concept of γ-ray tracking, made possible largely by technical advances in Ge detector segmentation. This leads to large gains in resolving power and also to new kinds of measurements, such as the event-by-event characterization of γ-rays, and the detection of high-energy, high-resolution γ-rays. Gamma-ray detector evolution is important for many types of physics.

Acknowledgements

We would like to thank F.S. Goulding, D. Landis and M. Maier for illuminating discussions. This work was supported by the Director, Office of Energy Research, Division of Nuclear Physics of the Office of High Energy and Nuclear Physics of the U.S. Department of Energy under Contract No. DE-AC03-76SF0098.

References

[1] M.A. Deleplanque, R.M. Diamond (Eds.), Gammasphere Proposal, Lawrence Berkeley National Laboratory Report 5202, 1988.
[2] P.J. Nolan, F.A. Beck, D.B. Fossan, Ann. Rev. Nucl. Part. Sci. 45 (1994) 561.
[3] C.W. Beausang, J. Simpson, J. Phys. G: Nucl. Part. Phys. 22 (1996) 527, and references therein.
[4] J. Simpson, Z. Phys. A 358 (1997) 139.
[5] A.J. Tavendale, G.T. Ewan, Nucl. Instr. and Meth. 25 (1963) 185.
[6] A. Johnson, H. Ryde, J. Sztarkier, Phys. Lett. 34B (1971) 605.
[7] F.S. Stephens, R.S. Simon, Nucl. Phys. A 183 (1972) 257.
[8] R.H. Pehl, R.C. Cordi, F.S. Goulding, IEEE Trans. Nucl. Sci. NS-19 (1972) 265, and references therein.
[9] P. Twin et al., Nucl. Phys. A 409 (1983) 343c.
[10] P.J. Nolan, D.W. Gifford, P.J. Twin, Nucl. Instr. and Meth. A 236 (1985) 95.
[11] R.M. Diamond, F.S. Stephens, LBL Report, 1981, unpublished.
[12] R.M. Diamond, in: D. Schapira (Ed.), Proceedings of the Conference. on Instrumentation for Heavy Ion Nuclear Research, Nucl. Sci. Research Conf. Series, vol. 7 Harwood, p. 259.
[13] P. Twin et al., Phys. Rev. Lett. 57 (1986) 811.
[14] F.S. Stephens, private communication.
[15] T.E. Drake et al., The TRIGAM Spectrometer Proposal, AECL, October 1992, unpublished.
[16] T.L. Khoo et al., Phys. Rev. Lett. 76 (1996) 1583.
[17] F.A. Beck et al., Proceedings of the International Conference on Nucl. Struct. at High Ang. Momentum, Ottawa, 1992, p. 364.
[18] F.A. Beck, Proceedings of the Conference on Phys. from Large Gamma-ray Detector Arrays, Berkeley, 1994, p. 154.
[19] J. Eberth, Prog. Part. Nucl. Phys. 28 (1992) 495.
[20] J. Eberth et al., Nucl. Instr. and Meth. A 369 (1996) 135.
[21] F.S. Goulding, D.A. Landis, IEEE Trans. Nucl. Sci. NS-41 (1994) 1145.
[22] D. Cline (Ed.), Gammasphere Baseline Review Document, Nuclear Structure Research Laboratory, University of Rochester, Report NSCR-366, 1991, p. 3.
[23] I.Y. Lee, private communication.
[24] G.J. Schmid et al., IEEE Trans. Nucl. Sci. NS-44 (1997) 975.
[25] G.J. Schmid et al., Nucl. Instr. and Meth., to be published.
[26] R. Brun, F. Bruyant, M. Maire, A.C. McPherson, P. Zanarini, GEANT3 Users' Guide, DD/EE/84-1, CERN, 1987.
[27] H. Yaver et al., private communication.
[28] K. Vetter et al., Nucl. Instr. and Meth., to be published.
[29] B. Hubbard-Nelson et al., Nucl. Instr. and Meth. A 422 (1999) 411.
[30] J. Eberth, private communication.
[31] G.J. Schmid et al., Nucl. Instr. and Meth. A 417 (1998) 95.
[32] T. Glasmacher et al., Phys. Lett. B 395 (1997) 163.

Reprinted from:
NUCLEAR SPECTROSCOPY AND REACTIONS, PART A
© 1974
ACADEMIC PRESS, INC.
New York San Francisco London

For Reference

III.D SEMICONDUCTOR DETECTOR SPECTROMETER ELECTRONICS

Fred S. Goulding and Donald A. Landis

LAWRENCE BERKELEY LABORATORY
UNIVERSITY OF CALIFORNIA
BERKELEY, CALIFORNIA

I. Examples of Spectrometer Systems 414
A. Introductory Remarks 414
B. Simple Spectrometer 414
C. Fast-Slow Coincidence System 416
D. Particle Identification System 418
E. Timing Systems 420
II. Basic Considerations in Energy Measurements 421
A. Introductory Remarks 421
B. Statistical Effects in Detectors 421
C. Noise Reduction 422
D. The Input Circuit and Preamplifier 428
E. Effects of Fluctuations in Detector Signal Rise Time 438
F. Degradation Factors at High Counting Rates 439
III. Design Factors in Electronic Modules for Spectroscopy 443
A. Linear Amplifiers 443
B. Pileup Rejectors 448
C. Baseline Recovery Circuits (dc Restorers) 449
D. Linear Gates 452
E. Biased Amplifiers 456
F. Pulse Stretchers 458
G. Discriminators and Single-Channel Analyzers 459
H. Nonlinear Elements for Analog Calculations 461
I. Analog-to-Digital Converters 462
J. Analog Multiplexers and Derandomizers 463
IV. Basic Considerations in Time Measurements 464
A. Introductory Remarks 464
B. Fast Timing of Particles with Thin Silicon Detectors 465
C. Fast Timing with Germanium γ-Ray Detectors 468

V. Design Factors in Electronic Modules for Fast Timing 471
A. Fast Amplifiers 471
B. Time Pickoff Discriminators 473
C. Time-to-Amplitude Converters 475
Appendices 476
A. Bipolar and Field-Effect Transistors 476
B. Miscellaneous Electronic Terms 480
References 480

I. Examples of Spectrometer Systems

A. Introductory Remarks

Nuclear experiments involve complex signal processing operations performed by functional electronic units. The use of standard modules facilitates the assembly of highly sophisticated systems, but optimum design of these systems requires knowledge of the design philosophies involved in both systems and modules. A few common systems will first be described as an introduction to the subject.

B. Simple Spectrometer

We restrict our attention to the measurement of radiation using semiconductor detectors. These convert the energy of individual photons or particles absorbed in the detector material into electrical signals (see Goulding and Pehl, Chapter III.A). Each detector signal consists of a short pulse of current, its duration being determined by the collection time for electrons and holes in the detector. The total charge signal is proportional to the energy absorbed by the detector. Signals arrive at random times, their average rate being determined by the radiation intensity.

The most important parameter in a nuclear spectrometer is its energy resolution. In an ideal system, absorption of photons or particles of a single energy produces signals of a single size from the detector, and the electronics feeds pulses of fixed amplitude to a pulse-height analyzer, which accumulates them in only one channel. The resulting spectrum contains spectral lines each only one channel wide, the channel number of each line corresponding to one energy of photon or particle. In practice, the spectral lines are broadened by several factors. As shown in Chapter III.A, Section I, some broadening of spectral lines is caused by statistical processes in the charge production in the detector. Further broadening is caused by electronic noise in the signal-processing electronics.

Figure 1 shows the elements of a typical spectrometer. Detector bias is adjusted to suit the particular detector; very thin detectors use low voltages (~10 V), but thick ones may require voltages as high as 5 kV. Electrical signals

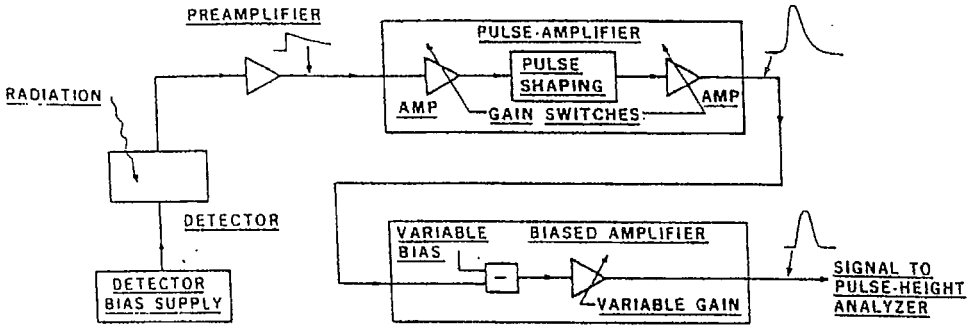

Fig. 1. Configuration of a simple spectrometer.

from the detector feed a preamplifier, which is in close proximity to it. The preamplifier feeds a pulse amplifier, often located some distance away, which provides signal amplification adjusted to suit the size of the input signals. An even more important function of the pulse amplifier is to shape the signal pulses to minimize the effect of electronic noise on signals. The pulse-shaping network is usually adjustable to permit optimization in an experiment.

Where a whole range of signals from zero to full amplitude is to be studied, the pulse-amplifier output is connected directly to a pulse-height analyzer. Many times, only those signals near the top of the signal amplitude range are of interest, so a biased amplifier is used to remove all signals below an adjustable bias level, and to amplify the resulting residues of signals, so that the interesting range of signal amplitudes fully utilizes the available analyzer channels.

While the general features shown in Fig. 1 occur in all nuclear spectrometers, details vary according to the particular application. The wide energy range covered by nuclear spectrometers—from 1-keV X rays to 100-MeV particles—makes it impossible to design an optimum system for the entire range. The importance of a given parameter changes radically as the energy changes; for example, electronic noise is the dominant contributor to resolution at low energies, but, at high energies, its effect is negligible compared with statistical effects in detectors.

These considerations lead to three groupings of spectrometers, although considerable overlap exists between these groupings:

(1) High-energy particle spectrometers are characterized by sensitivity to such factors as charge trapping in detectors and gain drifts in amplifiers, since the absolute amount of these effects increases nearly linearly with energy. On the other hand, electronic noise is usually negligible. Silicon detectors are often used at temperatures near room temperature in these applications.

(2) Gamma-ray spectrometers measuring energies greater than 30 keV use germanium detectors, since silicon is an inefficient absorber at these energies. Cooling the germanium detector to 77°K (or near to this) is essential to reduce

its leakage current to an acceptable value. In this energy range, electronic noise, detector statistics, and charge trapping are all important.

(3) In X-ray spectrometers (<30 keV) the resolution is dominated by electronic noise. To minimize this noise, silicon detectors are used at 77°K to reduce their leakage current, and a very sophisticated low-noise electronics system is employed.

C. Fast-Slow Coincidence System

A more complex system is often used in decay-scheme studies. In a typical case, an intermediate energy level Y may be populated from a single level X above it; the lifetime of the level Y may be very small (<10 nsec), before it decays to one of the lower-lying levels Z_1, Z_2, etc. The nucleus, decaying from its highest level X to Y, emits a γ ray of energy $X - Y$, and almost immediately afterwards, a further γ ray, which may have any one of the energies $Y - Z_1$, $Y - Z_2$, etc., is emitted as the deexcitation process continues. Since the emission of the individual γ rays is isotropic, two detectors can be placed a short distance away from the sample, one being used to select some fraction of the $X \rightarrow Y$ transition γ rays, while the other is used to observe some of the $Y \rightarrow Z$ transition γ rays. Both detectors might be germanium, but, in some applications, one might be a scintillation detector (to realize higher efficiency), or a particle detector if particle–γ-ray associations are to be studied. If the angular distribution of the $Y - Z$ relative to the $X - Y$ γ rays is to be studied, the angle subtended by the two detectors at the sample may be changed between successive experiments.

Figure 2 shows a typical system used for these studies. Each detector feeds a high-resolution spectrometer system, although the amplitude analysis in the B channel is performed only by a single-channel analyzer. This selects $X \rightarrow Y$ transition γ rays seen by detector B on the basis of their energy. The A channel contains a delay and linear gate, so that a signal can reach the pulse-height analyzer only when the single-channel analyzer in the B channel registers an X–Y transition γ ray. The delay is chosen to permit amplitude determination in the B channel early enough to gate the A channel output.

Relatively slow pulse shaping must be used to optimize the signal/noise ratio in the amplitude-measuring channels of spectrometers. Shaping times normally range from 1 μsec to 10 μsec, so the ability of these channels to recognize real coincidences is poor. Events not truly coincident may be accepted as coincident by the slow systems alone, resulting in a high chance-coincidence rate. The parallel fast channels shown in Fig. 2 overcome this difficulty by superimposing a very short (nsec) coincidence-time requirement on the coincidence requirements of the slow channels.

The fast channels may derive their inputs from the preamplifiers, or a fast signal pick-off may be made directly at the detector. The fast amplifiers are

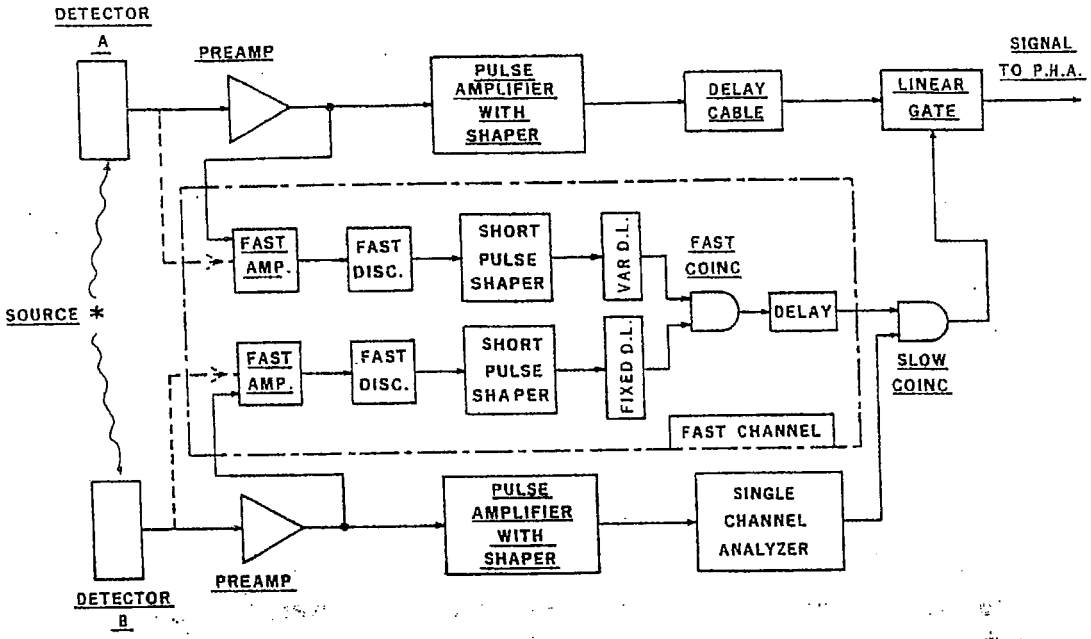

Fig. 2. A typical fast-slow coincidence spectrometer.

capable of amplifying the signals with minimum degradation in rise time. Fast discriminators remove low-level signals and noise pulses, and convert all pulses above the preset discriminator level into constant-amplitude output pulses, which are then shaped into short pulses of fixed duration τ. Following suitable short delays, inserted to compensate for minor transit time differences in the A and B fast channels, these pulses feed a fast-coincidence circuit which produces a fixed-shape output pulse only when an overlap occurs between its two inputs. A signal in the B channel starting at any time from $-\tau$ to $+\tau$, with reference to a signal in the A channel, is recognized as coincident with it, and vice versa. By making a slow coincidence between the coincidence output of the fast channels and the single-channel analyzer, a fast coincidence requirement is imposed, over and above the requirement for the B pulse to fall in a small amplitude range, before the A signal is allowed to go to the pulse-height analyzer.

The effect of a finite coincidence resolving time on the chance coincidence rate is easily analyzed:

Let $n_A(\text{sec}^{-1})$ be the total γ-ray signal rate in A channel; F the fraction of these γ rays that are truly coincident with events in the B channel; $n_B(\text{sec}^{-1})$ the total γ-ray signal rate in B channel; and 2τ the coincidence resolving time.

We then have the total time (sec^{-1}) when events in A channel sensitize the system to counts in the B channel as $2n_A\tau$; therefore, the chance coincidence rate is $2n_A n_B\tau$, and the true coincidence ratio is $F/2n_B\tau$.

The requirement for good energy resolution indirectly imposes a limitation on the maximum "singles" counting rate in the A and B channels, as it demands the use of relatively wide pulses (5 μsec or greater), with the result that pileup problems become important at even moderate rates. For the purpose of illustration, we will assume a singles rate of 50,000 pulses per second (i.e., a pileup probability of 25% for 5-μsec wide pulses), and that the fraction F is 0.01, and we will compare the true/chance ratio for a system using only slow channels with a resolving time of 200 nsec (i.e., 2τ), with that for a system with fast channels exhibiting a resolving time of 10 nsec. The calculated true/chance ratios are 1:1 in the first case, and 20:1 in the second, illustrating the great advantage of the fast-slow system.

D. Particle Identification System

In the previous example, certain conditions (fast coincidence between A and B, and the pulse amplitude within a small range in B) were imposed before γ-ray signals were presented to the pulse-height analyzer. More complicated conditions are often imposed; the particle identifier system as shown in Fig. 3 represents a good example. It is used in studies of nuclear reactions producing many types of particle, each with its own distribution of energies.

The identifier uses a thin ΔE detector, through which the particles pass, and an E detector in which the particles stop. Each particle leaves some energy in the ΔE detector, the fraction depending on the type of particle and its energy. Identification of the type of particle can be accomplished by using the ΔE and E

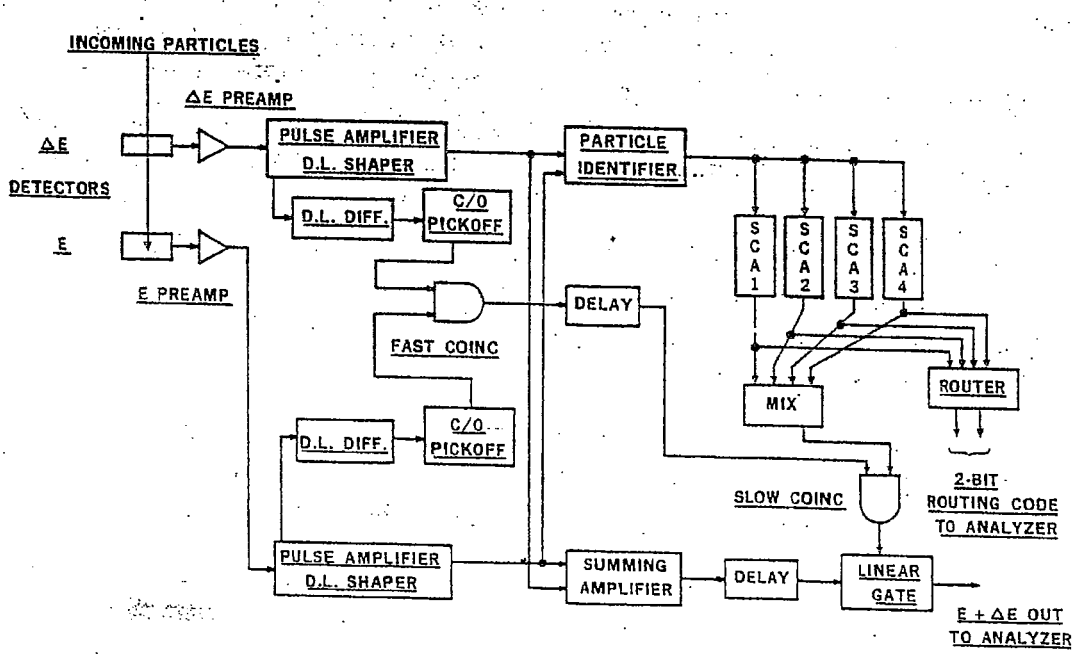

Fig. 3. A particle identification system.

signals, and performing a calculation based on the range–energy laws for charged particles in matter (i.e., silicon if silicon detectors are used). For a large range of charged particles, the range–energy law can be simplified to

$$R = A\,E^B \tag{1}$$

where R is the particle range, E its energy, B is almost a constant ($\sim$1.73 but changing for low velocity particles), and A depends on the type of particle and the absorbing material.

The relationship of Eq. (1) is frequently used for particle identification purposes (Goulding *et al.*, 1966), although the more accurate Bethe–Bloch range–energy equation can also be employed. If E is the energy deposited in the E detector, ΔE is the energy in the ΔE detector, and T is the ΔE detector thickness, we can write

$$T/A = (E + \Delta E)^B - E^B \tag{2}$$

By calculating the value of the right hand side of this equation for each particle stopping in the detector telescope, a signal is generated (T/A) whose amplitude is dependent only on the type of particle, not on its energy. The calculation may be carried out quickly (<5 μsec) in an analog calculator using logarithmic elements (see Section III.H) or in a computer in a much longer time.

When an analog calculation is used, the T/A pulse is available immediately to identify the particle. In Fig. 3 this pulse feeds a number of single-channel analyzers, each adjusted to select particles of only one type. The single-channel analyzer outputs drive a "router" that directs the energy analysis of each particle into a segment of the analyzer memory reserved for that type of particle.

Energy signals, produced by summing the E and ΔE signals, suitably delayed, are gated into the analyzer only if the particle is one of the selected types, and if fast coincidence conditions are met. In the example of Fig. 3, delay-line differentiators are used in the amplifiers, and a second delay-line differentiation is performed in each channel to produce a bipolar pulse. The zero-crossing point of this pulse is independent of pulse amplitude, so the crossover (c/o) pickoff output occurs at a fixed time in relation to the start of the detector signal. This method permits a reasonably fast coincidence to be made between two channels without the complexity of the separate fast channels used in the preceding example of a fast-slow system.

Using this particle identifier system, four energy spectra, each appropriate to one type of particle, are obtained. In recent years, on-line computers have found increasing use to perform the particle identification operation described here (see Borchers, Chapter III.E). The versatility and accuracy of the computer recommends it, but the time required to determine the type of particle makes it rather slow. Consequently, the analog particle identification scheme may be used to preselect events for more exacting computer processing, thereby reducing the

event rate into the computer, and making its computation time less objectionable. This illustrates an increasing trend toward utilizing good analog signal-processing electronics together with computers to utilize the best features of both.

E. Timing Systems

Our emphasis so far has been on pulse amplitude measurements. Time information might also be important—for example, in studying the lifetimes of excited states in nuclei, or in determining the distribution of flight times of particles along a fixed path. In many cases, the time distributions must be determined while measuring energies, as in the general system of Fig. 4.

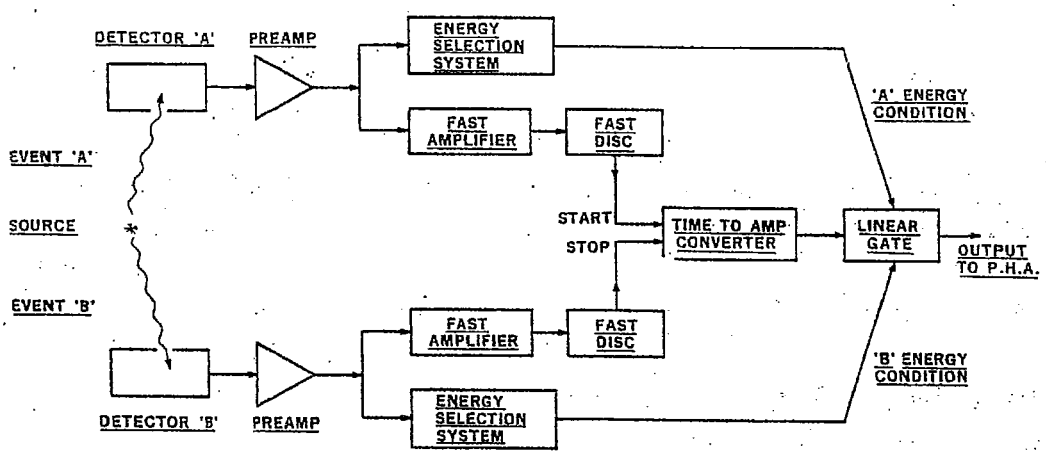

Fig. 4. A fast-timing system.

The fast channels associated with the two detectors are similar to those described in Section I.C. To utilize readily available pulse-height analyzers, it is convenient to convert time into amplitude distributions. To accomplish this, the fast-timing pulses from the A and B channels feed "start" and "stop" inputs on a time–amplitude converter (TAC) that produces an output pulse amplitude proportional to the time difference between pairs of pulses at its input. No output signal occurs if an A pulse is not followed by a B pulse within a preselected time. Section V.C discusses time–amplitude converters.

Energy requirements are often placed on the signals in A and B channels before permitting time analysis. To accomplish this result, spectrometer systems like that of Section I.B may be used with single-channel analyzers in the side channels to gate the output of the time–amplitude converter. Suitable delays are included in each channel to achieve the desired synchronization of signals at the linear gate.

II. Basic Considerations in Energy Measurements

A. Introductory Remarks

Many factors determine the energy resolution of spectrometers. The two major sources of degradation of resolution are statistical processes in the detector and electronic noise, which is due partly to fluctuations in detector leakage current, and partly to current fluctuations in the signal amplifying elements. Further degradation in resolution occurs at high counting rates due to baseline fluctuations, and pulse pileup. Fluctuations in the rise time of the detector signal may also be important in some applications. The magnitude of the degradation in resolution produced by most of these factors depends on the pulse shaper (or noise filter) employed in the pulse amplifier.

B. Statistical Effects in Detectors

In Chapter III.A, Section I.C, it is shown that the statistics of energy sharing between ionizing processes and lattice excitation cause fluctuations in the charge signal produced in the external circuit. Assuming a fixed energy E(eV) to be absorbed for each event in the detector, the full width at half maximum (FWHM) of the spectral line, expressed as an equivalent energy fluctuation, is given by

$$\Delta E = 2.35(FE\epsilon)^{1/2} \tag{3}$$

where F is the Fano factor, and ϵ is the average energy required to produce an electron–hole pair in the detector material (eV). The effective value† of F for silicon is 0.12, and a similar value applies to large germanium detectors. However, for unknown reasons, small volume (<1 cm^3) germanium detectors often exhibit values as low as 0.08. The value of ϵ in Eq. (3) is somewhat dependent on temperature. For silicon it ranges from 3.64 eV at 25°C to 3.80 eV at 90°K; for germanium, ϵ is 2.96 eV at 90°K.

Equation (3) may be used to assess the statistical detector contribution to resolution. Typical values are (1) Silicon at 77°K, for 10-keV X rays: $\Delta E = 160$ eV; (2) Germanium at 77°K, for 1-MeV γ rays: $\Delta E = 1.4$ keV; and (3) Silicon at 25°C, for 50-MeV α particles: $\Delta E = 11$ keV. Although the absolute value of ΔE rises as E increases, the percentage resolution falls as energy increases, ranging from 1.6% at 10 keV to only about 0.02% at 50 MeV.

Another physical process contributes to the energy resolution when measuring heavy charged particles (Linhard and Nielsen, 1962). Toward the end of their track in the detector, the particles become neutral while still possessing

† The value of F should, in principle, be determined by the charge production processes in the detector (Klein, 1968). In practice, trapping, and other unexplained factors in the detector material, degrade resolution. Hence the term "the effective value of F" in this text.

considerable kinetic energy. Their remaining energy can only be dissipated in atomic collisions and very little ionization is produced. As the process varies from one particle to the next, the "defect" in the signal is a statistically varying quantity. The contribution to energy resolution is negligible for light particles, but becomes significant for α particles, and may be dominant for heavy ions and fission fragments.

In an ideal detector, all the charge produced by photons or particles is collected to produce signal in the output circuit. In practice, some charge is lost, either by recombination, if the density of hole–electron plasma is high, or by trapping in the detector material during the collection process. The magnitude of the charge loss is usually small, but can become large where the plasma density is very high (e.g., fission fragments), or where the detector material exhibits substantial trapping. The effect of trapping becomes exaggerated where ionization is produced at random points in the detector volume, as in the case of γ-ray detection, since the amount of charge lost depends on the distance travelled by the carrier (hole or electron) susceptible to trapping. Although trapping is not a fundamental property, and its magnitude varies with detector operating conditions, its contribution to resolution can be serious in many applications. More details are given in Chapter III.A.

C. Noise Reduction

1. *General Classes of Noise Sources*

All spectrometers use pulse shaping as a method of minimizing the sensitivity of the analyzed signal to noise from various sources. The performance of a spectrometer is dependent on choosing the correct pulse shaper for a given application, so it is important to understand the basic mechanisms involved in noise filtering by pulse shaping.

Important noise sources include:

(a) Leakage current in the detector, which, in its simplest form, consists of discrete hole–electron pairs randomly created in the material by thermal excitation. The detector surfaces may also contribute leakage current.

(b) Any shunt resistance across the signal input circuit.

(c) Fluctuations in the current flowing through the first amplifying element.

(d) Fluctuations in current in the input lead of the amplifying element.

(e) Fluctuations in currents, and thermal noise in resistors used in later amplifier stages contribute noise, but this should be small compared with input circuit noise.

(f) Miscellaneous additional sources, less basic than those cited earlier. These include ac ripple, extraneous noise from contacts in components

(including "excess" noise of carbon resistors), high-frequency pickup from radio and TV stations, and microphonic effects in the detector–amplifier system.

Noise sources fall into two major classes. The first contains those that inject charge pulses into the input circuit (in the same way as the detector signal does). These sources have in common the fact that they produce voltage *step functions* at the input of the amplifier due to the integration of injected charge pulses by the total input circuit capacitance. As both the signal and these noise pulses are integrated by the input capacitance, the signal/noise ratio, for these sources only, is independent of input capacitance. We will call the contribution of these noise sources *step noise.*

The second class is typified by the fluctuations in current in the first amplifying element. They are equivalent to random sequences of *delta functions* of voltage at the input, whose magnitude is independent of the input circuit capacitance. The signal/noise ratio, in this case, is inversely proportional to the input circuit capacitance, so it is important to reduce the capacity to a minimum. This second type of noise will be termed *delta noise.*

Other types of noise sources occur in practice, which are not as basic as step and delta noise. They include noise due to charge injected slowly into the input circuit (e.g., surface noise in detectors), and noise due to the input amplifying element, and later stages, not represented by the simple delta-function voltage generator. In general, noise falling in these categories can be reduced by choosing suitable components, and its contribution to resolution can be made small.

Figure 5 shows the equivalent input circuit used to represent the signal, and the two basic types of noise. Photons or particles releasing a total charge Q in the detector produce voltage steps of amplitude Q/C at the preamplifier input, where C is the total input circuit capacitance. The individual electrons injected at random into the input circuit by the detector, and by other sources of leakage, produce steps of amplitude q/C at the preamplifier input (where q is the

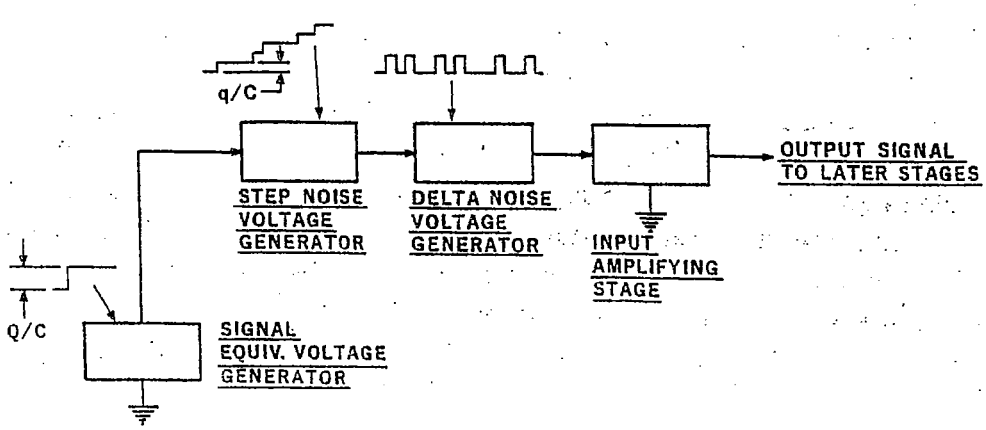

Fig. 5. Equivalent input noise sources in a spectrometer.

charge on the electron). Finally, fluctuations of current in the input element are represented by the delta voltage generator, the *area* of each delta pulse being proportional to q, and independent of C.

2. *Pulse Shaping*

a. General principles. Pulse shaping is carried out primarily to emphasize the signal as compared with the noise. All pulse shapers used in nuclear amplifiers perform some form of differentiation and integration. Differentiation serves the dual purpose of limiting the duration of any signal to a reasonable time to prevent its interfering with later signals, and also limiting the step noise, which would otherwise build up to an intolerable amount. Integration is required to average out fluctuations in delta noise.

A rough picture of the effect of a pulse shaper can be obtained by assuming that its effect is to restrict any measurement of the input signal to a period T_m. If the signal step input is accumulated for a time T_m, the signal output will be proportional to T_m. On the other hand, since the average number of delta-noise pulses is proportional to T_m, the fluctuation in this number, which determines the delta-noise output, is only proportional to $T_m^{1/2}$. Therefore the noise/signal ratio for delta noise must be proportional to $1/T_m^{1/2}$.

A different picture emerges for step-noise. Again, the fluctuation in the number of noise pulses is proportional to $T_m^{1/2}$, but each noise step is integrated for a time proportional to T_m, so the step noise at the output is proportional to $T_m^{3/2}$. Therefore, the noise/signal ratio for step noise is proportional to $T_m^{1/2}$.

These intuitive conclusions are correct for all shaping networks; as the characteristic shaping time is changed, delta noise changes as $T_m^{-1/2}$, while step noise changes as $T_m^{1/2}$. As the total noise is the quadrature sum of both, an optimum measurement time must exist. Unless other factors become more important than noise performance, it is best to operate at this optimum measurement time.

These general considerations show what occurs as the characteristic time constant of a given shaper is changed. Now, we must consider the factors that favor one pulse shape as compared to another. We assume that the output signal amplitude is measured at a fixed time T_m on the signal. The amplitude measured for a given signal is then the true signal amplitude plus (or minus) the cumulative effect of all noise steps (and deltas) occurring before T_m. It is convenient to define a *step-noise residual function* $R(t)$ that represents the effect at T_m of a unit-size noise step occurring t seconds before T_m. This function can be derived theoretically from knowledge of the pulse-shaping network parameters, or can be measured experimentally. It may be shown that the total mean square step-noise amplitude at T_m is

$$n_s \int_0^\infty \{R(t)\}^2 \, dt$$

n_s = average number of unit size noise steps per second.

As our purpose here is only to compare the influence of one pulse shape compared with another, we will not be concerned with absolute noise levels. It is useful therefore to derive a *step-noise index* reflecting only the effects of the pulse shaper. On this basis, n_s need not be included but the output signal amplitude S at the time T_m should be, as its value depends on the pulse shaper. As the factor of importance is the ratio of noise to signal, a convenient step-noise index is given by

$$\langle N_s^2 \rangle = (1/S^2) \int_0^\infty \{R(t)\}^2 \, dt \tag{4}$$

As is well known, the response of a network to a delta function is the differential of its step-function response. Following an analogous procedure to that used for step noise, the delta-noise residual function will be $R'(t)$, and the delta-noise index will be given by:

$$\langle N_\Delta^2 \rangle = (1/S^2) \int_0^\infty \{R'(t)\}^2 \, dt \tag{5}$$

The entire effect of pulse shapers on the signal/noise ratio is contained in Eqs. (4) and (5). Once $R(t)$ and S are established for various pulse shapes, evaluation of their relative noise performance is simply a matter of evaluating the indices $\langle N_s^2 \rangle$ and $\langle N_\Delta^2 \rangle$. The fact that $\{R'(t)\}^2$ appears in Eq. (5), while $\{R(t)\}^2$ appears in Eq. (4), implies that $\langle N_s^2 \rangle$ is always dimensionally equal to $\langle N_\Delta^2 \rangle t^2$, in agreement with our earlier intuitive conclusion about the effect of measurement time on step and delta noise.

Two quite different types of pulse shapers may be used in nuclear pulse processing systems. The commonest uses passive elements of fixed value to generate the desired output pulse shape. This type of shaper is called *time-invariant* to distinguish it from the *time-variant* pulse shaper where values of shaping elements are switched in synchronism with input signals. In the time-invariant class of shaper, the function $R(t)$ is the same as the signal output pulse shape since all noise steps are treated in exactly the same way as signals. However, $R(t)$ is not the same as the signal shape in the case of time-variant shapers, because the processing of a given noise step depends on its time of occurrence in relation to a signal.

Due to the limited nature of this account, we will not deal here with time-variant shapers, but will discuss three time-invariant shapers to illustrate their general features. More detailed treatments are available in the literature (Goulding, 1972).

b. Trapezoidal pulse shaper (time-invariant). This is difficult to realize in practice, but its simplicity is useful in pointing to general principles that affect the noise performance of various pulse shapes. Figure 6 shows the output signal pulse shape, and the functions $R(t)$, $R'(t)$, $\{R(t)\}^2$, and $\{R'(t)\}^2$ appropriate to this pulse shaper. As the output signal has been normalized to unity amplitude,

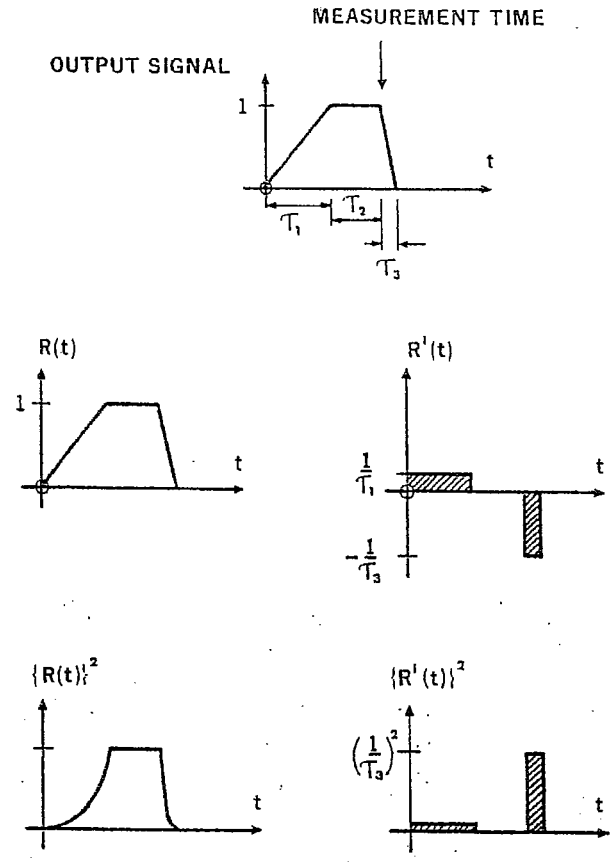

Fig. 6. Signal and noise functions for a trapezoidal pulse shaper (time-invariant).

computation of the noise indices for this shaper is simply a matter of determining the area under the functions $\{R(t)\}^2$ and $\{R'(t)\}^2$.

Derivation of the function $R(t)$ is the key step in calculating the noise indices for any shaper. As this shaper is time-invariant, $R(t)$ is the same as the signal response.

Computing the areas under $\{R(t)\}^2$ and $\{R'(t)\}^2$, we have

$$\langle N_s^2 \rangle = \tau_2 + (\tau_1 + \tau_3)/3 \tag{6}$$

$$\langle N_\Delta^2 \rangle = (1/\tau_1) + (1/\tau_3) \tag{7}$$

These relationships conform to our general conclusion regarding the effect of changes in the pulse time scale for the two noise components. If we apply the constraint that the whole pulse shall not occupy a total time greater than T, a time dictated by pileup considerations at high counting rates, the best noise performance is achieved by making $\tau_2 = 0$ and $\tau_1 = \tau_3 = T/2 = \tau_0$. This corresponds to a symmetrical triangular shape peaking at τ_0:

$$\langle N_s^2 \rangle = 2\tau_0/3 \tag{8}$$

$$\langle N_\Delta^2 \rangle = 2/\tau_0 \tag{9}$$

As we will see in the next section, a flat top is desirable to reduce the effects of fluctuations in detector signal rise time; the consequent noise degradation caused by a short flat region can be determined from Eqs. (6) and (7).

Using this example, several general conclusions are forthcoming:

(i) The step-noise index is proportional to the pulse time scale.
(ii) The delta-noise index is inversely proportional to the time scale.
(iii) Delta noise results mostly from the fast changing parts of the signal.

Assuming a maximum total pulsewidth, dictated by counting-rate considerations, this implies that symmetrical pulse shapes are preferred, and that pulse shapes like a triangle, where the rate-of-change is constant during rise and fall, give the best delta-noise performance.

c. Equal RC integrator and differentiator. A common pulse shaper employs an RC differentiator, and an RC integrator, each having the same RC time constant. While this network has been superseded by more sophisticated shapers in recent years, primarily to achieve better performance at high counting rates, some aspects of its behavior warrant consideration.

Normalizing to unity peak signal amplitude the signal response is given by

$$\text{Output} = (t/\tau_0)e^{1-(t/\tau_0)} \tag{10}$$

where τ_0 is the RC time constant.

As the network is time-invariant, the $R(t)$ function is the same as the signal response. We have

$$\langle N_s^2\rangle = \int_0^\infty \frac{t^2}{\tau_0^2} \exp\left\{2\left(1-\frac{t}{\tau_0}\right)\right\}dt = 1.87\,\tau_0 \tag{11}$$

$$\langle N_\Delta^2\rangle = \frac{1}{\tau_0^2} \int_0^\infty \left(1-\frac{t}{\tau_0}\right)^2 \exp\left\{2\left(1-\frac{t}{\tau_0}\right)\right\}dt = \frac{1.85}{\tau_0} \tag{12}$$

These results can be compared directly with the symmetrical triangle results of Eqs. (8) and (9), remembering that both waveforms peak at a time τ_0 after the start of the signal. However, it should also be remembered that the triangle is complete in a time $2\tau_0$, while the long tail on the RC integrator–differentiator pulse shape persists for a very long time. Therefore, in using a triangular shaper, it is obviously desirable to peak at a larger value of τ_0 than when using the RC shaper, thereby reducing the delta noise. For the purpose of illustration, suppose the RC shaper peaks at 1 μsec while the triangle peaks at 2 μsec. We then have

	Triangle	RC Shaper
$\langle N_s^2\rangle$	1.33×10^{-6}	1.87×10^{-6}
$\langle N_\Delta^2\rangle$	1.00×10^{6}	1.87×10^{6}

We see that the triangle is better with regard to both noise indices while returning to the baseline in a shorter time.

d. Gaussian-shaped pulse. Most modern nuclear pulse amplifiers employ a shaper containing a single RC differentiator, and several RC integrators having the same RC time constant (Fairstein and Hahn, 1965). If the number n of RC integrators is sufficient, a quasi-Gaussian-shaped pulse results with the form, normalized to unity amplitude at a peaking time τ_0, given by

$$\text{Output} = \left(\frac{t}{\tau_0}\right)^n \exp\left\{n\left(1 - \frac{t}{\tau_0}\right)\right\} \tag{13}$$

Taking $n = 4$, the output pulse is given by

$$\text{Output} = \left(\frac{t}{\tau_0}\right)^4 \exp\left\{4\left(1 - \frac{t}{\tau_0}\right)\right\} \tag{14}$$

When analyzed in the same way as in the previous examples, the noise indices are

$$\langle N_s^2 \rangle = 0.90\ \tau_0 \tag{15}$$

$$\langle N_\Delta^2 \rangle = 2.04/\tau_0 \tag{16}$$

The Gaussian-shaped pulse approaches the symmetry of the symmetrical triangle, so it is reasonable to compare the two cases with the same peaking times. Therefore, Eqs. (15) and (16) should be compared with Eqs. (8) and (9). The delta-noise performance is essentially the same for the two cases, but the step-noise index of the Gaussian is about 40% worse than that of the symmetrical triangle. Also, the Gaussian pulse tail extends for some time past the end of the triangle.

On the basis of these results, a symmetrical-triangle shaper would be preferred to either the Gaussian or the RC integrator–differentiator shapers. However, the delay lines required in triangular shapers are inconvenient to use, and suffer from secondary problems. Consequently, use of the Gaussian shaper has become common practice whenever time-invariant shapers are used.

D. The Input Circuit and Preamplifier

1. *General Features*

In the previous section, we discussed the role of pulse shaping in reducing the effect of noise of both types on signal amplitude measurement. However, the absolute magnitude of these types of noise, as well as that of any additional types, is determined by the physical processes occurring in various elements in the input circuit, and in the input stage of the preamplifier. Optimum choice of components, and their operating conditions is therefore important.

a. Preamplifier and detector configurations. A charge Q, released in a detector, flows into an input circuit of total capacitance C, and produces a

voltage signal Q/C. A simple form of preamplifier amplifies this voltage signal. For example, a 1-keV X ray releases about 5×10^{-17} C of charge in a silicon detector, producing a signal of only 10 μV in 5 pF, a typical total input capacity. On the other hand, a 100-MeV particle produces 1 V in a similar system.

In a voltage-sensitive system, the output signal is inversely proportional to the total input capacitance. As the detector capacity usually varies with bias voltage, and may change with temperature and time, the output signal is not stable. Consequently, the charge-sensitive preamplifier configuration shown in Fig. 7 is commonly used. It uses an operational amplifier, with a feedback capacitor C_F to the input, acting as a charge integrator. The output signal is Q/C_F if the gain within the feedback loop is large, so is almost independent of C, the shunt input capacitance.

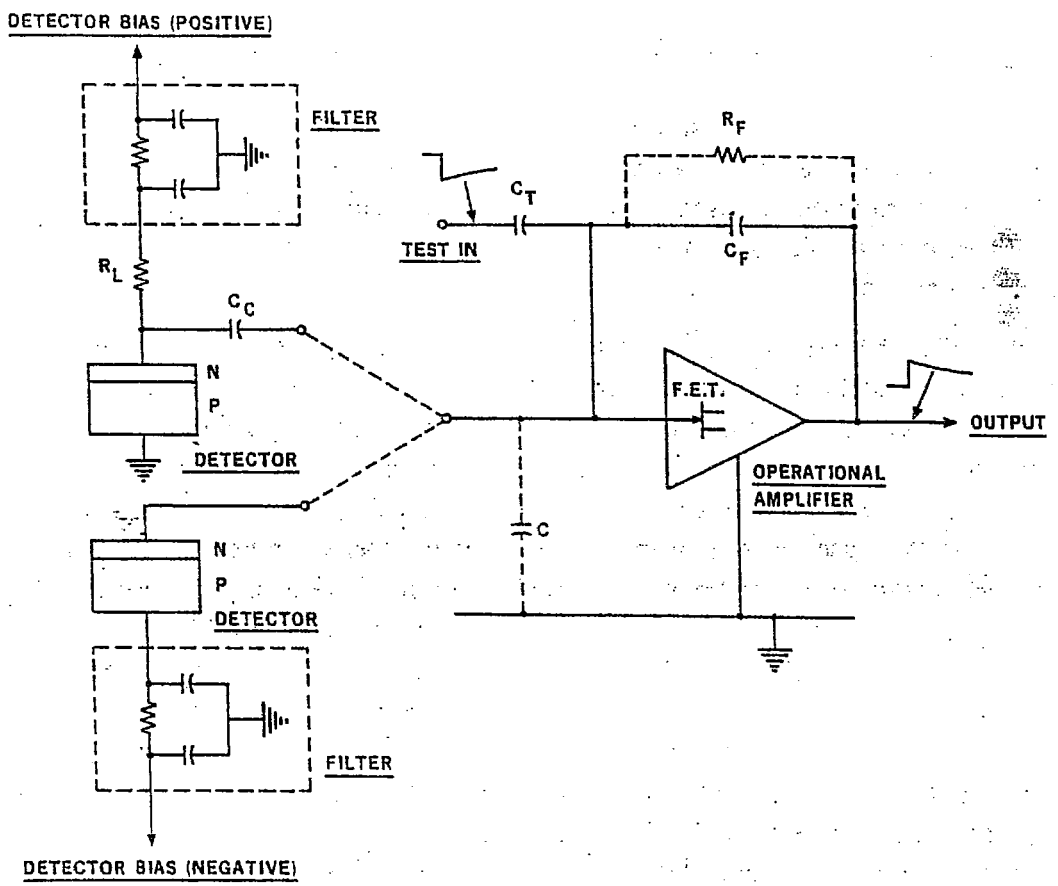

Fig. 7. Charge-sensitive preamplifier configuration.

Two types of detector connection are used depending on the application; both are shown in Fig. 7. In the dc connection shown in Fig. 8, detector leakage current flows in the preamplifier input, and the design must allow for this. However, its use eliminates the stray capacitance to ground of the coupling capacitor C_C and load resistor R_L used in the ac-coupled circuit shown in Fig. 7, thereby effecting an improvement in signal/noise ratio. The dc connection is

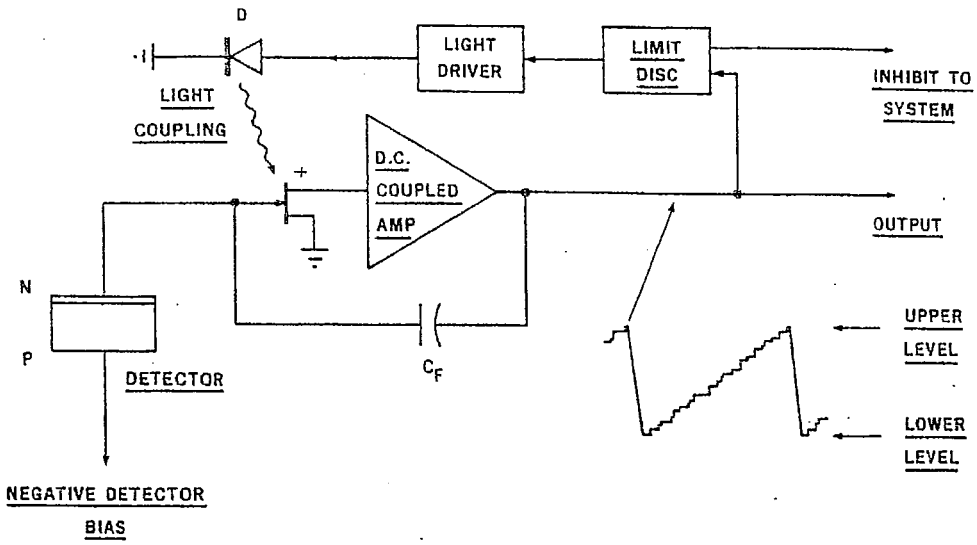

Fig. 8. Pulsed-light feedback method of discharging the feedback capacitor.

always used in X-ray systems, and in most germanium γ-ray systems. The detector and field-effect transistor are cooled in a cryostat to low temperatures. The ac connection is used in less critical systems, like those employed in high-energy particle experiments; where the detector and preamplifier are operated at room temperature.

b. The recharge path in charge-sensitive preamplifiers. The resistor R_F serves to discharge the feedback capacitor C_F to prevent the operational amplifier stages from being overloaded by pileup of input pulses. The decay time constant $R_F C_F$ must be made long compared with the amplifier pulse shaping times. In typical germanium γ-ray systems, and particle spectrometers, values of $R_F C_F$ of 500 μsec are common, but much larger values are required in high-resolution X-ray systems. This implies values of R_F ranging from 200 MΩ to 10^5 MΩ. Such resistors are bulky, adding capacitance from input to ground, and they rarely behave as pure resistors in the frequency range of interest for nuclear pulse amplifiers. The frequency variation of R_F causes a complex decay shape on output pulses that causes serious problems in the behavior of spectrometers at high counting rates. R_F also acts as a parallel resistive impedance generating noise in the input circuit.

Many recent X-ray spectrometers use a pulsed feedback method (Landis *et al.*, 1971) to discharge the capacitor C_F, and the resistor R_F is omitted. A scheme of this type is shown in outline in Fig. 8. A dc detector connection is used, and C_F is discharged by pulsing a light emitting diode D which couples by a light path to the field-effect transistor. When the light is turned on, it produces current in the drain to gate junction of the field-effect transistor (which is photosensitive) to discharge C_F. In normal operation, both detector leakage and the charge in signals cause a slow rise in the output voltage; when this reaches the upper discriminator level, the light-emitting diode is turned on to discharge

C_F, and to force the preamplifier output down. When the output level reaches the lower discriminator level, the light is turned off, and the preamplifier returns to its normal counting mode. During the reset period, and for a reasonable interval thereafter, the whole pulse processing system is deactivated by a waveform derived from the limit discriminator, thereby avoiding any adverse effects resulting from the large negative reset signal. In a high-resolution X-ray system, the silicon detector leakage is typically in the 10^{-14} A range, the feedback capacitor is 0.2 pF, and the voltage swing permitted at the preamplifier output is two volts. Light pulses occur about once every 10 sec in the absence of radiation in the detector. The reset time is about 5 μsec, a negligible time compared with the time between resets, even at high counting rates.

2. *Physical Sources of Noise*

Nuclear spectrometers use detectors having a wide variety of sizes, and capacitances, and operating at temperatures ranging from room temperature to 77°K (occasionally even at 4°K) with consequent large variations in detector leakage. This makes optimization of the input circuit a complex problem. Although field-effect transistors† are universally employed as the first amplifier, the type of FET used, its temperature of operation, the values of the feedback components, and even the choice of pulse shaper and its characteristic time constants, are all intimately linked to the type of detector, its operating temperature, and the energy range to be studied. Understanding the interrelationships between these various parameters requires knowledge of noise mechanisms, and the effect of pulse shaping on their contributions to the resolution.

a. Delta-noise contributions. Delta noise (see Section II.B) is due almost entirely to the FET if no significant series resistances (e.g., due to poor contacts) are present in the input circuit. Channel noise (Van der Ziel, 1962) in field-effect transistors can be represented by a voltage generator v_Δ in the input circuit whose mean square value is given by the formula

$$\langle v_\Delta{}^2 \rangle = 4kT R_{eq}\, \Delta f \quad (\text{volts})^2 \tag{17}$$

where k is Boltzmann's constant, T = temperature (°K), R_{eq} = equivalent noise resistance of the FET, and Δf = the frequency increment on which v_Δ is observed.

The value of R_{eq} is generally assumed to be

$$R_{eq} = \frac{0.7}{g_m}\left(1 + \frac{C_{gs}}{3C}\right) \tag{18}$$

where g_m = transconductance of the FET, C_{gs} = gate-source capacitance, and C = total input circuit capacity.

† The reader not familiar with the operation of bipolar and field-effect transistors should

For practical purposes it is convenient to approximate this relationship by

$$R_{\text{eq}} \simeq 1/g_m \tag{19}$$

The total delta noise at the amplifier output is given by integrating this noise over the passband of the system. If the gain–frequency characteristic of the pulse shaper is represented by $G(f)$, and if $\langle V_\Delta{}^2 \rangle$ is the mean square value of the delta noise (voltage) at the amplifier output, we have

$$\langle V_\Delta{}^2 \rangle = \int_0^\infty (4kT/g_m)\{G(f)\}^2\, df \quad (\text{volts})^2 \tag{20}$$

If the measured signal amplitude at the amplifier output produced by 1-eV energy absorption in the detector is S_0, the output delta noise can be expressed in terms of equivalent energy fluctuation E_Δ in the detector as

$$\langle E_\Delta{}^2 \rangle = (1/S_0{}^2) \int_0^\infty (4kT/g_m)\{G(f)\}^2\, df \quad (\text{eV})^2 \tag{21}$$

It is convenient to discuss noise in terms of a voltage-sensitive configuration (the same final result applies to a charge-sensitive stage if the feedback components are regarded as being in parallel with the input circuit), in which case the value of S_0 can be expressed as

$$S_0 = (qP_0/\epsilon C) \tag{22}$$

where P_0 = the peak amplifier output for a unit voltage step at the preamplifier input, ϵ = the average energy absorbed per hole–electron pair produced in the detector, q = charge on the electron, and C = total input circuit capacitance. Combining Eqs. (21) and (22) we have

$$\langle E_\Delta{}^2 \rangle = \left\{\frac{4k\epsilon^2}{q^2}\right\}\left\{\frac{TC^2}{g_m}\right\}\left[\frac{1}{P_0{}^2}\int_0^\infty \{G(f)\}^2\, df\right] \quad (\text{eV})^2 \tag{23}$$

The final main term in this expression is controlled by the pulse shaper, the second term is mainly dependent on the field-effect transistor, its temperature, and the detector capacitance, while the first term depends only on the detector material.

Equation (23) is the frequency–domain equivalent of the time domain Eq. (5) in Section II.C.2, but it contains the physical parameters of the input circuit, and can therefore be used to calculate the absolute value of the noise for a specific pulse shaper. The time–domain relationships of Section II.C.2, however, are better suited to comparing the various types of pulse shaper, so, if one type of pulse shaper is analyzed using Eq. (23), relationships similar to those developed in Section II.C.2 can be used to obtain absolute values of the noise for any other type of pulse shaper. A convenient pulse shaper to use as a standard is the equal time constant RC integrator–differentiator network. For this network

$$P_0 = e^{-1} \qquad \text{and} \qquad G(f) \doteq 2\pi f \tau_0/(1 + 4\pi^2 f^2 \tau_0{}^2)$$

where τ_0 is the RC time constant in the shaper. Substituting this into Eq. (23), and performing the integration, we obtain the result:

$$\langle E_\Delta{}^2 \rangle = 0.5 \frac{k\epsilon^2}{q^2} \frac{TC^2}{g_m} \frac{e^2}{\tau_0} \tag{24}$$

where $\langle E_\Delta{}^2 \rangle$ is the mean square value of the energy resolution contribution due to FET channel noise.

b. Step-noise contributions. As seen in Section II.C, sources of step noise include leakage currents and shunt resistance in the input circuit. Leakage current is produced both by the detector and by the field-effect transistor, while shunt-resistance noise arises mainly in the feedback resistor.

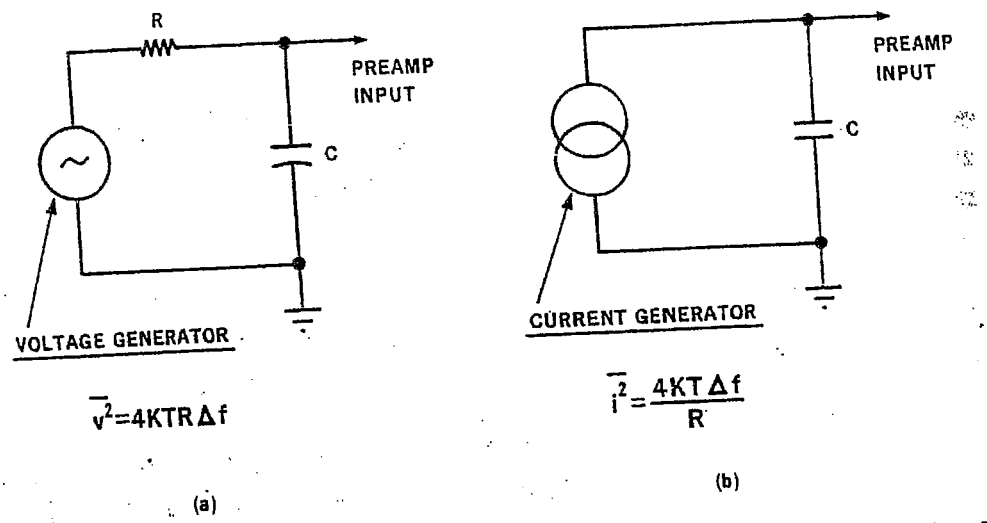

Fig. 9. Equivalent circuits for shunt resistance noise: (a) General case; (b) when $RC \gg$ time constant of pulse shaper.

The noise introduced by shunt resistance is minimized by making the value of the resistance very large. Figure 9a shows the effective input circuit for resistance noise. The mean square noise $\langle v^2 \rangle$ in the shunt resistance R is given by

$$\langle v^2 \rangle = 4kTR\,\Delta f$$

where Δf is a small frequency increment.

The mean square value of the noise voltage developed across the input capacitance C in the frequency increment Δf, centered on the frequency f, is then given by

$$\langle v^2 \rangle = 4kT(R/(1 + 4\pi^2 f^2 C^2 R^2))\,\Delta f \tag{25}$$

If the amplifier passband is narrow, Eq. (25) implies that variation of R produces maximum noise when

$$R = 1/2\pi fC \tag{26}$$

When R is increased to a large value, the noise approaches zero. This is the condition desired in low-noise preamplifiers.

A signal measurement time of τ_0 is approximately associated with a passband centered on a frequency $f = 1/2\pi\tau_0$, so the condition applied to R, derived from Eq. (26) is

$$RC \gg \tau_0 \tag{27}$$

If this condition is met, Eq. (25) becomes

$$\langle v^2 \rangle = (kT/\pi^2 f^2 C^2 R)\Delta f \tag{28}$$

This equation leads to the equivalent input circuit shown in Fig. 9b, where the resistor is replaced by a noise current generator. The mean square fluctuation in a saturated current I is given by the formula

$$\langle i^2 \rangle = 2qI\Delta f \tag{29}$$

Across a capacity C, this produces a mean-square voltage $qI\Delta f/2\pi^2 C^2 f^2$. Comparing this with Eq. (28), we see the resistor R can be replaced by an equivalent saturated current I_{eq} given by

$$I_{eq} = 2kT/qR \tag{30}$$

To compare the shunt resistor noise contribution with that due to leakage currents, it is only necessary to compare the value of I_{eq} given by Eq. (30), with the value of the leakage currents. For example, a resistor of $10^{12}\ \Omega$ at 77°K is equivalent to a current of about 10^{-14} A. As this is typical of the detector and FET leakages in silicon X-ray spectrometers, values of $R \gg 10^{12}\ \Omega$ must be used—this is only realized satisfactorily by using the pulsed-light feedback method of Fig. 8. A much smaller value of R is tolerable in high-energy γ-ray spectrometers, where germanium detectors exhibiting 10^{-10} A leakage current are often used, and in particle spectrometers where detectors are used at room temperature.

Equation (29) permits calculation of the total step noise due to input circuit currents, and shunt resistance, if the current I is interpreted as the sum of the *absolute* values of all currents, plus the current equivalent of shunt resistance as given by Eq. (30). The mean square voltage produced by this noise current across the preamplifier input is then

$$\langle v^2 \rangle = qI\Delta f/2\pi^2 f^2 C^2 \tag{31}$$

Using the gain–frequency characteristic $G(f)$ of the pulse-shaping network as in Eq. (20), the total step-noise contribution at the amplifier output is given by

$$\langle V_s^2 \rangle = \frac{qI}{2\pi^2 C^2} \int_0^\infty \frac{(G(f))^2}{f^2}\, df \tag{32}$$

Using the signal response of the amplifier in the same way as in Eqs. (21), (22) and (23), and applying it to step noise, we have

$$\langle E_s^2 \rangle = \left[\frac{\epsilon^2}{2\pi^2 q}\right] I \left[\frac{1}{P_0^2} \int_0^\infty \frac{(G(f))^2}{f^2}\right] df \quad (\mathrm{eV})^2 \tag{33}$$

The final term of Eq. (33) is dependent on the pulse shaper used in the amplifier, and is analogous to the expression in Eq. (4), where the pulse-shaper behavior is expressed in the time domain. As discussed for delta noise, Eq. (33) can be used to calculate the absolute value of step noise for one type of pulse shaper, and the relationships in Section II.B used to modify the result for any other shaper. For the equal time-constant RC integrator–differentiator, the mean square value of the step noise, expressed as equivalent energy absorption in the detector, is given by

$$\langle E_s^2 \rangle = \frac{\epsilon^2}{4q} I e^2 \tau_0 \tag{34}$$

where e is the base of natural logarithms.

c. Overall behavior with time constant. As indicated by Eqs. (24) and (34), the step noise rises with increasing pulse-shaper time constant, while the delta noise decreases. Figure 10 shows the overall behavior expected for a typical case. The total input leakage is assumed to be 10^{-13} A, the detector is assumed to be silicon used at 77° K, while the FET is assumed to exhibit a g_m of 5 mA/V, and is operated at 100° K. A total input capacitance of 5 pF is assumed. The left scale indicates the mean square resolution expressed in hole–electron pairs ($\overline{N^2}$)

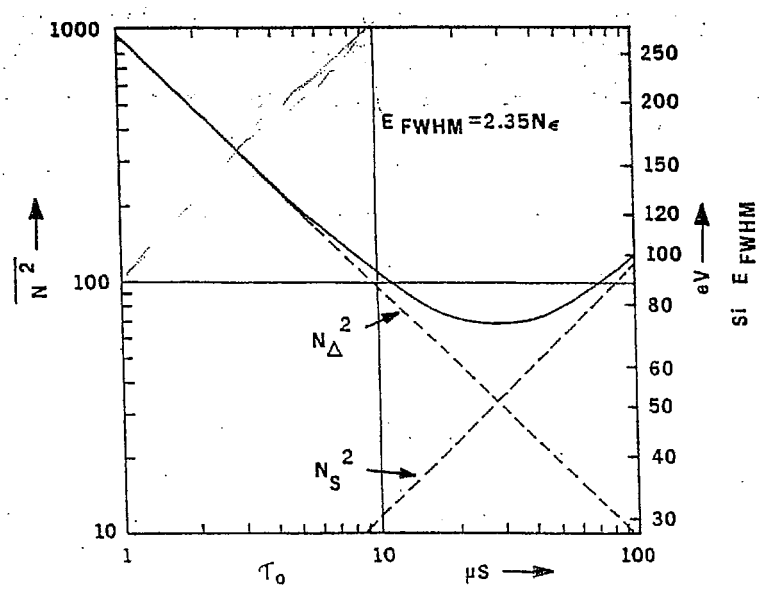

Fig. 10. Resolution as a function of time constant. (Silicon detector at 77° K, FET 5 mA/V at 100° K, 5-pF total capacitance, 10^{-13}-A total leakage.)

while the right scale shows the energy resolution in eV. Similar graphs can be constructed for any set of parameters, but the results should only be used as a guide, as measured results generally deviate significantly from the calculated ones due to extraneous noise sources. To modify the results for other types of pulse shaper, calculations like those discussed in Section II.B should be used.

d. Optimization of the field-effect transistor. The FET contributions to noise are represented by the second term ($\langle E_\Delta{}^2\rangle \propto (TC^2/g_m)$) in Eq. (23), and by the second term (I) in Eq. (33), where I is partially due to gate current in the FET. Lowering the FET temperature reduces its gate leakage by a factor near two for every 10°C fall in temperature. It also reduces the delta noise, in a direct sense due to the appearance of T in Eq. (23), and also in an indirect way, as the mutual conductance of the FET increases when T is reduced. This results from the increase in carrier mobility in the FET channel at low temperatures. Experience has shown, however, that an optimum temperature exists for the operation of a given FET in low-noise preamplifiers. The best FETs generally optimize in the region of −130°C; to achieve this temperature in a liquid-nitrogen cryostat, a heater is often used for the FET.

Choice of a particular type of FET for a given application depends partly on its ability to behave well when cooled, but the term C^2/g_m appearing in Eq. (23) is the major factor governing the choice of FET.

We have already pointed out the importance of reducing the capacity C to a minimum. To do this, stray capacitance should be minimized, and special FET packages are sometimes used, but the detector capacity, which is included in C, and which is dictated by the size of the detector, is always present. Small X-ray detectors exhibit about 1-pF capacitance, planar germanium γ-ray detectors are usually about 10 pF, large coaxial detectors might be 50 pF, while very thin silicon particle transmission detectors range as high as 1000 pF. No one type of FET can be matched to all cases.

The ratio of C_F/g_m (where C_F is the FET input capacity) is found to have an almost constant value ϕ for FETs representing the limit of the state of the art; for large area structures both g_m and C_F are large, and vice versa for small structures. If the detector capacity is C_D, the term C^2/g_m appearing in Eq. (23) can be written as

$$\phi(C_F + C_D)^2/C_F$$

This has a minimum value when $C_F = C_D$, so, by choosing the FET on the basis of satisfying this condition, the signal/noise ratio is optimized. While this result is only approximate, the general trend is obeyed, and it is best to use a large area FET with high-capacity detectors, and vice versa.

e. Resolution of detector and amplifier combination. Statistical effects in the charge production in the detector, and those due to electronic noise, can be combined in quadrature to yield the energy resolution of a spectrometer for different radiation energies. Figures 11 and 12 show the resolution of silicon and

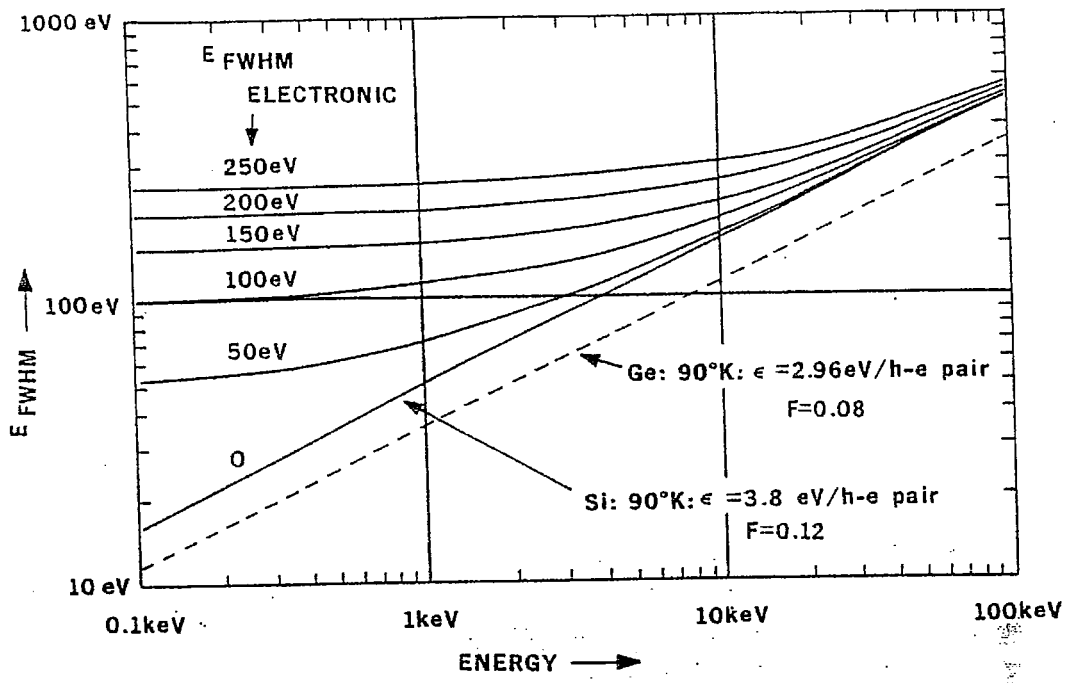

Fig. 11. Energy resolution of a silicon detector system as a function of energy and electronic noise in the range 0.1 to 100 keV. The best achievable germanium detector resolution is also shown.

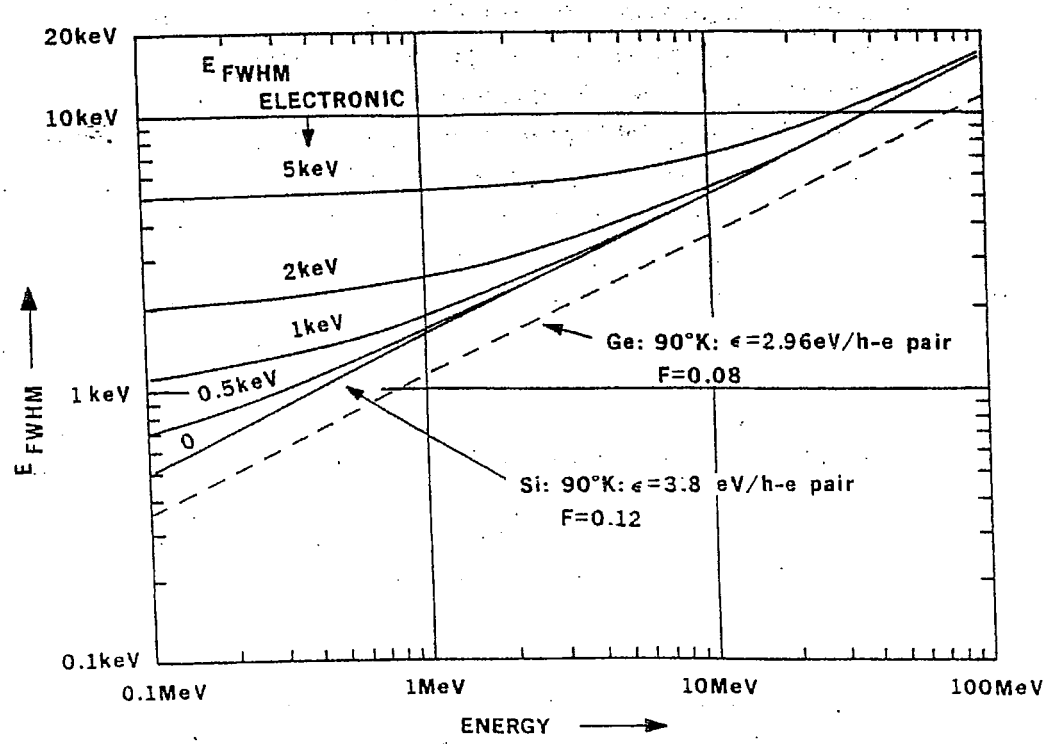

Fig. 12. System energy resolution in the range 0.1 to 100 MeV (see Fig. 11).

germanium detector systems as a function of energy, and of the electronic noise in the systems. Figure 11 covers the low energy range; the main curves are for a silicon detector used at 77°K; the detector contribution alone for an outstanding germanium detector is also shown. Figure 12 shows the behavior at high energies. Figure 11 is applicable to X-ray systems, while Fig. 12 is more useful for high-energy particle, and gamma-ray spectrometers. As indicated in Section II.B other statistical effects in detectors must be added to those shown in these figures, particularly if high-energy particles or heavy ions are measured. For γ-rays of energy below 1 MeV, and for X-ray detectors, the curves of Figs. 11 and 12 represent the actual performance when good (low-trapping) detector materials are used.

E. Effects of Fluctuations in Detector Signal Rise Time

In most applications, the rise time of the detector pulse, which depends on collection of charge in the detector, is much shorter than the measurement time of the pulse shaper. Sometimes, however, short time constants are used in the shaper, and the rise time of the detector signal may be a significant fraction of these times. Changes that occur in detector pulse rise time then result in changes in amplitude of the amplifier output signal. This is particularly true where the output pulse shape exhibits a sharp peak (the triangular pulse shape is an example).

Two specific effects occur in nuclear spectrometers due to the sensitivity of output pulse shape to detector pulse rise time variations. In particle experiments, the varying ranges of particles of different energies produce changes in the signal rise time. If the pulse shaper is such that the output is sensitive to detector pulse shape, a nonlinearity in the overall output versus energy response results. This effect can be quite large if suitable precautions are not taken to guard against it.

An even more important consequence occurs in γ-ray spectrometers. The γ-rays interact at random places in the detector volume, and the varying source of charge in the detector produces statistical fluctuations in the pulse shape. Typically, the rise time varies from 50 to 100 nsec. The absolute value of the pulse-amplitude spread introduced by this effect is proportional to the size of the signal. Therefore, even if the spread caused by rise time fluctuations is small compared with other contributions (e.g., electronic noise) at low energies, it may become quite significant at high energies. In practice, it becomes important at energies greater than 500 keV when using large germanium detectors; it therefore becomes a factor, in addition to those described in Section II.B, in the selection of the optimum pulse shaper for these applications.

From the foregoing discussion it is clear that pulse shapes exhibiting rather flat tops should be used to reduce the effect of detector signal rise times. As seen in the discussion of the trapezoidal time-invariant pulse shaper in Section II.C.2, a small penalty in noise must result from provision of a flat top on the pulse, and

this general conclusion applies to all shapers. However, at high energies, electronic noise is usually a minor contributor to resolution, and it is reasonable to select a network optimized for the effect of detector signal rise time variations. The Gaussian-shaped pulse, or, preferably, a trapezoid produced by a time-variant shaper (Radeka, 1972), represent good choices for these high-energy γ-ray spectrometers.

F. Degradation Factors at High Counting Rates

1. *General Remarks*

In our noise analysis, we tacitly assumed that each signal could be treated as a separate entity modulated by noise. However, each signal is also superimposed on the residue of all previous signals. The interference between signals can conveniently be studied by breaking the time domain into three regions.

(a) Two pulses may occur within the normal signal pulse width thereby grossly changing the amplitude of one or both signals. This process, called "pileup," is handled by providing a pileup rejector circuit that inspects for pulse pileup. and rejects one or both pulses from the analysis system if pileup is sensed.

(b) Secondary effects normally produce a low-level aftershock following each pulse that may interfere with a following signal. The low level of the aftershock precludes its detection by rejection circuits; consequently, one objective in spectrometer design is to eliminate aftershocks.

(c) Long-term baseline fluctuations are inevitable in any pulse measuring system. In effect, all pulse amplitude measurements are made with reference to a reasonable time average of the baseline—this implies extracting the ac components of the amplifier output. As the average level of the signal pulse train must be zero (after ac coupling), the pulse baseline (assuming positive pulses) is depressed by an amount proportional to the product of counting rate, pulse width, and average amplitude. To remove the effect of this varying baseline, a dc restorer reestablishes a baseline at zero (or a known reference level) in the pulse amplitude measuring system. If the dc restoration system is made to respond very quickly to departures of the baseline from zero, it will respond to noise, and will significantly worsen the noise performance of the spectrometer. However, if it responds very slowly, it will permit serious fluctuations of the baseline to occur, and the resolution at high counting rates will be degraded. Therefore, careful choice of the response time of a baseline restorer must be made to match it to the application, taking into account the appropriate balance between noise and counting-rate factors.

Additional secondary effects may arise at high counting rates, and care must be taken to avoid them. In particular, the long signal pulses present in amplifier

(and preamplifier) stages prior to the main differentiator will stack up to change the effective operating point of these stages. Due to this factor, the main differentiator of the pulse shaper is usually placed early in the amplifier: integrators can be placed late with advantage. Despite this precaution, care must be taken to recognize the possibility of stack up in the front end stages, and to design them to maintain virtually constant gain over their full operating range. Otherwise gain fluctuations will result, with disastrous consequences to resolution.

We will now examine, in more detail, the three time regions responsible for major degradations of performance at high counting rates.

2. *Pulse Pileup*

Pileup will be discussed with reference to Fig. 13a. Signals are measured at their peak time T_m, and vanish well into baseline noise at T_w. The effects of pileup between two signals whose starts are separated by T_0' are as follows:

(a) If $T_0' < T_m$, both peak amplitudes are changed and both pulses should be rejected.

(b) If $T_m < T_0' < T_D$ (where $T_D = T_w - T_m$), only the second amplitude is affected, and only that pulse should be rejected.

(c) If $T_0' > T_D$, no interference in amplitude occurs.

A pileup rejector satisfying these conditions will reject the same total number of pulses as would be rejected by an inspector that rejected all pulses that follow an earlier pulse within a time T_w (since $2T_m + (T_D - T_m) = T_w$). This fact permits simple calculation of the losses due to the pileup rejector. For an input counting rate n, the output counting rate is given by

$$N = ne^{-nT_w} \tag{35}$$

This equation indicates that the output rate peaks as the input rate reaches a value $1/T_w$, then decreases for further increasing input rate.

The effects of pileup are directly dependent on the total width of the signal. By using a symmetrical pulse as illustrated by the Gaussian-shaped pulse of Fig. 13b, noise performance can be improved while maintaining T_w smaller than for the asymmetrical pulse of Fig. 13a.

The methods used to achieve pileup rejection will be discussed in Section III.B. In principle, they consist of delaying the measurement of any signal pulse until inspection circuits have determined that it is not subject to interference by other pulses. If such interference is present, the measurement of the pulse is not performed.

3. *Aftershock Effects*

Unless care is taken in the design of the pulse processing system, and components are carefully selected, signal pulses in the system can produce

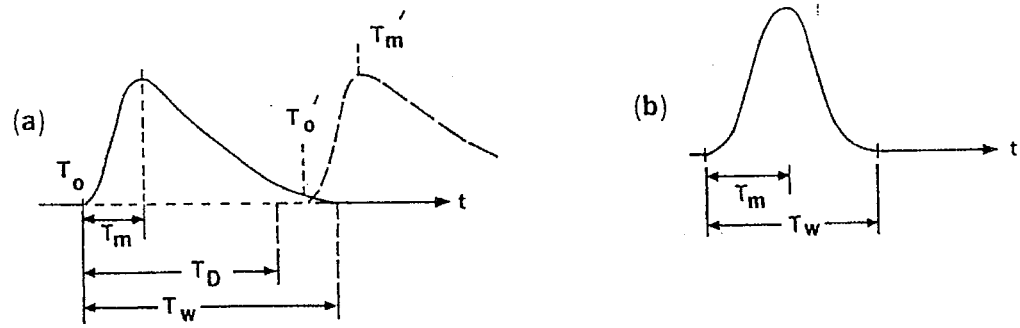

Fig. 13. Illustration of signal pileup: (a) *RC* differentiator–integrator pulses; (b) ideal Gaussian-shaped pulse.

significant effects considerably later than the main pulse. The commonest source of such effects in the system is the presence of *RC* differentiators, other than the one required in the main pulse shaper. Suitable circuit design, as discussed in the following paragraphs, can largely avoid this problem; however, spurious effects, not so easily identified, may also cause aftershocks. The feedback resistor in a preamplifier can produce these effects, while charge storage in surface layers of the detector, or in the field-effect transistor, can cause similar problems in pulsed-light feedback preamplifiers (see Section II.D). Long term energy storage and multiple reflections in delay lines also contribute to aftershock when delay lines are used in pulse shapers. Even transistors in the output stages of amplifiers can be a source of such effects. These are but a few of the sources of low-level disturbances following signal pulses; to identify them (and other sources) and establish their effect on the resolution of a spectrometer at high counting rates is a difficult problem.

A differentiator is essential in the pulse shaper to return the output pulse to its baseline in a reasonable time, and thereby to reduce pileup effects. In certain cases, a second differentiator having the same, or nearly the same, value as the first may be used to produce a bipolar pulse which achieves area balance between the positive and negative parts of the pulse in a short time, so that the baseline between pulses is a true zero, and is independent of counting rate. While double differentiation causes a penalty in delta-noise performance (this can be analyzed by the method of Section II.C), the bipolar pulse it produces eliminates the long term baseline fluctuations which must be circumvented by other methods if unipolar pulses are employed.

Apart from the use of a second differentiator to deliberately develop a bipolar pulse (where this is desired), it is important to avoid second, or multiple, differentiators, comparable in time constant to the primary differentiator in the pulse shaper. The effect of a second differentiator, whose time constant is a few times longer than the one used in the shaper, is to produce a reverse-polarity overshoot following the pulse, the duration of the overshoot being determined

primarily by the second differentiator. Its amplitude, expressed as a fraction of the signal, is approximately equal to the ratio of the two time constants. This overshoot constitutes an aftershock, and any second pulse falling on it will be distorted. Since the overshoot subtracts from the second pulse, it has the effect of distorting spectral peaks on the low-energy side, the degree of broadening increasing at high counting rates. On the other hand, multiple differentiators produce a complicated aftershock pattern with as many zero crossings as there are extra differentiators, so their effect on spectral peaks is more complicated.

These arguments lead to the conclusion that any additional differentiator, over and above the one in the pulse shaper, should have a very long time constant compared with it. If the system resolution capability is 0.1% (not an uncommon value), any second differentiators should be at least 10^4 times longer in time constant than the one used in the pulse shaper. This implies that ac couplings in the system should be avoided where possible, or should have time constants greater than 0.1 sec. If a shorter time constant ac coupling occurs in the signal path, it is essential that a compensation circuit be included to correct for its effect. One unavoidable differentiator is the feedback resistor–capacitor combination in resistive-feedback preamplifiers. The RC time constant is usually in the range of a few hundred microseconds; it is therefore only removed from the pulse-shaper time constant by a factor between 10 and 1000. "Pole-zero" cancellation (Nowlin and Blankenship, 1965), as discussed in the next paragraph, must be employed to correct for this RC differentiator, otherwise the behavior at high counting rates is seriously degraded.

Figure 14 shows the arrangement used to achieve pole-zero cancellation for the additional differentiator C_1R_1. The resistor R_C appearing across the main shaper differentiator capacitor C is the key component in achieving the cancellation. The transmission of the circuit is given by

$$\text{Transmission} = \frac{j\omega C_1 R_1}{1 + j\omega C_1 R_1} \frac{R}{R + R_C/(1 + j\omega C R_C)}$$

where $j = (-1)^{1/2}$ and $\omega = 2\pi f$.

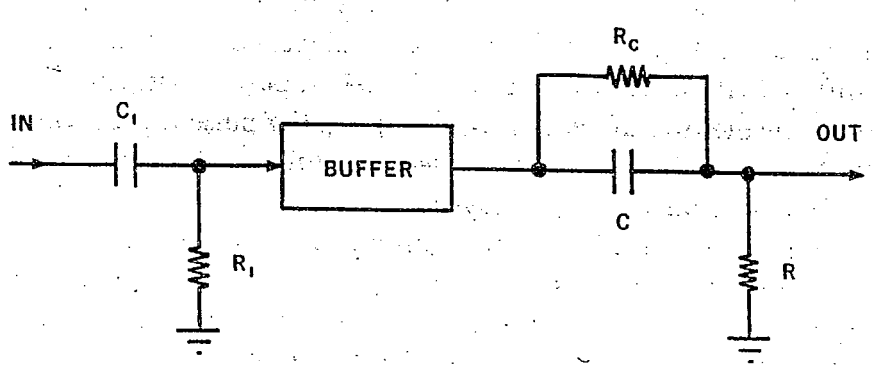

Fig. 14. Pole-zero cancellation circuit.

By making $CR_C = C_1R_1$, $1 + (R_C/R) = n$ and $C_1R_1 = n\tau_0$, this expression becomes

$$\text{Transmission} = j\omega\tau_0/(1 + j\omega\tau_0)$$

which corresponds to a single RC differentiator of time constant τ_0. If n is large, the conditions for cancellation of a pole and a zero simplify to $R_C = nR$, and $\tau_0 = CR$. By choice of R_C, it is therefore possible to modify the response of the circuit of Fig. 14 to correspond to a single RC differentiator whose time constant is approximately CR.

4. *Long Term Baseline Fluctuations*

Even if suitable pileup rejection methods are used to eliminate those pulses that pileup in the main part of the pulse, and if aftershock effects are reduced to negligible proportions, random time fluctuations in the signal pulse rate produce a randomly fluctuating baseline after any ac coupling, and this fluctuation modulates the amplitude of signals. To overcome these baseline fluctuations, and also to remove any dc drift components present in the baseline, it is necessary to provide dc restoration immediately before the circuits used to measure the pulse amplitude. These dc restoration circuits are discussed in Section III.C.

The counting rate at which long term baseline fluctuations contribute a given degradation to resolution is related to the area of the signal pulses. The larger the area of the pulses, the larger is the baseline shift to maintain the average value of the signal sequence at zero. Based on this reasoning, it is clearly advantageous to use symmetrical pulses, so that their peak height is as large as possible for a given area. It is also desirable to reduce the pulse width to as small a value as possible, consistent with adequate noise performance.

III. Design Factors in Electronic Modules for Spectroscopy

A. Linear Amplifiers

1. *General Considerations*

Linear amplifiers are key components in nuclear spectrometers. Their primary function is to amplify the signals received from the detector–preamplifier combination to a level (commonly 10 V max) at which the later circuits can perform accurate amplitude analysis, but an equally important function is to shape the signal pulses so as to yield the best possible energy resolution in the spectrometer. Section II discussed pulse shaping, so we will deal here only with its practical aspects, and with other factors of importance in the design and use of linear amplifiers.

2. *Linearity*

Linearity of the input/output characteristic is required to simplify interpretation of spectra recorded in the analyzer. Its early importance is stressed by the name "linear amplifier" often used in nuclear spectrometry. A crude specification of linearity might require that the centroid of a peak should be no more than 10% of its peak width from its correct position on a linear calibration line. As the peak width, expressed as a fraction of the energy, varies according to the energy and application, this cannot be converted directly into a permissible change of gain. Generally gain variations should be less than 0.01% to 0.1%, depending on the application, for any signal within the design range of amplitudes.

3. *Stability*

The gain of the amplifier must be stable, both with temperature changes, and as a function of time. A requirement that all gain changes be within 0.01% to 0.1% (depending on the application), under normal operating conditions, and during the period of an experiment, is reasonable. If gain changes exceed this amount, significant degradation of energy resolution of the system may result.

Meeting these linearity and gain stability requirements requires the use of large amounts of negative feedback in amplifier stages. The operational amplifier stage shown in Fig. 15 is now commonly used as a basic building block. In some cases, an integrated circuit is used for the amplifier portion of the block, while in others, discrete transistors are used; in either case the value of G is very large, and the current flow in the input to the amplifier is negligible. When these conditions are met, the junction of $R1$ and $R2$ is a virtual ground, not moving significantly on signals, and the overall stage gain is given by

$$V_{\text{out}}/V_{\text{in}} = -R2/R1 \tag{36}$$

The stability of overall amplification therefore depends on $R2$ and $R1$; low-temperature-coefficient, stable metal-film resistors are used for these components. Rise time requirements on the operational amplifier limit the values of $R1$ and $R2$ to the range from about 100 Ω to 10 kΩ.

The operational amplifier provides a very low output impedance that is convenient for driving later stages, pulse shaper networks, and terminated output cables. The differential input shown in Fig. 15 is also valuable. If the signal is fed to the positive input point, and the input end of $R1$ is grounded, the stage behaves as an amplifier with no phase change, exhibiting a high input and low output impedance. Its gain is given by

$$V_{\text{out}}/V_{\text{in}} = (R2+R1)/R1 \tag{37}$$

If carefully matched transistors are used at the input elements, or single-chip pairs of transistors are used, as in many integrated circuits, the offset voltage ΔV

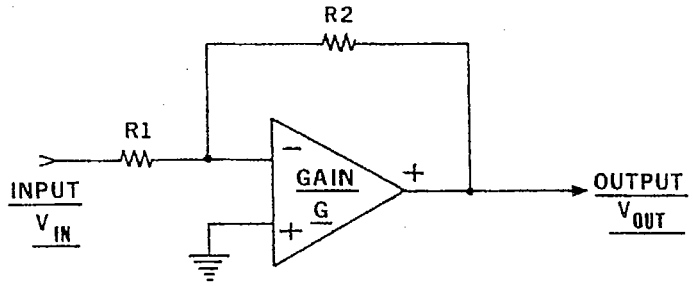

Fig. 15. Basic operational amplifier building block.

between the two input points for zero output can be very small, and almost independent of temperature and time. The offset ΔV is multiplied by the total gain of cascaded dc coupled stages to produce an amplifier output offset that might drive the output stage well beyond its normal operating range. However, if ΔV is small, as in well-balanced integrated circuits, gains as high as 10,000 can be used in a dc coupled amplifier while producing less than 1 V offset at the output. This capability reduces the need for ac coupled stages, simplifying the problem of avoiding multiple differentiators, as required by the consideration of Section II.F.3.

4. *Overload Performance*

Good overload performance is necessary in order to handle the very wide range of signal amplitudes encountered in most nuclear amplifiers. The negative feedback used in linear amplifier stages holds the gain constant in the normal working range, but overload signals drive stages past that range, feedback is lost, and long recovery may follow. Stages that are dc coupled largely eliminate this problem. Improvement in overload performance is also achieved by reducing the pulse width by placing the single differentiator as early as possible in the amplifier. Care must then be taken to avoid the introduction of hum and low-frequency noise into stages after the differentiator.

All linear amplifiers contain gain controls covering a wide range (usually over 100:1) to permit their use in a variety of experiments. The location of the gain controls in the amplifier chain is a compromise. For best overload behavior, signals should be attenuated to the desired degree as early as possible. However, such an attenuator reduces the preamplifier noise as well as the signal, so the main amplifier noise may become dominant. General-purpose linear amplifiers have both early and late gain controls, or the gain switch operates on attenuators positioned at several appropriate points in the amplifier chain. This permits optimization of signal/noise and overload performance for a given application.

5. *Pulse Shaping*

Location of the integrator part of the pulse shaper is less critical than that of the differentiator. Usually it is included in one of the late stages, but before the

final stage which serves as an output driver. The simplest type of integrator is an RC circuit placed between two stages of the amplifier. When used together with a single RC differentiator of equal time constant, the pulse shaper discussed in Section II.C.2.c is realized. Component values are switched to optimize signal/noise for a given application. As explained in Section II.C more complex forms of shaper can be used with advantage. The commonest is the Gaussian pulse shaper using a single RC differentiator and multiple RC integrators. The equivalent of multiple RC integration is usually achieved by complex feedback in one or more of the later amplifier stages.

Unipolar pulse shapers are preferred for good noise performance, but bipolar pulses, generated by two short time constant differentiators, are useful in many applications. The balanced waveform (i.e., balance achieved in a short time) avoids any shift of the baseline between pulses, thereby maintaining the operating points of the late stages of the spectrometer at their design values, independent of counting rate. Further advantages include reduction of low-frequency noise, hum and microphony, better overload characteristics than amplifiers using unipolar pulse shapers, and the availability of a zero crossing point in the output waveform to use for many fast timing purposes (see Section I.D for an example). Bipolar shaping is available in many general-purpose linear amplifiers for use where the ultimate in energy resolution is not essential.

The common type of bipolar pulse shaper used in linear amplifiers employs delay lines. Figure 16 shows two types of delay-line differentiators. The first type, shown in Fig. 16a, employs an operational amplifier $A2$ to sum the original signal (fed via $2Z_0$), and a delayed and inverted version of the signal, the delay being provided by a delay-line terminated at both ends in its characteristic impedance Z_0. Precise return of the output signal to the baseline after the pulse

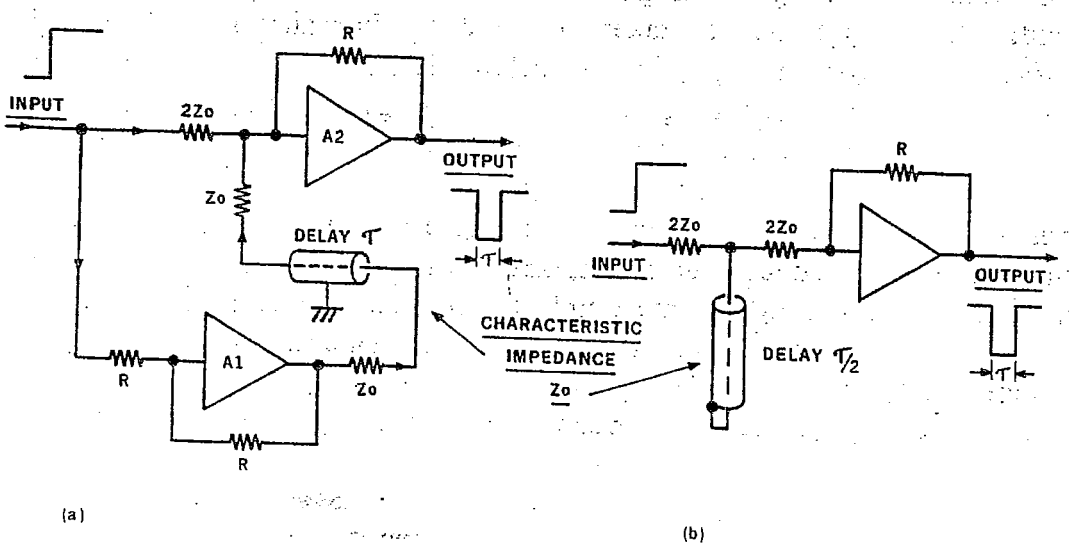

Fig. 16. Delay-line shapers: (a) Delayed-subtraction method; (b) shorted delay line.

width τ can be achieved even if the input signal is an RC differentiated step function, such as is produced by a resistor-feedback preamplifier. To accomplish this result, it is only necessary to adjust the gain of the delayed-signal path to a value (just below unity) at which the delayed signal equals the input signal level at time τ after its start.

Figure 16b shows the simpler shorted delay-line shaper. The simplicity of this arrangement is attractive, but slight capacitive or other mismatches at the line output produce more serious "rings" than the arrangement of Fig. 16a, in which both ends of the line are correctly terminated. The shorter line required for the circuit of Fig. 16b, for a given output pulse width, is also a useful feature. In some amplifiers, the complex scheme of Fig. 16a is used for the first differentiator, providing pulses for energy analysis purposes, and a second delay-line differentiator like that shown in Fig. 16b is then used to provide bipolar pulses for crossover timing, or other purposes. The performance of the second differentiator is less critical than that of the first (due to the possible overload effects in early stages), so the limitations of the shorted delay-line differentiator (Fig. 16b) can be tolerated.

6. *Pole-Zero Correction*

All modern linear amplifiers provide adjustable pole-zero cancellation for the RC differentiation produced in resistor-feedback preamplifiers, unless they are specially designed for pulsed light, or other pulsed feedback systems. The pole-zero scheme described in Section II.F.3 is used, and adjustment is made by adjusting the resistor R_C of Fig. 14.

7. *Input Connections*

The great majority of linear amplifiers use a single coaxial cable to connect the signal from the preamplifier. The input attenuator in the amplifier is designed to terminate the cable in its characteristic impedance. Generally speaking, the preamplifier output impedance also matches the cable at its end, thereby providing good cable matching at both ends, and minimizing ringing due to slight high-frequency mismatches.

In applications where extraneous noise or hum is likely to be induced in the signal cable, other methods of connecting from the preamplifier are sometimes used. One uses a current driver at the output of the preamplifier. The high output impedance of the preamplifier prevents inductively coupled low-frequency currents from flowing in the center wire of the cable, and thence into the amplifier input. Another arrangement that is used more commonly, and more effectively, to suppress a range of frequencies of inductively coupled noise, is the differential-input scheme shown in Fig. 17. A double wire shielded cable is used, with the induced voltages in the extra wire cancelling those in the main signal wire. As the two wires are in close proximity along their entire length, and

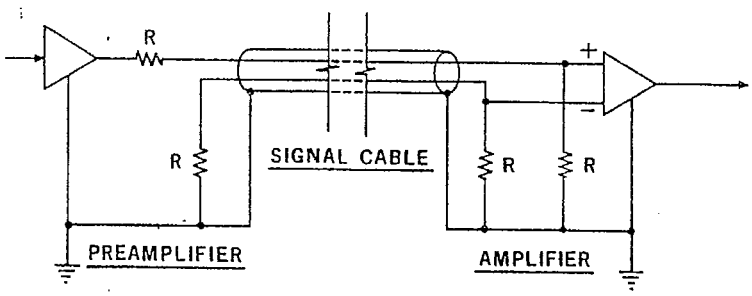

Fig. 17. Amplifier differential input circuit to minimize extraneous noise pickup.

are terminated in the same impedances, cancellation can be almost perfect. This is the recommended method of operation in very noisy locations.

B. Pileup Rejectors

Pileup is defined as mutual interference between the main parts of pulses (see Section II.F.2). If pulses subjected to such interference are not rejected, gross distortion of the amplitude spectrum is caused at high counting rates. A pileup rejector must recognize pulses subject to pileup, and provide control pulses for a linear gate to reject these pulses. The inspection is usually performed on short differentiated signals (rather than on the signals shaped for optimum signal/noise).

A typical pileup rejector is shown in Fig. 18. It is driven by the short signal shown in waveform (ii), which is obtained by differentiation and amplification of the preamplifier signal. Each signal exceeding the discriminator threshold triggers† a one-shot that generates an inspection period (iii) during which the AND gate inspects for further fast signals. If such a signal occurs (as in the second half of waveforms (i) and (ii)), it sets the "pileup flip-flop" producing an output waveform that inhibits signals at a linear gate included in the main signal processing channel. Any signal reaching its peak while the flip-flop is set is rejected. If further fast signals occur during pileup periods, the associated slow signals are rejected, and they initiate their own inspection periods to seek possible interferences with later signals. This is the purpose of the "up-dating" feature in the one-shot.

If the fast discriminator threshold is set too high, pileup by small signals will not be recognized, but if set too low, an unnecessarily large fraction of signals will be rejected due to the discriminator triggering on noise. The noise level in a fast signal channel is much higher than in a slow one, so the fast discriminator threshold cannot be set very low, and very small signals will not be detected by

† A slight delay is included in the path via the updating one-shot and the gate, to prevent the signal that triggers the one-shot from being recognized as a pileup signal.

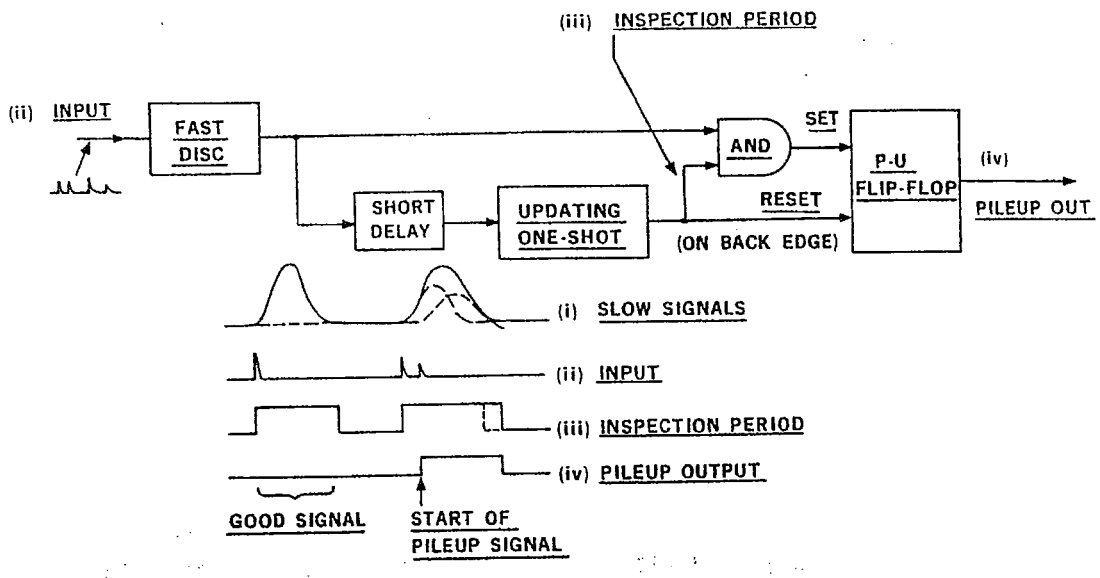

Fig. 18. Operation of a pileup rejector.

the fast discriminator. A slower measurement would improve the rejector's ability to recognize small signals, but its ability to resolve two closely spaced signals, and not to regard them as one, would be impaired.

Other methods of pileup rejection are sometimes used. As seen in waveform (i) of Fig. 18, pileup causes a change of signal shape; therefore any circuit capable of checking that a signal conforms to the prescribed shape (within limits imposed by noise) can be used to recognize pileup. The only simple scheme for achieving this is to double differentiate the signal to produce a zero crossover, and to check that this crossover occurs at the correct time with reference to the start of the signal.

An additional feature, often included in pileup rejectors, permits rejection of abnormally slow detector pulses. Many semiconductor detectors contain undepleted regions from which slow diffusion of radiation-induced ionization occurs. This process is very slow compared with normal charge collection so, after shaping in the amplifier, small pulses are produced which cause background in the final spectrum. A pileup rejector, examining the shape of signals, excludes signals containing substantial slow components.

C. Baseline Recovery Circuits (dc Restorers)

1. *General Comments*

Comparison of a pulse amplitude with a dc level requires that the pulse baseline be defined. This is important in analog-to-digital converters, discriminators, single-channel analyzers, linear gates, and biased amplifiers. The output baseline of a linear amplifier varies with counting rate, and is subject to dc drifts,

so the pulse baseline must be established prior to any further processing. This function is performed by a dc restorer at the input of many modules.

For most applications, signals are unipolar, and the dc restorer need only handle single-polarity pulses. While balanced bipolar signals introduce no baseline shift after ac couplings, the area balance is usually not exact, and baseline restoration is also required. This demands a baseline restorer handling both positive and negative signal excursions.

2. *Unipolar and Bipolar Diode Restorers*

The simplest dc restorer, as shown in Fig. 19, uses a signal diode to clamp the baseline between signals, the diode switching from low to high impedance when a signal occurs. The signal feeds through capacitor C to the output, which is clamped by the current I flowing in diode D. The low diode impedance (kT/qI, or 25 Ω for 1-mA current), together with C, provides a short differentiating time constant except during signals. A positive input signal, of sufficient amplitude, reverse biases the diode, so that its impedance becomes large. The differentiating time constant thereby becomes large during signals.

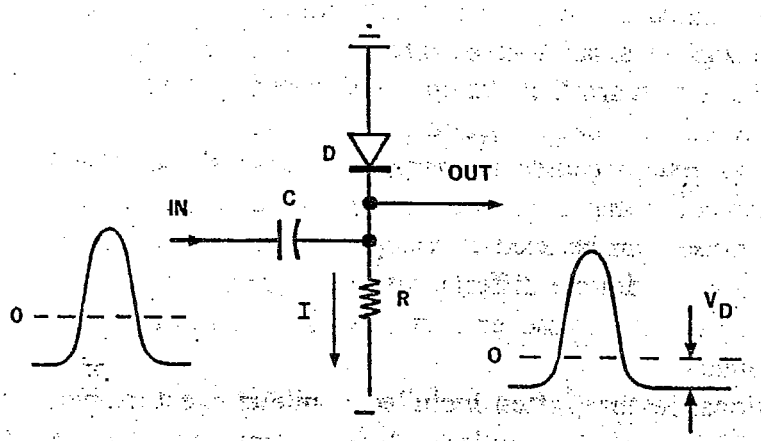

Fig. 19. Unipolar dc restorer using a semiconductor diode.

The noise performance of a system may be seriously degraded by dc restoration, as the short time constant existing when no signal is present modifies the overall system pulse shaping. Since this time constant changes during signals, the system behaves as a time-variant shaper (Radeka, 1967). To ensure only a small degradation in resolution due to the restorer, it is necessary to use a restoration time constant much longer than the main shaper time constant. However, if the restoration time constant is too long, it will fail to respond to fast baseline fluctuations. A compromise must be made between these competing requirements.

In the restorer shown in Fig. 19, the charge stored in C during the signal pulse is removed via the diode between pulses. At high counting rates, this increases

the average current through D by an amount βI where β is the signal duty factor. As the incremental diode impedance is kT/qI, and kT/q is 25 mV at room temperature, the baseline will be depressed by a voltage of 25β mV.† At high duty factors this shift is intolerably large. Consequently, the more complex restorers described in the next section are used in high-resolution spectrometers. As the output baseline is fixed by the voltage drop V_D in diode D, which is temperature dependent, practical dc restorers must also include temperature compensation, often achieved by balancing the drop in diode D against that in a similar diode.

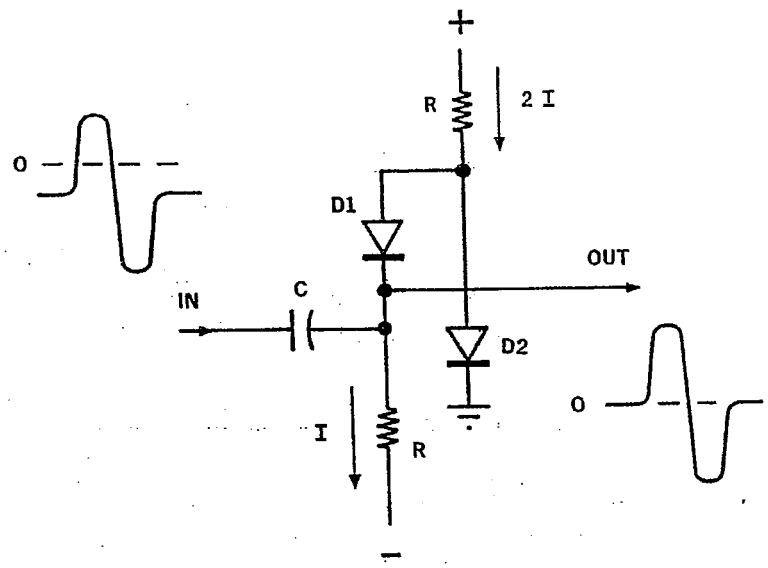

Fig. 20. Bipolar dc restorer.

A version of the simple diode restorer that can handle bipolar pulses (Robinson, 1961), at the same time as providing temperature compensation, is shown in Fig. 20. In the rest condition both diodes pass a current I; diode $D1$ becomes nonconducting on the negative portion. The diode impedances are in series, so the effective restoration time constant is twice that of the unipolar restorer.The bipolar dc restorer may also be used to clamp the baseline of unipolar pulses of either polarity, but it operates incorrectly when the duty factor approaches 50%. At duty factors above 50%, the circuit regards the peak of the pulse as its baseline, and restores accordingly.

3. *Active Unipolar and Bipolar dc Restorers*

The intolerably large baseline shifts exhibited by simple restorers, and the fact that the diodes fail to unclamp on small signals, thereby limiting the

† We assume here that the change in current through the diode is only a small fraction of its steady current I; otherwise the nonlinearity of the diode characteristic must be taken into account.

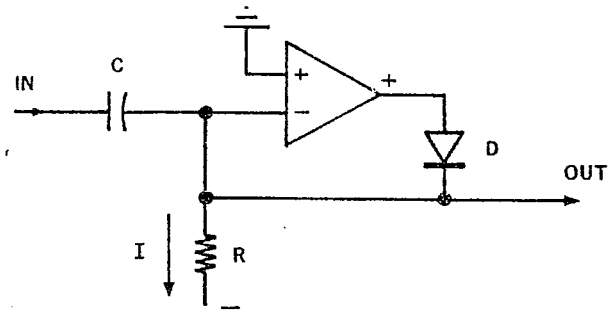

Fig. 21. Active unipolar dc restorer.

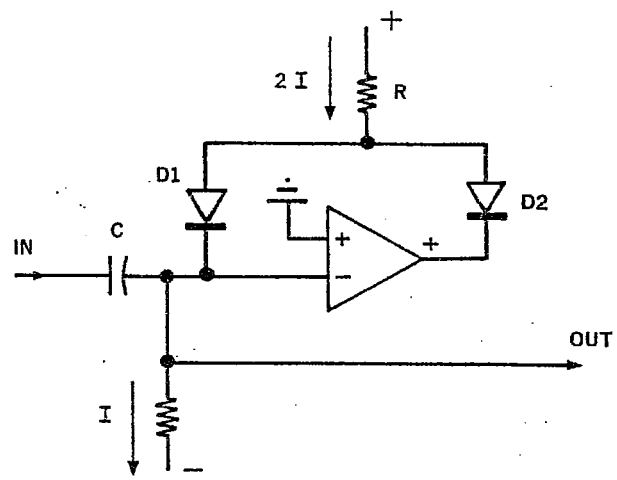

Fig. 22. Active bipolar dc restorer.

dynamic range of the restorers, has led to the development of restorers in which the nonlinear characteristics of diodes are amplified (Chase and Poulo, 1967; Gere and Miller, 1967). Two examples derived directly from the simple diode restorers are shown in Figs. 21 and 22. The voltage movement at the output, due to changes in diode current, is reduced by driving the other end of the diode with an amplifier of controlled gain (~10). The effective impedance from output to ground in the rest condition is reduced by this factor, when compared with simple restorers. The impedance changes to a high value on very small signals.

D. Linear Gates

A linear gate transmits signals under the control of an external waveform. Ideally the gate should switch from one state to the other quickly (in 100 nsec or less), should totally transmit the signal when open, but transmit no signal when closed, and should not inject a significant pedestal or switching spikes into the output signal.

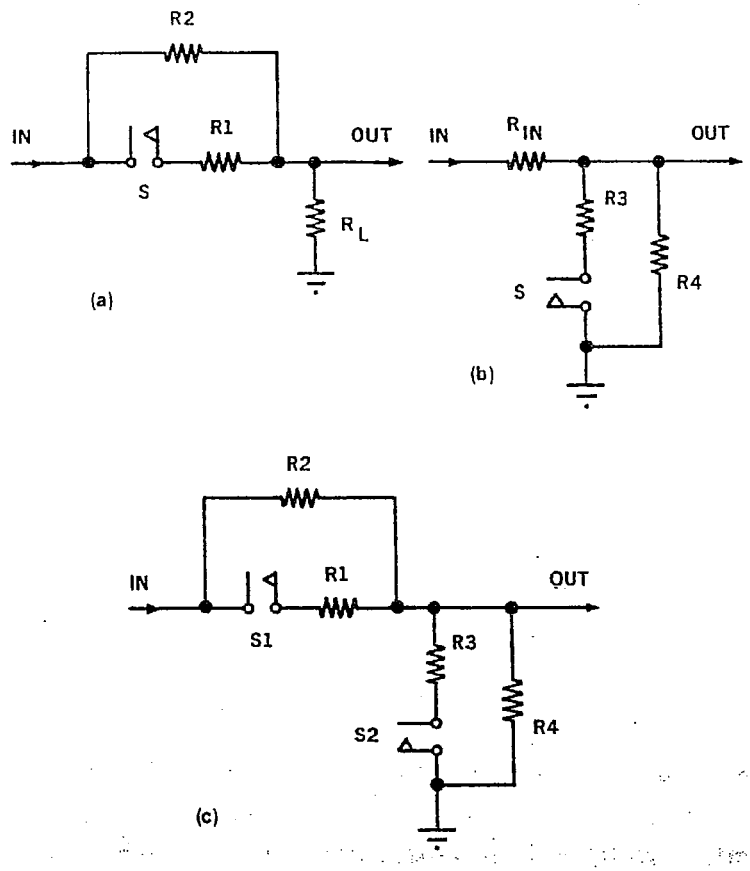

Fig. 23. Basic types of linear gate: (a) Series; (b) shunt; (c) series-shunt.

Most linear gates, as shown schematically in Fig. 23, employ electronic switches in the series path (a), in shunt with the output (b), or in both positions (c). Ideal switches exhibit zero impedance when in the *on* condition, and infinite impedance in the *off* condition.

Practical electronic switches exhibit series ($R1$) and shunt ($R2$) impedances that degrade their performance. The transmission of the series switch is $R_L/(R_L+R_1)$ in the *on* state, and $R_L/(R_L+R_2)$ in the *off* state. The *on* transmission approaches unity only if the load R_L is very large compared with R_1, but R_2 must be many times larger than R_L to make the *off* transmission approach zero. These considerations impose severe limitations on the performance of simple linear gates. The same limitations arise in the shunt gate (b). These difficulties are largely circumvented by using the series-shunt gate (c), where the switch $S2$ is closed when $S1$ is open and vice versa. Apart from the improvement in the on/off transmission ratio, the synchronous operation of the two switches reduces transient effects produced by the switching operation.

One implementation (Goulding, 1965) of the series-shunt gate is shown in Fig. 24, in which transistors $T1$ and $T2$ are the switches. In the *open* condition of the linear gate $T1$ is in its saturated *on* state with the current I flowing in its

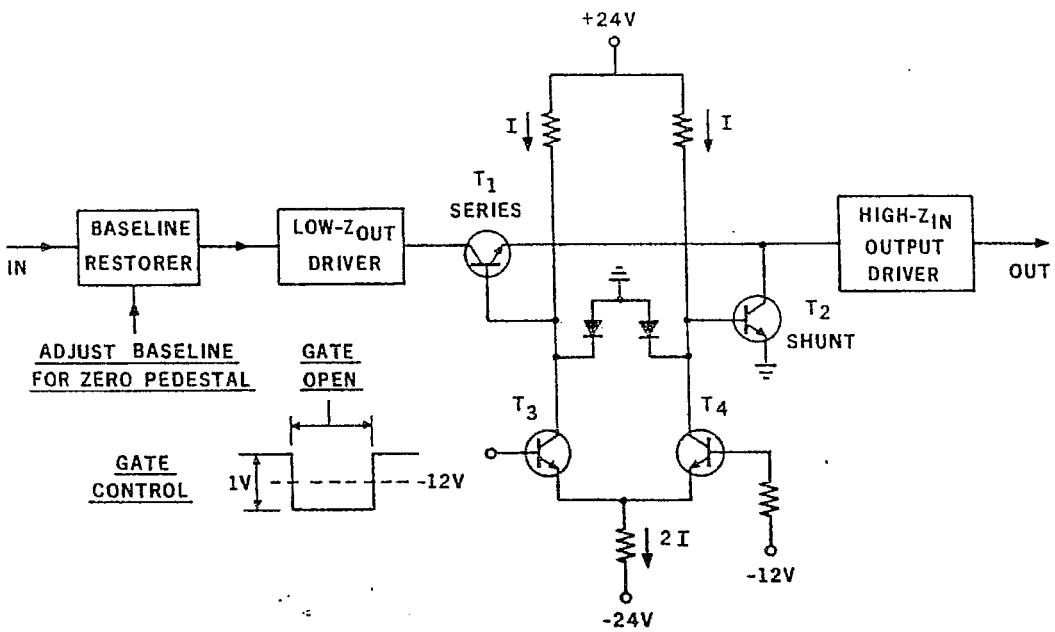

Fig. 24. Series-shunt transistor linear gate.

base. On the other hand, the current in $T4$ holds $T2$ off. The voltage drop across $T1$ is essentially zero, so the gate output is held at the same potential as its input. The gate is switched to its *closed* position by switching the current switch (containing $T3$ and $T4$) to turn $T1$ off and $T2$ on; $T2$ then clamps the output at zero potential. The reference level in the dc restorer is adjusted to realize zero pedestal when the gate switches.

While the 100 nsec or so required for this gate to switch is usually tolerable, faster switching is required in some cases. The diode-bridge linear gate shown in Fig. 25 is often employed in these cases, with very fast Schottky-barrier diodes acting as the switching elements. In the open condition of the gate, a current I_1 is switched to flow through the bridge from top to bottom, as shown in Fig. 25a. All four diodes are conducting, and the input and output are connected together via the (low) diode impedances. The gate is closed by reverse biasing all diodes in the bridge as shown in Fig. 25b.

A completely different type of linear gate is shown in Fig. 26 (Battista, 1970). It is composed of an operational amplifier in which the input transistors are switched to control the gate. In the closed position of the gate, transistor $T6$ conducts the current I, so that $T5$ is nonconducting. The signal input transistor $T1$ is therefore nonconducting, and the feedback loop is from the output via R_{F2} to the base of $T3$. The gate is opened by raising the base potential of $T5$ above that of $T6$, so that $T5$, $T1$, and $T2$ are all brought into conduction, while $T6$, $T3$, and $T4$ are made nonconducting. The feedback loop is then from the output via R_{F1} to the base of $T1$. The signal gain is then given by $-R_{F1}/R_{A1}$. As shown in Fig. 26, a single integrated circuit contains $T1$–$T6$. The balanced characteristics

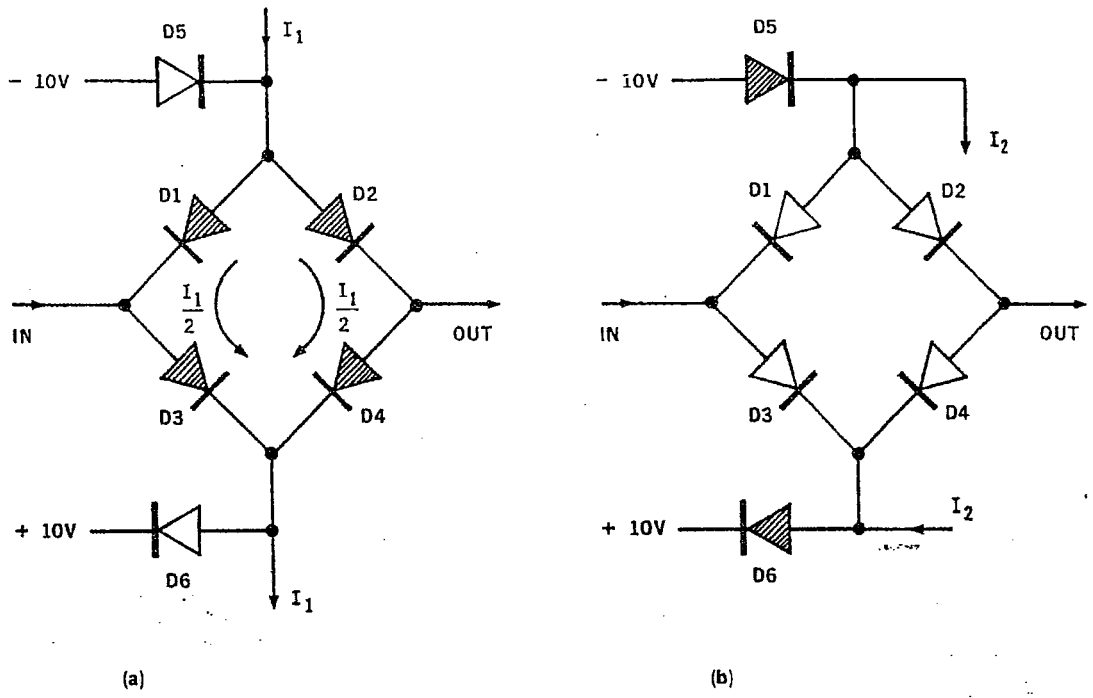

Fig. 25. Diode-bridge linear gate: (a) Open state; (b) closed state.

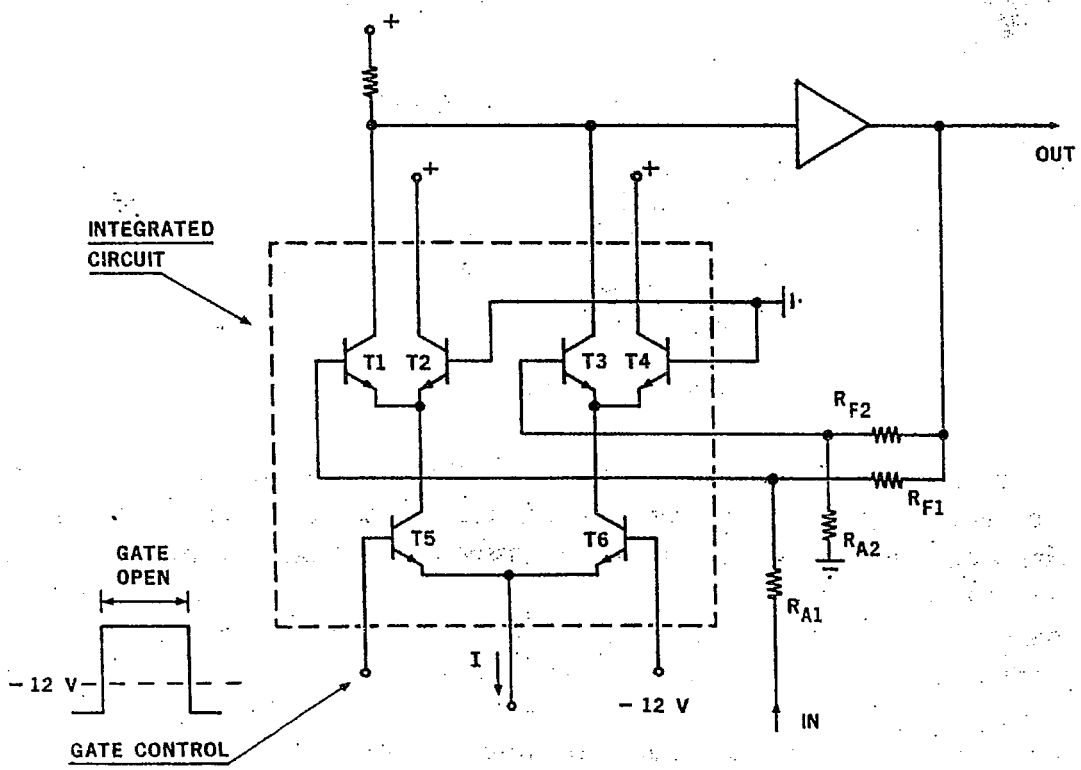

Fig. 26. Operational amplifier linear gate with switched input circuit.

of the transistors used in an integrated circuit are desirable in this linear gate to reduce the pedestal produced at the output when the gate is switched. The availability of differential inputs in this type of gate permits its use with, or without, phase inversion. The use of negative feedback around the gate, and high frequency transistors within the loop, results in fast switching, typically 10–50 nsec.

E. Biased Amplifiers

Biased amplifiers are used to expand the high-energy part of a spectrum (neglecting the low-energy parts) to observe fine structure in high-energy spectral lines. A preset bias is subtracted from all signals, the resulting negative signals are rejected, and the positive residues of other signals are amplified.

The simplest form of biased amplifier is shown in Fig. 27. A diode cuts off the portion of signals smaller than the baseline restorer reference voltage. That portion of signals passed through the diode is then amplified by the output amplifier. The ideal diode characteristics would abruptly change from infinite impedance for negative bias to zero impedance for forward bias. In practice, while the diode impedance is suitably high in the reverse direction, and quite low when in the forward direction, the transition between these two regions is not abrupt. Transmission through the diode changes slowly as the diode voltage changes over a range of about 1 V, so serious non-linearity exists over much of the output voltage range.

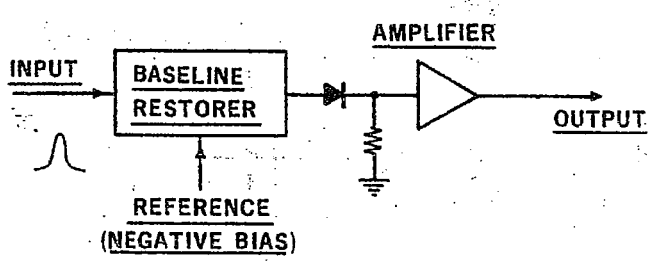

Fig. 27. Simple biased amplifier.

Further problems with simple biased amplifiers include signal feeding through the diode capacity, producing small output pulses for signals smaller than the bias level, and the fact that the signal passed by the diode becomes very narrow for signals that only just exceed the bias level. Unless the output amplifier stage exhibits short rise time, the varying width of its input signal will produce nonlinearity. The switched linear gate shown in Fig. 28 reduces these non-linearities. A linear gate (e.g., the series-shunt gate of Fig. 24) connecting the input and output circuits is normally closed, but is opened by the discriminator whenever an input signal exceeds the bias level. The portion of the signal above the bias level is thereby passed on to the output amplifier.

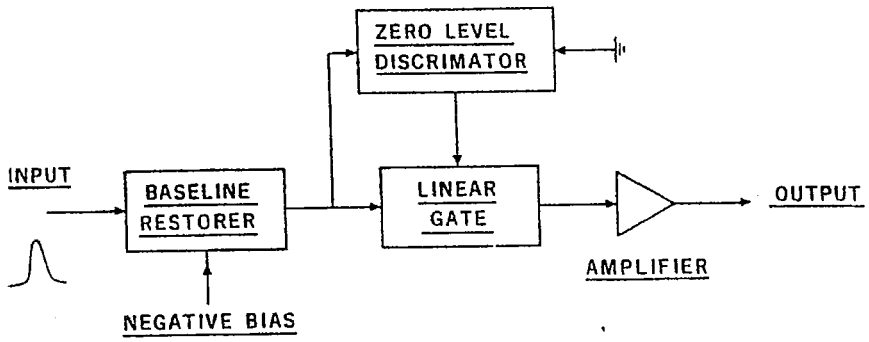

Fig. 28. Biased amplifier based on a linear gate.

The width variation in the output signal from a biased amplifier may produce nonlinearity in the overall response of a spectrometer. This results from slow response in the linear gate, in the output amplifier of Fig. 28, or in later parts of the analysis system, like the analog-to-digital converter in the pulse-height analyzer, which cannot respond linearly to very narrow pulses. A pulse stretcher is normally included in the output of a biased amplifier to provide a wide pulse for the later circuits. This stretcher must handle the widely varying input pulse widths without exhibiting amplitude nonlinearity.

It is often preferable to stretch the signal pulse prior to performing bias cutting. By sampling the stretched pulse, a flat topped, fixed width output pulse is realized. A biased amplifier employing this principle is shown in block form in Fig. 29. In this circuit, a pulse stretcher follows the initial baseline restorer. The pulse is stretched only when its amplitude exceeds the bias level as sensed by the discriminator, and until the time (determined by the discriminator) when the input pulse is essentially back to its baseline. A peak detector, included in the

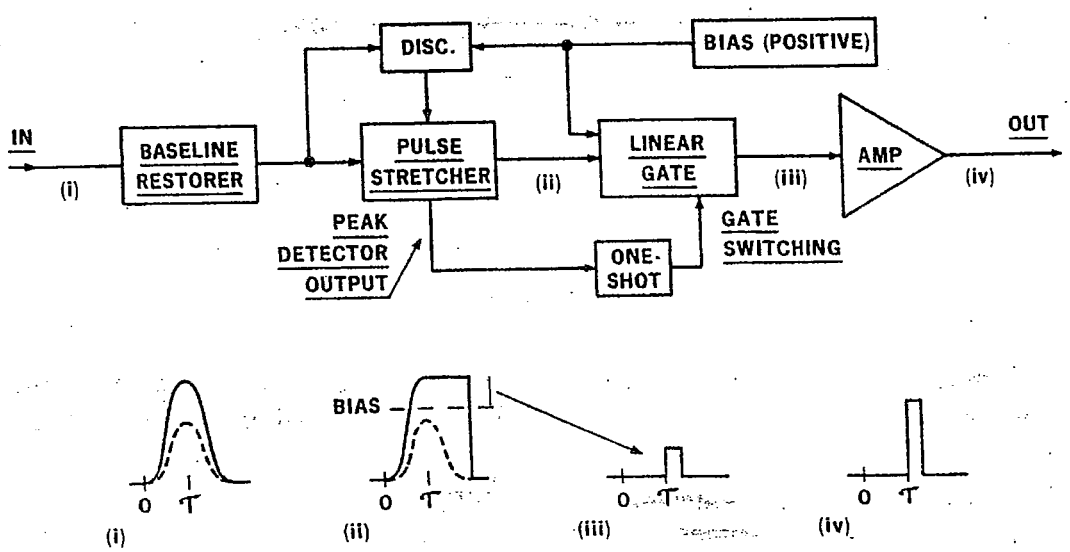

Fig. 29. Biased amplifier using a pulse stretcher.

stretcher, provides a timing pulse at the peak time. This pulse, suitably delayed and shaped, is used to switch the linear gate to its open position shortly after the input signal peak time. The linear gate produces an output pulse, equal to the difference between the stretched signal and the bias level, which is then amplified by the output amplifier. The rectangular output pulse is ideal for later parts of the spectrometer.

F. Pulse Stretchers

An ideal stretcher accepts any pulse, even of very narrow width, and produces a stretched output pulse of the same amplitude as the input pulse, retaining this amplitude for a long time. The simplest form of stretcher, shown in Fig. 30, uses a diode D to charge a memory capacitor C to the peak value of the signal. This simple arrangement has the following limitations:

(1) Unless C is large and the discharge current I is small, the memory is short. On the other hand, if C is large it is difficult to charge it to the peak signal amplitude in a short time. If I is small, and C large, the memory is long but the circuit cannot respond to pulses at a high rate.

(2) Feedthrough via the diode capacity, and extraction of charge stored in the diode during its short conducting period, cause the removal of some of the charge from C on the back edge of the signal [dotted line in Fig. 30, waveform (b)]. This can cause nonlinearity in the input/output characteristic of the stretcher.

(3) The nonlinear impedance and temperature sensitivity of the diode cause nonlinearity and instability.

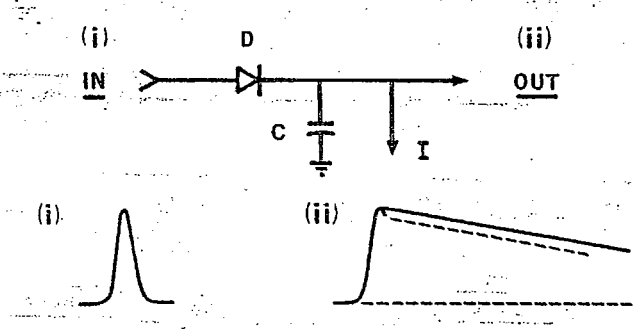

Fig. 30. Simple pulse stretcher.

A block diagram of a stretcher designed to overcome these problems and to provide the performance required in nuclear pulse processing is shown in Fig. 31. The linear gate is normally open, so signals pass through into input (i) of the difference amplifier. Feedback, via the charging circuit to the input (ii) of the difference amplifier, forces it to follow input (i) as long as the required movement is in a positive direction. Any negative movement at input (ii),

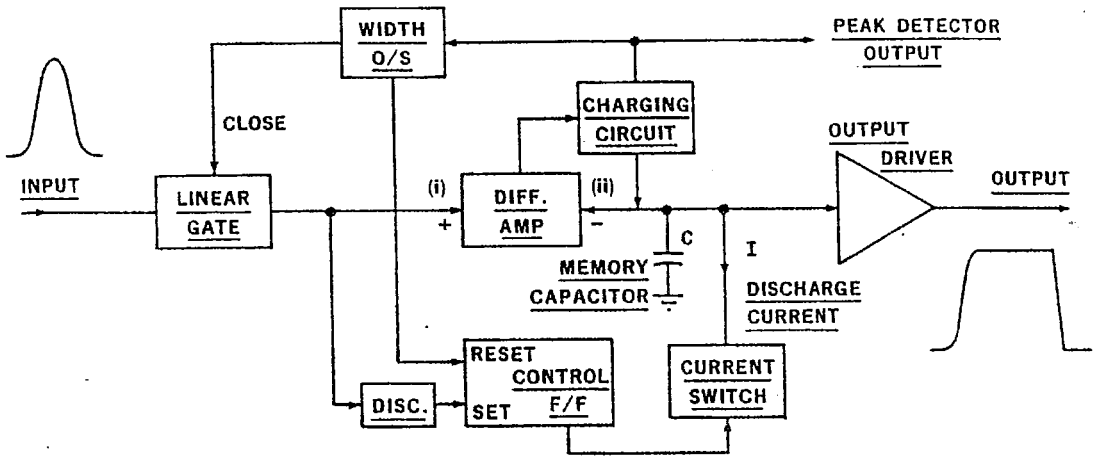

Fig. 31. Typical pulse stretcher used in spectrometers.

however, is produced only by the discharge current I, as long as it is present. When any signal exceeds the discriminator level, the control flip-flop is set, removing the discharge current I, so the memory capacitor C in the input (ii) of the difference amplifier charges to the input signal peak, but cannot discharge after the peak. It therefore retains the peak signal amplitude.

The sudden drop in charging current after the peak of the pulse is sensed to provide the peak-detector output, which triggers the width one-shot closing the input gate for a fixed time to prevent further signals from entering the stretcher until the later signal processing electronics has dealt with the first signal. Relaxation of the width one-shot resets the control flip-flop, thereby permitting the discharge current I to flow again, and rapidly discharging C back to its initial condition. When this is accomplished the input linear gate is opened, and the stretcher can process further signals.

It is essential that all loading on the memory capacitor C be kept to a minimum. Consequently, the input impedances of both the difference amplifier, and the output driver, must be very large (FETs are often used), and the diodes used in the charging and discharging paths must exhibit very low leakage, as well as being fast, with little charge storage, and very low capacity. The quality of the memory capacitor itself is also important, polystyrene film capacitors are often used in this position.

G. Discriminators and Single-Channel Analyzers

At one time, single discriminators were used to determine the amplitude distribution of pulses. By counting the number of times a discriminator fired, the integral of all counts above the discriminator level was accumulated. Moving the level in increments permitted the amplitude spectrum to be deduced. Later, multiple discriminators and scalers were used to reduce the time required to

produce a spectrum, and also to improve statistics. This was the forerunner of the modern pulse-height analyzer which uses more sophisticated methods of sorting and storage. However, discriminators are still used as elements in many functional units (e.g., in pulse stretchers—see Section III.F), and are used in pairs in single-channel analyzers (SCAs), which produce an output only when a signal amplitude lies between the two discriminator levels. Single-channel analyzers are generally used now to select pulses in one analysis channel, the output being used to gate another channel, so that the only signals processed in it are coincident with the SCA output pulses. Examples of applications of single-channel analyzers occur in Sections I.C and I.D.

All discriminators use a nonlinear element (usually sensitive to voltage changes at the input) in a circuit that triggers to produce a standardized output pulse only when the input pulse amplitude exceeds the discriminator threshold. The positive feedback used to provide triggering results in "backlash"; that is, relaxation of the circuit only when the signal amplitude falls some distance below the triggering threshold level. This behavior is illustrated in Fig. 32. A useful result of backlash is the insensitivity of the circuit to noise on the tail of the signal. Many discriminators are designed to define the level at which relaxation occurs independently of the triggering threshold level. It is important that a discriminator should not produce partial outputs for input signals below the threshold level, as this may result in the system threshold being defined by circuits later than the discriminator which are not designed for stability.

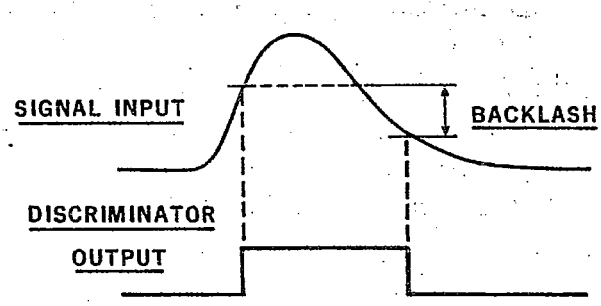

Fig. 32. Illustration of "backlash" in a discriminator.

The stacking of a pair of discriminators to produce a single-channel analyzer is illustrated in Fig. 33. The circuit logic is largely self-explanatory. An output is required for signal pulse (2), but not for (1) or (3). Signal (1) fails to trigger either discriminator so no output results; signal (2) triggers only the lower discriminator, while signal (3) triggers both discriminators. The timing and coincidence circuits strobe the condition of the two discriminators shortly after the peak of the input signal. The coincidence circuit produces an output only if the lower level, but not the upper level, discriminator has triggered. The output pulse time is defined by an external strobe pulse, or by an internal timing circuit

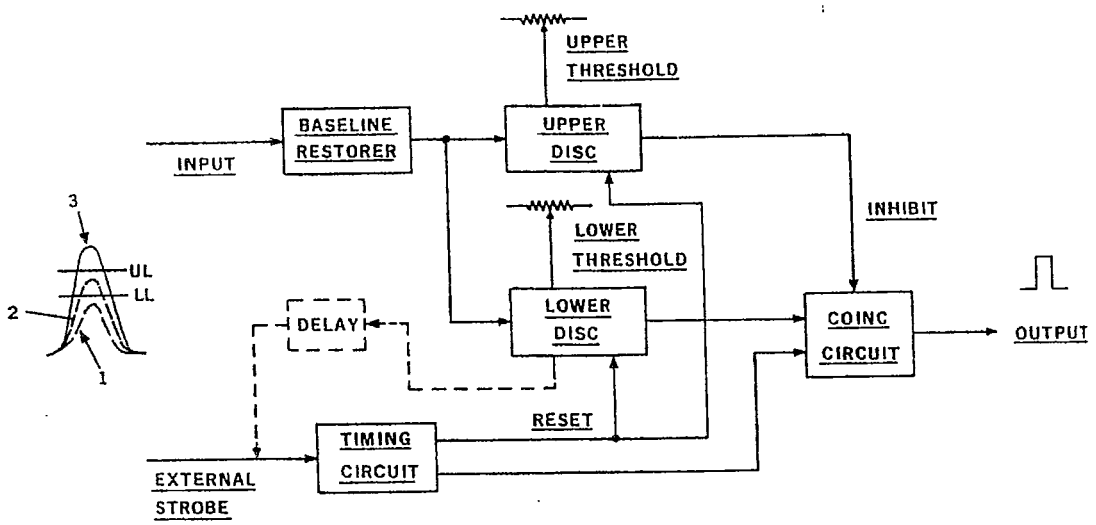

Fig. 33. Block diagram of a single-channel analyzer.

(shown dotted). The external strobe is often supplied by a zero-crossing pickoff circuit when bipolar signals are used.

H. Nonlinear Elements for Analog Calculations

Special applications exist where nonlinear processing of signals is required. One case in point is that of the particle identifier (see Section I.D), where an arbitrary power of the signal amplitude must be derived. In other cases, the product or ratio of two signals must be calculated. A logarithmic element provides a convenient way of achieving these calculations in an analog fashion in a relatively short time.

The basic logarithmic element used in these applications is a semiconductor junction diode. The relationship between the forward current I and junction voltage V is given by

$$V = \frac{nkT}{q} \ln \frac{I + I_0}{I_0} \tag{38}$$

where I_0 is a saturation current determined by the junction parameters, and n is usually near to unity in value. The value of I_0 is normally very small compared with I, so this relationship can usually be simplified to

$$V = \frac{kT}{q} \ln I - \frac{kT}{q} \ln I_0 \tag{39}$$

This provides the desired logarithmic relationship between the current and voltage. However, series bulk resistance of a semiconductor diode invalidates the relationship at high currents (>1 mA). For this reason the simple diode element is not generally used as a logarithmic element. Instead, the equivalent

relationship between the emitter-base voltage of a transistor and its collector current is more commonly used. In this arrangement the emitter region is very heavily doped, therefore presenting very little series impedance, and the base current is very small, so it produces very little voltage drop.

A typical logarithmic converter circuit is shown in block form in Fig. 34. In this arrangement a high-gain operational amplifier, which requires virtually no input current, is used to force the base-emitter potential of the feedback transistor to a value where its collector current is equal to I_{in}. The emitter-base voltage of the transistor is then used as the output, its magnitude is proportional to the logarithm of the input current. In practice, precautions must be taken to avoid feedback oscillations in the circuit, and initial dc conditions must be established.

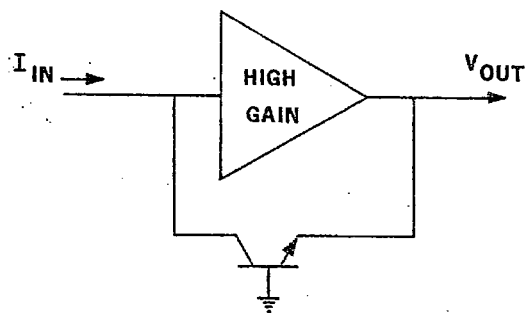

Fig. 34. Block diagram of a logarithmic function generator.

Other methods of performing analog calculations have been used, including the use of a field-effect transistor as a multiplier, but the logarithmic element provides the most versatile tool.

I. Analog-to-Digital Converters

The final step in the signal processing system of any nuclear spectrometer is to convert the amplitude of the signal, often of very short duration, into digital information. In a pulse-height analyzer, this digital information determines the memory address to which a count must be added.

The basic process used in all analog-to-digital converters is to compare the analog input level (a stretcher is used to remember the peak signal level) to an internally generated level which is directly associated with a digital output generator. While this can be achieved in various ways, the linear ramp method illustrated in Fig. 35 is commonly used in nuclear spectrometers. In this scheme, a pulse, produced by the stretcher at the signal peak, starts a linear ramp generator, and, at the same time, permits high-frequency clock pulses to feed a scaler. When the ramp level equals the stretched signal level, clock pulses to the scaler are inhibited, and the number then stored in the scaler is a linear representation of the signal amplitude. At this point, the later digital processing

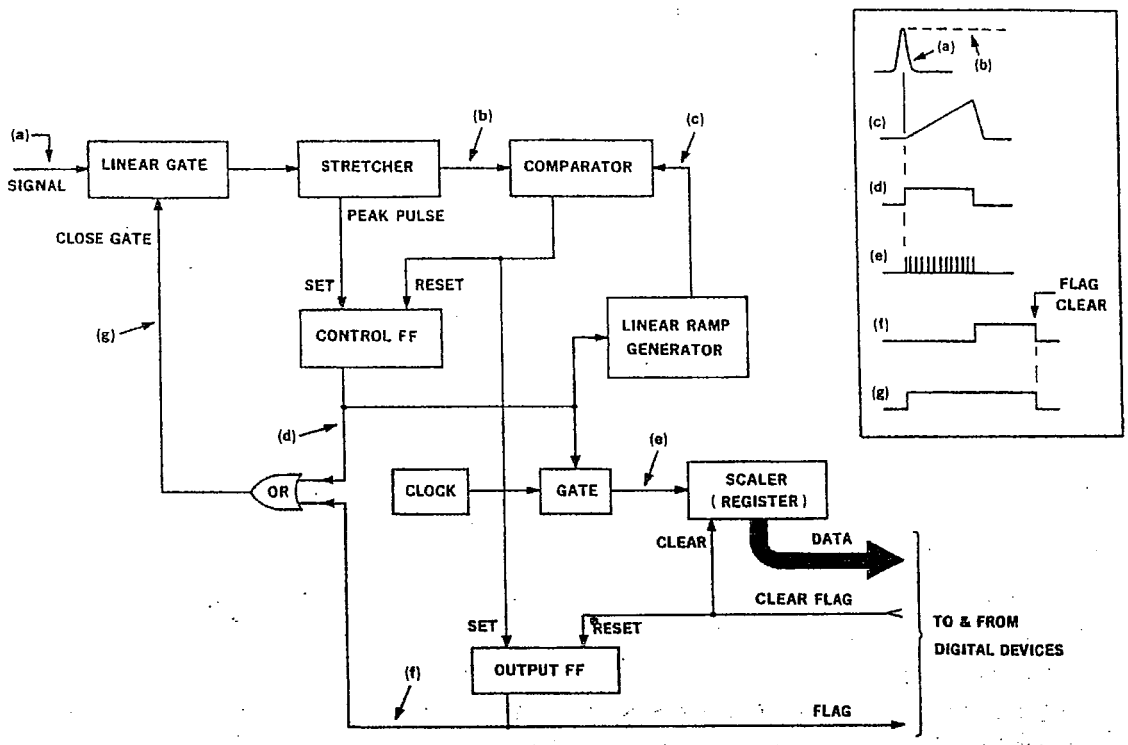

Fig. 35. Block diagram of a ramp-type ADC.

system is flagged to indicate the availability of data in the ADC register. When the digital system completes processing, it so indicates by clearing the ADC flag, thereby freeing the ADC to process further signal pulses. The input gate on the ADC prevents signals entering the system while an earlier signal is being processed.

The coding time of an ADC is an important parameter in a system, as it is often the major factor determining the rate at which events can be handled. For example, if the clock rate in Fig. 35 is 50 MHz, and coding in 4096 channels is required, the coding time is over 80 μsec. This time can be reduced by operating at higher clock rates, but 100 MHz represents the practical limit in this direction. Alternatively, a binary successive-approximation method (Cottini *et al.*, 1963) can be used, although this method becomes quite complicated if good differential linearity is to be achieved. The brevity of this review prohibits further description of the binary successive-approximation method, but the interested reader can find further details in the literature (Kandiah *et al.*, 1969; Robinson *et al.*, 1968).

J. Analog Multiplexers and Derandomizers

Two common problems are encountered in complex spectrometer systems that can be handled by multiple pulse stretchers. The first case is that where an

event is represented by several simultaneous input signals; for example, the passage of a particle through a multidetector telescope producing signals from each detector. In principle, each signal could feed a separate ADC, and the digital output could be processed. However, ADCs are quite complex and accurate tracking of several ADCs is difficult to achieve. For these reasons, it is convenient to store the signal pulse amplitudes in stretchers (one per input), and to time-multiplex the stretcher outputs in sequence into a single ADC. This device is called an analog multiplexer.

A second kind of problem arises due to the long coding and storage cycle times of ADCs, and of the associated digital system. These times often extend to 100 μsec or more, and severely limit the capability of the system to handle high signal rates. As nuclear events occur at random times, severe dead-time losses occur at average signal rates far below the regular pulse rate capability of the ADC. It is therefore important, in many cases, to provide a "queuing" device, commonly called a "derandomizer," in which the randomly occurring input signals can be retained, and fed to the ADC at a rate compatible with its processing capability. It may be shown that a relatively small store (e.g., four events) serves to reduce dead-time losses almost to zero, until the random arrival rate approaches the regular rate capability of the ADC. The function of the queuing store can be performed by a number of stretchers with appropriate circuitry to shuttle signals from one to the other both when input signals arrive, and when the ADC accepts a signal.

The circuits involved in derandomizers and analog multiplexers, while logically quite simple, become rather complex in their details. The reader is therefore referred to the literature for details (Robinson *et al.*, 1969; Robinson and Gin, 1969).

IV. Basic Considerations in Time Measurements

A. Introductory Remarks

Energy measurements are of primary importance in nuclear spectrometry, but accurate timing information is often required in addition. For example, the time delay between two detector signals may be used to determine the velocity of a particle. As the velocities of nuclear particles approach that of light, and reasonable flight paths are typically only measured in centimeters, timing accuracies of 0.1 nsec may be required. Timing information is also used in studies of the time correlation between pairs of events. This type of study has been vital in unraveling the complexity of nuclear energy level schemes.

Optimization of time measurements using semiconductor detectors is a complex problem requiring a knowledge of detector properties, and of the limitations of various circuits used to determine the precise time of a pulse.

Measuring the time of flight of a particle is entirely different from timing γ rays, both in regard to detectors, and in the critical associated timing circuits. While the same modules may be used in the later stages of each system, the optimum methods of processing the signals prior to these modules are quite different. We will now discuss the methods used in these two cases.

B. Fast Timing of Particles with Thin Silicon Detectors

1. *Detector Signal Pulse Shape*

Thin silicon detectors can be used to derive both time and energy information on particles stopping in, or passing through, them. We assume that the detector (either surface-barrier or diffused-junction) is totally depleted, and that the applied voltage is sufficient to make the electric field at all points high enough to achieve the saturation velocity for holes and electrons in silicon (about 10^7 cm/sec). Under these conditions, the maximum collection time for any carrier produced in the thickness T cm of a detector is equal to 100 T nsec. On this basis, a 10-μm thick silicon detector, typical of transmission detectors used for heavy-ion detection, should collect all the charge in 0.1 nsec. If the plasma density in the particle track is very high, such as occurs with very heavy ions or fission fragments, the time taken for the erosion of the plasma by the electric field increases the signal rise time significantly, the increase depending on the electric field, and on the direction of the particle track in relation to it. Observations indicate that detector signal rise times of a small fraction of a nanosecond can be achieved in many cases, although direct observation on this time scale is not possible.

2. *Circuit Considerations*

To achieve fast timing the pulse amplifier must introduce minimum noise, and the degradation in signal rise time must be small. The final timing signal is derived from a fast discriminator, so we must consider fluctuations in the time at which signals cross a fixed level. These fluctuations are related to the noise, and to the rate at which the signal crosses the level. The latter factor is determined by the size of the signal, by its rise time, and by the point on the front edge of the signal at which the discriminator is set to trigger.

The signal rise time is partly determined by the amplifier, and partly by its connection to the detector. Fast amplifiers can be designed to exhibit rise times of 1 to 2 nsec. The circuit must be designed and constructed to avoid "rings" on signals as these seriously distort the time spectrum. This is best accomplished by using a simple voltage-sensitive front end for the amplifier, thereby avoiding any phase shift rings that would arise in a feedback configuration.

The input circuit is also very critical in determining the signal rise time, and in avoiding ringing on signals. Figure 36a shows the precautions commonly

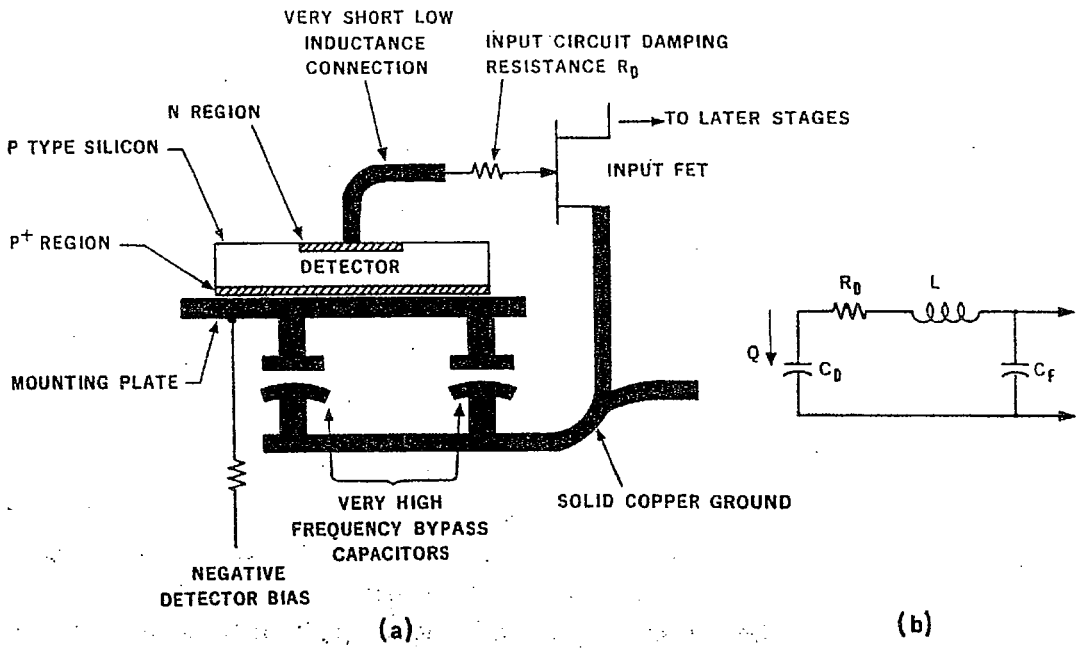

Fig. 36. Input circuit of preamplifier for fast timing: (a) Mechanical configuration; (b) equivalent circuit.

employed in the input circuit. The input amplifier must be mounted in close proximity to the detector, and the input circuit loop must have minimum inductance. The large detector capacitance leads to these stringent mechanical requirements. The equivalent circuit shown in Fig. 36b will be used to illustrate the problems. The input capacity C_F of the FETs used in these applications is typically 50 pF. The capacitance C_D of a *silicon* detector is given approximately by

$$C_D = 1.05A/T \tag{40}$$

where A is the detector area (cm^2), and T is its thickness (cm), and C_D is in pF. The value of the inductance of a straight wire of circular cross section is given by

$$L = 0.002\, l\, [2.3 \log(4l/d) - 0.75] \tag{41}$$

where L is the inductance (μH), l is its length (cm), and d is its diameter (cm).

If the wire between the detector and FET is 1-cm long, and its diameter is 0.05 cm, Eq. (41) yields an inductance of 0.01 μH, while, if the detector area is 0.25 cm^2, and its thickness 10 μm, its capacity is 275 pF. The resonant frequency of the input circuit (assuming $C_F = 50$ pF) is then about 250 MHz. The critical damping resistance for the input circuit is given by

$$R_D = 2(L/C)^{1/2} \tag{42}$$

where C is the series input circuit capacity (~40 pF). This is about 30 Ω in the

present case. The rise time of the signal appearing across the FET input, in this case, is much greater than 1 nsec, thereby degrading the overall rise time of the system. Reducing the length of the detector connection, and increasing its size (e.g., by using a flat beam lead) to reduce its inductance, is required to avoid this degradation. The value of the damping resistance is then chosen for critical damping.

Noise in the first amplifying stage is a limiting factor in timing, as it modulates the point where the signal crosses the discriminator threshold. As seen earlier, delta noise becomes dominant at short time constants. Its main source (see Section II.D.2) is the input amplifier. Combining Eqs. (17) and (19), the mean square equivalent input noise produced by an FET is given approximately by

$$\langle v_n^2 \rangle \simeq (4kT/g_m)\Delta f \tag{43}$$

where g_m is the transconductance of the FET, and Δf is the bandwidth of the system. For 200-MHz bandwidth (rise time for 10 to 90% is about 2 nsec), and with an FET exhibiting a mutual conductance of 50 mA/V when operated at room temperature, the value of $\langle v_n^2 \rangle$ is 64×10^{-12} V^2, corresponding to an RMS noise level of 8 μV. The equivalent full width at half maximum spread is about 19 μV. This reflects in a timespread which depends on the rate at which the signal crosses the discriminator threshold (measured in V/sec), which depends on the signal rise time, and on the size of the signal. For a 1-MeV deposition of energy in the detector, a total shunt input capacitance of 325 pF, and a system rise time of 2 nsec, the maximum rate of rise (referred to the input) is about 6.8×10^4 V/sec. Combining this with the FWHM noise (19 μV), we deduce a time spread (FWHM) of about 250 psec. Increasing the energy deposition in the detector reduces this value in inverse proportion to the energy.

From these arguments, the following general relationship can be derived

$$\Delta t \simeq (4C/E)(\tau/g_m)^{1/2} \tag{44}$$

where Δt is the time resolution (FWHM in psec) caused by noise, C is the total input circuit capacity in pF, τ is the rise time in nsec, E is the energy in MeV, and g_m is the FET transconductance in mA/V. This result represents a limit to the performance that can be realized, but it can only be achieved if noise is the dominant factor determining time resolution.

Optimum choice of the input field-effect transistor for these applications should be based on the effect of its input capacity on the signal size, and the effect of the transconductance on the noise produced by the FET. It can be shown that the optimum value of C_F is equal to the detector capacity C_D. This is difficult to achieve if C_D is large, as the power dissipation in FETs exhibiting high g_m and high C_F is prohibitive. For this reason, we limited the value of C_F to 50 pF in the earlier example.

The discriminator used to "pickoff" the time signal may be set at a fixed level, or may trigger at a level proportional to the signal amplitude. The time pickoff derived from a fixed-level discriminator "walks" as the signal amplitude changes, an undesirable feature unless signals are of relatively fixed amplitude, although a "walk corrector" may be used to correct for this effect. Usually, it is preferable to use a discriminator triggering at a fixed fraction of the signal amplitude. Optimum choice of the signal fraction used for time pickoff is dependent on a number of considerations which change according to the application. However, a few general rules may be stated:

(a) If the detector signal pulse shape is constant, the best fraction to use is that where the discriminator fires on the fastest rising part of the signal. This implies setting the level well above the rounded initial start of the signal rise (caused by multiple integration in the amplifier).

(b) If fluctuations in the rise time of the basic signals occur, such as in many semiconductor detectors, the discriminator should be set to trigger at the smallest possible fraction of the signal amplitude, consistent with avoiding triggering too frequently on noise, and with avoiding the initial rounded part of the signal rise.

C. Fast Timing with Germanium γ-Ray Detectors

1. *Detector Signal Pulse Shape*

Gamma rays interact randomly through a detector volume producing small regions of ionization. For low γ-ray energies, absorption in the detector material causes a nonuniform distribution of interactions through the volume, but the distribution becomes nearly uniform for high-energy γ rays. The shape of the output signal, which is the summation of hole and electron components, depends on the relative magnitude and duration of these components; therefore, the rise time exhibits statistical fluctuations.

Figure 37a shows the locations of three interactions, one near the middle of the detector and one near each contact. Germanium detectors are normally operated at high voltages, resulting in uniform electric fields adequate to produce velocity saturation for carriers (10^7 cm/sec), so the movement of each carrier produces a constant current in the external circuit until the carrier is collected. Assuming that the detector is 1-cm thick, the pulse shapes shown in Fig. 37b result. Signals for three events are shown, and also for events at intermediate positions in the detector. This picture assumes that the charge produced by an interaction is localized in a very small region. This is reasonably valid for γ rays of energy below 1 MeV interacting by a photoelectric process, where the photoelectron range is well below 1 mm. The signal is more complex when a γ ray interacts by Compton scattering, followed by a photoelectric process, as these events occur at different points in the detector volume.

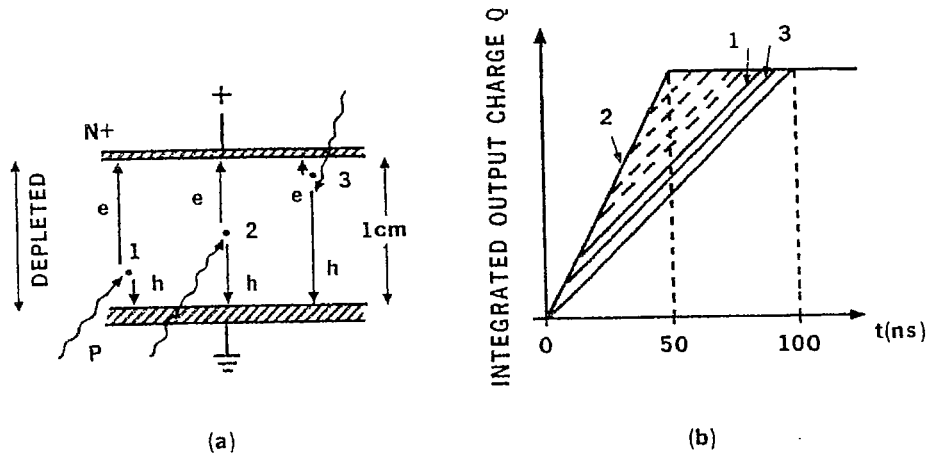

Fig. 37. Charge collection in a thick planar detector: (a) Events at three locations are shown; (b) output signal charge as a function of time.

The planar geometry shown in Fig. 37 produces a rather simple distribution of pulse shapes. More complex shapes occur in coaxial detectors, particularly of the closed-end type. However, the pulse shapes of Fig. 37 can be used for discussion of the general aspects of timing.

2. *Circuit Considerations*

Circuit considerations in fast timing with germanium γ-ray detectors are similar in some respects to those described in Section IV.B.2, but a number of major differences arise. The detector capacity is generally smaller, so the mechanical configuration of the input circuit is less critical. This is fortunate as germanium detectors must be mounted in a cryostat. Also, the signal rise time is rather slow in γ-ray systems, so the rise time of the amplifier is less critical than in fast particle timing experiments. On the other hand, variations in the rise time of signals are large, and they cause problems in timing measurements with γ-ray detectors.

Amplifier noise causes a spread in γ-ray timing measurements, just as for particles (see Section IV.B.2), but the longer detector signal rise time changes the importance of amplifier rise time (τ). The noise is proportional to $\tau^{-1/2}$, but the rate of crossing of the discriminator level may be determined either by the detector or by the amplifier. If the detector signal rise time is dominant, speeding up the amplifier results only in an increase in noise, and therefore worse timing. On the other hand, if the amplifier determines the final signal rise time, speeding it up increases the noise, but despite this, an overall improvement in timing results. Therefore, an optimum amplifier rise time must exist for germanium γ-ray detector timing experiments.

The effect of integration in the amplifier is more complex than indicated by these simple considerations. For example, Fig. 38 shows the effect of a 10-nsec single-*RC* integrator on a typical detector signal. In this case, which is fairly

typical of germanium γ-ray detector systems, the slower rate of crossing caused by setting the discriminator below the level shown in this figure will degrade time resolution. Therefore, an important effect of slowing down the amplifier is to prohibit setting the discriminator at a very low level on the signal. This competes with an obvious desire to set the discriminator to a low level to reduce the timing spread due to signal rise time variations in the detector (see Fig. 37b).

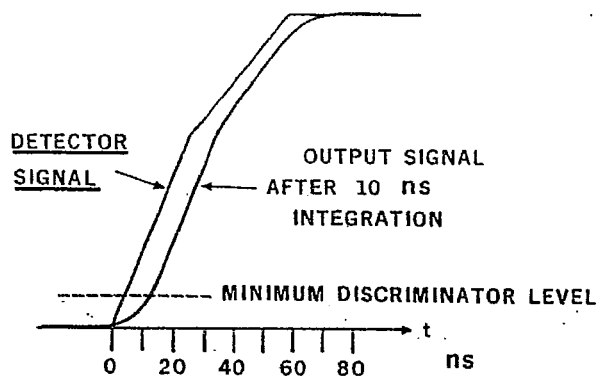

Fig. 38. Effect of a 10-nsec integrator on the front edge of a typical signal.

This discussion has centered on fixed-size signals. As signals vary in size, the time pickoff provided by a fixed level discriminator changes, producing a "walk" with amplitude. A discriminator designed to change its threshold level in proportion to the signal amplitude (a fractional discriminator) overcomes this problem, or some method of walk compensation may be used in the later data processing system to correct the time information derived from a fixed level discriminator.

The distribution of time delay between an event and the time pickoff signal is examined in Fig. 39. As seen in Fig. 39a, a discriminator set to a level βA_0 produces timing signals delayed by βt_0 (where t_0 is the rise time of the fast signal) after events occurring in the central region of the detector. Events near the detector faces, as shown in the inset of Fig. 39a (a fraction 2β of the total events), produce delays uniformly distributed from βt_0 to $2\beta t_0$. If no spread occurred due to noise, the time distribution shown in Fig. 39b would be observed, but in a normal system (~5-nsec resolution) the time distribution shown in Fig. 39c is seen. This distribution only applies if a fractional discriminator is used. Varying the fraction β alters the relative proportions of pulses appearing in the main peak, and those in the delayed tail.

That part of the time resolution due to noise is inversely proportional to the signal amplitude, since the noise is fixed in amplitude while the rate of rise of a signal is proportional to its amplitude. Therefore, while fractional discriminators and walk correctors can be made to produce timing signals almost independent

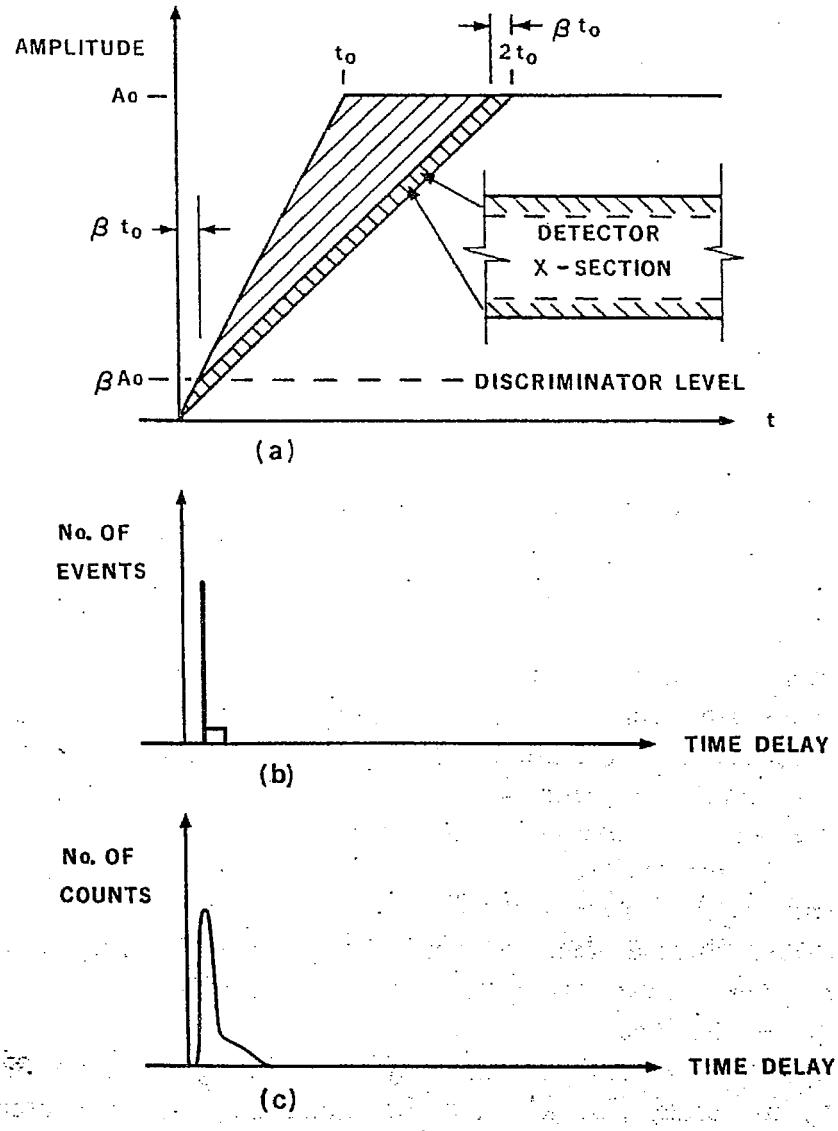

Fig. 39. Showing the predicted time distribution of discriminator triggering: (a) Range of pulse shapes; (b) time distribution in a noiseless system; (c) time distribution in a normal system.

of pulse amplitude, the timing resolution always degrades as the γ-ray energy decreases.

V. Design Factors in Electronic Modules for Fast Timing

A. Fast Amplifiers

The primary function of fast amplifiers is to amplify signals derived from detectors or preamplifiers without significantly degrading their rise time. Normally such amplifiers present a 50-Ω input impedance to match the

characteristic impedance of the input cable, and the output circuit is designed to feed a terminated 50-Ω cable with negative signals of at least 1-V amplitude. The matched input-output system permits cascading several amplifiers to achieve the overall gain required in a system, while avoiding possible "ringing" on signals due to cable mismatches.

Gain stages used in fast amplifiers use very high frequency transistors ($f_T \simeq 2000$ MHz), usually in feedback-pair configurations producing voltage gains in the 10–20 range, with rise times in the 1–2-nsec range. Although negative feedback is employed to stabilize the gain, and to flatten the gain versus frequency characteristic, the amount of feedback is much lower than in the amplifiers used in the energy-analysis channels of spectrometers. As a result, the gain stability is poorer, but ringing on signals due to phase shifts within the feedback loop, which are of great importance in fast amplifiers, are minimized. An important consideration in the design of fast amplifiers is the requirement that the amplifier rise time should be independent of signal amplitude and counting rate.

The signal pulse-shaping requirements in fast amplifiers are quite different from those discussed for spectrometer amplifiers (see Section II.C.2). In most cases, the amplifier rise time should be as fast as possible, and is limited only by the transistors employed. Deliberate integration may sometimes be employed to reduce noise when the overall signal rise time is dominated by the detector charge-collection process (see Section IV.C.2). On the other hand, differentiation is usually required prior to the first amplifier to avoid signal pileup at high counting rates. Shorted delay-line differentiation (using coaxial cables) is normally employed in very fast systems, but RC and bipolar differentiators may be used in some situations.

The signal/noise factors in fast timing systems differ greatly from those in the slow energy-measuring channels. At the short shaping times used in fast channels, delta noise is dominant, and step noise need not be considered (see Section II.C.2). The best signal/noise ratio is achieved by using a preamplifier with a reasonably high input impedance to amplify the signals prior to feeding the 50-Ω cable to the fast amplifier. If the input shunt resistance is made large enough to give an input time constant long compared with the system rise time, its noise contribution can be neglected. The main noise source is then the input amplifying device. At high frequencies, either transistors or very high transconductance FETs are best used for this stage. Equivalent noise resistances of about 20 Ω can be achieved, producing input equivalent RMS noise levels of only 8 μV or so in systems with rise times of 2-nsec. If the gain of the whole preamplifier is low, the noise (13-μV RMS) in the input resistance (50 Ω) of the fast amplifier may be a significant contribution to the total system noise. The effect of these noise levels on time resolution is related to the size and rise time of the signal as discussed in Sections IV.B and IV.C.

B. Time Pickoff Discriminators

As discussed in Section IV.C.2, fixed level discriminators (usually called leading-edge discriminators) are sometimes used for fast time pickoff, but the dependence of their triggering time on the size of a signal is undesirable, so discriminators triggering at a constant fraction of the signal amplitude are now also used. In either case, an element capable of switching very quickly when a signal crosses a preset threshold level is required. The tunnel diode provides the ideal element in this regard, and is used almost exclusively as the triggering device in fast discriminators. This contrasts with the slow discriminators discussed in Section III.G.

The operation of a tunnel diode discriminator will be described in terms of Fig. 40 which shows the forward current–voltage characteristic of a typical tunnel diode. In the region from 0 to A, the built-in field in the junction region produces free carriers by a tunneling action, so the diode exhibits a very low impedance ($\sim 5\ \Omega$). Driving the diode in the forward voltage direction past A reduces the built-in junction field, so tunneling ceases, and the current through the diode decreases (a negative resistance region). However, further forward bias causes minority carrier injection, and the current increases as shown.

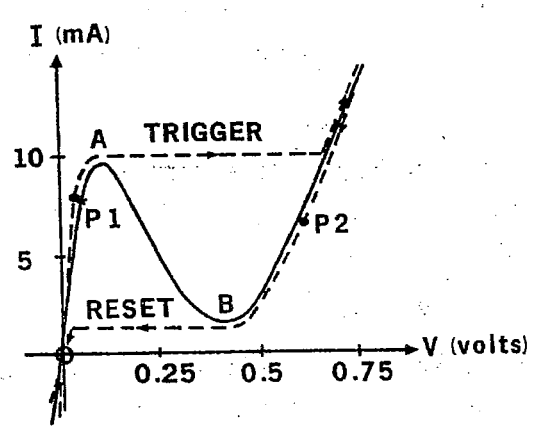

Fig. 40. Characteristic of a tunnel-diode discriminator.

To use the device as a discriminator, the diode is biased to a point P1, and the signal increases the diode current until the peak point A is passed. The diode switches very rapidly to its high voltage state at this point. If the signal is larger than required to pass this point, it drives the diode current up the right branch of its characteristic. When the signal is removed, point P2 is reached. To reset the diode back to its original condition, a reset pulse is applied that reduces the diode current below its minimum point B. Due to the storage of minority carriers in the bulk, the reset action is much slower than the triggering, which only involves turning off the tunneling action.

1. *Considerations in Leading-Edge Discriminators*

To achieve satisfactory timing, leading-edge discriminators must be set to a very low level on signals, so that the walk due to variations in signal amplitude is kept at a small value. This frequently means setting the threshold so low that the discriminator fires at a high rate on noise pulses. This is undesirable, as it produces false timing signals. An arrangement that overcomes this problem is to use two discriminators, one set to a very low level on the signal, even within the noise, while the other is set above the noise level to trigger only when true signals occur. The signal from the lower level discriminator, delayed by a short time, then samples the high discriminator condition to determine whether a signal has occurred. In this way, the lower level discriminator provides the timing pulses, but they only appear at the output when a true signal occurs.

Even when this arrangement is employed, signal amplitude variations produce walk in the timing signals. Consequently correction of the walk is necessary. This may be achieved in several ways:

(a) By measuring the time delay between firing of two discriminators set to different levels of the signal, an extrapolated zero time for the signal can be determined. This extrapolated leading-edge timing technique depends on there being no change in the slope of signals between the two discriminator levels; as this is often not true (e.g., germanium γ-ray detector signals) the technique has limited value.

(b) The walk may be corrected by modifying the output of the time-to-amplitude converter (or the digital data derived later) by a suitable function calculated from a slow signal pulse-height measurement. The correction can be empirically adjusted for best results.

2. *Constant-Fraction Discriminators*

Automatic correction for the effects of signal amplitude variations (assuming constant shape) can be made by discriminating at a level that is a constant fraction of the signal amplitude. The best way to achieve this is to shape the signal, prior to the discriminator, so that a bipolar signal reaches it. The front edge of the signal can then be used to set the discriminator at a suitable level above noise, and the discriminator can be adjusted to reset at the zero-crossing point of the bipolar pulse. Assuming a linear system, fed with a constant detector pulse shape, the zero-crossing time is independent of the signal amplitude.

Figure 41 illustrates the method of pulse shaping used to achieve these objectives (Chase, 1968). The operation is largely self-explanatory; it is obvious that the zero-crossing time at the output depends partly on the signal rise time, on the fraction β determined by the attenuator, and on the delay τ. The discriminator is set to fire at a level A above noise, and it resets accurately at the

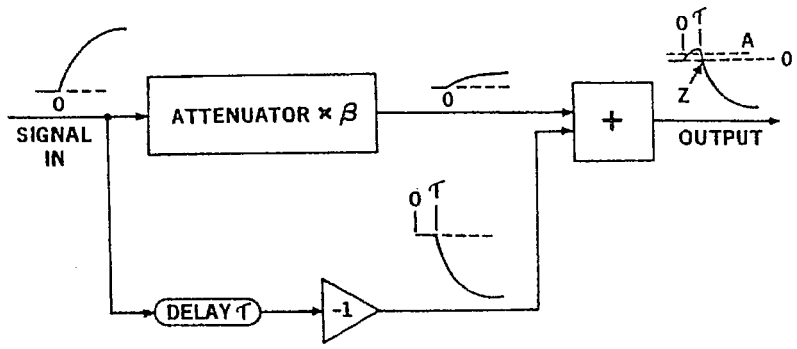

Fig. 41. Pulse shaping for a constant-fraction discriminator.

zero crossing point. Adjustment of the fraction β can be made to achieve the best rate of crossing of zero for the signal amplitude range of interest; this achieves the best time resolution. The general considerations involved in choice of the fraction β are outlined in Section IV.C.2.

The zero-crossing discriminator (probably a tunnel-diode circuit) must provide the backlash implied by its triggering at level A and resetting at zero. Also, as the time information is derived at the zero-crossing time, the circuit should be designed to reset as fast as possible. This dictates that the tunnel diode peak point A (Fig. 40) should be used for the reset point, unlike the case of a leading-edge discriminator.

C. Time-to-Amplitude Converters

Time-to-amplitude converters (TAC) are used to produce output pulses whose amplitude is linearly proportional to the time delay between pairs of pulses fed successively to *start* and *stop* inputs. The full-scale time range is made adjustable so that time distributions as short as 10 nsec or as long as several μsec in total span can be studied. Apart from the requirement that the time-to-amplitude conversion be reasonably linear, it is also essential that the conversion be stable, and that the equivalent time spread introduced into the measurement by the TAC be very small. Timing accuracies as low as 10 psec (FWHM) have been achieved in the best situations.

A typical TAC is shown in block form in Fig. 42. The basic time-to-amplitude conversion is carried out by using the *start* pulse to switch a constant current I into an integrating capacitor C, and by stopping the current flow when a *stop* pulse occurs. The actual current switching is accomplished by fast diodes $D1$, $D2$, and $D3$ controlled by bistable circuits switched by the input pulses. These diodes exhibit very low charge storage effects, and introduce only small stray capacities. These are essential features for fast linear conversion. Furthermore, the capacitor C, and its ground connection, must introduce no high-frequency rings.

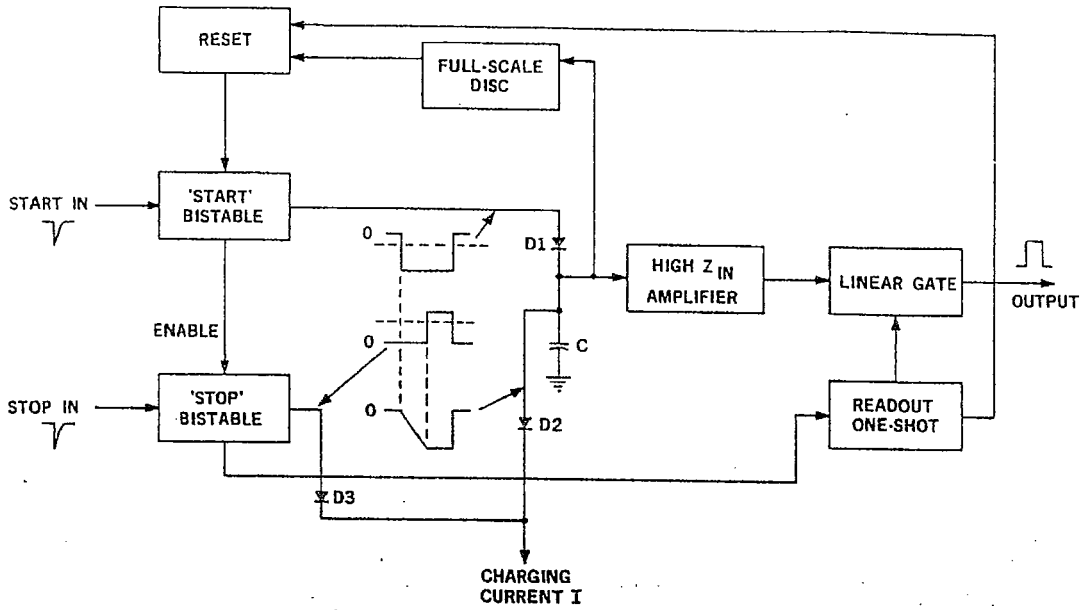

Fig. 42. Block diagram of a time-to-amplitude converter.

The circuit shown in Fig. 42 satisfies the following conditions:

(1) The *stop* bistable flip-flop is only triggered when a *stop* input pulse occurs within the selected time range after a *start* pulse. Any *stop* pulse not meeting this requirement is neglected.

(2) Further *start* or *stop* pulses do not interfere with a measurement in progress.

(3) If a *start* pulse is not followed by a *stop* pulse within the selected time range, the circuit resets rapidly at the end of the range, and is ready for a further *start* pulse. No output pulse occurs.

(4) An output pulse occurs immediately after a valid *stop* pulse, while the integrating capacitor remembers the voltage stored on it during the timing period. The system is reset immediately after the end of the output pulse.

Appendices

A. Bipolar and Field-Effect Transistors

The biggest single revolution in nuclear electronics in the past 15 years has been due to the use of transistors. The reliability of semiconductor devices, as compared with the vacuum tubes used earlier, has made possible a much higher level of sophistication in signal- and data-processing in nuclear experiments. It is not unusual for a single nuclear experiment to require as many as 10,000 transistors to operate continuously, and with absolute reliability, for long

periods of time. We hope that this brief exposition will lead to more general reading on the topic (Shive, 1959).

Bipolar transistors, invented by Shockley in 1950, represented the first dependable semiconductor amplifying devices. Like most semiconductor devices, these depend on the behavior of a junction in a semiconducting crystal, where the dominant electrically active impurity in the lattice changes from one producing free electrons (i.e., valency-five or a *donor* in a valency-four lattice), to one producing free positive holes (i.e., valency-three or an *acceptor*). By various procedures, it is possible to produce flat interfaces between *n* regions (donors dominant), and *p* regions (acceptors dominant), which are referred to as "junctions." The operation of most semiconductor devices depends on the behavior of the free electrons and holes at these junctions. An electron leaving an *n* region, where it is a *majority* carrier, and diffusing or being injected into a *p* region then becomes a *minority* carrier in this region, and vice versa for holes travelling in the reverse direction. It is important to recognize that a charge carrier can exist in a region where it is in the minority for quite a long time (up to several milliseconds in some cases) before it combines with the opposite type of carrier to disappear.

Figure 43 shows the conditions existing in a semiconductor junction in equilibrium with no externally applied voltages. In the *n* region, the donor atoms have released electrons to acquire a positive charge; these positive charges are fixed in the lattice, while the electrons are free to move. Similarly, acceptor atoms become fixed negative charges in the *p* region by capturing electrons,

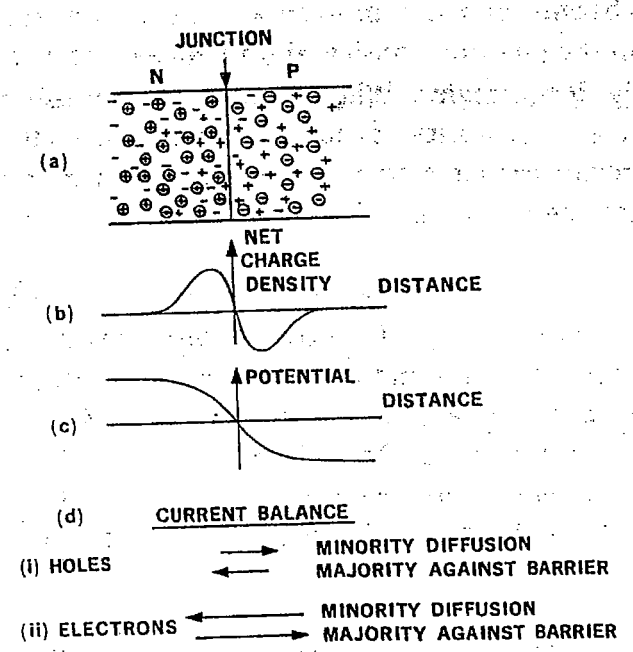

Fig. 43. Equilibrium conditions in a semiconductor junction.

thereby producing free holes. Thermally induced diffusion of the free holes and electrons naturally leads to passage of these carriers across the junction, so a dipole charge layer is produced, as shown in Fig. 43b, resulting in the potential distribution of Fig. 43c.

The balance between electron and hole currents flowing across the junction in this condition is important in device applications. Figure 43d indicates the balance conditions. Flow of the majority carrier from either side of the junction to the other is resisted by the potential barrier of Fig. 43c. On the other hand, a minority carrier at one side of the junction can diffuse from deep within its region to the junction where its crossing is aided by the potential distribution existing there. In the equilibrium condition the potential adjusts itself to produce a detailed balance between the electron currents in the two directions, and between the two hole currents. The relative magnitude of the electron and hole currents depends on the relative doping levels in the *n* and *p* regions. If the *n* region is more heavily doped than the *p* region, the electron currents will be greater than the hole currents.

The equilibrium condition shown in Fig. 43 is rarely of interest in devices; in general, we are more interested in the perturbation caused by applying an external voltage to the junction. The behavior then depends on whether the applied voltage tends to reduce the potential barrier of Fig. 43c (forward bias) or to increase it (reverse bias). In the first case, the reduction of the barrier permits increased flow of majority carriers from one side of the junction to the other side where they become minority carriers. This process can be used to inject large currents of minority carriers into a region. Furthermore, if the emitting region is very heavily doped compared with the region receiving the carriers, the current flow in the junction consists almost entirely of minority carriers injected into the lightly doped region. When a junction is reverse biased, the effect is to suppress the flow of majority carriers from one side to the other. On the other hand, the minority carrier diffusion currents shown in Fig. 43d remain almost unchanged since their value is controlled by diffusion from regions remote from the junction.

The operation of a bipolar transistor depends directly on the considerations of the last paragraph. Figure 44 shows a *pnp* transistor structure (in an *npn* transistor, the roles of holes and electrons are reversed) consisting of a piece of semiconductor in which a thin *n* region (only a few micrometers thick) is interposed between *p* regions. One of the *p* regions, called the "emitter," is very heavily doped compared with the *n* region, which is called the "base." When the emitter junction is forward biased it efficiently injects holes into the base region. The other *p* region, called the "collector," is reverse biased with reference to the base, so it collects holes that diffuse through the thin base layer to the collector junction. In practice, the only holes lost are the few that recombine with electrons in the base, so the collector current is nearly equal to the emitter

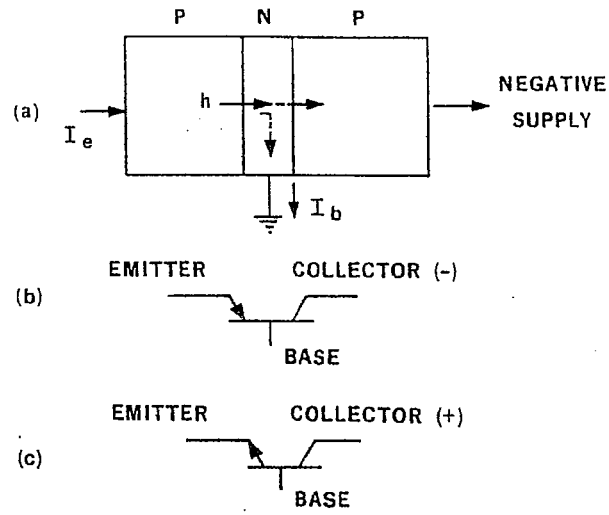

Fig. 44. (a) Operation of a bipolar transistor; (b) symbol for a *pnp* transistor; (c) symbol for a *npn* transistor.

current, while the base current is very small. By modulating the base potential with reference to the emitter, a relatively large collector current can be controlled with very little flow of current in the base. The large current gain (β) from base to collector is the transistor property of most importance in practical applications.

The symbols used for *pnp* and *npn* transistors are shown in Figs. 44b and 44c. The arrow in the emitter lead denotes the direction of positive current flow. Two operating modes are commonly encountered in transistor circuits. In amplifiers, the transistor operates more or less as described in the last paragraph; that is, in a linear mode. In pulse circuits, on the other hand, the transistor is used as a switch. Its *off* condition is obtained by applying a base potential to reverse bias the emitter-base junction, thereby preventing injection at the emitter junction. Virtually no collector current then flows. The *on* condition is achieved by forward-biasing the emitter junction. If a collector load resistance is high, the *on* condition may cause the collector-base reverse bias to fall essentially to zero, the transistor is then said to be operating in the *saturated* condition. As the collector is no longer able to accept all the carriers injected by the emitter into the base, the base current must rise.

The undesirably low input impedance (for some applications) seen at a transistor base has led to the use of another semiconductor amplifying device, the field-effect transistor, shown schematically in Fig. 45. In this device a thin *n* layer of material† provides a conducting path between the heavily doped (n^+) source and drain connectors (conduction is by majority carriers, and, unlike the

† This is an *n*-channel FET; *p*-channel FETs are also used.

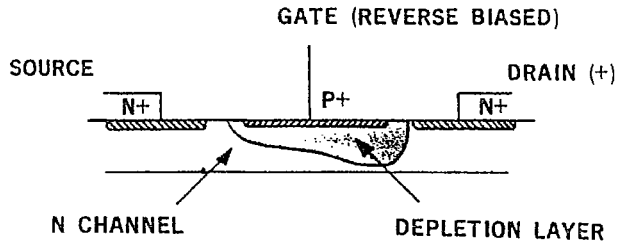

Fig. 45. Diagram of a field-effect transistor.

transistor, does not depend on minority carrier injection). A *p–n* junction is formed on the surface of the conducting channel as shown in Fig. 45. Reverse biasing this junction causes an increase in the potential barrier (see Fig. 43c) existing in equilibrium at the junction, driving electrons from a depletion layer as shown in Fig. 45. Increasing the bias increases the thickness of the depletion layer, pinching-off the conducting channel between source and drain. Therefore, modulation of the gate–source potential controls the drain current. As the gate junction is reverse biased, it exhibits a very high input impedance which is well matched to a radiation detector. For this reason, field-effect transistors are almost exclusively used as input amplifiers for detector signals.

B. Miscellaneous Electronic Terms

Many electronic terms used in this chapter may be unfamiliar to readers. Definitions are given in elementary electronic and semiconductor texts, or in general reviews, such as that of Fairstein and Hahn (1965) cited in the table of references. In some cases, the reader will note interchangeable use of European and American terms (e.g., transconductance or mutual conductance to represent the ratio of the change of drain current to the change of gate-source voltage of an FET). We hope this is not confusing. The term Shottky barrier is used to represent a metal–semiconductor barrier which behaves in many respects like the semiconductor *p–n* junction described in Appendix Section A. However, the lack of carriers injected in the bulk semiconductor results in fast current turn off in Shottky barriers as compared with *p–n* junction diodes.

References

Battista, A. (1970). *Nucl. Instrum. Methods* **80**, 172.
Chase, R. L. (1968). *Rev. Sci. Instrum.* **39**, No. 9, 1318.
Chase, R. L., and Poulo, L. R. (1967). *IEEE Trans. Nucl. Sci.* NS-14, No. 1, 83.
Cottini, C., Gatti, E., and Svelto, V. (1963). *Nucl. Instrum. Methods* **24**, 241.
Fairstein, E., and Hahn, J. (1965). *Nucleonics* **23**, No. 11, 50.
Gere, E. A., and Miller, G. L. (1967). *IEEE Trans. Nucl. Sci.* NS-14, No. 1, 89.

Goulding, F. S. (1965). *In* The Series-Parallel Transistor Switch as a Linear Gate, p. 121 of "Instrumentation and Techniques in Nuclear Pulse Analysis." Nat. Acad. Sci. Nat. Res. Council Publ. 1184.

Goulding, F. S. (1972). *Nucl. Instrum. Methods* **100**, 493.

Goulding, F. S., Landis, D. A., Cerny, J. and Pehl, R. H. (1966). *IEEE Trans. Nucl. Sci.* NS-13, No. 3, 514; (1964). *Nucl. Instrum. Methods* **31**, 1.

Kandiah, K., Stirling, A., and Trotman, D. L. (1969). An Analogue-to-Digital Converter Employing Recycled Successive Approximations. At. Energy Res. Establishment Rep. AERE-R6111.

Klein, C. A. (1968). *IEEE Trans. Nucl. Sci.* **NS-15**, No. 3, 214.

Landis, D. A., Goulding, F. S., Pehl, R. H., and Walton, J. T. (1971). *IEEE Trans. Nucl. Sci.* NS-18, No. 1, 115.

Linhard, J., and Nielsen, V. (1962). *Phys. Lett.* **2**, No. 5, 209.

Nowlin, C. H., and Blankenship, J. L. (1965). *Rev. Sci. Instrum.* **36**, 1830.

Radeka, V. (1967). *Rev. Sci. Instrum.* **38**, 1397.

Radeka, V. (1972). *IEEE Trans. Nucl. Sci.* **NS-19**, No. 1, 412.

Robinson, L. B. (1961). *Rev. Sci. Instrum.* **32**, 1057.

Robinson, L. B., and Gin, F. (1969). *Nucl. Instrum. Methods* **75**, 125.

Robinson, L. B., Gin, F. and Goulding, F. S. (1968). *Nucl. Instrum. Methods* **62**, 237.

Robinson, L. B., Gin, F., and Cingolani, H. (1969). *Nucl. Instrum. Methods* **75**, 121.

Shive, J. N. (1959). "Semiconductor Devices." Van Nostrand Reinhold, Princeton, New Jersey.

Van der Ziel, A. (1962). *Proc. IRE.* **50**, 1808.

CONTRIBUTION TO THE NSAC LONG-RANGE PLAN

THE FUTURE OF GAMMA-RAY SPECTROSCOPY: GRETA, THE GAMMA-RAY ENERGY TRACKING ARRAY

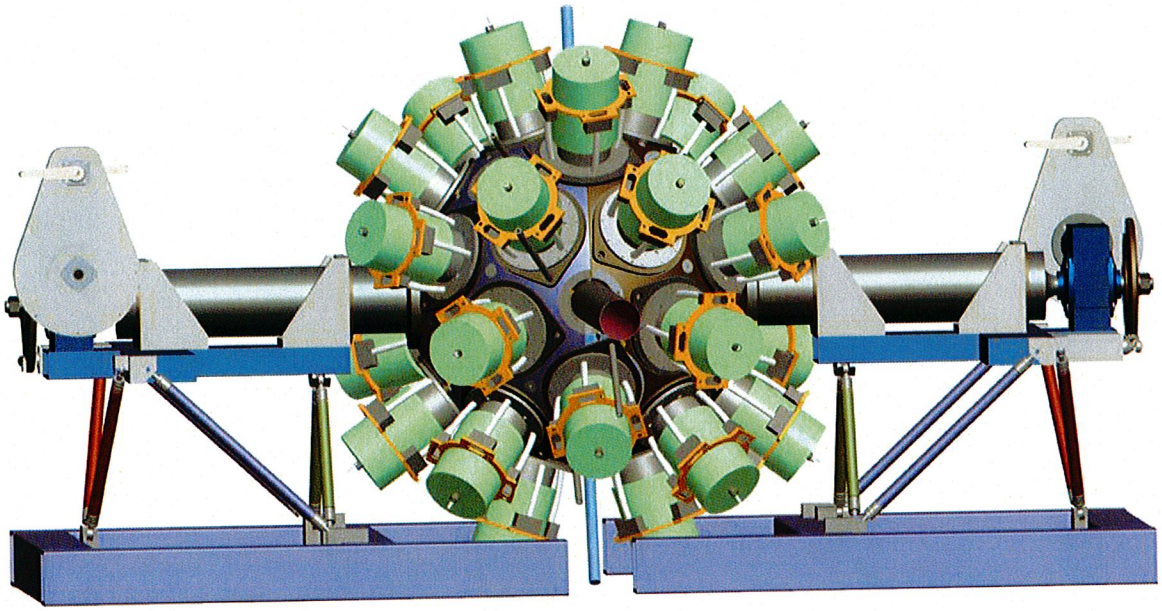

December 2006

CONTENTS

1 Executive Summary 4

2 Introduction 6

3 Physics Opportunities with GRETA and Gamma-Ray Tracking 8

- 3.1 How do extreme proton-to-neutron asymmetries affect nuclear properties, such as shell structure and collectivity?
  - 3.1.1 Doubly magic nuclei far from stability
  - 3.1.2 The alteration of shell structure far from stability
  - 3.1.3 Symmetries and excitation modes in exotic nuclei
  - 3.1.4 The nucleus as an open quantum system
- 3.2 What are the properties of nuclei at the limits of mass and charge?
- 3.3 What are the properties of nuclei at the limits of angular momentum?
- 3.4 Nuclear astrophysics, fundamental interactions and rare processes

4 Technical Accomplishments towards a 4π Gamma-Ray Tracking Array 19

5 Auxiliary Detectors for GRETA 21

6 Applications of Gamma-Ray Tracking Detectors 23

7 Cost Estimates for GRETA 23

8 The Path to GRETA: Progress and Milestones so Far 27

Appendix: The Management Structure of GRETINA 28

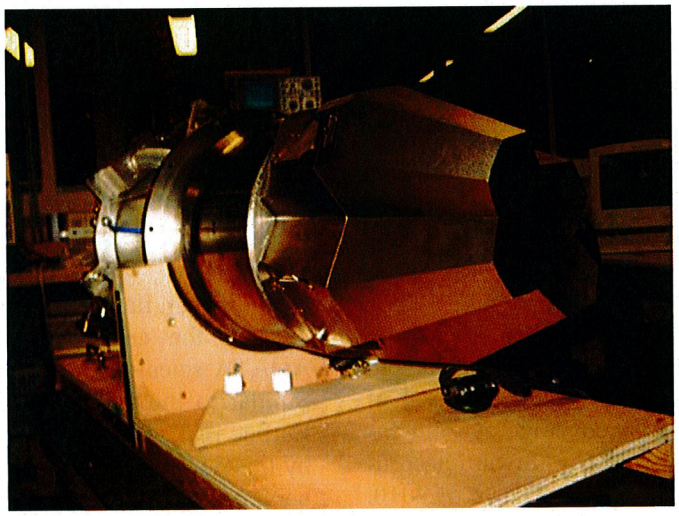

Photograph of the first quad-cluster Ge detector module which forms the basic building block of GRETINA and GRETA. (October 2006)

1. Executive Summary

This is a time of great opportunity in nuclear spectroscopy. The development of radioactive beam capabilities around the world is opening a new landscape for discovery, and the connections between nuclear structure studies and astrophysics, neutrino physics, and physics beyond the standard model are stronger than ever. New detector technologies are evolving which can meet the challenges of the new generation of experiments. Leading these is the technology of "γ-ray tracking" which can revolutionize γ-ray spectroscopy in a way that large arrays of γ detectors did a decade ago. During the last few years this technology has been shown feasible and GRETINA a 1π detector is under construction. However, the momentum in developing this technology to its full potential must continue towards GRETA, a full 4π calorimeter. GRETA will carry γ-ray spectroscopy into the next generation where it will be needed to fully exploit the science opportunities at radioactive beam facilities and increase the reach of stable beam facilities. In addition, γ-ray tracking technology will have important applications for science, medicine, and homeland security.

GRETA was first mentioned in the 1996 Long Range Plan (LRP) and became a recommendation in the subsequent LRP of 2002. In the 2003 NSAC report entitled "The Nuclear Physics Science Horizon: Projects for the Next Twenty Years" GRETA obtained the highest rank of "1" in both science and readiness categories. The physics justification and technical performance for a 4π γ-ray tracking detector were also well documented in the extensive report submitted by the National Gamma-Ray Tracking Coordinating Committee setup by the DOE Office of Nuclear Physics in 2002. A selection of physics highlights along with an up to date status of technical issues are contained in the present document.

As a first step towards GRETA, a physics-rich pilot program was devised to allow technical development to advance at full speed. This led to the proposal of GRETINA, a detector with 25% coverage of solid angle. The GRETINA project is moving forward according to schedule with a start of operation date of 2010. Our intention is to keep moving forward with γ-ray tracking in this country and to complete our original proposal to build the full 4π array GRETA, in order to fully optimize the physics potential of this new technology.

For most experiments, GRETA will improve the power of GRETINA by a factor of 10 -100. This will greatly extend the reach of the physics and allow advances in the study of nuclear structure, nuclear astrophysics, and fundamental interactions. For example, the alteration of shell structure and new collective phenomena at the two extremes of isotopic number can be studied with fast beams from ^{48}Ni to ^{80}Ni. The structure of heavy elements with Z larger than that of Sg (Z=106) can be studied with enough detail to help constrain and refine the theoretical calculations needed to make a more accurate prediction of the stability of super heavy elements. The search for hyperdeformed nuclei with 3:1 axis ratio at the very limits of angular momentum will be within reach with GRETA's 100 fold increase in sensitivity. Crucial capture reactions in element synthesis in nuclear astrophysics have extremely low cross sections which require detectors with the highest possible efficiency and ability to reject background. In the area of fundamental interactions GRETA's high spatial resolution and efficiency will bring a large increase in sensitivity to many measurements; including tests of QED and CPT from studies of positronium annihilation, and measurements of V_{ud} obtained from the superallowed β-decay of ^{10}C.

The GRETINA construction project has developed all the advanced technology needed for GRETA. The first detector module with 4 highly segmented irregularly shaped crystals closely packed in a single cryostat has been produced. Signal digitizers with the required resolution and sampling rate have been fabricated and are in use. Signal decomposition and tracking software has already demonstrated the required position resolution and speed. The data acquisition system with sufficient computing power and storage capability has been designed and prototyped.

In Europe a competitive γ-ray tracking germanium shell detector, AGATA, is advancing. It will be used at the European radioactive and stable beam facilities. At present, the collaboration between GRETINA and AGATA scientists in technology R&D is very strong. Similar to the US, the nuclear physics community in Europe realizes the vast range of opportunities offered by this device and the demand for its use is expected to be very large. Clearly, continuing development toward GRETA is essential to our competitive position in the field of γ-ray spectroscopy.

Detailed GRETA cost projections have been based on the current GRETINA project. As GRETINA contains all the key technologies, the cost scaling should be reliable and have very little uncertainty. Following the DOE project scheme for escalation and contingency, we estimate a total project cost of $42M beyond the GRETINA phase and a project completion date in 2016. The development would steadily lead to ever-increasing physics reach and flexibility as the device grows from 1π to 4π. However, many key physics goals require the complete shell for success.

In summary we would like to quote from the 2002 NSAC Long Range Plan Overview and Recommendations section (page 9),

"The detection of gamma-ray emissions from excited nuclei plays a vital and ubiquitous role in nuclear science. The physics justification for a 4π tracking array is extremely compelling, spanning a wide range of fundamental questions in nuclear structure, nuclear astrophysics, and weak interactions. This new array would be a national resource that could be used at several existing stable and radioactive beam facilities, as well as at RIA."

With GRETINA now under construction we are moving towards this goal. We strongly urge the timely completion of the full 4π system GRETA.

2. Introduction

The unique strongly interacting aggregation of fermions that we call the atomic nucleus displays a remarkable diversity of phenomena and symmetries. Its behavior and structure continues to surprise and fascinate as unexpected properties are revealed by fresh experimental opportunities arising from increasingly sensitive instrumentation along with new accelerator developments. A central component in the highly successful US nuclear structure program has been through the utilization of γ-ray spectroscopy techniques, in particular, using Gammasphere. The latter's resolution, granularity, efficiency, and ability to be used in conjunction with a powerful suite of auxiliary detector systems, have made it an unsurpassed device for studying rare and exotic nuclear properties. (Over 600 refereed publications and 100 PhD theses have been written utilizing data from this detector so far.) It is therefore extremely exciting that at the same time as a major new radioactive beam accelerator facility initiative is on the horizon that huge advances in our γ-ray detection capabilities are also possible. Such a next generation detector system would allow us to capitalize on the science opportunities prior to and when the new accelerator facility was completed. Indeed, as stated in the 2002 NSAC Long Range Plan (Overview and Recommendations, page 9),

"The detection of gamma-ray emissions from excited nuclei plays a vital and ubiquitous role in nuclear science. The physics justification for a 4π tracking array is extremely compelling, spanning a wide range of fundamental questions in nuclear structure, nuclear astrophysics, and weak interactions. This new array would be a national resource that could be used at several existing stable and radioactive beam facilities, as well as at RIA."

While the present state-of-the-art detector arrays, which consist of large volume germanium crystals surrounded by a suppression shield, have pushed this particular detector technology to its limit, it has become apparent that significant further gains in sensitivity will be possible as a consequence of an innovative and new design paradigm utilizing the concept of γ-ray energy tracking in electrically segmented Ge crystals. These new opportunities have arisen from technical innovations first realized by the US γ-ray spectroscopy community. The new 4π detector design mentioned above which was already discussed in the 1996 Long Range Plan is called GRETA (Gamma-Ray Energy Tracking Array). It would contain about 120 (30 quad-cluster modules) co-axial Ge crystals each segmented into 36 portions and arranged in a highly efficient 4π geometry. GRETA would have about 100 times the sensitivity of Gammasphere for selecting weak exotic signals, and thus give as big a jump in capability compared to Gammasphere as Gammasphere was to the previous generation of detector systems.

The improved sensitivity or resolving power is due to the new technique of "tracking", which identifies the position and energy of γ-ray interaction points in the detector segments. Since most γ rays interact more than once within the crystal, the energy-angle relationship of the Compton scattering formula is used to "track" the path of a given γ-ray. The full γ-ray energy is obtained by summing only the interactions belonging to that particular γ-ray. In this way there are no lost scatters into suppression shields (which cover nearly 50% of 4π in Gammasphere) and so a much higher overall efficiency can be achieved, for example, by a factor of 6 (GRETA vs Gammasphere) and 100 (GRETA vs MSU SeGA array) for a single 1 MeV γ-ray. An efficiency gain of about 20 times over Gammasphere is also expected for 15 MeV γ rays. Other key design benefits of a highly segmented Ge array include high energy resolution, high counting rate capability (a factor of ~5 over Gammasphere), good position resolution (1.4 degrees versus 6 degrees for Gammasphere) which is critical for Doppler shift corrections since many experiments involve high recoil velocities, the ability to handle high multiplicities without a high double-hit probability, and the ability to pick out low-multiplicity events hidden in a high background environment due to background rejection by direction. Another asset is that the high segmentation also makes high precision linear polarization γ-ray measurements possible. The modularity of the detector design makes it extremely versatile and flexible for use in many different configurations.

In 2003, after major R&D efforts had validated the GRETA concept to show that building a tracking detector array was feasible, and that a first class physics case existed, the DOE gave the go ahead for a mission need decision on GRETINA (CD0). GRETINA, which comprises ¼ of GRETA, is a logical first phase for a staged approach to GRETA. GRETINA itself will provide a large gain in sensitivity compared to existing systems for addressing an important range of scientific questions and especially for studying nuclei far from stability at existing rare isotope accelerator facilities.

The gains in performance are most significant for fast beam experiments such as fragmentation reactions, and quasi-elastic processes such as Coulomb excitation and transfer reactions. Progress on all the essential components of GRETINA, which will comprise of 28 36-fold segmented Ge crystals in 7 cryostats, is proceeding extremely well and is on track for a start of operation date in 2010.

The aim of this document is to keep the momentum going with regard to γ-ray tracking in this country and to argue that we should complete our original intention from 1996, namely to build the complete 4π array GRETA, in order to fully optimize the physics potential of this new technology. This is supported by the recommendation contained in the 2002 Long Range Plan and the major report from NSAC in 2003 entitled "The Nuclear Physics Science Horizon: Projects for the Next Twenty Years" in which GRETA obtained the highest rank of "1" in both science and readiness categories. In addition there is a major effort in Europe to build a 4π highly-segmented germanium shell, called AGATA, similar in concept to GRETA. The US nuclear structure community, which conceived of this next revolutionary step in γ-ray detection capability, is therefore poised and eager to complete a next generation 4π γ-ray spectrometer with unsurpassed sensitivity and discovery potential, GRETA.

The present document is arranged as follows. In the next section some key physics goals are presented where the capabilities of GRETA over existing detector systems are emphasized in each case. The technical accomplishments towards a 4π γ-ray tracking array are then documented. New auxiliary triggering detectors which will play an essential role in the success of GRETINA and GRETA are discussed followed by some applications of "γ-ray tracking" technology. Next the cost estimates and timeline of GRETA are presented along with a brief summary of progress and milestones so far. In the appendix an outline of the management structure of the GRETINA project is given.

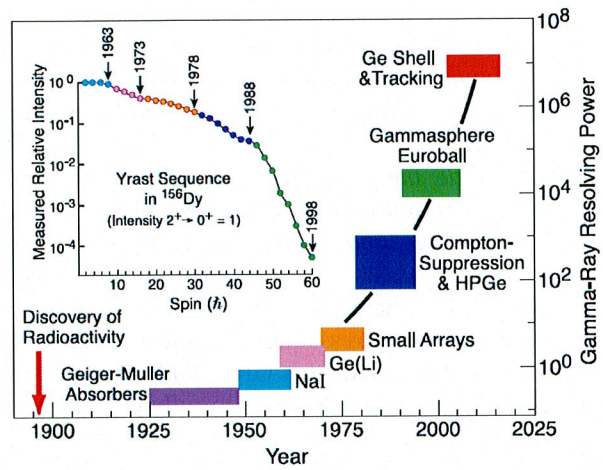

Evolution of γ-ray detector technology. The large gain provided by a Ge shell and tracking is clearly shown. The calculated resolving power is a measure of the ability to observe faint emissions from rare and exotic nuclear states. This is illustrated in the left hand insert, which indicates the strong inverse relationship between resolving power and the experimental observational limit. Taken from the NSAC 2002 Long Range Plan document, page 132.

3. Physics Opportunities with Gamma-Ray Tracking

In the 2002 NSAC Long Range Plan for Nuclear Science a number of key physics themes and questions were selected for special discussion and which outlined future priorities of investigation for our field. They include,

- *What are the limits of nuclear existence?*
- *How do weak binding and extreme proton-to-neutron asymmetries affect nuclear properties?*
- *How do the properties of nuclei evolve with changes in proton and neutron number, excitation energy, and angular momentum?*

It is now accepted that a γ-ray energy tracking detector will be needed to address these questions. This is of course one of the reasons that GRETINA has been approved for construction. However to fully capitalize on the science opportunities at existing, and future facilities, a full 4π array is essential.

Of course the gains made possible with GRETA will be specific to the type of physics experiment being performed. For example, the previous figure refers to a high multiplicity experiment. In the following Table and Figure the improvement in resolving power or sensitivity of GRETA is calculated and compared to GRETINA, Gammasphere or SeGA for a variety of different experiments and reaction types.

The physics impact of GRETA will cover a broad range of topics and its use will be in high demand. For example, at the 2004 RIA Facility Workshop, GRETA was a critical device in a very large fraction of the proposed experiments. In fact much time was spent discussing how it would be moved from beam line to beam line. The experimental examples below offer only a brief sampling of the richness of questions that GRETA will ultimately touch upon.

3.1. How do extreme proton-to-neutron asymmetries affect nuclear properties, such as shell structure and collectivity?

3.1.1. Doubly Magic Nuclei Far from Stability

Nuclear shell structure has been an underlying theme of nuclear structure physics for over 50 years, and earned the Nobel Prize for J. Hans D. Jensen and Maria Goeppart-Mayer in 1963. The "magic" nuclei, with a closed shell of protons or neutrons, serve as landmarks in the chart of the nuclides, analogous to the inert noble gases in the periodic table. Of special interest are "doubly magic" nuclei such as ^{40}Ca and ^{208}Pb, which together with their immediate neighbors have long been the focus of extensive study. Light neutron-rich nuclei, however, indicate that the shell structure of nuclei near stability cannot be reliably extrapolated to the drip lines. It is thus especially exciting that beams of new doubly magic nuclei are becoming available. Initial studies of the region around ^{132}Sn are already possible, but can be greatly improved at the next-generation facilities; the more exotic neutron-rich ^{78}Ni and proton-rich ^{100}Sn regions will need to await a facility like RIA. By employing GRETA at such a facility, it should be possible to make detailed studies of all three of these new doubly-magic regions. Such studies are great importance for both nuclear structure and astrophysics.

Measurements of Coulomb excitation of magic and doubly magic rare isotopes provides crucial information on the collectivity of low-lying excitations, on the underlying nuclear shape (through the reorientation effect), and on their magnetic moments (through transient field or recoil-in-vacuum techniques.) The superb energy resolution afforded by GRETA will be important for multi-step Coulomb excitation, but also for cases where low-energy ("safe") Coulomb excitation is performed with cocktail beams and the excited levels of the various beam components lie close in energy.

Single-particle transfer reactions such as (d, p) or (d, ^{3}He) in inverse kinematics, reveal the energy and strength of the single-particle and single-hole excitations relative to the closed shells. Studies with these reactions will not only identify new single-particle states, but also provide measurements of the spectroscopic factors, related to the single-particle purity of the observed levels. Inverse kinematics is required,

Experimental Technique or Reaction Type	$\langle E_\gamma \rangle$ MeV	v/c	M_γ
1. Stopped - Hi E_γ	5.0	0.0	4
2. Stopped - Low E_γ	1.5	0.0	4
3. Hi-spin - Normal Kinematics	1.0	0.04	20
4. Hi-spin - Inverse Kinematics	1.0	0.07	20
5. Coulex/Transfer	1.5	0.1	15
6. Fast Beam Fragmentation	1.5	0.5	6
7. Fast Beam Coulex - Hi E_γ	5.0	0.5	2
8. Fast Beam Coulex - Low E_γ	1.5	0.5	2

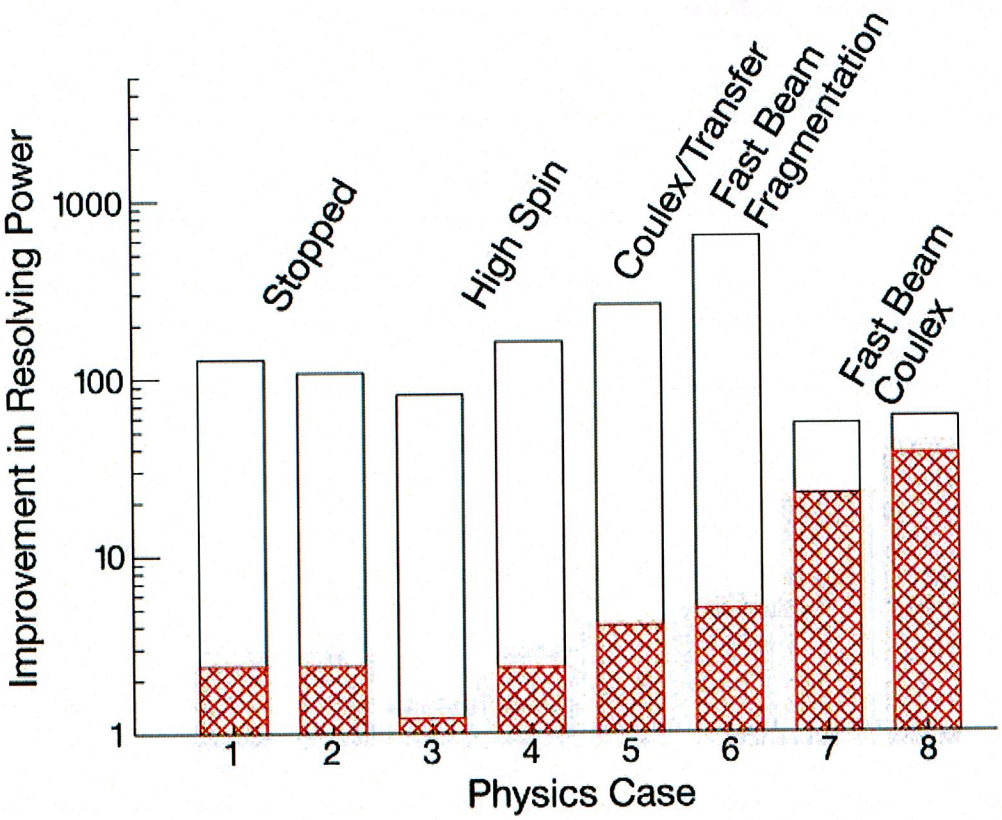

Top: Table showing the variety of different experimental techniques or reaction types along with characteristic γ-ray energies, recoil velocities and γ-ray multiplicities. Bottom: Improvement in resolving power or sensitivity of GRETA compared to Gammasphere or SeGA (whichever array was optimally suited) for a variety of different experimental cases given in the Table above. The red hatched bars correspond to the expected performance of GRETINA. The calculations do not consider any contributions from auxiliary detectors.

however, which together with the energy loss of the heavy beam in the target limits the energy resolution available from detection of the light reaction products alone. Detecting the γ transitions from excited states not only allows the excitation energy to be determined precisely, but also provides additional data from angular correlations. Since GRETA comprises a highly efficient Ge shell, it can serve as a superb γ-ray calorimeter, determining the excitation energy of the excited beam with excellent specificity.

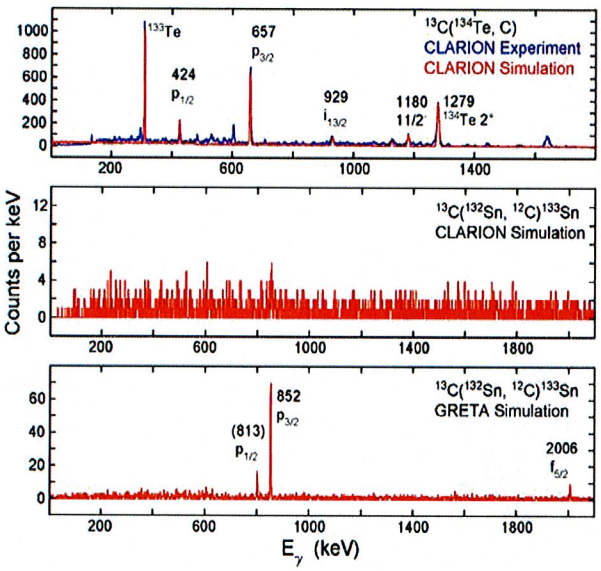

Simulation of GRETA performance for single-particle transfer reaction studies. The upper panel shows the spectrum (blue) from the ^{134}Te + ^{13}C reaction, obtained with CLARION at the HRIBF. Unless otherwise indicated, transitions are from excited states in ^{135}Te. The spectrum in red is the corresponding simulated spectrum for CLARION which overlaps the experimental spectrum extremely well. The middle panel is a simulation for CLARION for the ^{132}Sn + ^{13}C reaction, with a beam that is fifty times weaker than in the top panel. The bottom panel is the corresponding simulation for GRETA.

The sensitivity gain from using GRETA for such transfer studies is illustrated above by the case of an exotic ^{134}Te beam incident on a ^{13}C target. Single-particle states populated in ^{135}Te following neutron transfer were clearly seen in an experiment at the HRIBF, using the CLARION array of segmented clover detectors and the HyBall CsI array. The top panel in the figure shows the measured CLARION spectrum in blue, and a simulated spectrum in red. The second panel shows the corresponding simulated spectrum for a similar experiment using a ^{132}Sn beam, available at the HRIBF but at a factor of fifty weaker in intensity. The third panel shows the simulated spectrum from GRETA, using the same weak ^{132}Sn beam. Clearly, GRETA will greatly extend the reach of transfer studies and open the way to a new generation of experiments exploring the evolution of nuclear shell structure far from stability. In addition to its high detection efficiency, the very high angular resolution is critically important for these experiments and for Coulomb excitation studies, both of which exhibit recoil velocities around 0.1c.

3.1.2. The Alteration of Shell Structure Far from Stability

The shell structure of atomic nuclei close to stability is well established. Pronounced shell closures define the effective degrees of freedom needed for a quantitative understanding of the atomic nucleus. The nuclear potential is well-parameterized and theoretical frameworks explain many experimental facts. For atomic nuclei away from stability decreasing nucleon binding energy and the large neutron-to-proton asymmetry lead to modifications in the nuclear potential and the spin-isospin component of the nucleon-nucleon interaction drives changes in the single-particle structure. This, together with the increased role of many-body correlations, leads to the disappearance of shell closures established close to stability and to the emergence of new magic numbers. For the lightest nuclei, such changes have already been observed experimentally at current facilities with present-day detectors. For example, established shell closures at N=8, N=20, N=28 have been observed to disappear for neutron-rich nuclei, while a new magic number has emerged at N=16.

Experimentally, the first indications for shell closures traditionally come from mass measurements. To establish that a magic number has vanished, it is necessary to measure effective single-particle energies or to determine experimentally that the ground state wave function of a presumed magic nucleus has a significant admixture from the shell expected to be above the shell closure. The quantitative determination of such admixtures can be accomplished in single-nucleon removal and single-nucleon addition reactions, both with fast exotic beams and with reaccelerated exotic beams. Such experiments depend crucially on the correct identification of the final states. In most applications these final states are particle-bound and can be tagged by coincidence measurements with γ-rays. Compared to

precisely measuring the momentum of the scattered particle in a spectrograph, γ-ray experiments have the advantage of allowing for much thicker reaction targets, thus extending the scientific reach of any facility. Gamma-rays traverse matter with known attenuation and multiple scattering of the projectile in a thick target does not affect their energy resolution. Complementary information on the strength of the coupling between ground-state and excited-state wave functions can be achieved by measuring the transition matrix elements between states. By comparing different probes (for example hadronic, electromagnetic, and isoscalar probes) one can begin to separate the proton- and neutron-contributions to the observed collectivity.

The sensitivity of any such measurement and the scientific reach of any facility depend directly on the resolving power of the γ-ray spectrometer used. GRETA will have superior resolving power for fast-beam experiment compared to any other γ-ray detector. This increased resolving power translates directly into added discovery potential.

For example, with GRETA it will be possible to characterize the shell structure of Z=28 nickel isotopes $^{52-76}$Ni (N=24-48) at the NSCL Coupled Cyclotron Facility. GRETA will enable definitive measurements with fast beams from ^{48}Ni-^{80}Ni (N=20-52) at facilities under discussion (200 MeV/nucleon heavy-ion driver, 400 kW beam power). The experimentally accessible nickel isotopic chain ^{48}Ni-^{80}Ni covers three major shell closures (N=20, 28, 50) with the lightest and heaviest isotopes both very weakly bound, effectively amplifying shell-modifying effects. ^{48}Ni is located beyond the proton dripline and ^{80}Ni is expected to have a neutron-separation energy of less than 4 MeV. This unique scientific reach across three shell closures makes the nickel isotopes a key laboratory for studying the modification of shell structure in atomic nuclei.

Zirconium (Z=40) isotopes will provide complementary information to nickel, covering isotopes from the proton-dripline to close to the neutron-dripline. GRETA will enable definitive measurements of the wave functions with fast beams for ^{75}Zr-^{115}Zr (N=35-75) at future facilities and ^{79}Zr-^{108}Zr (N = 39-68) at the NSCL CCF.

The doubly-magic nucleus ^{100}Sn (Z=50, N=50) as well as ^{99}Sn (N=49) will be accessible for in-beam γ-ray reaction studies with GRETA at future fast beam facilities, together with tin isotopes ranging to ^{139}Sn (N=89), reaching into the astrophysically important r-process path.

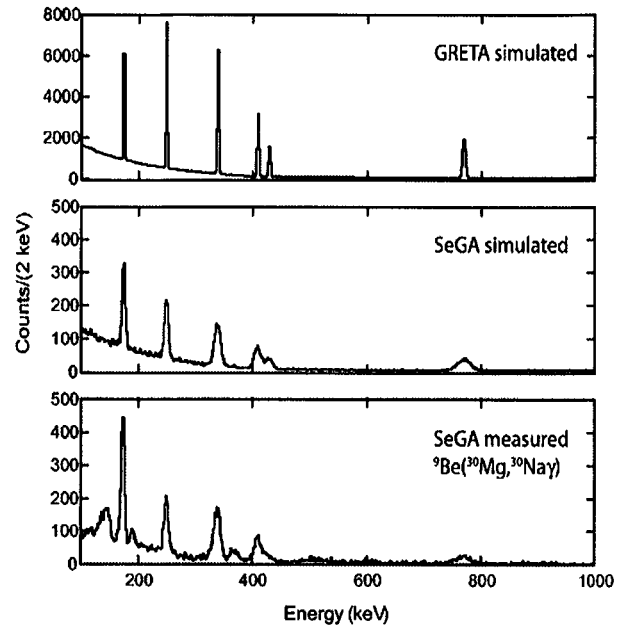

Comparison of current data taken with the SeGA array with simulations of SeGA and GRETA. Note the significant increase in statistics and improved resolution with GRETA.

3.1.3. Symmetries and Excitation Modes in Exotic Nuclei

Critical Point Symmetries

A remarkable feature of heavy nuclei is the emergence of novel collective properties that are not apparent in few-body systems. Such regularities can often be described in terms of many-body symmetries, which simplify the interpretation by introducing simple degrees of freedom. One recent example of emergent collectivity focuses on rapid changes in structure that occur in mass regions where nuclear shapes suddenly switch with the addition of only one or two nucleons. The classical theory of phase transitions has been applied to describe these changes of nuclear shapes and has offered new insights into the transitional behavior of finite many-body systems in general.

A specific example is the case of the rapid change from spherical to ellipsoidal deformation. This can be understood in terms of a transition between coexisting spherical and deformed phases. When these phases have equal energies, a phase transition occurs. Nuclei which lie at this "critical point" (such as ^{152}Sm) have been successfully described in terms of new analytic

critical-point models, which predict a number of characteristic spectroscopic signatures. Understanding these phase transitions of nuclear shapes requires studying the evolution of structure across many nuclei. This is illustrated in the figure which shows the locus of expected shape transition regions over a large swath of the nuclear chart. Most of the regions of interest lie off the valley of stability (e.g. neutron-rich Mo-Zr or rare-earth nuclei). These can be reached by using deep-inelastic reactions with either intense stable beams or reaccelerated neutron-rich beams from radioactive beam facilities. Properties of ground-state sequences need to be measured and GRETA will be essential for these studies.

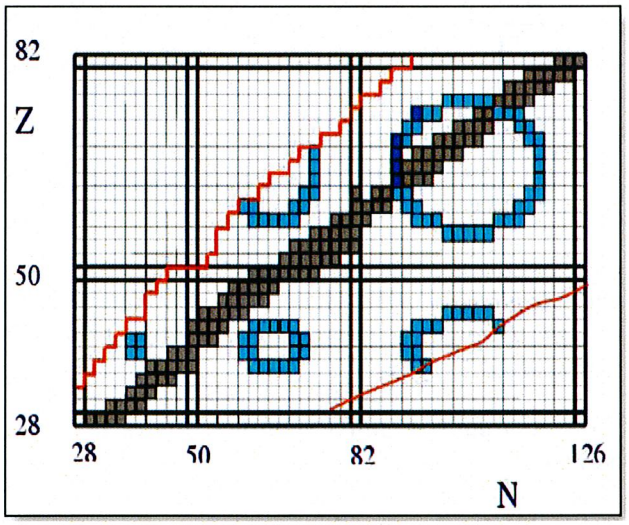

The expected locus (in blue) of nuclei showing the critical-point behavior of the rapid phase change from spherical to ellipsoidal deformation (taken from the RIA brochure "The Science of the Rare Isotope Accelerator (RIA) – A Brochure from the RIA Users Community", February 2006).

The sensitivity gain from using GRETA for such deep-inelastic studies is illustrated by the case of a ^{238}U beam incident on a ^{170}Er target. The ground-state rotational structure, of the target-like fragment after a 1n-transfer channel, was clearly seen in an experiment using the Gammasphere+CHICO combination. The top panel in the figure shows the measured Gammasphere spectrum, while the second panel shows the corresponding simulated spectrum. The third panel shows the spectrum from GRETA, in combination with Super-CHICO, assuming the sequence is in a 6n-transfer channel (with a cross-section approximately 300 times less than the 1n-transfer). Clearly, GRETA will extend the reach of deep-inelastic studies and open the way to a new generation of experiments exploring the evolution of nuclear structure and emergent collective properties far-from-stability.

Examples of experiments on symmetry properties of mass A~100 nuclei made possible by GRETA include, (a) Using multi-nucleon transfer reactions with stable beam and target combinations, such as ^{96}Zr or ^{100}Mo and ^{238}U or ^{208}Pb to study ^{104}Zr, ^{106}Mo; (b) Coulomb excitation of re-accelerated neutron-rich beams (to a limit of 10^4 beam pps) to measure transition rates in, for example, ^{108}Zr and ^{112}Mo.

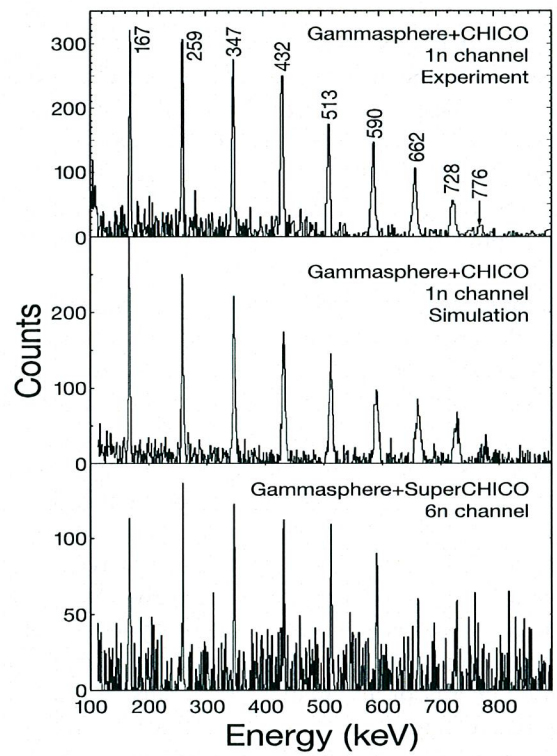

The gain in experimental sensitivity using GRETA (together with a state-of-the-art heavy ion detector) for multi-nucleon transfer or Coulomb excitation reactions, compared with the present state of the art γ-ray detector Gammasphere. The upper panel shows data taken using Gammasphere and CHICO to study the 1n transfer channel from reactions of a ^{238}U beam on ^{170}Er target. The middle panel shows the corresponding simulated spectrum. The lower panel shows a simulation for a 6n transfer reaction (assumed to have a cross section 300 smaller than the 1n transfer channel) that would be possible using GRETA and SuperCHICO.

Dipole Resonances
Collective dipole excitations are a general phenomenon of finite fermion systems. In atomic nuclei they can, for instance, arise from out-of-phase oscillation of the proton and neutron "fluids" giving the well known Giant Dipole Resonance (GDR) at excitation energies of ~15-20 MeV. In metallic clusters, E1 modes have been observed corresponding to positive ions oscillating against the electron cloud, and more recently there have been predictions for dipole modes in quantum dots due to the motion of the confined electrons and holes.

While the GDR is the dominant E1 mode in nuclei there is evidence for an excess of E1 strength at significantly lower energies in the vicinity of the 1-neutron emission threshold. This strength is usually referred to as the Pygmy Dipole Resonance (PDR). In analogy to the GDR, the PDR has been interpreted as a collective oscillation of a core of equal numbers of neutrons and protons against a neutron excess. The occurrence of non-statistical low-lying E1 strength can influence (γ,n) reaction rates, for example, in hot stellar scenarios for nucleosynthesis.

So far, the majority of information on the PDR has come from Nuclear Resonance Fluorescence experiments on stable nuclei and Coulomb dissociation experiments on neutron-rich unstable nuclei. GRETA will provide a powerful new tool to study and characterize "resonant" states near to particle threshold using high-resolution γ-ray spectroscopy, and specifically γ-ray coincidences. In these experiments the PDR will be excited by heavy-ion Coulomb/inelastic scattering at ~20 MeV/A. With this method either stable or unstable nuclei (i.e. neutron-rich radioactive beams) can be studied. GRETA's increased efficiency for high energy γ rays will give a factor of ~30 improvement for the detection of high-Eγ (6 MeV) – low-Eγ (1 MeV) coincidences, and the 4π coverage and high granularity will be needed to cleanly isolate the low γ-ray multiplicity events that will characterize the decays of these states.

3.1.4. The Nucleus as an Open Quantum System

A nucleus is not an isolated system; it interacts with its environment and communicates with other nuclei through decays and captures. If the continuum space is not considered, this communication is not allowed: the system is closed; such an approximation is often made in nuclear structure calculations. In exotic, weakly-bound nuclei, particle and cluster thresholds appear particularly low; hence, their properties are strongly affected by open, or scattering, channels. The proximity of the scattering continuum in weakly bound and unbound nuclei, implies that these nuclei cannot be properly described without taking into account the coupling between discrete states and the continuum of positive energy states, thus one must treat bound, resonant and continuum states on an equal footing. In addition to the cases at the neutron and proton driplines, threshold phenomena are expected at higher excitation energy where new decay channels open up. Here, a good example is particle decay competing with γ decays in rotational bands. How GRETA can help us make significant progress in this exciting areas of current research is discussed below.

Decay studies of neutron-rich nuclei
Decay spectroscopy is the best method to discover and study the low energy levels in new neutron-rich nuclei. Such measurements charting the evolution of single-particle states and the deformation of very neutron-rich isotopes are likely to be first to observe the predicted changes in the shell structure. However, to achieve this goal, advances in the production of exotic isotopes as well as γ-ray detection are necessary.

Decay spectroscopy experiments rely on the efficient detection of γ rays and GRETA will offer an order of magnitude in efficiency compared to systems presently in use. In addition, the high granularity of each detector element in GRETA combined with digital signal processing will allow new opportunities in the selection of rare signals associated with β- decays. In particular, shallow-penetrating β particles compared to deep-penetrating γ rays can easily be identified and separated. The identification of β-delayed γ radiation at rates below one ion per hour may become feasible. At present such limits are at about 100 ions/hour.

With production rates expected for a future major US radioactive beam facility it should become possible to study the decay properties of all r-process nuclei between N=50 and N=82, as well as significantly advance studies between the N=82 and N=126 shell closures.

Proton emitter studies
With the departure from the line of β stability the binding energy of constituent nucleons (protons on the proton-rich side and neutrons on the neutron-rich side) decreases until the nucleons become unbound at the driplines. Small binding energy can lead to halos, a larger diffuseness of the nuclear potential, and a mix-

ing of bound states with the continuum. In addition, unbound nucleons can be spontaneously emitted from a nucleus. At the neutron dripline profound changes in nuclear structure are expected. On the proton-rich side protons are confined temporally by the Coulomb barrier and new phenomena are expected to set in gradually. However, the proton dripline can be accessed experimentally now while the neutron dripline studies are limited to only a handful of light nuclei. New detection techniques, such as γ-ray tracking, will allow precise mapping out of the transition between well confined and open nuclei across the proton drip line.

The limit of nuclear existence on the proton rich side of the line of β stability is delineated by nuclei spontaneously emitting protons. Proton emitters are a unique laboratory for studying quantum tunneling through a 3-dimensional Coulomb barrier. They are also a source of information on nuclear structure far from the line of stability as proton decay rates depend on the single particle content of proton decaying states, which depends on the shape of the nuclear potential, and on the strength of the pairing interaction. Proton decay studies can be also combined with in-beam γ-ray spectroscopic methods offering a glimpse at these loosely bound nuclei at high excitation energy and angular momentum.

Gammasphere coupled to the Argonne Fragment Mass Analyzer has successfully studied excited states in several deformed proton emitters along the island of deformation between Z=50 and N=82. (Similar studies have been performed at ORNL using the Recoil Mass Spectrometer and CLARION γ-ray array.) Figures a) and b) below contain γ-ray spectra obtained for the deformed proton emitters ^{145}Tm and ^{131}Eu, respectively.

Both proton emitters were produced with cross sections of about 300 nb and are representative of the current experimental limit. In panel a) of the following figure a regular sequence of γ rays can be easily seen and was interpreted as a $\pi h_{11/2}$ decoupled ground state rotational band. The spectrum in panel b) of the following figure is much more complex as several rotational bands are present close to the yrast line. In order to discern the ^{131}Eu decay level scheme γ–γ coincidences have to be measured. The γ–γ data obtained with Gammasphere are inconclusive. Thus to make progress in these studies better γ-ray detection capabilities are needed.

Using the fact that the efficiency of GRETA is 40% (4 times that of Gammasphere) and that GRETA crystals (which cover twice the solid angle compared to Gammasphere crystals) can count up to 50 kHz (5 times that of Gammasphere), resulting in an increase of the maximum beam current by 2.5, then a factor of 40 = 4^2x2.5 increase will be obtained in the number of detected γ–γ coincidences. This will certainly make the determination of the ^{131}Eu structure possible. Similar arguments apply to other well deformed proton emitters such as, ^{117}La. In addition, in-beam studies could now be extended to deformed odd-odd proton emitters such as, ^{130}Eu and ^{144}Tm, which are produced with cross sections of about 30 nb.

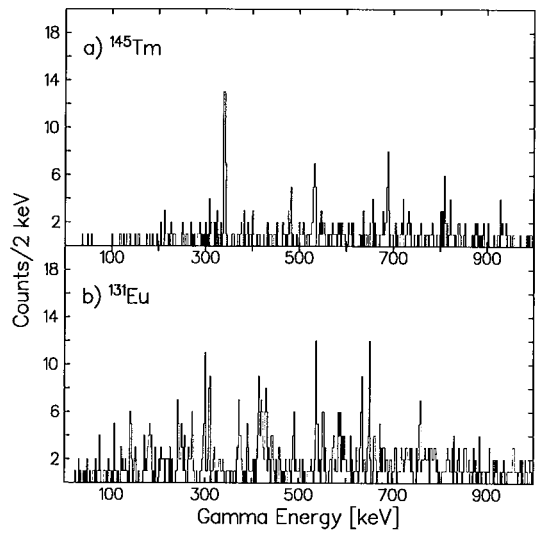

Current state-of-the-art prompt γ-ray spectra correlated with the deformed proton emitters a) ^{145}Tm and b) ^{131}Eu. These data were collected using Gammasphere. GRETA will allow an improvement factor in statistics of ~40 pushing dripline spectroscopy to new levels of sensitivity.

Discrete charged-particle decay in A ~ 60 nuclei

A challenging, "new" decay mode has been uncovered in the A~60 mass region. Single and often multiple discrete-energy proton- and alpha-particle decays have been observed from the highly deformed to otherwise shell-model spherical structures. The cross sections for these decays are very small and their observation was only possible by combining the power of Gammasphere with auxiliary charged-particle arrays, first the Microball and then a Si wall coupled to the Microball. To further explore these exotic decays and to uncover the underlying physics behind these decays the power of GRETA coupled with new highly segmented charged-particle arrays will be needed. New areas of such decay will also be found in the proton rich nuclei up to around ^{100}Sn. A first example may be the recently reported ^{94}Ag proton-decay.

3.2. What are the properties of nuclei at the limits of mass and charge?

Heavy Element Research

The quest for superheavy nuclei and an understanding of their formation and stability has always been a defining challenge for nuclear structure physics. Their very existence depends on stabilization by quantal shell effects, at charge Q>100e the Coulomb energy is sufficient to destroy the stability of any conventional drop of nuclear matter. Studying the coalescence of nuclei which can form these systems, the fission barriers which inhibit their instant decay, and the modes of excitation they can sustain, all provide details of the delicate balance of forces which are in play. Thus, these studies deepen and generalize our understanding of all nuclei.

For many years the most fruitful avenue of research in this field has been synthesis of superheavy nuclei through heavy ion fusion. Their existence and relative stability can be determined by observation of the groundstate decay modes. This research has taken us from Z=98 to Z=113, by cold fusion of ^{208}Pb and ^{209}Bi and heavy ions, and recent research suggests progress to Z=118 using hotter fusion of a ^{48}Ca with actinide targets. This approach has been critical in defining the topology of the mass surface in very heavy systems. However, as production cross-sections are extremely low, at the parts-per-trillion level, addressing the issues underlying the causes of stability are difficult.

In this century, a new paradigm for understanding superheavy nuclei, through the detailed spectroscopy of slightly lighter elements has already made important contributions to our understanding of all heavy systems. A new field of γ-ray spectroscopy has started on nuclei with $Z > 100$. Already, the shapes of these very heavy systems have been conclusively determined, and the spin-dependence of the fission barriers studied. The location of critical states at the Fermi surface have been determined, both in studying spectroscopy of odd-A nuclei and by locating K-isomeric states. The latter results have directly challenged the issue of locating gaps in the single-particle sequence in the heaviest nuclei. These experiments have only become possible with recoil separators, to identify successful synthesis, and the γ detector arrays of the Gammasphere generation. Even in the best cases, fusion is at the parts-per-million level, and spectroscopy is at the very limit of what is feasible. We continue to refine our experiments and are approaching experiments at the tens of parts-per-billion level. To make further real progress, to the parts-per billion level, a new generation of detectors is critical.

The GRETINA array will allow substantial progress to be made in this field when operated with recoil separators like the Fragment Mass Analyzer (FMA) at ANL or the Berkeley Gas-filled Separator (BGS) at LBNL. High intensity heavy ion beams, of hundreds of particle nanoamps, are needed to produce the nuclei of interest. The beams are sufficiently intense that large target wheels are needed to prevent melting. Prompt γ spectroscopy, the study of γ rays emitted during coalescence and cooling at the synthesis position, is limited by countrate as the dominant fission reaction process produces γ rays copiously. The new generation of detectors with digital pulse processing, can be tuned for high countrates, and can sustain rates 5-10 times higher than traditional systems. Further, the compact nature of the array will allow the residues to be more efficiently collected, and the beam-dump better shielded. In all, a factor of 100 improvement should be feasible, leading to experiments in the parts-per-billion regime. This should allow detailed spectroscopy above Z=104 to be started for the first time.

GRETA will allow even more sensitive studies. At the target position, another significant gain can be made in "high-fold" detection of more than one γ-ray, possibly increasing sensitivity by another order of magnitude. Perhaps more significant are the prospects of performing high resolution calorimetry; determining the spin dependence of the fission barrier by measuring the entry distribution of γ rays in nuclei which survive coalescence and determining if and how it falls at very high atomic numbers. These measurements provide unique insights into the coalescence mechanism, particularly determining which partial waves lead to fusion. Until very recently, the conventional assumption was that only very low partial waves can contribute. However, it is now clear that this is not so. Perhaps the biggest gain can be achieved in delayed isomer spectroscopy. Locating GRETA at the focal plane of a gas-filled spectrometer (which allows the most efficient collection of heavy residues) could provide an experimental environment in which isomers formed with cross-sections well below the part-per-billion level could be measured, in nuclei with $Z > 106$. In this case, the tracking capability will be essential in suppressing γ backgrounds, as at very low production levels, it becomes essential to understand the genesis of each photon detected.

3.3. What are the properties of nuclei at the limits of angular momentum?

Nuclear Hyperdeformation

The shape of the atomic nucleus is governed by a delicate interplay between macroscopic liquid-drop properties and microscopic quantal effects. As discussed above, the heaviest elements survive only because of shell stabilization. Their ability to sustain rotational states above 20ħ indicates that the fission barrier may be more robust than previously thought. A similar situation occurs for hyperdeformed (HD) nuclei, which are associated with a third minimum in the potential energy surface of rapidly rotating nuclei. The extreme deformation (approaching a 3:1 major-to-minor axis ratio) is predicted to occur at the very limits of sustainable angular momentum before the nucleus undergoes fission. The observation, and detailed spectroscopy, of HD structures will allow us to study the interplay between macroscopic shape effects (the role of the surface is of particular importance), shell stabilization, and angular momentum. There have been suggestions of the first glimpses of HD in the rare-earth and actinide regions but definitive identification of discrete-line HD sequences will be a major achievement for nuclear physics.

Understanding the conditions of formation, survival, and decay of these exotic nuclei will be extremely challenging. There is likely to be only a small entry window in the excitation energy-spin plane, close to the fission limit, through which to populate these states. Entrance channel effects (for instance, static and dynamical shape distortions) might determine the delicate balance required for their formation. The survival of HD structures is dependent on the fission barrier and shape relaxation effects. We will learn a great deal on these topics by studying HD nuclei which lie at the extremes of nuclear deformation and angular momentum. In order to address all these issues GRETA will be an absolute necessity.

The sensitivity gain from using GRETA for this type of high-angular-momentum experiment is illustrated by the case of ^{108}Cd. A weak rotational structure, with an intensity of ~10^{-3} of the total fusion cross-section has been seen at high angular momentum in an experiment with Gammasphere. This structure corresponds to a very deformed prolate shape, possibly exceeding a 2:1 major-to-minor axis ratio. The top panel shows the measured Gammasphere spectrum (black) together with the corresponding simulated spectrum (red). This is the observational limit for current detector arrays - a band with intensity of 10^{-4} would not be seen today (middle panel). The bottom panel shows a simulation from GRETA where we have assumed the band is 10 times weaker still (i.e. an intensity of 10^{-5}). This ~100 fold increase in resolving power will open the way to a new generation of experiments at high angular momentum and the detailed investigation of topics such as hyperdeformation using intense stable beams available today and re-accelerated neutron-rich beams from future radioactive beam facilities.

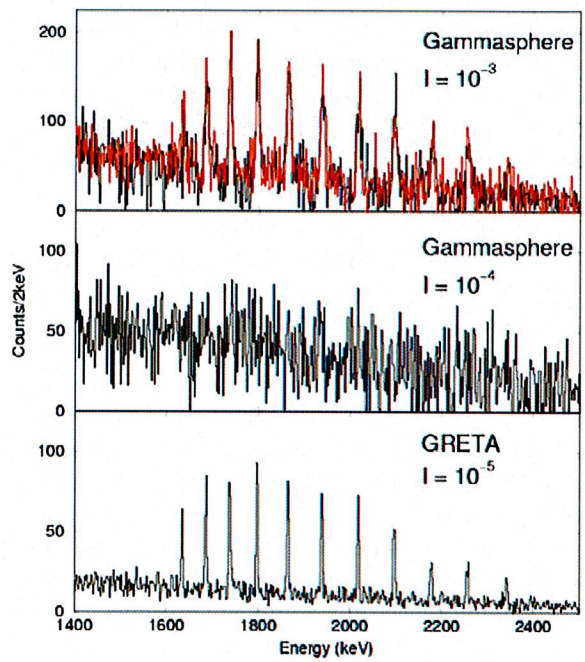

Simulation of GRETA performance for high multiplicity γ-ray data. The upper panel shows the spectrum (black) of the very deformed rotational band in ^{108}Cd obtained with Gammasphere using 4-fold data. This band carried ~0.1% of the reaction cross-section. The spectrum in red is the corresponding simulated spectrum for Gammasphere. The middle panel is a simulation for Gammasphere assuming the band carries 0.01% of the intensity. This intensity is at (beyond) the sensitivity limit for Gammasphere. The bottom panel is a simulation for GRETA assuming the band has an intensity of 0.001% (100 times weaker than the structure presently observed).

A specific example of a hyperdeformation experiment would be the reaction of a ^{48}Ca beam on a ^{64}Ni target to produce ^{108}Cd, where recent calculations predict hyperdeformed structures at a spin of ~70ħ. This is beyond the reach of today's experimental sensitivity, but

within the reach of GRETA. In addition, reaccelerated radioactive beams of, e.g. ^{94}Kr, will give access to neutron-rich Cd isotopes up to ^{114}Cd, where hyper-deformed structures are predicted to be favored at even lower spins and where GRETA's 100 fold increase in sensitivity will be needed to compensate the lower beam intensity.

3.4. Nuclear astrophysics , fundamental interactions and rare processes

3.4.1. Nuclear Astrophysics

Nuclear astrophysics is concerned with the impact of the microscopic aspects of nuclear structure and reactions on the macroscopic phenomena we observe in our universe. There are a number of measurements in the area of nuclear astrophysics that will benefit greatly from a highly efficient γ-ray tracking detector array such as GRETA. For example:

Low-Energy Capture Reactions
Nuclear reactions play the crucial role in the energy production and element synthesis in most astrophysical sites, and models of these environments require the rate and energy release of the relevant nuclear reactions as critical input. Thermonuclear capture reactions are the most important, since they provide the pathway to forming heavy nuclides out of lighter nuclides. Furthermore, because hydrogen and helium comprise 99% of the baryonic matter in the Universe, and because they have the lowest Coulomb barriers, almost all heavy element charged particle nuclear reactions in the cosmos involve interactions with isotopes of H and He, burning them as fuel to form even heavier nuclides. The determination of the rates of such reactions, by both direct and indirect techniques, is the focus of much international effort.

Direct measurements of reactions such as $^{12}C(\alpha,\gamma)^{16}O$ or $^{14}N(p,\gamma)^{15}O$ at very low energies are of great interest, but are also very time consuming because of their extremely low cross sections. To provide the required high beam intensities, these measurements are usually performed by bombarding solid targets with intense (several μA) beams of light ions, which would preclude the use of recoil separators. Therefore, capture γ rays are often detected in singles. These signals can be easily masked by backgrounds from cosmic rays and natural radioactivity in a typical experimental hall. Surrounding such a target with a tracking detector like GRETA could reject the majority of the background γ rays, while giving a very high efficiency for detecting the capture γ rays of interest. There are many (~30) important measurements of this type that would benefit from this approach. It should be noted that these experiments will require beam times of a month or more.

Many studies of stellar explosions involve inverse capture reactions of radioactive ion beams on gas targets. By the time of GRETA, it is highly likely that gas jet targets in which the high density gas is localized to ~ 2 mm coming out of a nozzle will have been developed for this class of experiment. The use of γ-ray tracking detectors like those in GRETA closely-packed around the target will help reduce the very high backgrounds from 511 keV annihilation radiation along with cosmic-ray induced events. GRETA will provide high efficiency for ~MeV γ rays, and high energy resolution to reconstruct the cascade γ-ray decays in cases where there is a reasonably high level density. Of the order of ~20 important measurements would benefit and be made possible using GRETA.

Nuclear Structure Studies
This category of measurements is very broad, and includes studies used for indirect determinations of important reaction rates. Specifically, nuclear levels that may dominate an astrophysical reaction rate are populated by a reaction different from that occurring in the cosmos, and the decay properties of those levels (branching ratios, lifetimes, spins and parities, level densities) are measured. These studies are particularly important near the proton- and neutron-dripline, where structure information is both greatly lacking and is very important for studies of stellar explosions. The high efficiency of GRETA will allow studies to go several mass units closer to the drip line than possible with current arrays. There are hundreds of studies that can benefit, utilizing both stable and radioactive beams.

3.4.2 Fundamental Interactions and Rare Processes

A γ-ray tracking array like GRETA with high efficiency, high segmentation and thus high spatial resolution, and excellent background rejection could be used to perform important experiments in weak interaction physics. One possible experiment would be a greatly improved measurement of the superallowed branching ratio of the β-decay of ^{10}C. The strength of superallowed β decays can be simply related to the V_{ud} element of the CKM matrix. The decay of ^{10}C is the least susceptible of the superallowed decays to theoretical

uncertainties. The superallowed branching ratio of ^{10}C can be measured by observing a γ-ray cascade, and the largest systematic error in such a measurement is caused by accidental pileup of 511 keV photons. Very high spatial resolution in GRETA would essentially remove this error from current measurements, allowing an improvement in the precision of the branching ratio of a factor of 10 or more.

GRETA with its extremely good spatial resolution and high detection efficiency would also be useful in further studies of positronium annihilation. An experiment with only one week of data acquisition could improve existing measurements of positronium annihilation to four and five photons, which test QED predictions at high orders of α. This experiment would also significantly improve limits on Charge Conjugation Symmetry violating currents. The decay of polarized positronium in a highly segmented detector could provide an extremely sensitive test of CPT. Measurements of β-γ correlations could be improved in an array with good spatial resolution. Several cases would be interesting as tests of recoil-order weak interaction form factors including ^{22}Na, ^{14}O, and ^{20}Na-^{20}F, ^{24}Na-^{24}Al, and ^{28}Al-^{28}P. A particularly interesting, although challenging, experiment would be investigating the β-γ correlation of polarized ^{19}Ne in order to study the parity mixing of the $1/2^+$,$1/2^-$ levels in ^{19}F. This could help resolve the current uncertainty in nuclear parity-violating meson couplings.

4. Technical Accomplishments towards a 4π Gamma-Ray Tracking Array

The concept of a γ-ray tracking detector array was proposed in 1994, and after about ten years of R&D, the technology was in place to construct such a detector. The Department of Energy made the Critical Decision-0 (CD0) for GRETINA in August 2003 to construct a tracking detector covering one-fourth of the total solid angle. Since then the project has proceeded according to schedule and is planned to be completed in 2010. In the following, we will give a short summary of technical accomplishments.

Detector

The critical detector technology is the manufacture of two-dimensionally segmented coaxial germanium detectors which provide signals with sensitivity for locating interaction points in three dimensions. In addition, the crystals should have large volume and be shaped into tapered irregular hexagon shapes for close packing into a spherical shell with high solid angle coverage. We have been working closely with a detector manufacturer to develop such detector. The final prototype has three tapered crystals in a cryostat, each segmented into 36 segments. Extensive tests have demonstrated that this detector will meet the requirements of γ-ray tracking. The geometric design of GRETINA uses 120 crystals packed in 30 cryostats. The first production 4-crystal detector module was ordered and was delivered at the end of 2006.

Electronics

Determining the interaction position in three dimensions requires a detailed analysis of the pulse shapes. The pulse shape needs to be recorded at sampling rate about 10 MHz and a resolution of at least 12 bits. We have produced a prototype signal digitizer using commercially available parts. To reduce the amount of data to be stored, online processing in the electronic module generates energy, time, and trigger information, as well as capture of the relevant portion of the pulse shape for signal decomposition by a computer farm in real time. A trigger and timing system will carry out complex trigger decisions and distribution clock and trigger information to GRETINA and auxiliary detectors. The design of the production version of both the digitizer and trigger modules is completed and the modules will be fabricated and be available for testing in early 2007.

Signal decomposition

In order to perform γ-ray tracking, the positions and energies of the γ-ray interactions in the Ge (usually several Compton scattering events, followed by photoelectric absorption) must be accurately determined from the signal waveforms. The procedure must handle cases where two or more interactions occur within one of the detector segments. An algorithm to perform this "signal decomposition" has been developed, by combining several methods such as Singular Value Decomposition, adaptive grid search, and constrained least-squares. It utilizes calculated signal waveforms, and incorporates such effects as the preamplifier response and two different types of cross talk. We have shown experimentally that this algorithm can achieve an average position resolution of at least 2 mm.

It is important that the signal decomposition be performed in real time, so that large quantities of waveform data need not be stored. However, this requirement means that the signal decomposition forms the data acquisition bottleneck; computational speed is therefore very important. On the current generation of 2 GHz processors, the algorithm requires less than 10 ms of CPU time per hit segment. With advances in processing power from multi-core CPUs, this performance will be sufficient to meet our requirements.

Tracking

The tracking process uses the energies and positions of the interaction points produced by the signal decomposition to determine the scattering sequence for a particular γ-ray. Algorithms have been developed to track events based on Compton scattering, pair-production and photo electric interactions. Tracking efficiency achieved ranged from ~100% to 50% with γ-ray multiplicity changed from 1 to 25. The current tracking algorithm needs ~10% of the planned computing power.

End-to-End tests

The three-crystal prototype detector has been subject to several end-to-end tests with all of the 111 segments instrumented with signal digitizers. Measurements were carried out using γ-ray sources, and with γ rays produced in-beam at both the 88-Inch Cyclotron at LBL and the NSCL at MSU. At MSU, γ-particle coincidence data were taken with fragments detected in the S800 spectrograph. The full data analysis process, including event building, signal decomposition, and tracking, was performed. Results indicated that a position resolution of about 2 mm (RMS in all three dimensions) can be achieved with the prototype system.

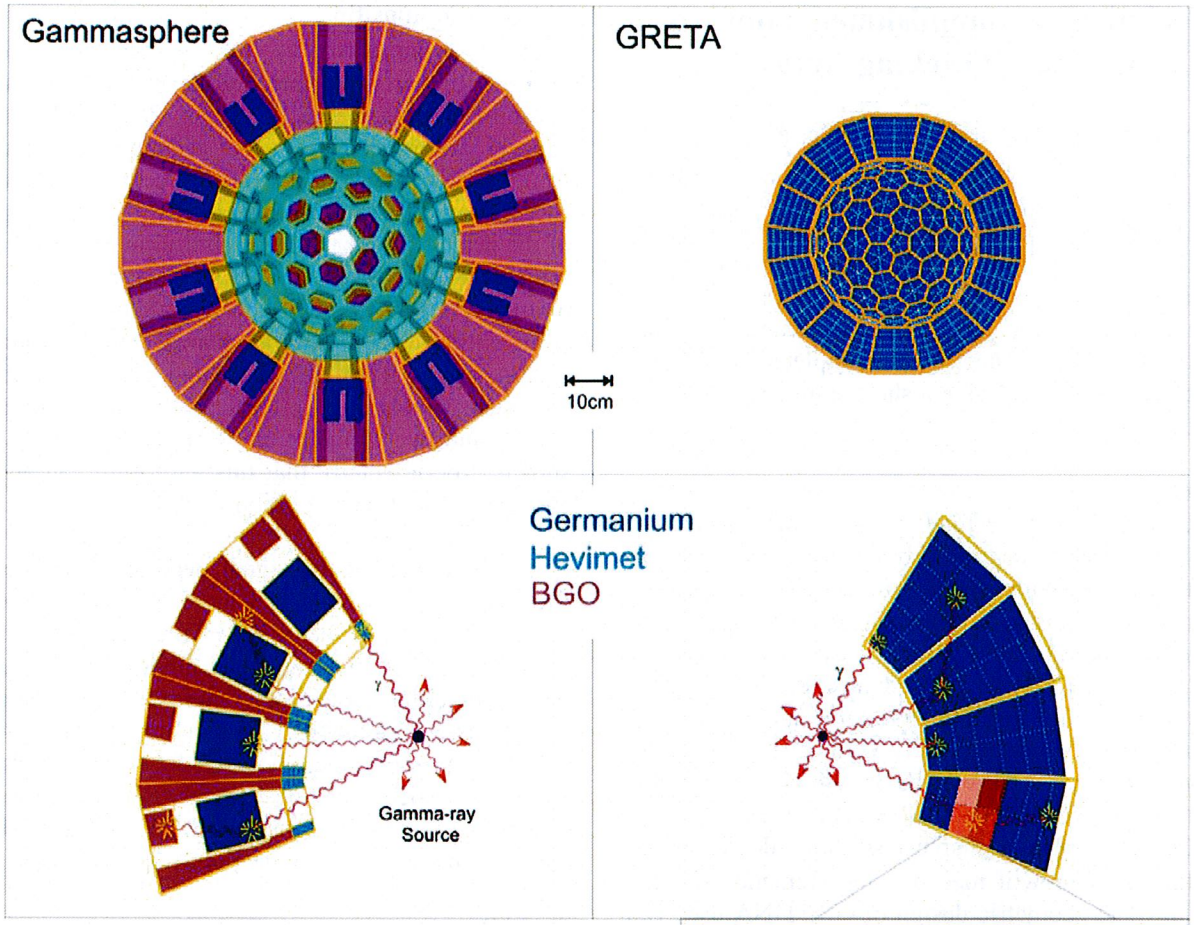

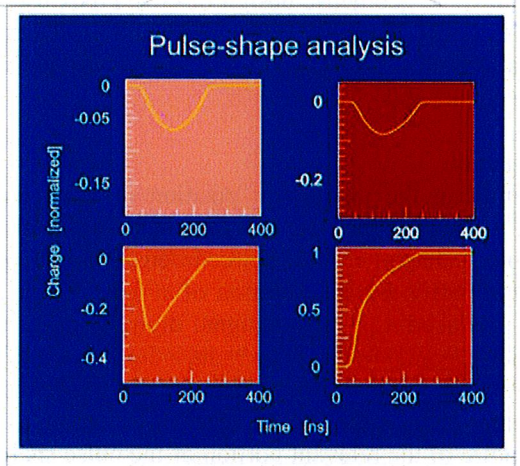

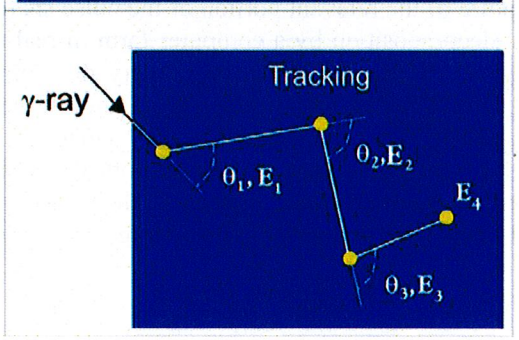

This figure illustrates the basic principles of γ-ray tracking. Instead of individually shielded Ge detectors and collimators, as in Gammasphere, a tracking array will consist of a closed shell of segmented Ge detectors. Pulse-shape analysis of signals from segments containing the interaction(s), as well as analysis of transient signals in adjacent segments, allows the determination of the three-dimensional locations of the interactions, and their energies. Tracking algorithms, which are based on the underlying physical processes such as Compton scattering or pair production, are able to identify and separate γ rays and to determine the scattering sequence. Note, while the topmost drawings are to scale, to illustrate the dimensions of the arrays, the expanded drawing showing 4 individual detectors are not to scale. They are shown to illustrate the two different concepts, and the gain obtained by removing Compton suppressors and hevimet absorbers. Gamma rays, which hit a Compton suppressor or an absorber, are lost for spectroscopic purposes.

5. Auxiliary detectors for GRETA

Auxiliary detectors continue to play a very important role in γ-ray spectroscopy with Gammasphere where they augment tremendously the physics that can be achieved. With GRETA, a number of auxiliary detectors will play an even more important role. A major advantage of GRETA, in addition to its higher efficiency, is the energy resolution for in-beam studies, as emphasized in Section 3. This results from the considerably smaller opening angle (~2° in θ and ϕ compared to 7° for Gammasphere). But in order to make good use of this angular resolution for Doppler corrections the angle of the recoiling nucleus must now also be determined with comparable angular resolution.

Thus a new generation of auxiliary detectors is needed with higher segmentation and higher counting rate capabilities than any of the existing devices which include, (i) **Microball**: a 95-element 4π-CsI(Tl) detection system for protons and alpha particles, (ii) **HERCULES:** a 64 element fast scintillator-system that can count and separate fusion evaporation residues with high efficiency in the presence a copious amounts of fission and elastic scattering, (iii) **CHICO**: a 4π parallel-plate avalanche counter that can identify deep inelastic and Coulomb excitation in nearly symmetric reactions, (iv) **Si-strip detectors**: highly segmented high resolution charged particle detection systems, and (v) a "**Neutron Shell**" consisting of 30 liquid scintillators for neutron counting.

Below we summarize some of the next generation auxiliary detectors along with examples of the physics opportunities where these devices are essential.

Nanoball
The Nanoball is a new highly segmented light charged particle system with 4π solid angle coverage. This detector will have the same segmentation as the current Microball but it will use much faster scintillators. This will allow the same exit channel selection and recoil direction determination, higher counting rates and preserve the ability to determine optimally the nuclear spin direction event by event. This device will often be coupled to a Si ΔExE Wall and/or the Neutron Shell. One of the important areas of study where the Nanoball is essential is the structure of nuclei with $N=Z$, $Z-1$ and $Z-2$ for mass regions below A~100, such as:

- Spectroscopy in $N=Z$ nuclei
- The "charge independence" of heavier isospin multiplets
- The discrete-energy charged particle decay from excited states

In these studies, the combination of the Nanoball, Si Wall, the Neutron Shell and GRETINA/GRETA will be unsurpassed in providing the necessary channel selection, recoil correction capability and high energy resolution for particle spectroscopy.

SuperHERCULES
SuperHERCULES is a highly segmented evaporation residue detection system. It will use fast plastic detectors coupled to phototubes with a segmented anode. It will have a higher segmentation than the current HERCULES detector. SuperHERCULES provides a way to study the structure of heavy nuclei that is complementary to the setups using a magnetic separator. It will provide a unique tool for studying fusion reactions induced by light projectiles where the recoil energies are too low for magnetic separators. In addition, many evaporation residues in the neighborhood of ^{254}No are beyond the reach of a separator acceptance because they require production by (HI, αxn) reactions.

The combined use of the Nanoball with the Neutron Shell and in some instances with SuperHERCULES will be crucial for both channel selection and high-resolution spectroscopy of the structure at high spins using fusion reactions near the barrier in the mass regions A~80, 60 and A~40. Here a few current topics of interest are:

- Discrete line proton and alpha decay of highly deformed structures around A~60, and searches for such decays in the neighboring A~40 and A~100 mass regions.
- Multi-particle multi-hole excitations and "high-purity" terminating states in the $40 \leq A \leq 48$ region.

MicroWall (a phoswich detector system)
This detector is a fast plastic plus CsI(Tl) phoswich arrangement to provide Z resolution and sustain higher rates than the Microball. It will have a segmentation comparable to that of SuperHERCULES.

With the advent of the CARIBU and the future "RIA" facility it becomes necessary to explore all possible avenues to study the properties of the neutron rich nuclei for which only beams can be produced. Such reac-

tions have been used at HRIBF to study neutron-transfer in reactions like $^{134}Te(^{13}C, ^{12}C)^{135}Te$, see Section 3.1.1. In these reactions the projectile-like fragments are stopped in suitable absorbers while the target-like fragments (TLF) are emitted at larger angles with increasing cross sections and decreasing energies. This detector will detect the TLFs and provide the necessary angular resolution, *Z* identification, and time of flight information, as well as handling the high counting rates required for these studies.

SuperCHICO

SuperCHICO is a 4π position-sensitive heavy-ion detector with an angular resolution of $1^\circ \times 1^\circ$ for θ and ϕ respectively as compared to the $1^\circ \times 7^\circ$ for the current CHICO detector. Such a detector is required for the kinematic reconstruction of transfer, Coulomb excitation, and fission reactions and will lead to nearly an order of magnitude improvement in γ-ray energy resolution. This will greatly expand the opportunities for advancing nuclear structure studies to higher spin, heavier mass and to odd-*Z* nuclei. The physics opportunities provided include exploring the evolution of collective motion, single particle pairing correlations, and unusual isomeric configurations with increase in spin, isospin, or excitation energy.

In the figure below we show the contributions to the energy resolution for a typical fusion reaction $^{58}Ni(^{48}Cr,\alpha 2n)^{100}Sn$ at 170 MeV and a 0.5 mg/cm^2 thick target. They are: (a) intrinsic Ge resolution shown as magenta, (b) GRETINA/GRETA opening angle contribution in brown, (c) target thickness contribution in blue, (d) recoil cone contribution without recoil detection shown in dashed cyan, (e) recoil contribution after recoil detection with a device having 2° opening angle (SuperHERCULES), (f) Total resolution for a 2.0 MeV γ-ray without recoil correction (dashed-red curve) has a maximum FWHM of 17.0 keV, and (g) Total resolution with recoil correction with FWHM of 5.4 keV. For comparison with the same reaction, Gammasphere with HERCULES (4° opening angle) has uncorrected and corrected FWHM values of 20.3 and 11.3 keV, respectively.

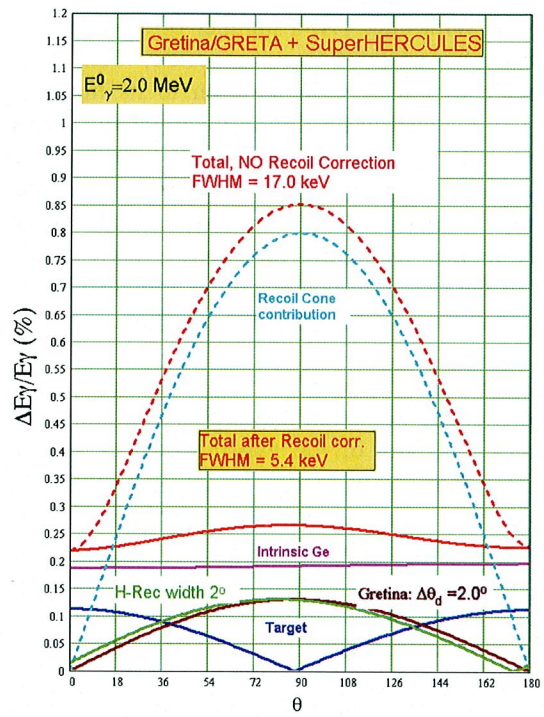

Contributions of energy resolution from various sources for the reaction $^{58}Ni(^{48}Cr,\alpha 2n)^{100}Sn$. If uncorrected, the angular distribution of the recoil direction dominates the energy resolution. See text for details.

The above reaction is the best case scenario. For other reactions (transfer, deep inelastic reactions, etc.) with much larger recoil velocities the detection of the recoils is even more important.

6. Applications of Gamma-Ray Tracking Detectors

Gamma-ray tracking, for all practical purposes, is an entirely new technique in γ-ray detection, enabled for the first time by the new detector technologies that are now being developed. Tracking has important applications for science, technology, medicine, and societal issues such as homeland security.

An important application to homeland security is the detection of nuclear materials, with an emphasis on imaging and sensitivity. Tracking provides the possibility of achieving higher detector efficiency, higher peak to total ratio (rejection of the Compton shelf), and better background rejection than conventional detectors in a variety of applications. Urgent homeland security needs represent an immediate application of this new technology. It should improve capabilities for a variety of diverse threats from the use, deployment or transport of nuclear materials. There is a critical need for more sensitive detectors to detect and locate approximately kg size strategic nuclear materials at a distance, monitor boarder crossings, and for nuclear surveillance.

Tracking has applications in diverse areas of science such as astrophysics (Compton telescopes, polarimetry), and diagnostic medical uses (PET, Compton imaging). All of these applications are currently active areas of research in many institutions throughout the country. A common thread between them is the need for electrically segmented detectors, the need for robust tracking algorithms, and the need for data acquisition capabilities that are necessary to implement them.

7. Cost Estimates for GRETA

In this section, we give a high level summary of the cost and schedule of GRETA. The estimated cost to complete GRETA, beyond the cost of GRETINA, is $42M including escalation and contingency. The schedule is determined by the delivery of the germanium detector modules. We used the same delivery rate, 4 modules per year, as the GRETINA modules, and if funded the project could be completed in 2016.

Schedule

The figure on the following page shows the schedule of the high level WBS elements of GRETA. This schedule prevents conflict with GRETINA. The plan is to continue procuring detector modules after the final order for GRETINA modules has been placed. The project starts in FY08 with the preparation for the long-lead time procurement of the first four detector modules. The first order for detector modules is issued in FY09. In order to manage a continuing resolution scenario, all big orders are placed in early February. A new batch of electronics and computing systems is procured and assembled to instrument the detector modules delivered for the long lead procurement. The design of the 30 module detector support structure then starts. In parallel, preparations to place the contract for the remaining 19 detector modules will be underway. Production starts in FY11.

In FY10, after all GRETINA detector modules are received, we start receiving GRETA detector modules. We use the same approach used for GRETINA: the detectors are procured one year in advance, and they start being delivered one year after the order. We assume that the vendor will be able to deliver detectors at the same rate they are planning to deliver now: four modules per year. All detector modules are received by FY15, and FY16 is used to assemble all the systems and to perform the qualification tests. Project Management and Environment and Safety are on going activities during the duration of the project.

ID	WBS	Task Name	Start	Finish
1	1	**GRETA**	**1/2/08**	**7/25/1**
2		Start Project	2/1/08	2/1/08
3		Prepare long-lead procurement	2/1/08	2/2/09
4		Authorization for long-lead procurement	2/2/09	2/2/09
5		Start Production	2/4/11	2/4/11
6		Project Complete	7/25/11	7/25/1
7	**1.1**	**Mechanical**	**11/4/0**	**7/20/1**
8	**1.1.**	**Design**	**11/4/0**	**7/30/1**
9		Support structure	11/4/0	7/30/1
10		Target chamber	2/10/1	7/30/1
11		LN System	2/10/1	7/30/1
12	**1.1.**	**Production**	**4/29/1**	**7/20/1**
13		Support structure	4/29/1	3/30/1
14		Target chamber	8/19/1	11/11/1
15		LN system	8/19/1	2/3/12
16		Assemble	3/30/1	7/20/1
17	**1.**	**Detector Module**	**2/3/09**	**12/8/1**
18	**1.2.**	**Detector Procurement**	**2/3/09**	**9/21/1**
26	**1.2.**	**Test/Characterize Module**	**2/3/11**	**12/8/1**
29	**1.**	**Electronics Systems**	**2/3/09**	**1/4/13**
30	**1.3.**	**Electronics for long-lead detectors**	**2/3/09**	**3/22/1**
31		Review electronics	2/3/09	7/23/0
32		Digitizers (1200 channels)	7/24/0	3/22/1
33		Trigger and Timing	7/24/0	3/22/1
34		Power supplies, cables, crates, rack	7/24/0	3/22/1
35	**1.3.**	**Electronics for production detectors**	**3/23/1**	**1/4/13**
36		Review electronics	3/23/1	9/9/10
37		Digitizers (2500 channels)	2/3/12	1/4/13
38		Trigger and Timing	2/3/12	1/4/13
39		Power supplies, cables, crates, rack	7/20/1	1/4/13
40	**1.**	**Computing Systems**	**2/3/09**	**5/23/1**
41	**1.4.**	**CS for long-lead detectors**	**2/3/09**	**3/22/1**
42		Review CS	2/3/09	7/23/0
43		Readout CPUs, switch, storage, wor	7/24/0	3/22/1
44		1/3 Processor farm	7/24/0	3/22/1
45	**1.4.**	**CS for production detectors**	**3/23/1**	**5/23/1**
46		Review CS	3/23/1	10/5/1
47		Readout CPUs, switch, storage, wor	2/3/12	1/4/13
48		1/3 Processor farm	2/3/12	6/21/1
49		1/3 Processor farm	6/21/1	5/23/1
50	**1.**	**System Assembly**	**2/3/11**	**7/25/1**
51		Long lead assembly	2/3/11	2/27/1
52		Preliminary assembly	6/21/1	4/24/1
53		Final assembly	1/5/16	7/25/1
54	**1.**	**Project Management**	**1/2/08**	**7/6/16**
55	**1.**	**Environment and Safety**	**1/2/08**	**7/6/16**

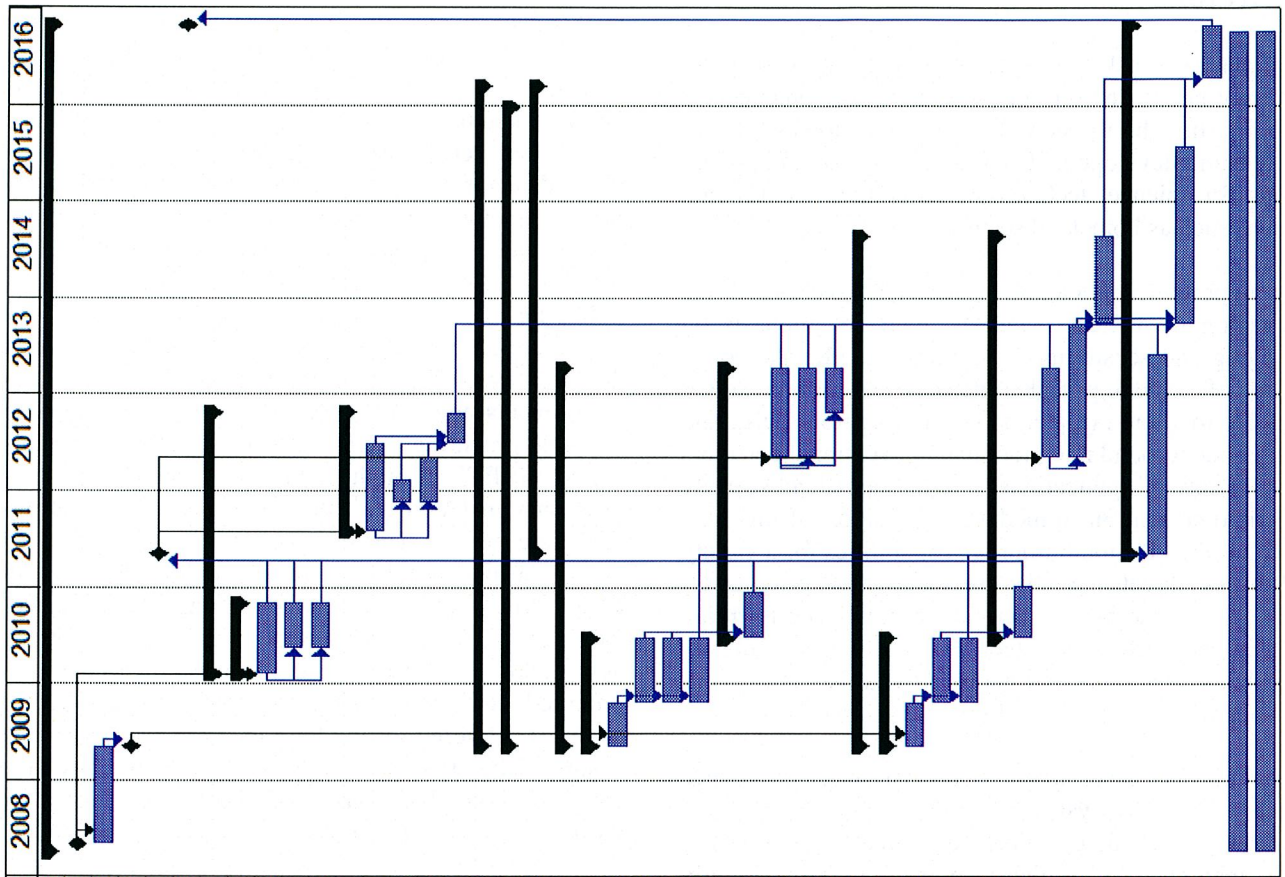

The detailed schedule for GRETA

Cost

Based on the schedule discussed above, we developed a funding profile in actual year dollars, as shown below. The table on the following page shows the breakdown cost summary for the GRETA in actual year dollars. All estimates have been inflated using escalation rates of 4% per year for material and labor assuming a funding profile that covers FY08 to FY16. This cost takes into account that GRETINA will be completed and its electronics, computing system and detector modules will be available to complete this 4π GRETA detector.

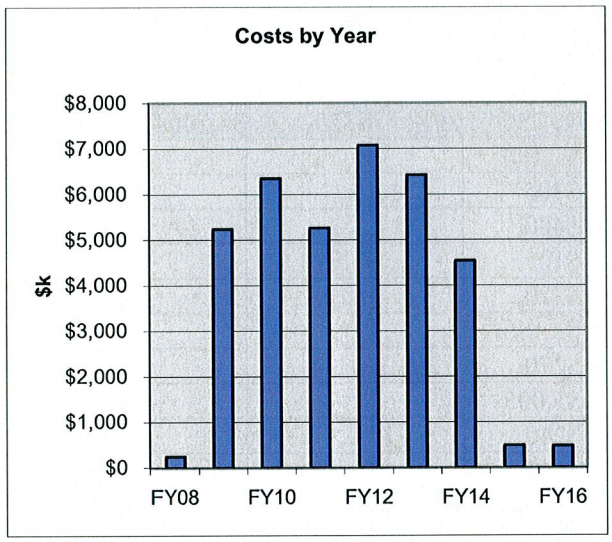

The funding profile for GRETA.

This cost estimate is based on the GRETINA cost estimate. It takes into account that most of the design is done during the GRETINA project, and that GRETA will concentrate mainly in the procurement of more detector modules, and hardware for the Electronics and Computing System, as well as the testing and assembly into a system. However, the Mechanical Systems will require a new design of the support structure, to accommodate the additional 23 detector modules (a total of 30 modules).

The cost of the materials was projected to larger quantities (which includes savings). We have contacted Eurisys and we projected the price estimate of the detector modules to be $1M per unit (in FY07 dollars). The detector price is derived by considering the unit price of €800k per module and an exchange rate Euro/Dollar of 1.25. In the current estimate, we applied escalation to this price. Although it is likely that we could obtain a fixed price contract in Euro, as we were able to do for GRETINA detectors.

Contingency allocation reflects the risk reduction due to knowledge and experience acquired with GRETINA. We have set the detector module contingency at 15%, which takes into account the risk of Dollar/Euro fluctuations in the exchange rate.

This cost estimate also assumes approximately the same level of redirected effort from Argonne National Laboratory, Lawrence Berkeley National Laboratory, the National Superconducting Cyclotron Laboratory at Michigan State University, Oak Ridge National Laboratory, and Washington University in St. Louis (for example, in the test and characterization of the detector modules, WBS 1.2.2 by MSU)

WBS	Description	Cost ($k)	Cont	Cont ($k)	Total ($k)
1	GRETA	$36,235	17%	$6,160	$42,395
1.1	Mechanical	$1,125	25%	$280	$1,406
1.1.1	Design	$380			
	Support structure	$325			
	Target chamber	$0			
	LN System	$55			
1.1.2	Production	$745			
	Support structure	$515			
	Target chamber	$55			
	LN system	$115			
	Assemble	$60			
1.2	Detector Module	$26,690	15%	$4,005	$30,694
1.2.1	Detector Procurement	$26,690			
1.2.2	Test/Characterize Module	$0			
1.3	Electronics Systems	$3,280	25%	$820	$4,100
1.3.1	Electronics for long-lead detectors	$1,100			
	Review electronics	$195			
	Digitizers (1200 channels)	$480			
	Trigger and Timing	$105			
	Power supplies, cables, crates, racks	$320			
1.3.2	Electronics for production detectors	$2,180			
	Review electronics	$270			
	Digitizers (2500 channels)	$1,005			
	Trigger and Timing	$240			
	Power supplies, cables, crates, racks	$665			
1.4	Computing Systems	$1,450	30%	$435	$1,885
1.4.1	CS for long-lead detectors	$530			
	Review CS	$155			
	Readout CPUs, switch, storage, workstations	$160			
	1/3 Processor farm	$215			
1.4.2	CS for production detectors	$920			
	Review CS	$160			
	Readout CPUs, switch, storage, workstations	$210			
	1/3 Processor farm	$300			
	1/3 Processor farm	$250			
1.5	System Assembly	$500	25%	$125	$625
	Long lead assembly	$175			
	Preliminary assembly	$190			
	Final assembly	$135			
1.6	Project Management	$2,955	15%	$445	$3,400
1.7	Environment and Safety	$235	20%	$50	$285

Table: The Cost of GRETA

8. The Path to GRETA: Progress and Milestones So Far

1994 – First discussions at LBNL

1995 - Duke Town meeting

1996 - GRETA mentioned in Long Range Plan document

1997 - First prototype segmented detector received and tested

1998 - Workshop on GRETA physics (LBNL) - Workshop on experimental equipment for RIA (LBNL) - GRETA Advisory Committee formed

1999 - Second prototype segmented detector received and tested

2000 - Workshop on GRETA physics (MSU) - Proposal for a GRETA module cluster submitted to DOE

2001 - National Steering Committee for Gamma-ray tracking in Nuclear Structure Physics formed - Santa Fe meeting (2002 LRP) presentation and discussion - Workshop on Digital Electronics in Nuclear Physics (ANL) - Workshop on Gamma-ray Tracking Detectors for Nuclear Science (U. Mass. Lowell)

2002 - GRETA mentioned in Overview and Recommendations section of the 2002 LRP –Gamma-ray Tracking Coordination Committee meeting (ANL) and report - Module cluster funded and ordered.

2003 - NSAC sub-Committee on Future Facilities presentation and report - Workshop on experimental equipment for RIA (ORNL) - GRETINA proposal written and submitted to DOE - CD-0 approval of GRETINA. Official start of project. - I.Y. Lee named as Contractor Project Manager and GRETINA Advisory Committee formed - Review of GRETINA project by LBNL -Review of GRETINA project by DOE

2004 - CD-1 approval for GRETINA - Facility Workshop for RIA at MSU - Workshop of GRETINA Detector Working Group at ORNL - Three Crystal Cluster prototype arrives in Berkeley - Workshop of GRETINA Software Working Group at LBNL - Workshop of GRETINA Electronic Working Group at ANL

2005 - CD-2A/3A approval for GRETINA -Workshop of GRETINA Software Working Group at FSU - First Quad-cluster module order sent out

2006 - Workshop of GRETINA Auxiliary Detector Working Group at St. Louis - Workshop of GRETINA Physics Working Group at FSU – Delivery of first Quad-cluster module (Dec)

For further information on the progress of GRETA/GRETINA over the past 4 years please see the annual newsletters which can be found at the official GRETA/GRETINA website http://grfs1.lbl.gov/

Appendix: The Management Structure of GRETINA

1. Management Advisory Committee

- James Symons (LBNL)
- Glenn Young (ORNL)
- Don Geesaman (ANL)
- Konrad Gelbke (MSU)

2. Contractor Project Manager

- I-Yang Lee (LBNL)

3. GRETINA Advisory Committee

- Con Beausang (Univ. of Richmond)
- Doug Cline (Univ. Of Rochester)
- Thomas Glasmacher (MSU)
- Kim Lister (ANL)
- Augusto Macchiavelli (LBNL)
- David Radford, **Chair** (ORNL)
- Mark Riley (FSU)
- Demetrios Sarantites (Washington Univ.)
- Kai Vetter (LLNL)

4. Working Groups and Chairs

- **Physics**: Mark Riley (FSU)
- **Auxiliary Detectors**: Demetrios Sarantites (Washington Univ.)
- **Electronics**: David Radford (ORNL)
- **Software**: Mario Cromaz (LBNL)
- **Detector Development**: Augusto Macchiavelli (LBNL)

This document was composed and edited by the GRETINA Physics Working Group, the GRETINA Advisory Committee and the Contractor Project Manager following a dedicated workshop entitled "The Future of Gamma-Ray Spectroscopy" held in Tallahassee FL, in August 2006. A list of participants along with presentations and a summary of the workshop can be found at http://fsunuc.physics.fsu.edu/gretina

Nuclear Instruments and Methods in Physics Research A 597 (2008) 233–237

Contents lists available at ScienceDirect

Nuclear Instruments and Methods in Physics Research A

journal homepage: www.elsevier.com/locate/nima

A digital signal processing module for gamma-ray tracking detectors ☆

M. Cromaz *, V.J. Riot [1], P. Fallon, S. Gros, B. Holmes, I.Y. Lee, A.O. Macchiavelli, C. Vu, H. Yaver, S. Zimmermann

Lawrence Berkeley National Laboratory, 1 Cyclotron Road, Berkeley, CA 94720, USA

ARTICLE INFO

Article history:
Received 11 June 2008
Received in revised form
15 July 2008
Accepted 16 July 2008
Available online 30 July 2008

Keywords:
Digital signal processing
Gamma-ray spectrometer
Digitizer
HPGe detector

ABSTRACT

We have designed and constructed an 8-channel digital signal processing board for the GRETINA spectrometer. The digitizer samples each of 8 inputs at 100 MHz with 12-bit resolution. Employing a large on-board FPGA, the board derives an energy, leading-edge time, and constant-fraction time from the input signal providing the functionality of a conventional analog electronics system. Readout and control of the digitizer is done over a VME bus. The digitizer's performance met all requirements for processing signals from the GRETINA spectrometer.

Published by Elsevier B.V.

1. Introduction

The recent development of gamma-ray tracking detectors [1–3] which employ HPGe detectors with segmented contacts has required the development of new electronic systems. Tracking detectors locate the position of charge deposition points in the Ge volume, which are the scattering points of the incident gamma ray, by examining the detailed pulse shape of the induced currents in the detector.

Unlike conventional Ge detector electronics, where only energy and timing information need to be extracted from the detector signal, tracking detectors require the waveform of each detector segment to be recorded during charge collection in the detector. This requires a digital electronics system to sample the signals from each segment with a high-speed, high-resolution analog to digital converter (ADC). The sampling rate and resolution of these ADCs must be sufficiently high to differentiate signals generated from different points in the detector and maintain the intrinsic high-energy resolution of Ge detectors required to perform gamma-ray spectroscopy.

Design and construction of this digitizer was undertaken to support research and development efforts for the GRETINA spectrometer [4,5]. This array will consist of twenty-eight 36-way segmented HPGe detectors and is designed to have a gamma-ray position resolution of less than 2 mm RMS. These boards served as a prototype for the production GRETINA digitizers and were tested extensively on a prototype segmented detector. As such, these digitizers implement the signal processing functionality needed for full signal analysis by the spectrometer.

2. Functional description

The digitizer board we have designed consists of the functional blocks shown in Fig. 1. A summary of board features is given in Table 1. The input signals are digitized independently by eight 12-bit, 100 MHz ADCs (Analog Devices AD9432BST-105). Other than a simple anti-aliasing filter no signal conditioning is applied to the input signal.

All data processing for the digitizer are performed by a single large field programmable gate array (FPGA) (Xilinx Virtex II XC2V3000) which includes approximately 3×10^6 system gates. Signal processing consists of four primary functions: the calculation of the signal energy, determination of the leading-edge and constant-fraction times, and extraction of the part of the trace relevant for signal decomposition. The pipeline architecture shown in Fig. 2 carries out these calculations. The data stream from each ADC is stored in a memory pipeline which is broken into four blocks of programmable length given by two parameters m and k. This pipeline is clocked at the ADC digitization frequency of 100 MHz. The information required by the data processing functions is accessed from the boundaries of the blocks (taps) as explained in the next section.

☆ This work has been supported by the Director, Office of Science of the US Department of Energy under Contract no. DE-AC02-65-CH11231.

* Corresponding author. Tel.: +1 510 486 4187; fax: +1 510 486 7983.
E-mail address: mcromaz@lbl.gov (M. Cromaz).
[1] Current address: Lawrence Livermore National Laboratory, 7000 East Ave., Livermore, CA 94550, USA.

0168-9002/$ - see front matter Published by Elsevier B.V.
doi:10.1016/j.nima.2008.07.137

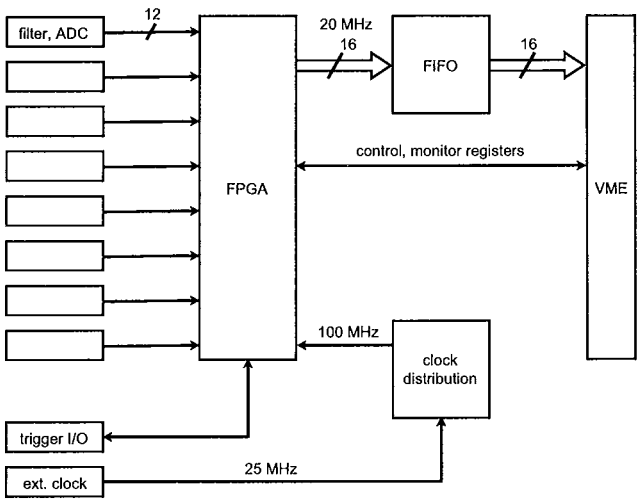

Fig. 1. Block diagram of the major elements of the GRETINA prototype digitizer board.

Table 1
A summary of characteristics and features of the prototype GRETINA digital signal processing module

Number of channels	8
Sampling rate	100 MHz
ADC resolution	12 bits
Input range	±1 V
Pipeline length	1000 samples
Signal processing	Energy, leading-edge and constant-fraction discriminator, trace windowing
Trigger modes	Self, external, validation
Form factor	6U VME 64x
Readout	VME A32/D32

Data processed by the FPGA, which includes the extraction of the relevant part of the trace as well as energy and timing information, are sent to a FIFO for output which can be read out over a VME interface. Control functions implemented in the FPGA are also controlled through registers accessible through the VME bus.

The digitizer operates synchronously with a common 100 MHz clock. This clock can be internally generated on the board for stand-alone operation or input externally to allow synchronization with other boards.[2] The external clock is operated at 25 MHz and is multiplied by 4 on the board.

2.1. Energy

A basic signal processing operation performed by the digitizer is calculating the energy of the incoming signal. An example of an energy spectrum from a ^{152}Eu source generated by the digitizer module from the central contact of a segmented HPGe detector is shown in Fig. 3. Pole-zero correction was not implemented on this prototype board and the counting rate was limited to 600 counts/s to prevent tailing. To achieve optimal signal to noise ratio, signal integration is necessary and this is done using a trapezoidal filtering algorithm [6]. This method has the advantage that it can be expressed as a recurrence relation with two adjustable parameters, m and k, which can be easily implemented with a memory pipeline

$$y_n = y_{n-1} + x_n - x_{n-k} - x_{n-k-m} + x_{n-m}. \quad (1)$$

[2] An ECL-driven sync input is provided that can reset the boards internal 48-bit clock to 0 allowing a set of digitizers to be synchronized to within one clock tick (10 ns).

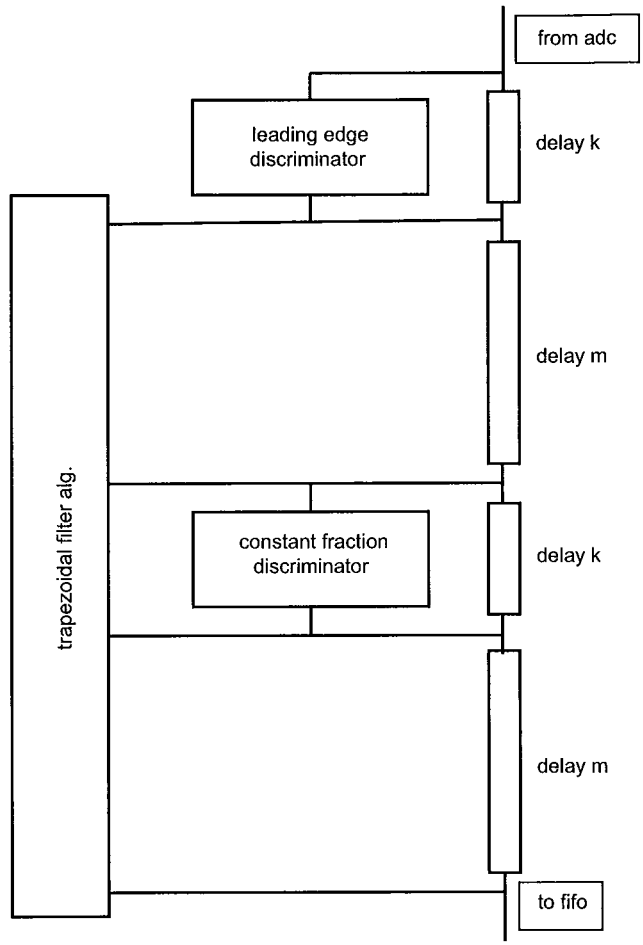

Fig. 2. Diagram showing the four segment pipeline used by each ADC channel and its relation to the three signal processing algorithms: energy, leading-edge discriminator time, and constant-fraction discriminator time.

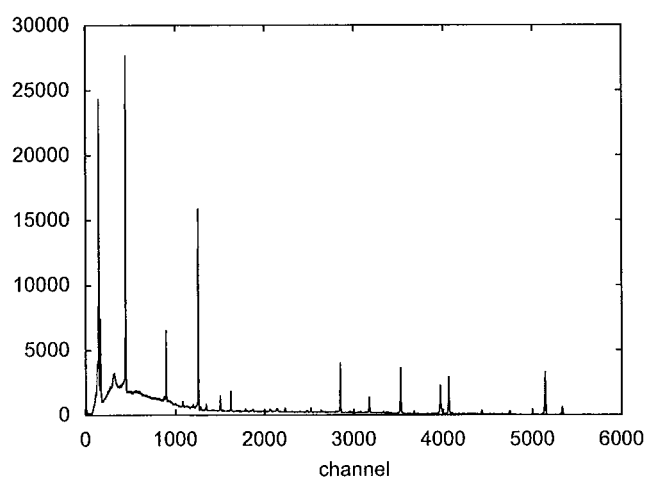

Fig. 3. Spectrum of a ^{152}Eu calibration source from the central contact of the GRETINA Q1 prototype detector generated by the digital signal processing module.

This relation requires the pipeline be sampled at four taps as shown in Fig. 2. Optimal shaping for a HPGe detector requires signal integration, corresponding to the time $2k+m$, of approximately 10 μs corresponding to a total pipeline length of 1000 samples.

Due to the repeated sampling of the incoming signal from the above integration, the effective energy resolution is higher than the nominal 12-bit resolution provided by the ADCs. Given a 1000 sample integration, the improvement in effective resolution is up to 5 bits[3] in the case where series noise is dominant [7]. This gain in effective resolution allows one to maintain energy resolution while having a large dynamic range.

2.2. Timing

Accurate timing is required from a physics point of view to perform gamma-ray coincidence measurements and reduce random coincidence events. From a purely instrumentation point of view, events must be timestamped as a single crystal, consisting of 36 segments, that will be distributed over several digitizer boards and must be reassembled before signal decomposition can be performed. The board provides two algorithms to obtain the time of the event: a leading-edge discriminator and a more accurate constant-fraction discriminator. Both tasks are performed digitally by the FPGA on the signal pipeline shown in Fig. 2.

The leading-edge discrimination occurs promptly, between the first two taps in the pipeline. This allows it to participate in the boards trigger decision. The algorithm used by the leading-edge discriminator consists of a differentiator given by

$$y_n = x_n - x_{n-k}$$

followed by four successive applications of a 3-point binomial integration filter

$$y_n = x_n + 2x_{n-1} + x_{n-2}$$

to smooth the resultant differentiated signal.

The clock tick at which the resultant signal passes a programmable discriminator threshold is latched. Once the timestamp is latched, a noise timer is started to prevent spurious re-triggering of the discriminator. This noise timer is programmable and is generally set equal to the typical charge collection time of the detector. The timestamp is 48-bits long so that all timestamps within a 33-day period of the last board synchronization are unique.

The second timing method used by the board is a digitally implemented constant-fraction discriminator. Unlike the leading-edge discriminator, to first order the constant-fraction discriminator is independent of the amplitude of the signal. As with an analog constant-fraction discriminator, the digital implementation subtracts a fraction a of the delayed signal from the incident signal and determines the time of the zero crossing:

$$y_n = x_{n-k} - ax_n.$$

This floating point operation would be resource intensive and slow on an FPGA and we write the above expression in terms of an integer shift

$$y'_n = \frac{x_{n-k}}{a_b} - x_n$$

where $a_b = \log_2(1/a)$ yielding fractions which are inverse powers of 2 (0.5, 0.25, 0.125,...).

[3] Following Poisson statistics, given a sampling error e, the energy integration over 1000 channels results in the error being reduced by $e/\sqrt{1000} \approx e/32 = e/2^5$.

Also, in the interest of saving FPGA resources, instead of calculating the zero crossing directly, the value of y'_n on each side of the zero crossing is output so the exact time of the signal can be inferred through linear interpolation.

2.3. Trigger

Due to the high computational cost of signal decomposition, it is essential for gamma-ray tracking detectors to have efficient, flexible triggering systems. Upon receipt of a valid trigger, the leading-edge and constant-fraction times, the energy and the relevant section of the waveform are latched into memory for subsequent readout. This module supports three triggering modes: internal or self-trigger, external trigger, and validation trigger. Each of the 8 channels on the board are triggered independently.

In self-trigger mode, the trigger fires when the input signal passes the leading-edge trigger threshold. Both the level and polarity of this threshold are programmable on a channel-by-channel basis.

Validate trigger mode is similar to self-trigger mode in that the leading-edge discriminator initiates the trigger. However, in validate mode, an additional validate signal must be provided by the user within a programmable time window to complete the trigger.

External mode enables asynchronous triggers to be generated regardless of the shape of the incoming waveform. The external trigger is initiated by an ECL logic signal input into the front panel. For these events, the leading-edge time, which normally serves as the event timestamp, is given by the clock pulse on which the external trigger signal was input.

Regardless of the trigger mode, the board generates an ECL pulse for each channel when its leading-edge discriminator is crossed. This pulse (available from the front panel) is very useful when generating a trigger from several digitizer boards or when using external detectors and electronics to create a compound trigger. For example, a standard trigger used in our multiple-crystal HPGe tests takes the leading-edge discriminator from the central contacts of each crystal, generates a coincidence, and passes it to the individual digitizer boards as an external trigger.

2.4. Trace window

The trace length required to compute the positions of the interaction points is given by the charge collection time which is approximately 400 ns or 40 samples. The extracted trace must be kept as short as possible to avoid overwhelming the readout section of the board and data acquisition system at high rates. A programmable window consisting of an offset and window length are provided to give the board this functionality. In the case of self- or validate triggering modes, the offset is taken from the leading-edge discriminator while for external mode it is taken from when the external trigger logic signal arrives.

3. Control interface and data readout

The control interface and readout is performed by mapping two memory regions from the address space of the VME crate controller to the digitizer board. A 256 byte section is mapped into VME A16/D16 space is used to configure the board. Here, channels can be enabled or disabled, thresholds and various time windows can be set.

The single FIFO VME address is mapped repeatedly into 256k contiguous words in A24/D32 space for data readout. This allows

the FIFO to be read out in VME block mode for more efficient data transfers.

The data format used by the digitizer board reflects the segment-by-segment independence of the data. The data for each detector segment comprises a 12 byte header containing the board's id and the parameters calculated from the signal as described in Section 2. Following the header is a variable length trace as defined by the trace window. There is no guarantee that events in the data stream from near-simultaneous triggers among the 8 channels of the board will be time-ordered. Detailed timing information must be obtained from the event's timestamp.

The board can be read out using either a polled or an interrupt driven readout system. Polled systems access a word in configuration space of the digitizer module to determine fill status of the output FIFO. Interrupt driven systems rely on an interrupt generated by the board when the FIFO is half-full.

4. Performance characteristics

The digitizer is required to meet performance criteria in energy resolution, linearity, and data rate. A basic test of the performance of the digitizer is measured by the noise when the input to the digitizer is terminated. This relates to the intrinsic ADC noise as well as to contributions from the digitizer board itself. At one standard deviation, the trace noise was 0.3 bits whereas 0.5 bits are given by the ADC specification [9]. This also implies that the noise contribution from the digitizer itself is very small.

The energy resolution of the digitizer was measured and compared to that of a conventional analog system (Tennelec TC244 spectroscopy amplifier, Amtek 8000A multichannel analyzer). To investigate the noise characteristics of the digitizer with regards to energy resolution, our input was a tail pulser (Ortec 448 research pulser) superimposed with a white noise source, provided by an Agilent 33250A function generator. The pulser was set up to model our detector and preamplifier with a risetime of 100 ns and a fall time of 50 μs. The amplitude of the noise source was varied to model realistic noise values for HPGe detectors. The results of these tests are shown in Fig. 4. The integration time of the digitizer was set to 4.4 μs with a flat-top length of 0.32 μs. This is equivalent to a peaking time of 2 μs for the Tennelec amplifier. The energy resolution of the digitizer is only slightly worse than that of the analog system, with the energy resolution of the analog system being an average of 16% better over all measured noise levels. However, we do not expect this to have a significant impact on the sensitivity of the array.

The integral linearity of the digitizer was measured with an Ortec 448 research pulser at maximum amplitude of 400 mV, which corresponds roughly to a 2 MeV pulse with our HPGe/preamplifier set up. The integration time of the digitizer was set to 4.5 μs and the length of the flat-top was 0.32 μs. We chose a set of pulse amplitudes to span the input range of the digitizer. Plotted in Fig. 5 is the deviation of energy values from a linear fit as a function of pulse height. The maximum deviation from a linear fit, which corresponds to the integral linearity, was found to be 0.0017%.

To measure the differential non-linearity, we employed a tail pulser and a ramp to sample all signal amplitudes in the input range of the digitizer. This pulser and ramp were constructed as an integral unit specifically designed for these measurements. Compared against a reference Wilkinson ADC, the differential non-linearity introduced by the pulser and ramp themselves were less than 1%. To remove any correlations in the ramp the pulser was triggered randomly using a gamma-ray source. The test took 2 days with 1.45×10^8 counts collected. The resultant spectrum is shown in Fig. 6. We determined the differential non-linearity of the digitizer, defined as the maximum excursion from the average, to be 3.76% with a 0.87% RMS deviation.

The differential non-linearity in the energy measurement can be understood in terms of the differential non-linearity of the ADC [8]. The ADC has a typical differential non-linearity of ±0.5 of the least significant bit (LSB) [9] corresponding to a RMS value of 0.3 LSB or 30%. Such a large value would be unacceptable for peak shape analysis if the energy was determined by the differential non-linearity of a single ADC channel. However, the energy of the gamma ray using the trapezoidal filter is derived from the sum of many samples taken over a wide range of ADC channels. For example, for $m = 4.5\,\mu s$, the energy is derived from 450 independent amplitude measurements. The preamplifier has a decay time of 50 μs meaning the 450 numbers are digitized at different amplitudes. As a rough estimate, the differential non-linearity of the derived energy will be reduced by a factor of about 20 due to the random nature of the differential non-linearity of the ADC. On this basis the energy spectra would have a differential non-linearity of 1.5% RMS, compared to the measured RMS differential non-linearity of 0.87%.

The data rate from the digitizer over the backplane is 19 MB/s. This was measured using A32/D32 block transfers using direct

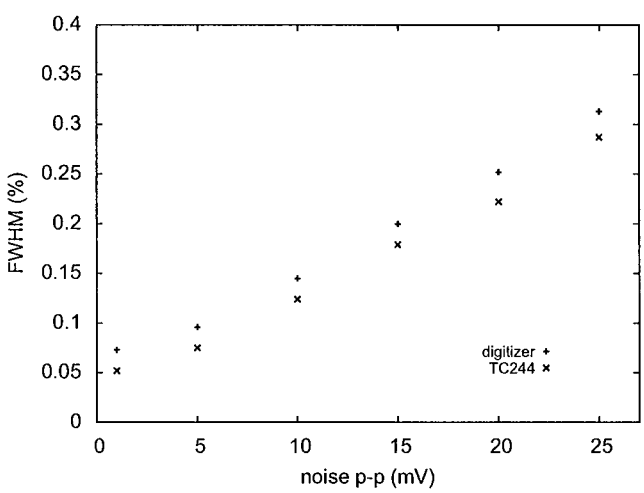

Fig. 4. Resolution as a function of noise added to a tail pulser. An analog system (Tennelec TC244 spectroscopy amplifier coupled to an Ampek 8000A MCA) is compared with the GRETINA digitizer board.

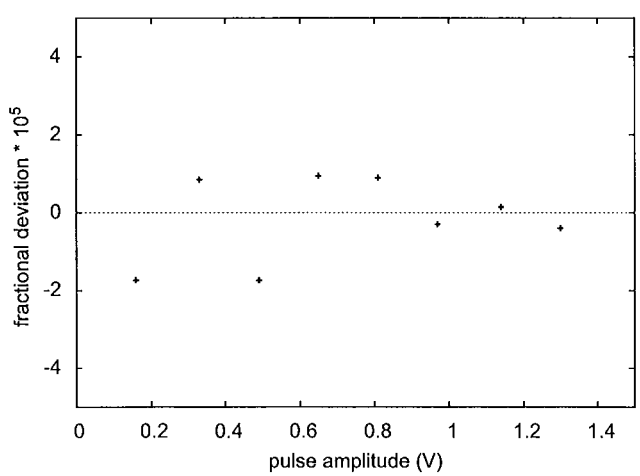

Fig. 5. Integral linearity as given by the fractional deviation of channel positions from a linear fit. The maximum deviation was found to be 0.0017%.

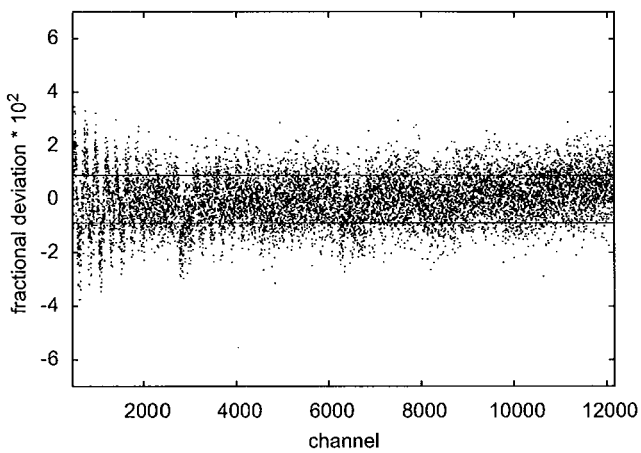

Fig. 6. Differential linearity as given by the fractional deviation of channel position over the usable dynamic range of the digitizer. The maximum deviation was found to be 3.76% with a RMS deviation is 0.87%. The two black lines show the one standard deviation error due to counting statistics.

memory access (DMA) from a CES RIO2 VME CPU board utilizing a 350 MHz PowerPC processor. The CPU utilization during this test was only 2%, indicating this was not limiting the readout rate. Given that a standard trace length for signal decomposition is 500 ns or 50 samples, the data rate with all 8 channels operating is roughly 18 500 events/s.

5. Conclusion

We have developed an 8-channel prototype digitizer board to process signals from segmented HPGe detectors used for gamma-ray tracking with the GRETINA spectrometer. These boards provide a 12-bit dynamic range and are capable of continuously digitizing their inputs at 100 MHz. Algorithms implemented in a FPGA calculate signal energies, times, and derive trigger information from the input trace eliminating the need for conventional analog signal processing electronics. Performance of the board was found to meet expectations with the exception of differential non-linearity which was higher than expected. We believe this reflects the intrinsic differential non-linearity of the ADC chip and an improvement will be seen when we use 14-bit ADC chips in the production version of the digitizer module. In addition to these measurements, in-beam experiments have been carried out and the system was found to perform well.

This digitizer board will essentially be used intact for the production GRETINA system. The main modifications made to the production board will be increasing the number of channels per board from 8 to 10, the addition of a serial trigger system to allow for more complex triggering decisions, and the use of a larger though less expensive FPGA (Xilinx Spartan XC3S5000). The first of these new boards has been completed and is being tested. The digitizer is expected to be ready for when the GRETINA spectrometer begins its experimental program in early 2011.

References

[1] I.Y. Lee, Nucl. Instr. and Meth. A 422 (1999) 195.
[2] K. Vetter, et al., Nucl. Instr. and Meth. A 452 (2000) 105.
[3] K. Vetter, et al., Nucl. Instr. and Meth. A 452 (2000) 223.
[4] J.T. Anderson, et al., IEEE Trans. Nucl. Sci., accepted for publication.
[5] ⟨http://grfs1.lbl.gov⟩.
[6] V.T. Jordanov, G.F. Knoll, Nucl. Instr. and Meth. A 345 (1994) 337.
[7] G.F. Knoll, Radiation Detection and Measurement, third ed., Wiley, New York, 1999, p. 631.
[8] I.Y. Lee, to be published.
[9] AD9432 data sheet, Analog Devices.

Nuclear Instruments and Methods in Physics Research A 345 (1994) 337–345
North-Holland

NUCLEAR INSTRUMENTS & METHODS IN PHYSICS RESEARCH
Section A

Digital synthesis of pulse shapes in real time for high resolution radiation spectroscopy

Valentin T. Jordanov *, Glenn F. Knoll

Department of Nuclear Engineering, The University of Michigan, 2355 Bonisteel Blvd., Ann Arbor, MI 48109, USA

(Received 18 January 1994)

Techniques have been developed for the synthesis of pulse shapes using fast digital schemes in place of the traditional analog methods of pulse shaping. Efficient recursive algorithms have been developed that allow real time implementation of a shaper that can produce either trapezoidal or triangular pulse shapes. Other recursive techniques are presented which allow a synthesis of finite cusp-like shapes. Preliminary experimental tests show potential advantages of using these techniques in high resolution, high count rate pulse spectroscopy.

1. Introduction

The theory of optimal pulse shaping in high resolution spectroscopy has been well developed and published in number of articles and textbooks. While the ideal cusp shape has been cited to give the best signal-to-noise ratio, it has been recognized that this pulse shape is not practical because of its theoretically infinite time duration [1,2]. In a typical spectroscopy configuration employing a charge sensitive preamplifier, two generalized types of noise are of significant importance: step and delta noise [1,3]. When delta noise is predominant, the optimum pulse shape for a finite pulse duration is the symmetrical triangular shape [1,4]. In addition to electronic noise, the pulse height measurement is subject to other sources of fluctuations such as statistical variations in the number of charge carriers, microphonic effects, charge loss due to trapping, etc. [5]. An additional consideration is the sensitivity of the pulse shaping techniques to variations in the detector charge collection time. Ballistic deficit and charge trapping effects can noticeably reduce the resolution of spectrometers when shapers producing short pulses with sharp peaks are used. It has been demonstrated that these effects can be reduced by using flat-topped shapes [1,6,7].

This paper describes a technique for synthesis of optimal pulse shapes (symmetric triangle and symmetric trapezoid) for high resolution, high throughput spectroscopy, using fast recursive digital algorithms. The technique also allows synthesis of other shapes such as finite cusp-like and flat-topped cusp-like shapes. The algorithms are suitable for real time implementation, require only simple hardware, and offer flexibility in the adjustment of the output pulse shapes.

* Corresponding author. Present address: Amptek Inc., 6 De Angelo Dr., Bedford, MA 01730, USA.

2. Synthesis of trapezoidal and triangular pulses

In common spectroscopy systems, the detector–preamplifier configuration is followed by a prefilter circuit (pole-zero cancellation, CR differentiation) that produces a pulse with short rise time followed by a long exponential tail. In the following development, we assume this type of input signal with amplitude normalized to one and a decay time constant of τ. The rise time of the pulse, for now, will be considered to be very short. An example of the exponential signal is sketched in Fig. 1a.

The initial problem we have addressed is to develop an efficient algorithm to convert this exponential pulse to a pulse with true trapezoidal shape. We will first carry on the analysis in the continuous time domain, and then apply the results in the discrete time domain.

The output $s(t)$ of a linear time-invariant system is given by the convolution integral

$$s(t) = \int_{-\infty}^{+\infty} v(t')h(t-t')\,\mathrm{d}t', \tag{1}$$

where $v(t)$ is the input signal and $h(t)$ is the impulse response of the system. For real-time signal processing the system must be causal, i.e. the output at given moment depends only on present and previous values of the input signal. As a result the upper limit of

Elsevier Science B.V.
SSDI 0168-9002(94)00165-4

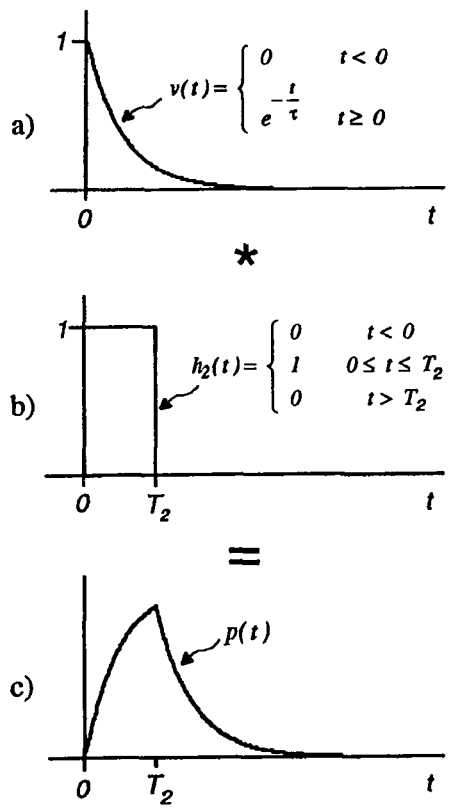

Fig. 1. Convolution of an exponential input signal (a) with rectangular function (b) and the output response of the system (c).

integration in Eq. (1) can be truncated at the moment of time t at which the output of the system is evaluated. Our goal is to find a causal system with finite impulse response which, when used in Eq. (1), will transform an exponential input signal into a trapezoidal shape. The convolving function should also be simple and practically realizable.

2.1. Convolution with rectangular and truncated ramp functions

First consider a system with a simple rectangular impulse response, also called a moving average system. The digital implementation of this system in radiation spectrometry has been previously described [8]. An example of a unit rectangular function is shown in Fig. 1b. The output response of the moving average system to an exponential input signal (Fig. 1a) is presented in Fig. 1c. The result of the convolution of an exponential signal with a unit rectangular function is described by the following equations

$$p(t) = \int_0^t e^{(t'-t)/\tau}\, dt' = \tau(1 - e^{-t/\tau}), \quad 0 \leq t \leq T_2 \tag{2}$$

and

$$p(t) = \int_0^{T_2} e^{(t'-t)/\tau}\, dt' = \tau\, e^{-t/\tau}(e^{T_2/\tau} - 1), \quad t > T_2. \tag{3}$$

The response of the system for $t < 0$ is zero. Note that the only time dependent terms in Eq. (2) and Eq. (3) are exponentials. An important feature of the output signal is that, after reaching a maximum, it decays with the same time constant as the time constant of the input signal.

Another simple convolving function is the truncated ramp (or saw-tooth) function. Fig. 2b shows a unit slope truncated ramp function with duration T_1. The response of this system to an exponential signal (Fig. 2a) is depicted in Fig. 2c. The output response of this system is given by

$$r(t) = \int_0^t t'\, e^{(t'-t)/\tau}\, dt' = \tau t - \tau^2(1 - e^{-t/\tau}),$$
$$0 \leq t \leq T_1 \tag{4}$$

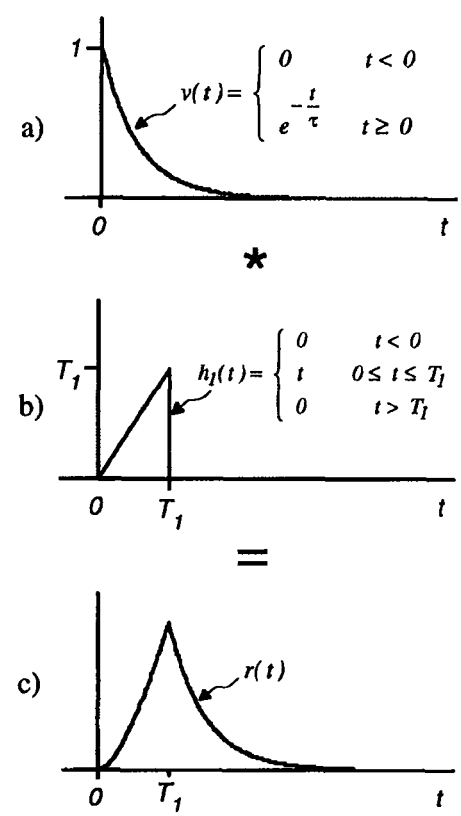

Fig. 2. Convolution of an exponential input signal (a) with unit slope truncated ramp function (b) and the response of the system (c).

and

$$r(t) = \int_0^{T_1} t' \, e^{(t'-t)/\tau} \, dt'$$
$$= \tau \, e^{-t/\tau}\left(\tau + e^{T_1/\tau}(T_1 - \tau)\right), \quad t > T_1. \tag{5}$$

Again the response of this system for $t < 0$ is zero, and this case will be omitted in the following discussions. Eq. (4) has two time dependent terms – one is linear and the other is exponential.

2.2. Impulse response of the trapezoidal shaper

We next will develop the conditions under which a flat-topped trapezoidal shape can be synthesized. Taking the definitions of $r(t)$ and $p(t)$ from above, consider a function $f(t)$ defined as

$$f(t) = r(t) + \tau p(t) + a p(t - T_1), \tag{6}$$

where a is a parameter. It is assumed also that $T_1 \le T_2$. Further, for simplification, the function describing the output signal of the system in given time interval will be indicated using two indices referring to the beginning and end of the interval, e.g. $f_{01}(t)$ denotes $f(t)$ in the time interval $0 \le t < T_1$, $f_{12}(t)$ implies $f(t)$ for $T_1 \le t < T_2$, etc. Using this convention and defining a moment of time $T_3 = T_2 + T_1$, Eq. (6) can be rewritten as three separate equations

$$f_{01}(t) = \tau t, \tag{7}$$

$$f_{12}(t) = \tau^2(1 - e^{-t/\tau}) + \tau \, e^{-t/\tau}\left(\tau + e^{T_1/\tau}(T_1 - \tau)\right) + a\tau(1 - e^{-(t-T_1)/\tau})$$
$$= \tau^2 + a\tau + \tau \, e^{-(t-T_1)/\tau}(T_1 - \tau - a), \tag{8}$$

$$f_{23}(t) = \tau^2 \, e^{-t/\tau}(e^{T_2/\tau} - 1) + \tau \, e^{-t/\tau}\left(\tau + e^{T_1/\tau}(T_1 - \tau)\right) + a\tau(1 - e^{-(t-T_1)/\tau}). \tag{9}$$

Eq. (7) represents the linear rising slope of the desired trapezoidal shape. The next step is to find the condition under which $f(t)$ is constant in the interval $T_1 \le t \le T_2$. This condition can be determined from Eq. (8). Since $f_{12}(t)$ must be time independent, it is necessary that $T_1 - \tau - a = 0$ or $a = T_1 - \tau$. For the case in which $a = T_1 - \tau$, Eq. (8) and Eq. (9) reduce to

$$f_{12}(t) = T_1 \tau, \tag{10}$$

$$f_{23}(t) = \tau^2 \, e^{-(t-T_2)/\tau} + \tau(T_1 - \tau). \tag{11}$$

This choice of $a = T_1 - \tau$ is assumed for the remainder of this analysis. If the trapezoidal shape is to be symmetric, the signal must decay to zero at $T_3 = T_2 + T_1$. Let the response of the system be written as

$$s(t) = f(t) + q(t) \tag{12}$$

where $q(t)$ is the specific function that results in $s(t)$ becoming a symmetric trapezoidal function defined as

$$s_{-\infty 0}(t) = 0, \tag{13}$$

$$s_{01}(t) = \tau t, \tag{14}$$

$$s_{12}(t) = T_1 \tau, \tag{15}$$

$$s_{23}(t) = T_1 \tau - \tau(t - T_2), \tag{16}$$

$$s_{3\infty}(t) = 0. \tag{17}$$

The specific solution for $q(t)$ can be found from Eq. (7) and Eq. (10) through 17. The result is that $q(t) = 0$ in the time interval $-\infty < t < T_2$, and in the rest of the time domain $q(t)$ is defined by

$$q_{23}(t) = -\left[\tau(t - T_2) - \tau^2(1 - e^{-(t-T_2)/\tau})\right] \tag{18}$$

and

$$q_{3\infty}(t) = -\left[\tau^2 \, e^{-(t-T_2)/\tau}\right]. \tag{19}$$

Eqs. (4), (5), (18) and (19) show that $q(t)$ has the same shape as $r(t)$ but with opposite polarity and a delay in time of T_2

$$q(t) = -r(t - T_2). \tag{20}$$

Thus, a system with properties that transform an exponential to a trapezoidal shape has been determined. In the case of $T_1 = T_2$ the trapezoid is reduced to a triangular shape. It should be noted that other constraints can be applied regarding the shape and duration of trailing edge of the trapezoidal pulse, and asymmetric shapes can be obtained. However, a symmetric shape is generally preferred for optimum signal-to-noise ratio in the measurement of pulse height [3].

From the distributive property of convolutions, the impulse response of the system can be written as

$$h(t) = h_1(t) + \tau h_2(t) + (T_1 - \tau) h_2(t - T_1) - h_1(t - T_2), \tag{21}$$

where $h_1(t)$ and $h_2(t)$ are the impulse responses of the truncated ramp system and the moving average system respectively. The impulse response of the trapezoidal shaping system is shown in Fig. 3b. In this example $T_1 = \tau$. This response is synthesized by simple functions and is suitable for real time digital implementation.

3. Digital implementation of the trapezoidal shaper

Consider an exponentially-decaying input signal that is digitally sampled at equal intervals of time. In what follows, we will measure time in units of the sampling period. The input signal at time i will be written as $\nu(i)$. The first step in the synthesis is to convolve the sampled input signal with a rectangular function. Since it is required that the convolution be performed in real

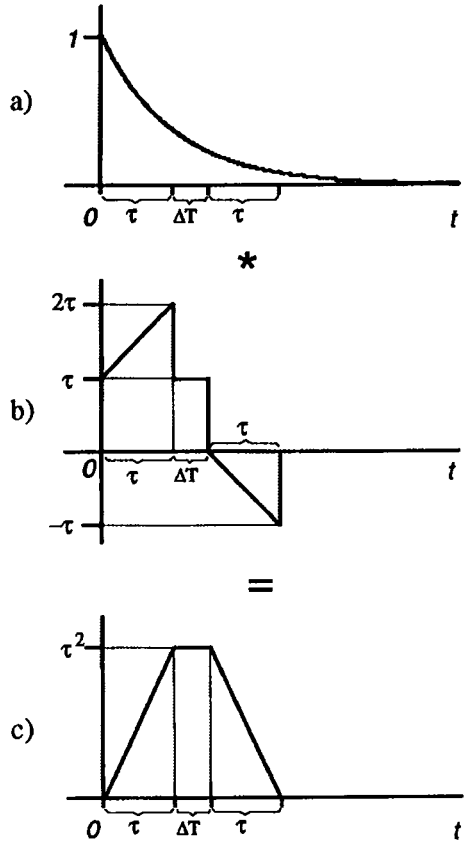

Fig. 3. Convolution of an exponential input signal (a) with trapezoidal shaper impulse response (b) and the output response of the system (c).

time, it is convenient to use a recursive convolution algorithm. The recursive form of moving average system is given as

$$p(n) = \sum_{i=0}^{n} \nu(i) - \nu(i-l)$$

or

$$p(n) = p(n-1) + \nu(n) - \nu(n-l), \quad n \geq 0, \tag{22}$$

where $\nu(n)$ is the prompt sample at time n and $\nu(n-l)$ is a sample at a time that is delayed by l relative to n. We will denote l as the length of the convolution function.

The initial conditions that are imposed will determine the offset of the output signal. It is usually required that the offset be zero, so that the initial condition can be defined as

$$\nu(n) = 0, \quad n < 0. \tag{23}$$

Further, we assume that the same initial condition is met for the recursive algorithms to be discussed later.

The next step is to define a recursive algorithm for convolution using a truncated ramp function. Again it is assumed that the slope of the ramp is equal to unity. Under these circumstances the recursive form of the convolution can be written as

$$r(n) \sum_{i=0}^{n} \left\{ \sum_{j=0}^{i} \nu(j) - \nu(j-k) - \nu(i-k')k \right\}$$

or

$$r(n) = r(n-1) + p(n) - \nu(n-k')k, \quad n \geq 0 \tag{24}$$

Here $p(n)$ represents a moving average (Eq. (22)) with length k, and k' is a delay parameter. Three different impulse responses can be obtained depending upon the choice of value of k', as shown in Fig. 4. For the trapezoidal shaping discussed above it is necessary that k' be set equal to k.

Recursive convolution algorithms using higher order polynomial truncated functions can be constructed in fashion similar to that described for the truncated ramp case. For instance, a convolution with a trun-

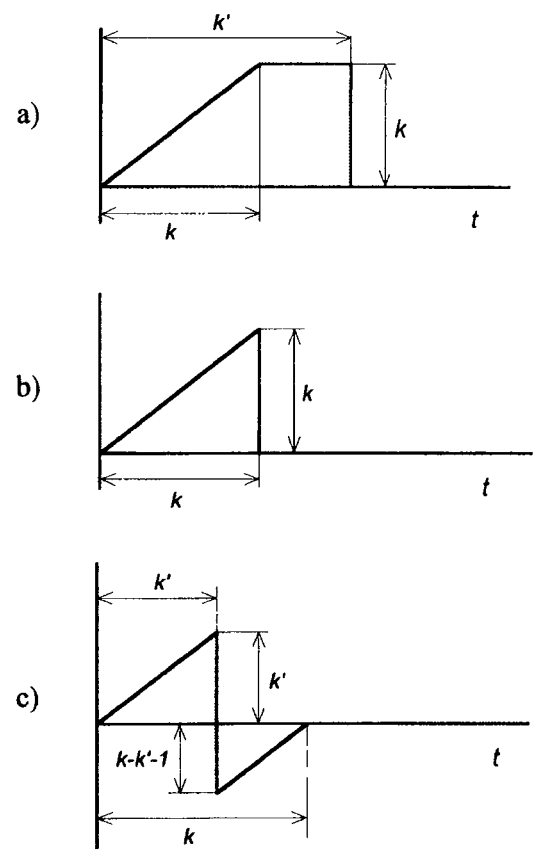

Fig. 4. Impulse response of a truncated ramp system at different values of the delay parameter k'. (a) $k' > k$, (b) $k' = k$, (c) $k' < k$.

cated $(k^2+k)/2$ function can be written in recursive form as

$$u(n)=\sum_{l=0}^{n}\left\{\sum_{i=0}^{l}\left\{\sum_{j=0}^{i}\nu(j)-\nu(j-k)-\nu(i-k')k\right\}-\nu(l-k)\frac{k^2+k}{2}\right\}$$

or

$$u(n)=u(n-1)+r(n)-\nu(n-k)\frac{k^2+k}{2},\quad n\geqslant 0, \tag{25}$$

where $r(n)$ is truncated ramp convolution with length k (Eq. (24)). Convolution with higher order polynomial functions requires operations with large integer numbers resulting in an increased complexity of the system. Thus, we will limit our considerations here to systems with rectangular and truncated ramp impulse responses.

The response of the trapezoidal shaper discussed previously in the continuous time domain can be written in the form of a recursive algorithm in the discrete time domain. It is assumed that the decay time constant of the sampled exponential signal is equal to M. The rise time of the trapezoidal shape is set to k and the duration of the flat top of the trapezoidal shape is equal to $m=l-k$. From Eq. (21), the response of the system can be written as

$$s(n)=r(n)+Mp(n)+(k-M)p(n-k)-r(n-l). \tag{26}$$

From Eq. (22) and Eq. (24) the response of the system can be expressed in terms of sampled input signal

$$s(n)=\sum_{i=0}^{n}\sum_{j=0}^{i}[\nu(j)-\nu(j-k)]-\nu(i-k)k+M\sum_{i=0}^{n}[\nu(i)-\nu(i-l)]+(k-M)\sum_{i=0}^{n}[\nu(i-k)-\nu(i-l-k)]-\sum_{i=0}^{n}\sum_{j=0}^{i}[\nu(j-l)-\nu(j-k-l)]-\nu(i-k-l)k. \tag{27}$$

Let

$$d^{k,l}(j)=\nu(j)-\nu(j-k)-\nu(j-l)+\nu(j-k-l). \tag{28}$$

The substitution of Eq. (28) into Eq. (27) yields

$$s(n)=\sum_{i=0}^{n}\sum_{j=0}^{i}d^{k,l}(j)+d^{k,l}(i)M. \tag{29}$$

The recursive form of Eq. (29) is given by

$$s(n)=s(n-1)+p'(n)+d^{k,l}(n)M,\quad n\geq 0, \tag{30}$$

where

$$p'(n)=p'(n-1)+d^{k,l}(n),\quad n\geq 0. \tag{31}$$

Eqs. (30) and (31) define a recursive algorithm for generating a symmetric trapezoidal shape from a sampled exponential input signal. When $k=l$ the system response results in a symmetric triangular shape. Using Eqs. (30) and (31), a simple hardware configuration can be assembled using only a small number of standard digital pulse processing building blocks. A simplified block diagram of the trapezoidal shaper is depicted in Fig. 5.

Three programmable delay pipelines [9] are used for providing the necessary time shift of the sampled input signal. In subsequent steps, the signal passes through arithmetic units according to the algorithm described by Eqs. (30) and (31). All building blocks are integer arithmetic devices using signed variables. It should be noted that the digital processor passes just one digital value per processed pulse to the multichannel analyzer corresponding to the peak value of the shaped pulse. The approach is an extension of that employed in our previous work [8] where a similar

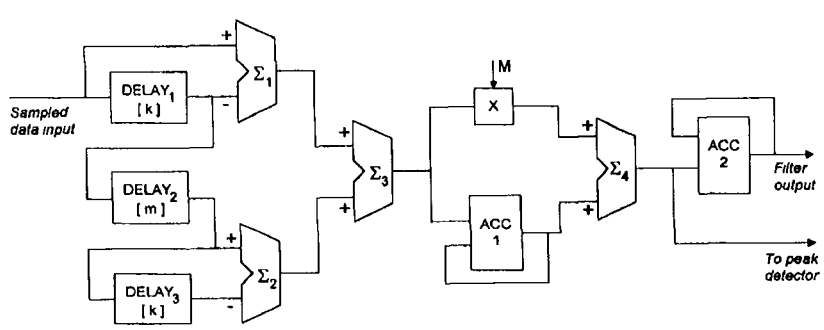

Fig. 5. Block diagram of digital trapezoidal/triangular shaping system. The building blocks are as follows: Σ – adder/subtracter; ACC – accumulator, X – multiplier; DELAY – delay pipeline.

threshold-free approach for detecting peaks has been described. Peaks are detected by monitoring sign changes in the result of the addition that precedes the final accumulation. When the noise level is high or when the sampling ADC misses some codes, measures need to be taken to avoid erroneous peak detection, especially in the case of a flat-topped pulse. Details of the peak detection process are given in refs. [8,10,11].

4. Other digital recursive algorithms

The recursive algorithms described in previous sections allow a variety of different shapes to be synthesized in real time. When the time constant of the exponential input signal is comparable to the length of the convolution function the methodology described for the trapezoidal signal can be applied but with

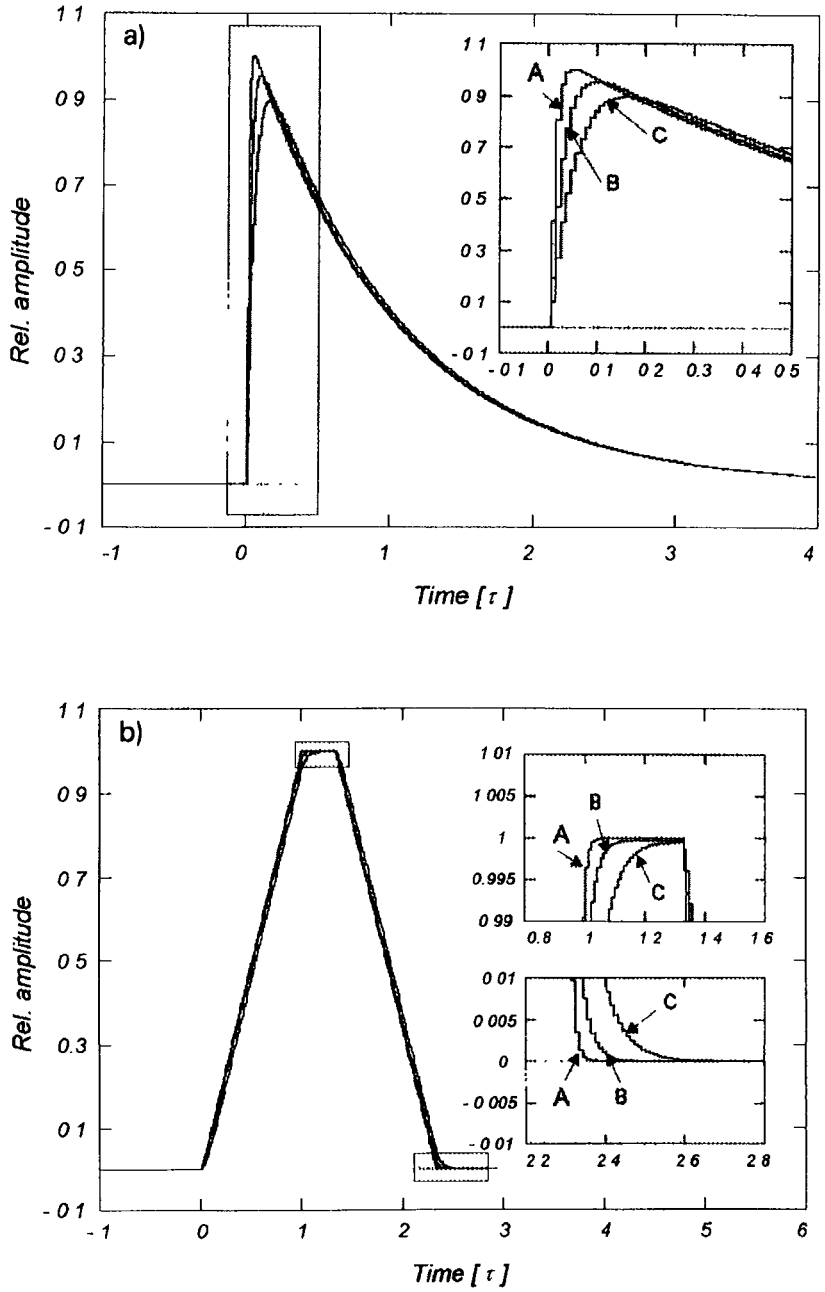

Fig. 6. Exponential pulses (see text) with different rise time (a) and the corresponding trapezoidal pulse shapes (b).

Table 1
Digital recursive algorithms and the corresponding output responses to a step input signal

INPUT $v(n)$	RECURSIVE ALGORITHM	DELAY l	PULSE SHAPE
	$s(n)=s(n-l)+v(n)-2\,v(n-k)+v(n-2k)$		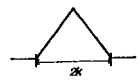
	$s(n)=s(n-l)+v(n)-v(n-k)-v(n-l)+v(n-l-k)$	$l=k+m$	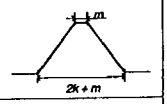
	$p(n)=p(n-l)+v(n)-v(n-l)$ $s(n)=s(n-l)+p(n)-v(n-k)\,l$	$l=2k+l$	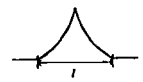
	$p(n)=p(n-l)+v(n)-v(n-k)+v(n-l)-v(n-l-k)$ $s(n)=s(n-l)+p(n)-[v(n-k)+v(n-l)]\,k-v(n-l)+v(n-l-k)$	$l=k+m$	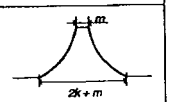

significantly different outcome. With the proper choice of parameters, finite cusp-like and flat-topped cusp-like shapes can be obtained. Optimization of the shapes often requires a solution of transcendental equations and the resulting pulse shape will be asymmetric. In this section, however, we will discuss a different case for which the input signal has a long decay constant and can be approximated as a step function. This circumstance holds when the output signal from a charge sensitive preamplifier is directly digitized [12].

First, consider the case of a step input. Using a rectangular convolving function, trapezoidal or triangular responses can be obtained. Cusp-like or truncated cusp-like pulse shapes can be synthesized using the recursive algorithms given by Eq. (24). Table 1 summarizes the recursive algorithms and corresponding pulse shapes. Because of the bipolar impulse responses of the systems shown in Table 1, the amplitude of the shaped pulse is independent of any dc offset of the step input signal. Thus, the technique is directly applicable to the signal from a reset type preamplifier as well as that from a conventional resistive feedback preamplifier.

5. Simulations and preliminary experimental tests

5.1. Calculated response

In the previous sections we considered the rise time of the exponential pulse to be very short. In reality, however, the rise time of the signals is finite and depends on variety of factors: finite rise time of the analog circuits, CR networks in the path of the signal, finite charge collection time, etc.

We have therefore investigated the effect of finite rise time on the trapezoidal shaping steps that have, to this point, been illustrated for input pulses of zero rise time. The assumed input pulse shape was modified to be of the form

$$v(t)=\frac{l}{\tau-\theta}\left(e^{-t/\tau}-e^{-t/\theta}\right), \tag{32}$$

where θ now accounts for the finite rise time of the pulse. In Fig. 6a, three input pulses (A, B, and C) are shown with values for τ/θ of 0.01, 0.025 and 0.05, respectively. In each case, the total charge (area under $v(t)$) has been kept constant. The rise time of the trapezoid is equal to decay time constant of the exponential signal. The amplitude of the output from trapezoidal shaper is given in units τ^2. The flat top of the trapezoidal pulses in Fig. 6b has a duration of $\frac{1}{3}$ of the decay time constant τ. The highlighted areas show the parts of the trapezoid which are affected the most by the variations in the rise time of the exponential pulse. Note that the maximum amplitude of the shaped output is the same for all three cases or, in other words, the output is free of the effects of ballistic deficit over this range of variation of the input rise time. The advantage of trapezoidal shaping in avoiding resolution loss due to ballistic deficit in germanium spectrometers has been previously recognized [1,6,7]. The time duration of the flat top must be long enough to accommodate the rise time variations, but should be made no longer than necessary to minimize the total pulse length and consequent effects of pile-up. One feature of the

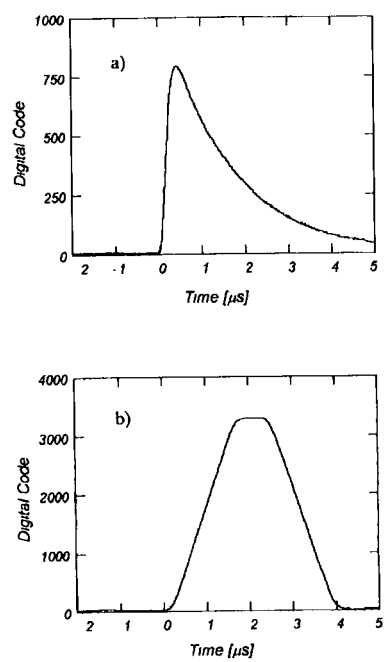

Fig. 7. Sampled input pulse (a) and corresponding trapezoidal shape (b). The decay time constant is 1.5 μs and the flat top duration of the trapezoidal shape is 800 ns.

Table 2
Energy resolution of the digital trapezoidal/triangular shaper at different settings, and the energy resolution data which were obtained using a quasi-Gaussian shaper at the same measurement conditions

PULSE SHAPE	HPGe DETECTOR (^{60}Co - 1.33 MeV)			X-RAY DETECTOR (^{241}Am - 59.4 keV)		
	T_F* [μs]	T_W [μs]	FWHM [keV]	T_F* [μs]	T_W [μs]	FWHM [keV]
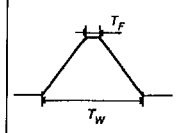	0	6.8	17.35	0	7.2	1.12
	0.2	7.0	9.28	0.2	7.4	1.12
	0.4	7.2	2.43	0.4	7.6	1.12
	0.6	7.4	2.41	0.6	7.8	1.13
	0.6	3.2	3.40	0	3.8	1.31
	T_p [μs]	T_W† [μs]	FWHM [keV]	T_p [μs]	T_W† [μs]	FWHM [keV]
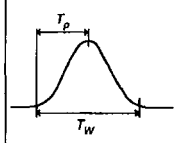	2	5.5	5.74	2	5.5	1.38
	4	11	2.41	4	11	1.18
	6	16	2.10	--	--	--
	12	30	1.98	--	--	--

* This entry is the delay $m = k - 1$ (see Eq. (28)–(31)).
† Width of the pulse at 2% of the amplitude.

present digital approach to shaping is that the flat top duration can be easily adjusted to suit the application by a simple change in choice of delay settings.

5.2. Experimental measurements

In order to test the techniques for synthesis of triangular and trapezoidal shapes, a prototype system was assembled that implements the algorithms developed earlier in this paper in a personal computer (PC) on a pulse-by-pulse basis. While this configuration is not the full hardware implementation we envision for the finished system (such as illustrated in Fig. 5), it is capable of testing the principles at data rates that are limited by data transfer and processing time in the PC. A full hardware implementation would impose no rate limitations, and maximum throughput would be set only by pile-up considerations.

In our prototype, the input pulses were obtained from the fast output of a spectroscopy amplifier (Ortec 673) [13]. This signal has a rise time (10–90%) of approximately 220 ns and an exponential decay time constant of either 1.5 or 3.5 μs (these are approximate values and depend on pole-zero adjustment). This pulse was sampled using a 10-bit ADC (AD9020) operating at 50 MHz. Time slices of up to 20 μs length were temporarily stored for each pulse in a FIFO buffer and then transmitted to the PC for implementation of the recursive shaping algorithms. The output of the shaper was then stored in a multichannel spectrum based on a trigger provided by the peak sensing algorithms similar to those described in ref. [8]. For comparison purpose, the quasi-Gaussian analog output of the same spectroscopy amplifier was also supplied to a conventional multichannel analyzer.

A typical time slice including the input signal and the corresponding trapezoidal shape output pulse is shown in Fig. 7. A digital gain of 4 was used so that the amplitude of the shaped signal is approximately 4 times greater than the amplitude of the exponential signal.

We used two detectors to evaluate the performance of the digital shaping system. The first was a p-type HPGe with 30% relative efficiency, while the second was a p-i-n photodiode used as X-ray detector. The counting rate was kept low (less than 1 kcps) in order to ensure that pile-up would have no significant effect on the recorded spectra. Table 2 summarizes the obtained results.

The data presented in Table 2 shows the superiority of the digital trapezoidal/triangular shaping system compared with the quasi-Gaussian shaper. Specifically, the digital system allows a shorter shaping time to be chosen at equivalent energy resolution, compared with the quasi-Gaussian shaper. This advantage will be most important at high counting rates where pile-up is a major consideration. By increasing the duration of the flat-topped part of the trapezoid, the effects of ballistic deficit are eliminated. It is also evident that, in the case of a detector with a very short charge collection time (the X-ray detector), the energy resolution is independent of the duration of the flat part of the pulse shape which is in good correspondence with theoretical predictions [1,3]. In obtaining these results we have found that proper adjustment of pole-zero is critical to provide an input pulse with a single exponential decay.

The results shown in Table 2 indicate a distinct advantage of the prototype digital shaper over the analog system used for comparison purposes. However, several words of caution are in order in interpreting these preliminary results. The system used to obtain these data operated in quasi-real time, and was not a true on-line processor of the type illustrated in Fig. 5. While we are reasonably confident that such a system could produce similar results, that capability has not yet been demonstrated. Also, the analog shaping amplifier used for comparison purposes is a common commercially available unit, but may not represent the ultimate performance that could be obtained with a custom designed analog pulse processing system.

6. Conclusion

Recursive algorithms for the digital synthesis of trapezoidal and triangular pulse shapes have been de-

veloped. Priority was given to real time applicability of the shaping steps and their simplicity. The technique offers flexibility through simple software adjustment of the shape parameters depending on the characteristics of the detector. Particularly, it has been demonstrated that by varying (digitally) just one parameter (the duration of the flat top of the trapezoid) an effective elimination of the effects of ballistic deficit from an HPGe detector can be achieved.

References

[1] V. Radeka, IEEE Trans. Nucl. Sci. NS-15 (1968) 455.
[2] P.W. Nicholson, Nuclear Electronics (Wiley, New York, 1974).
[3] F.S. Goulding, Nucl. Instr. and Meth. 100 (1972) 493.
[4] F.S. Goulding, D.A. Landis and N.W. Madden, IEEE Trans. Nucl. Sci. NS-30 (1983) 301.
[5] K. Debertin and R.G. Helmer, Gamma- and X-ray Spectrometry with Semiconductor Detectors (North-Holland, Amsterdam, 1988).
[6] F.S. Goulding et al., presented at IEEE NSS, San Francisco, Nov. 1993.
[7] S.M. Hinshaw and D.A. Landis, IEEE Trans. Nucl. Sci. NS-35 (1990) 374.
[8] V. Jordanov and G.F. Knoll, IEEE Trans. Nucl Sci. NS-40 (1993) 764.
[9] V. Jordanov, EDN 37 (Nov. 12, 1992) 200.
[10] F. Hilsenrath, H.D. Voss and J.C. Bakke, IEEE Trans. Nucl. Sci. NS-32 (1985) 145.
[11] T.H. Wilmshurst, Signal Recovery from Noise in Electronic Instrumentation, 2nd ed. (Adam Hilger, Bristol, 1990).
[12] T. Lakatos, Nucl. Instr. and Meth. B 62 (1991) 289.
[13] Ortec 673 spectroscopy amplifier and gated integrator manual (Ortec, 1984).

Gamma Ray Energy Tracking In-Beam Nuclear Array

Electronics: Requirement Document

Document # GRT-3-041115

November 2, 2005
(upgraded June 12, 2007)

Fred Bieser, I-Yang Lee, Augusto Macchiavelli, John Weizeorick, Sergio Zimmermann

Accepted and Approved by:

Sergio Zimmermann _____Date_____

I-Yang Lee _____Date_____

Electronics: Requirement Document
Gamma Ray Energy Tracking In-Beam Nuclear Array (GRETINA)

Revision History

Revision No.	**Pages Affected**	**Effective Date**
Revision 0	Entire document	November 2, 2007
Revision 1	Entire document	June 12, 2007

1 SCOPE 1
2 GENERAL 2
2.1 Purpose 2
2.2 Precedence 3
2.3 Authority 3
3 ELECTRONICS SYSTEM PRIMARY REQUIREMENTS 3
3.1 Front-End 3
3.1.1 Pre-amplifier Energy Resolution 3
3.1.2 Noise per Segment 3
3.1.3 Digitizer Sampling Rate 4
3.1.4 Dynamic range and required resolution of ADC 4
3.1.5 Non-Linearity 4
3.1.6 Final Energy/Gain Stability 4
3.1.7 Pre-Amp Rise Time 5
3.1.8 Maximum Hit Rate per Crystal 5
3.1.9 Maximum Energy of Central Contact 5
3.1.10 Maximum Energy of Segment 6
3.2 Data Readout 6
3.2.1 Readout Data Rate 6
3.2.2 Data Loss 6
3.2.3 Digitizer Information 6
3.2.4 Readout of Adjacent Segments 7
3.2.5 Pipeline Depth 7
3.3 Trigger Logic 8
3.3.1 Leading Edge Discriminator 8
3.3.2 Trigger Latency 8
3.3.3 Trigger Algorithms 8
3.3.4 Prompt and Delayed Coincidence Triggers 9
3.3.5 Trigger Losses 9
3.3.6 Trigger Information 9
3.3.7 Trigger Blocking ("Throttling") and Trigger Loss Reporting 10
3.3.8 Turning Off Level 1 Trigger Outputs 10
3.4 Clock and Timing 10
3.4.1 Time Stamp Increment 10
3.4.2 Long Term Clock Stability 10
3.4.3 Clock Jitter 10
3.4.4 Clock Skew 11
3.4.5 Timestamp 11
3.4.6 Clock Synchronization and Verification 11
3.5 Other Requirements 11
3.5.1 Reconfigurability and Logic Expansion 11
3.5.2 Testability 12
3.5.3 Spare Components and Modules 12
4 INTERFACES 12
4.1 Computing System 12
4.1.1 Hardware 12

4.1.2 Software 13
4.2 Detector Modules 13
4.2.1 Pre-Amplifiers 13
4.2.2 High Voltage 13
4.2.3 Test Inputs 13
4.2.4 Pre-amp/Digitizer Cable and Connector Crosstalk 14
4.2.5 Pre-amp/Digitizer Cable Attenuation and Lenght 14
4.3 Auxiliary Detectors 14
4.3.1 Readout 14
4.3.2 Trigger 14
4.3.3 Fast Strobe 15
4.3.4 Time Stamp 15
4.3.5 Clock Synchronization and Verification 15
4.3.6 Location 15
4.4 Physical 16
4.4.1 Floor Space 16
4.4.2 Cooling 16
4.5 Electrical 16
4.5.1 Power 16
4.5.2 Safe Voltage and Current 16
4.5.3 Ground 16
4.5.4 Cables and Connectors 16
4.5.5 Crate and Module 17
5 REFERENCES 18

1 SCOPE

This LBNL GRETINA Project Engineering Note specifies the Electronic System Requirements. Figure 1 shows the block diagram of the GRETINA Electronics and Computing Systems. The Electronics System is defined on the GRETINA Conceptual Design Report and includes the following subsystems:

a) Pre-amplifiers
b) Digital Signal Processing Modules
c) Global Trigger and Timing Modules
d) Power Supplies
e) Cables
f) Crates and racks.

We will now give a short description of the system. The gamma-ray interacts with the germanium crystal and induces charge in the crystal segments. The pre-amplifier integrates this charge and drives an analog voltage on the cable to the Digital Signal Processing (DSP) cards. The DSP cards digitize and process this information. If the data passes some threshold criteria, the DSP card issue a message to the Local Trigger and Timing Module (LTT), which routes this information to the Global Trigger and Timing Module (GTT). The GTT collects information from all LTT and also from auxiliary trigger modules, and uses this information to make a global trigger decision. Once this decision is made, it sends back to the LTT modules a trigger command, which then routes the information to the DSP cards. The DSP saves the data into an interface memory. Later on, the Readout Computer reads the data from each DSP FIFO and sends the data to the computing system, which processes and builds the event. The LTT and GTT modules also provide clock information to the electronics.

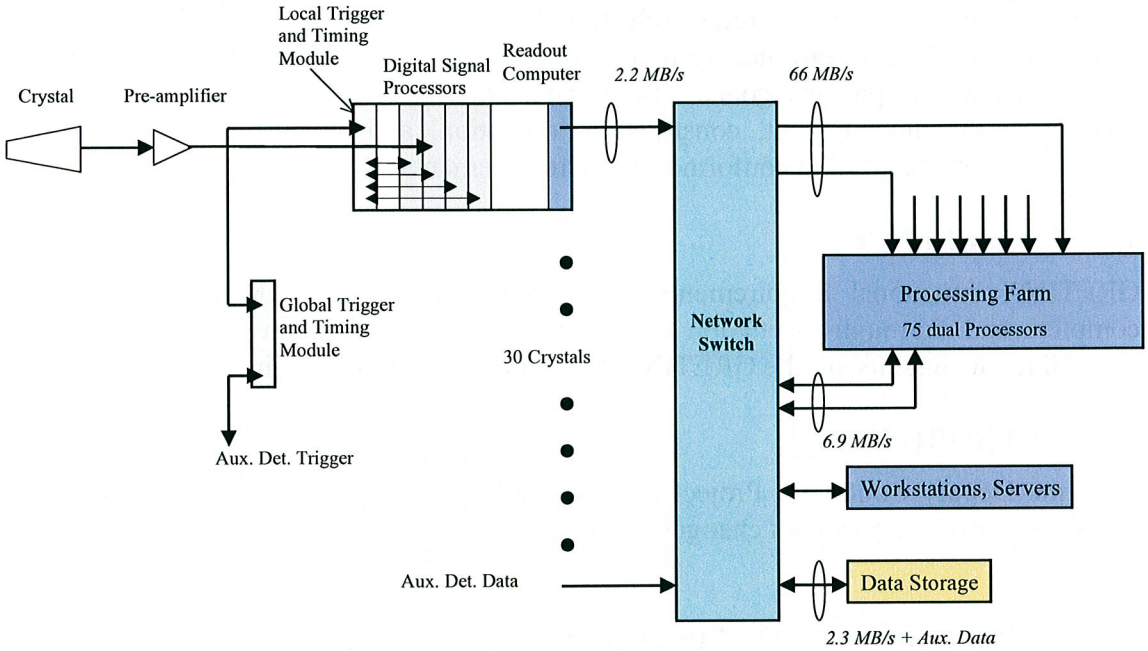

Figure 1. GRETINA Electronics and Computing Systems

The trigger hardware is designed to provide a method of reducing the overall data flow. It provides a method of event selection to reduce the data going to the computer farm. The computer farm does the final event selection. The trigger hardware should be designed as flexible as possible to allow the trigger algorithm to be modified without redesigning the hardware.

The main function of the trigger logic is to determine when a trigger has occurred and to notify the Digitizer Modules. When the Digitizer Modules are notified that a trigger has occurred they must decide which data is to be saved for readout and sent to the computer farm.

The trigger system should have two trigger levels. The level-1 triggers are a self-triggering threshold set for each segment or the central contact. The level-2 triggers are the response generated by a trigger module(s) after analyzing the level-1 triggers from the digitizer modules and trigger data from auxiliary detectors. The data sent to the level-2 trigger module from the Digitizer Modules may vary based on the triggering method selected by the user. The level-2 trigger will be sent to each digitizer module, which will prepare the appropriate data for readout. The data readout will typically be information regarding the net charge collected from segments with a level-1 trigger, and image charge signals from segments neighboring these segments.

2 GENERAL

2.1 PURPOSE

This document describes the primary electronics system requirements for GRETINA and it is based on the GRETINA Functional Requirements, as described in the GRETINA

Project Execution Plan (PEP, refer to Section 3 of reference [1]). It describes the overall requirements of the electronics system, and what is needed to achieve the Functional Requirements and physics goals. Secondary requirements, specifications and plans relating to the development, construction, operation, and support of the GRETINA Electronic Systems need to conform to these requirements.

2.2 PRECEDENCE

GRETINA Functional Requirements take precedence over this document. While a complete and thorough discussion of requirements is included in this document, the controlling documents are the GRETINA Functional Requirements, not this note.

2.3 AUTHORITY

Only the Deputy Contractor Project Manager authorizes approval of this document for initial release and subsequent changes, in accordance with the GRETINA PEP [1].

3 ELECTRONICS SYSTEM PRIMARY REQUIREMENTS

3.1 FRONT-END

3.1.1 PRE-AMPLIFIER ENERGY RESOLUTION

The pre-amplifier energy resolution shall be ≤ 1.1 keV FWHM when connected to 10 pF input capacitance and 4 usec shaping time.

Justification: Our experiences with the GRETA Prototype and GRETINA Triplet shows us that it is reasonable to expect ~2.5keV FWHM at an energy of 1.33MeV (^{60}Co source), with peaking times of 4-5 usec. In general $FWHM^2 = Noise^2 + a*E$. The first term is the noise of the electronics and the second term is due to the statistics of carrier generation. In Gammasphere we have Noise ~ 1keV and the E term is ~ 2keV at ^{60}Co.
Status:

3.1.2 NOISE PER SEGMENT

The noise per segment shall be ≤ 7 keV (standard deviation) averaged at 35 MHz bandwidth.

Justification: Noise at higher frequencies affect the position resolution and noise at lower frequency affect the time resolution. This requirement has been achieved in previous detector/pre-amp combinations and, if this requirement is achieved, it is not the limiting factor in the position resolution (because these factors add in quadrature). Also, this noise ultimately affects the energy resolution, and limiting to this requirement will contribute to achieve the energy resolution required in Section 3.1.1.
Status:

3.1.3 DIGITIZER SAMPLING RATE

The digitizer sampling rate shall be ≥ 75 MHz, preferable 100 MHz. An anti-aliasing filter shall filter the digitizer inputs.

Justification: The characteristic rise time of the signal is determined by the transport properties of the charge carriers in the Ge crystal. This is a few 100 nsec for detectors of this size. A preamp with a bandwidth of 30 - 40MHz will preserve the position information and therefore a digitizer running at 100 MHz will be fast enough to recover the signal. The Functional Requirements of the PEP [1] require 75 MHz, but the availability of modern ADCs allows higher sampling rate with reasonable additional cost. Furthermore, when the digitizers are actually assembled in production quantities, this cost difference will be smaller.
Status:

3.1.4 DYNAMIC RANGE AND REQUIRED RESOLUTION OF ADC

The dynamic range of the ADCs shall be ≥ 12 bits, preferable 14 bits.

Justification: The requirement "Noise per Segment" (Section 3.1.2) asks for pre-amplifier resolution ≤ 7 keV and some gamma-rays may have as much as 30 MeV (most likely measured just on the central contact, see Section 3.1.9). For all channels of the digitizers to be identical and to be able to accommodate this large dynamic range (7 keV to 30 MeV) with minimum contribution to the ADC noise itself, a 14 bits ADC with RMS noise smaller than 1 bit is preferable. An option that will allow operating with 12 bits ADC is to have the central contact going into two input channels of the digitizer. One channel can be configured to measure low energy interactions and the other channel could be attenuate by 4 and then be used to measure the high energy interactions. However, this will require one special channel on the digitizers to be always assigned to the central contact, and we want to avoid this. External attenuators can also be employed, and all channels then can have the same configuration.
Status: We intend to design the digitizers with 14 bits ADCs.

3.1.5 NON-LINEARITY

The final integral nonlinearity as measured in the final energy spectrum shall be ≤ ±0.1% over the top 99% of the dynamic range. The final differential nonlinearity as measured in the final energy spectrum must be ≤ ± 1% over the top 99% of the dynamic range. The energy used for this characterization shall be estimated by the Digitizer digital signal processing unit.

Justification: Non-linearity affects position resolution.
Status:

3.1.6 FINAL ENERGY/GAIN STABILITY

The final energy/gain stability as measured in the final energy spectrum shall be ≤ ±0.2% per hour gain drift for ≤ ± 8°C temperature drift.

Justification: Experience with previous gamma-ray spectrometers (e.g., Gammasphere) has shown that these numbers are achievable at reasonable cost. Furthermore, they are adequate for the experiments we foresee with GRETINA.
Status:

3.1.7 PRE-AMP RISE TIME

The pre-amp rise time shall be ≤ 70 ns (10% to 90%) when we include the capacitance of the detector at the input. This will ensure a sharp enough rising edge on the energy step to determine where the interaction of the gamma-ray occurred within the germanium crystal.

Justification: The pulse shapes are used to find the position of the gamma-ray interactions inside the crystal. Simulations of the sensitivity of he position determination to the rise-time of the pre-amp have shown that up to 70 ns will allow to comfortable achieve the required 2 mm position resolution described in the Functional Requirements of the PEP.
Status:

3.1.8 MAXIMUM HIT RATE PER CRYSTAL

The pre-amplifier shall work with an average hit rate per crystal of 50 Kgamma-ray with 1 MeV energy without saturating.

Justification: (a) Saturation vs. pile-ups: The first stage of the crystal pre-amplifier is a charge sensitive unit, with a resistor discharging the integrating capacitor. Presently this time constant is ~1 ms. If the hit rate is too high, this portion of the pre-amplifier saturates (i.e., the voltage increases so much that the circuit is not linear anymore). Pile-up is the detection of another hit before the pre-amplifier output had the ability to return to the baseline noise. The amplitude of the second hit adds to the tail of the amplitude of the first hit. The pre-amplifier second stage has a pole-zero cancellation circuit, and it returns the output to baseline noise before the first stage. The time constant of this second stage is ~50μs. For example, assuming that two hits happen within 150μs, the amplitude error of the second hit is approximate 5%. Due to the time distribution of the hits, pile-ups will eventually occur. (b) Hit rate: GRETINA will run experiments that look for rare events. Usually, in these experiments a selective trigger is used to reduce the data rate. However, to obtain enough statistics in a reasonable time the front-end pre-amp will have to amplify hits at a very high hit rate. This will limit the useful rate to about 50 KHz.
Status: We have calculated the transfer function of the two stages of the preamplifier, and simulations have shown that the pre-amplifier doesn't saturate with 50 KHz hit rate.

3.1.9 MAXIMUM ENERGY OF CENTRAL CONTACT

The central contact shall be able to detect interactions up to at least 30 MeV.

Justification: Some experiments, for example, those to study the giant dipole resonance, will require this energy level.
Status:

3.1.10 MAXIMUM ENERGY OF SEGMENT

Segments shall be able to detect interactions up to at least 10 MeV.

Justification: Same as Section 3.1.9.
Status:

3.2 DATA READOUT

3.2.1 READOUT DATA RATE

The readout speed of GRETINA shall be $\geq$ 10 MB/s/crystal.

Justification: It has been estimated that GRETINA should be able to process at least 20,000 gamma-rays/secs in the processor farm. If a gamma-ray generate signals in 20 segments and generates ~120 bytes of data from each segment, we can estimate 2400 bytes of data per gamma-ray. If there are 20,000 gamma-rays/sec (as required in the Functional Requirements of the PEP) then the readout rate is 20,000 gamma-rays/secs $\times$ 2400 bytes/gamma-ray = 48Mbytes/sec total. Since there are 30 crystals this would give a data rate of 1.6 MB/s/crystal. With a readout speed $\geq$ 10 MB/s/crystal we are allowing for future improvements in the processing farm to increase the overall system data rate.
Status:

3.2.2 DATA LOSS

The electronics shall be fully pipelined and operate with minimum data loss for an average frequency rate of 50 Kgamma-rays of 1 MeV per crystal. The trigger system may be configured to reduce the readout data rate per Section 3.2.1. The pre-amplifiers may have pile-up, in which case the high resolution energy measurement may be inaccurate.

Justification: Data loss constitutes inefficiency and should be avoided.
Status: The compliance to this requirement needs simulation of the overall system. There is an inherited data loss associated with the time it takes for the leading edge discriminator logic associated with the central contact and segments to recover from a hit. Right now it is programmable in the digitizers with a 7-bits precision or 640 ns.

3.2.3 DIGITIZER INFORMATION

During normal operation the following minimum set of information shall be read out from each channel when an event occurs.

Table 1. Digitizer Information

Name	Description	# of Bytes
Channel Identification	An unique identification for each analog input from the digitizer module	2
Leading Edge Time (LED)	The content of the time stamp counter when the detector output crosses the threshold	6
Constant Fraction Time (CFT)	Constant fraction time and the signal amplitudes before and after the zero crossing.	Time stamp: 6 Amplitudes: 2x2 Total: 10
Integrated Energy	Energies determined from the trapezoidal filter with programmable time constants and pole zero cancellation	4
ADC Trace	ADC samples. It shall be programmable from 0 nsec to 10 usec, typical 500 ns. ADC samples recorded before the LED is also programmable (typically a few samples)	0 to 2000 bytes, typical, 100 bytes.
		Typical: 118 bytes Max: 2018 bytes

Redundant information may also be transferred to support fault detection (for example, trigger decision number, etc.). In addition to the event data the digitizer modules shall also provide all setup information that may be read out before each experiment. This setup information could include information about which version of FPGA code is being used along with the values of various parameters.

Justification: This is the required information to execute the signal decomposition and tracking algorithms running in the processor farm and to transmit the measured energy.
Status:

3.2.4 READOUT OF ADJACENT SEGMENTS

The Digitizer Modules shall read out the digitize waveform of the segments adjacent to the charge collecting segment.

Justification: When the gamma-ray interacts with the germanium crystal, it creates electrons and holes. The electrons drift to the central contact, while the holes drift to one segment (dubbed the "charge collecting" segment) where the charge is collected. Charge is injected in the segments adjacent to the charge collecting segment, and they also need to be readout.
Status:

3.2.5 PIPELINE DEPTH

The pipeline depth associated with each digitizer analog input shall be $\geq$ 20 μsec, preferable $\geq$ 100 μsec.

Justification: The pipeline depth is to accommodate the time required for a Level-2 trigger decision. GRETINA can run by itself or with auxiliary detectors. When GRETINA is running with no trigger data from auxiliary detectors, it is desirable to keep the trigger latency short to reduce the data storage inside the Digitizer Modules. In this case the total time for a level-1 trigger and level-2 trigger shall be $\leq$ 20usec. When GRETINA is running with auxiliary detectors it is desirable to make the trigger latency as long as possible. The longer latency will allow interfacing with slower devices and interactions. In this case it is preferable to design the pipeline with 100 usec deep. The limiting factor will be how much memory it is possible to allocate for a reasonable cost inside the digitizers.
Status: These pipelines will be located into the digitizer FPGAs. It is necessary to check how much memory blocks can be allocated to these pipelines.

3.3 TRIGGER LOGIC

3.3.1 LEADING EDGE DISCRIMINATOR

The leading edge of the detector signals shall be discriminated for the central contact and segment logic. Trigger information shall be exchanged between digitizer and trigger system when the leading edge discriminator (LED) of the central contact fires. The LED associated with the segments shall be used for hit pattern determination for some possible trigger algorithm.

Justification: In general, when the LED logic of the central contact fires, it means that some gamma-ray interacted with the crystal (unless it is noise above threshold) and the trigger system has to make a trigger decision about passing this information to the next level. Therefore, the digitizer has to send to the trigger the information about this gamma-ray.
Status:

3.3.2 TRIGGER LATENCY

The total time from the LED detection inside the Digitizer Modules until the return of the trigger decision shall be faster than the pipeline depth (see Section 3.2.5). This latency includes the time it takes the trigger data to reach the trigger module, the time it takes the trigger module to process the data, and how long it takes for the trigger notification to get back to the digitizer modules.

Justification: This latency will not incur in data loss due to pipeline depth.
Status:

3.3.3 TRIGGER ALGORITHMS

The initial trigger algorithms shall be the following:

a) Multiplicity: central contact coincidence multiplicity trigger as described in the GRETINA Preliminary Conceptual Design Report
b) Energy: central contact energy at lower resolution (which appears earlier in the digitizer, compared with the integrated energy for high resolution calculations). It can use the energy of a central contact or the sum of energies of central contacts.

When this energy falls within some pre-set window (within some low and high energy limit) a trigger decision is generated.

c) Pattern distribution: GRETINA shall trigger if the Trigger System detects coincidence of gamma-rays energy at lower resolution above threshold in any two pre-programmed central contact of the crystals.
d) Auxiliary detector trigger: GRETINA will receive an external trigger within the pipeline depth.

Justification: It is possible to envision many different trigger algorithms. However, we will have to focus in a few candidates to clearly define the scope of the project. We have selected the four algorithms described above, which should give a wide range of possibilities to accommodate different experiments. Typically the user will need to specify the trigger source and algorithm and then specify parameters associated with the selected trigger.
Status:

3.3.4 PROMPT AND DELAYED COINCIDENCE TRIGGERS

The trigger logic shall accept both prompt and delayed coincidence triggers in at least two time windows within the allowed overall trigger window.

Justification: A number of possible experiments will require coincidence between prompt and delayed events. More than two time windows will satisfy this need.
Status:

3.3.5 TRIGGER LOSSES

The Trigger System shall be lossless with an average Level 1 trigger frequency of 50KHz per crystal.

Justification: Lost of trigger information will possibly incur in losing good events with the consequent additional time to execute the experiments.
Status:

3.3.6 TRIGGER INFORMATION

During normal operation the Trigger System has to provide information to the DAQ system which allows tracing why a trigger decision was made. This trigger even data may be recorded together with the events for latter analysis. In addition to the event data the Trigger System shall also provide all setup information that may be read out before each experiment.

Justification: To analyze the data the user needs to know how the trigger was reached and configured.
Status:

3.3.7 TRIGGER BLOCKING ("THROTTLING") AND TRIGGER LOSS REPORTING

If the trigger rate becomes too high the trigger system shall block trigger requests and shall report this condition to the user.

Justification: Depending of the experiment setup or even a failure in the digitizers, the trigger rate can be too high for the Trigger System. If this condition occurs, the Trigger System may lose trigger information. This condition has to be reported to the user. The user can then reduce the trigger rate by modifying the trigger parameters to make the trigger more selective or even repair the system. The trigger blocking ('throttling") allows automatically disabling and enabling Level 1 triggers to bring the system to a rate that decreases trigger loss.
Status:

3.3.8 TURNING OFF LEVEL 1 TRIGGER OUTPUTS

There shall be a method of turning off individual Level 1 trigger outputs.

Justification: In case a channel becomes noisy or defective, we need the ability to disable it from the trigger system without further disrupting the system.
Status:

3.4 CLOCK AND TIMING

3.4.1 TIME STAMP INCREMENT

The time stamp in the digitizer modules shall be incremented at least once every ADC clock cycle (refer to Section 3.1.3).

Justification: Time information is usually derived with a Constant Fraction Discrimination technique. In this way, the interpolation between the ADC clock cycles provides sufficient time resolution to recover typical performance of germanium detectors (about 5 ns at 1 MeV).
Status:

3.4.2 LONG TERM CLOCK STABILITY

The clocks must have a long term stability of $\leq$ 50 ppm over a 4 week period.

Justification: This requirement means that after a month the Δt will be $\leq$ 120 seconds. Small variations on the clock frequency will not cause problems to GRETINA. This requirement is based on what is currently available at a reasonable cost without requiring temperature controls or time adjustments.
Status:

3.4.3 CLOCK JITTER

The clock jitter must be less than 1 ns RMS measured over a 1000 cycles.

Justification: To guarantee the timestamp resolution between different segments the jitter on the clock must be controlled to within 1 ns.
Status: We expect to obtain 100 psec.

3.4.4 CLOCK SKEW

The clock skew between modules and time variation after the initial alignment shall be less than 2 ns over a two week time period for $\leq \pm$ 8°C temperature drift.

Justification: With this stability, time calibration will only need to be done at the beginning and end of an experiment.
Status:

3.4.5 TIMESTAMP

The time stamp will be 48 bits and will be clocked once every 10 nsec.

Justification: The timestamp must be large enough to provide a unique number for at least 4 weeks.
Status:

3.4.6 CLOCK SYNCHRONIZATION AND VERIFICATION

The clocks in all digitizers and auxiliary detectors shall be synchronized with the same time stamp. There shall be a method to verify the time stamp synchronization between digitizers and auxiliary detectors and this method shall be independent of the method employed to synchronize the clocks.

Justification: Event data will be available in several digitizers and auxiliary detectors. In order to assemble the event, GRETINA needs accurate information about the time this data was recorded. Having an independent method to verify the synchronization avoid the same path used for the synchronization procedure (which could be damage or not properly set up).
Status: Could the independent verification be implemented with the pulse inputs of the pre-amplifiers?

3.5 OTHER REQUIREMENTS

3.5.1 RECONFIGURABILITY AND LOGIC EXPANSION

The electronic system shall be reconfigurable remotely. The FPGA shall have plenty of spare logic available after incorporating the present requirements to allow for future expansion (goal, < 40% utilized).

Justification: GRETINA will be used in different Nuclear Science experiments, which may require different hardware/firmware configurations. Firmware upgrades and revisions have to be easy to propagate through the system to decrease down time and maintenance costs. Enough spare logic inside the FPGAs will allow future expansion of the logic.

Status:

3.5.2 TESTABILITY

The GRETINA Electronics System as a whole shall be testable just with the readout computers (which are part of the Computing Systems) and independently of signals from the detector modules. The detector module test inputs (which inject charge into the pre-amps) shall also be part of the test procedure. Reasonable effort shall be made to make all complex electronic testable, independent of auxiliary electronics. For example, a digital input signal in a module can be tested with a digital output signal in the same module. Registers and memory in the modules shall be read/writeable where possible.

Justification: Commissioning and testing complex electronic systems requires substantial effort and failures and malfunctions are difficult to debug and isolate. Also, during the GRETINA development, not all system portions will be available at one specific time because they will be developed in parallel in different locations. Furthermore, there is a reasonable cost in designing, assembling and maintaining test stand with all units require for fully testing a module. Careful planning and integration of test features into the system and modules will considerably reduce commissioning, testing and debugging time and costs.
Status:

3.5.3 SPARE COMPONENTS AND MODULES

The GRETINA technical scope specifies the level of spare modules for the MIE (described in the GRETINA PEP. However, parts are becoming obsolete at a very fast pace. When possible, parts used in the electronic modules shall have more the one manufacturer. Where this is not possible, it is important to identify parts that may become obsolete during the design or during the useful life of GRETINA and purchase additional spares parts or assemble additional spare modules.

Justification: Parts are becoming obsolete in a very fast pace. It is not uncommon to have a part obsolete even before the end of a design or production. When this happens, it can result in expensive retrofits and a delay in the schedule. Reasonable effort should be taken to avoid this situation.
Status:

4 INTERFACES

4.1 COMPUTING SYSTEM

4.1.1 HARDWARE

The electronics has to interface with the other systems (computing, mechanical, liquid nitrogen, etc.)

Justification: The electronics is controlled, readout and monitor through the computer system. Therefore, it has to electrically interface with this system.
Status:

4.1.2 SOFTWARE

The Electronic System shall be controlled, monitored and readout over the local network as described in the Computer System Requirement document [2].

Justification: The electronics is controlled, readout and monitor through the computer system. Therefore, the software in the Computer System has to exercise the electronics to control, readout and monitor the Electronic System.
Status:

4.2 DETECTOR MODULES

4.2.1 PRE-AMPLIFIERS

The outputs of the pre-amps shall interface with the digitizer modules.

Justification: The output of the pre-amplifiers connects to the digitizer modules.
Status:

4.2.2 HIGH VOLTAGE

The HV noise and ripple shall not degrade the performance of the detector. The high voltage (HV) ramp up rate shall be ≤1 kV/minute even if the Computing and Electronics Systems are reset, and even if they crash or fail. A diode shall be mounted in series with the HV connection of the crystal.

Justification: The HV of the detector modules cannot change too quickly because it can damage the pre-amplifiers. The diode is to prevent voltage discharge of the crystal bias voltage and allow enough time for the user to restore the HV to avoid the effects of neutron damage.
Status:

4.2.3 TEST INPUTS

We shall be able to inject a "detector like" calibration and timing charge into the pre-amplifiers connected to the central contact and segments of the detector. The voltage injected shall be adjustable to better than 0.1% of the maximum output of the pre-amplifier (i.e., 30 MeV for the central contact and 10 MeV for the segment, refer to Section 3.1.9 and 3.1.10). The rise time can be fixed to <100 nsec. This test input shall be used to measure the energy linearity of the system. The time skew of the test inputs sent to the detector inputs shall be less than 2 ns.

Justification: A capacitor in series with the pre-amplifier input is used to inject charge. This capacitor is part of the detector module. Therefore, the precision of the charge injection is then constrained to the accuracy and stability of the voltage pulse and the characteristics capacitor. In this requirement we are referring to the voltage pulse. The objective of the test input is to allow for electronics calibration, and functionality and

accurate timing tests of the pre-amplifiers, digitizer inputs and clock system. Even portions of the DAQ system can be tested using these test inputs.
Status:

4.2.4 PRE-AMP/DIGITIZER CABLE AND CONNECTOR CROSSTALK

The maximum crosstalk between the pairs of the cable and pins of the connectors between the pre-amplifier and digitizers shall be < 0.04%. This shall be tested with one pair as the receiver and all other signals switching in the same direction.

Justification: We need to minimize the crosstalk on the cable and connectors. The detector requirements state that the total crosstalk between any two pre-amplifiers must be less than 0.2%.
Status: In Oct. 2004 we have done preliminary tests and 0.01% seems to be achievable. However, further tests have shown a crosstalk of 0.04%. This needs more investigation.

4.2.5 PRE-AMP/DIGITIZER CABLE ATTENUATION AND LENGHT

The cable type and length shall contribute to the energy resolution by no more then 0.1 keV at 60 keV, and less than 1 keV at 25 MHz. The difference in length shall contribute less than 1 ns to the signal transit time.

Justification: Cables have attenuation, which depends on the frequency. This attenuation has to be kept under control to avoid distorting the pre-amplifier waveforms. The pre-amp waveforms have to be time aligned. Therefore, the cable length between the pre-amps and digitizers has to be approximately the same. A 6" length variation adds <1 ns delay difference between the digitizer inputs.
Status: We need to test if we can meet this requirement with the prototype cable we received.

4.3 AUXILIARY DETECTORS

4.3.1 READOUT

Data from the auxiliary detectors shall be combined with the GRETINA data.

Justification: GRETINA will operate together with auxiliary detectors. It is reasonable to use the same Computing System to save the data of these auxiliary detectors.
Status: Since the event building system will probably use an Ethernet switch it will require that auxiliary detectors will be able to send their data out an Ethernet port. It would be desirable to have the format of the data match the GRETINA format. This format will be specified at a later date.

4.3.2 TRIGGER

The GRETINA trigger system shall provide 8 digital inputs with any logical combination to generate a trigger associated with auxiliary detectors. Also, it shall provide 8 digital outputs that inform when a Level-2 trigger occurred or other information about the Level-2 trigger status (e.g., if there is trigger losses, or multiplicity status, etc.)

Justification: The GRETINA trigger has to work together with the auxiliary detector trigger. Also, the digital outputs allow monitoring the status of the trigger system.
Status: Further work is required to specify the minimum set to interface GRETINA with the auxiliary detectors.

4.3.3 FAST STROBE

The GRETINA trigger system shall provide a Fast Strobe signal for the auxiliary detectors based on multiplicity algorithm (refer to Section 3.3.3). The Fast Strobe signal shall generated in <250 ns.

Justification: The GRETINA trigger has to work together with the auxiliary detector trigger. Some of these detectors don't have digital pipelines; the data is actually traveling on cables and the trigger decision has to be made before it arrives to the digitizers.
Status:

4.3.4 TIME STAMP

The auxiliary detectors shall provide their own time stamp with the same resolution as the GRETINA time stamp.

Justification: The auxiliary data collected from other detectors must be time correlated with the GRETINA data.
Status:

4.3.5 CLOCK SYNCHRONIZATION AND VERIFICATION

GRETINA shall provide clock and reset signals to synchronize the auxiliary detectors with GRETINA. Verification methods shall be implemented (such as pulse input similar to the GRETINA detectors) to verify that the auxiliary detector is properly synchronized with GRETINA.

Justification: The auxiliary data collected from other detectors must be time correlated with GRETINA.
Status:

4.3.6 LOCATION

The Electronic Systems shall allow space to accommodate possible inclusion of auxiliary detectors inside and outside the target chamber, as well as the support structure.

Justification: The auxiliary detector will need space, and the electronics around the support structure should be routed in order to allow for space for auxiliary detectors.
Status:

4.4 PHYSICAL

4.4.1 FLOOR SPACE

The electronic system requires TBD square feet at TBD meters from the detector.

Justification:
Status:

4.4.2 COOLING

The electronics shall require TBD BTU cooling system.

Justification: When electronics is powered it generates heat. This heat has to be removed from the area where the GRETINA detector modules and the electronics are assembled in order to avoid failures, improper behavior or early degradation of the components.
Status:

4.5 ELECTRICAL

4.5.1 POWER

The GRETINA electronics will require 110 Volts ??? Amps

Justification:
Status:

4.5.2 SAFE VOLTAGE AND CURRENT

All electronics with easy access shall be Class 1B (for example, digitizer and trigger modules). Class 1B is defined by LBNL's PUB3000, Chapter 8 as V<50V & P<1000W & 1000J, or 50V<V<20,000V & I<5mA & E=<5J. If not it shall to be enclosed.

Justification: Personal safety.
Status:

4.5.3 GROUND

GRETINA electronics shall be properly connected to a safe electrical ground.

Justification: Personal safety.
Status:

4.5.4 CABLES AND CONNECTORS

4.5.4.1 Signal, Power, Bias and Control/Monitoring

The detectors will be assembled in a mechanical structure and interconnected with the data acquisition through cables. These cables shall to be light enough for the mechanical structure to support it without deflecting more than the tolerance allowed by the

mechanical requirements. Also, the cable and cable/connector assembly shall be easily replaced in case of failure.

Justification: The GRETINA detector hemisphere must turn around the target and move away from the target. GRETINA has more than 1000 detector segments to instrument. The cable used and how they connect to the system must be selected carefully to avoid unnecessary strain in the mechanical structure.
Status: We have received (Sept 05) a prototype cable and we are presently testing it.

4.5.4.2 Power

The cables must be rated to handle the maximum voltage and current that the power supplies can generate.

Justification: Safety. Mitigate fire hazards.
Status:

4.5.4.3 Hazards

Any connector with exposed pins shall not deliver any life threatening current or voltage.

Justification: Safety.
Status:

4.5.5 CRATE AND MODULE

4.5.5.1 Modules

All the modules we design shall have fuses on the power supplies.

Justification: Safety. Mitigate fire hazards.
Status:

4.5.5.2 Crates

The crates shall have DC trip off within TBD ms if one of the following conditions occur:

- The voltage deviates > 2% from the adjusted nominal values
- An overload occurs
- The crates overheat
- A fan fails

It would be preferred if the crates included the ability to be remotely controlled and monitored. Parameters that we would like to monitor and control are:

- All voltages and currents
- Crate temperatures
- Status signals
- Remote control and monitor fan speed
- Set over and under voltage trip points, and current limits
- Turn the crate on and off remotely

- Remote "system reset"

The noise and ripple of the crates power supplies should be ≤ ??? mVpp.

Justification: For the DC trip, it is for electronics and personnel safety. Preferred requirements are for controlling and monitoring the crates and observe trents.
Status:

4.5.5.3 Other Safety Requirements:

All fabrication and installation shall meet all relevant regulations: OSHA, NEC, DOE, etc.

Justification: Safety and Environment. Mitigate fire hazards.
Status:

5 REFERENCES

[1] "Project Execution Plan for the Gamma Ray Energy Tracking In-Beam Nuclear Array (GRETINA)," Project # MIE-41-NL, May 2005, Revision 1.

[2] Mario Cromaz, Carl Lionberger, Alan Biocca, Chris Timossi, "MIE Computing Requirements for the GRETINA Spectrometer," GRETINA Doc # GRT-4-041212-01.1, LBNL, Dec. 12, 2004.

[3] "GRETINA Conceptual Design Report," Feb. 2004, revision Oct. 2005.